

Doctoral school in Physics - XXXV cycle



University of Trento

---

## Isolated objects in quadratic gravity

---

*Supervisor:*

Prof. Massimiliano Rinaldi

*Ph.D. candidate:*

Samuele Marco Silveravalle

Academic year 2021/2022

---

## Abstract

Quadratic curvature terms are commonly introduced in the action as first-order corrections of General Relativity, and, in this thesis, we investigated their impact on the most simple isolated objects, that are the static and spherically symmetric ones.

Most of the work has been done in the context of Stelle's theory of gravity, in which the most general quadratic contractions of curvature tensors are added to the action of General Relativity without a cosmological constant. We studied this theory's possible static, spherically symmetric and asymptotically flat solutions with both analytical approximations and numerical methods. We found black holes with Schwarzschild and non-Schwarzschild nature, naked singularities which can have either an attractive or repulsive gravitational potential in the origin, non-symmetric wormholes which connects an asymptotically flat spacetime with an asymptotically singular one, and non-vacuum solutions modeled by perfect fluids with different equations of state. We described the general geometrical properties of these solutions and linked these short-scale behaviors to the values of the parameters which characterize the gravitational field at large distances. We studied linear perturbations of these solutions, finding that most are unstable, and presented a first attempt to picture the parameter space of stable solutions. We also studied the Thermodynamics of black holes and described their evaporation process: we found that either evaporation leads black holes to unstable configurations, or the predictions of quadratic gravity are unphysical.

We also considered the possibility of generalizing Stelle's theory by removing the dependence from the only mass-scale present by including a new dynamical scalar field, making the theory scale invariant. Having a more complex theory, we did not investigate exotic solutions but limited ourselves to the impact of the new additional degrees of freedom on known analytical solutions. It was already known that in a cosmological setting this theory admits a transition between two de Sitter configurations; we analyzed the same problem in the context of static and spherically symmetric solutions and found a transition between two Schwarzschild-de Sitter configurations. In order to do that, we studied both linear perturbations and the semiclassical approximation of the path integral formulation of Euclidean quantum gravity.

At last, we tried to extract some phenomenological signatures of the exotic solutions. In particular, we investigated the shadow of an object on background free-falling light, and a possible way of determining the behavior close to the origin using mass measurements that rely on different physical processes. We show that, whenever these measurements are applied to the case of compact stars, in principle it could be possible to distinguish solutions where different equations of state describe the fluid.

---

*Everything we do is possible only thanks to all the people we have shared our lives with,  
but for this thesis I must give a special thanks to:*

*Ilaria “Lalla” Torti, who always pushes me forward when I need it and bring me back to  
earth when I deserve it,*

*all the people of the Trento branch of ADI, who have been companions in this city and  
comrades in academia,*

*and Alfio Bonanno, who believed in me more than I did and has been a friend through  
all these years.*

# Contents

<b>1</b>	<b>Introduction</b>	<b>5</b>
1.1	Outline of the thesis	12
1.2	Notes on units and adimensionalization	14
<b>2</b>	<b>Quadratic gravity</b>	<b>17</b>
2.1	General quadratic gravity and Stelle's action	18
2.1.1	Starobinski action and $f(R)$ theories	24
2.1.2	Einstein-Weyl gravity	27
2.2	Scale-invariant gravity	29
2.2.1	Scalar sector and Einstein frame formulation	32
<b>3</b>	<b>Analytical approximations and numerical methods</b>	<b>35</b>
3.1	Linear regime and linearized equations of motion	36
3.1.1	Non-vacuum case	38
3.2	Series expansion at fixed radius	40
3.2.1	Behavior close to the origin and autonomous dynamical system	45
3.3	Non-asymptotically flat solutions	46
3.4	Numerical methods	48
3.4.1	Shooting method	49
<b>4</b>	<b>The phase diagram of quadratic gravity</b>	<b>54</b>
4.1	The phase diagram of Einstein-Weyl gravity	55
4.2	The phase diagram of quadratic gravity	59
4.3	Non-vacuum solutions in the phase diagram	65
<b>5</b>	<b>Solutions of quadratic gravity</b>	<b>68</b>
5.1	Black holes	70
5.2	Naked singularities	73
5.2.1	Repulsive naked singularities	74
5.2.2	Attractive naked singularities	78
5.3	Wormholes	81
5.4	Compact stars	89
5.5	Black holes in scale-invariant gravity	96
5.5.1	Quadratic scale-invariant cosmology	98
<b>6</b>	<b>Quasi-normal modes and stability of the solutions</b>	<b>100</b>
6.1	Numerical methods for quasi-normal modes	101

6.2	Quasi-normal modes of solutions of quadratic gravity . . . . .	104
6.2.1	Quasi-normal modes of black holes in quadratic gravity . . . . .	106
6.2.2	Quasi-normal modes of exotic solutions in Einstein-Weyl gravity .	110
6.3	Quasi-normal modes of black holes in scale-invariant gravity . . . . .	116
<b>7</b>	<b>Semiclassical quadratic gravity and black hole Thermodynamics</b>	<b>122</b>
7.1	Black hole Thermodynamics and semiclassical gravity . . . . .	123
7.1.1	Hawking radiation and black hole evaporation . . . . .	123
7.1.2	The path integral approach to quantum gravity and black hole Thermodynamics . . . . .	130
7.1.3	Wald entropy . . . . .	132
7.2	Thermodynamics of black holes in quadratic gravity . . . . .	133
7.3	Semiclassical analysis of black holes in scale-invariant gravity . . . . .	139
7.3.1	Non-linear stability and transitions of Schwarzschild-de Sitter solutions . . . . .	145
<b>8</b>	<b>Phenomenological signatures of quadratic gravity</b>	<b>151</b>
8.1	Shadow of isolated objects . . . . .	152
8.2	Mass definitions and mass discrepancies . . . . .	154
<b>Conclusions</b>		<b>164</b>
<b>A</b>	<b>Tachyonic black holes</b>	<b>169</b>
<b>B</b>	<b>Rotating solutions and Newman-Janis algorithm</b>	<b>174</b>
<b>References</b>		<b>178</b>

# 1 Introduction

Gravity has always been the guiding light of Physics into field theories: the concept itself of field was introduced in Physics to describe the gravitational interaction in the eighteenth century, General Relativity was the first theory founded on the idea of relativistic fields, and its requirement of diffeomorphism invariance inspired the idea of gauge invariance, on which all theories of fundamental interactions are built. Nonetheless, while all the other interactions have a well-established and accepted description as Quantum Field Theories, a consensus on a quantum description of gravity is still lacking. The search for a theory of quantum gravity has been, in all likelihood, the single topic that attracted the interest of the largest number of theoretical physicists in all of history. The aim of my Ph.D., however, was not to look for a fully consistent theory of quantum gravity, rather it was to understand what could be the most common predictions of these theories in an actual physical context. For this reason we studied the most simple isolated objects, that are static, spherically symmetric and asymptotically flat, in some of the most common effective theories of quantum gravity, which are quadratic theories of gravity.

Our current description of gravity, that is General Relativity, has as fundamental object of investigation the metric tensor  $g_{\mu\nu}(x)$ , which defines the norm of any vector field  $v^\mu(x)$  at any point of the spacetime  $x$  as  $\|v(x)\| = (g_{\mu\nu}v^\mu v^\nu)(x)$ . To parallel transport a vector field  $v^\mu$  in the direction of a second vector field  $u^\nu$ , we introduce the covariant derivative  $u^\nu \nabla_\nu v^\mu = u^\nu (\partial_\nu v^\mu + \Gamma^\mu_{\nu\rho} v^\rho)$ , where  $\Gamma^\mu_{\nu\rho}$  is an affine connection which is usually taken to be the Levi-Civita one,

$$\Gamma^\mu_{\nu\rho} = \frac{1}{2} g^{\mu\sigma} (\partial_\nu g_{\sigma\rho} + \partial_\rho g_{\nu\sigma} - \partial_\sigma g_{\nu\rho}). \quad (1.1)$$

This choice guarantees that the norms of vector fields do not change during the transport, thanks to  $\nabla_\rho g_{\mu\nu} = 0$ , and that transporting a scalar field in the direction of  $v^\mu$  and then in the direction of  $u^\nu$  or the other way around has the same results, thanks to  $\Gamma^\mu_{\nu\rho} = \Gamma^\mu_{\rho\nu}$ . The dynamics of the spacetime can be completely extracted by its curvature, which can be quantified by the Riemann tensor  $R^\rho_{\sigma\mu\nu}$

$$[\nabla_\mu, \nabla_\nu] v^\rho = R^\rho_{\sigma\mu\nu} v^\sigma, \quad (1.2)$$

which can be expressed in terms of the Levi-Civita connection as

$$R^\rho_{\sigma\mu\nu} = \partial_\mu \Gamma^\rho_{\nu\sigma} - \partial_\nu \Gamma^\rho_{\mu\sigma} + \Gamma^\rho_{\mu\lambda} \Gamma^\lambda_{\nu\sigma} - \Gamma^\rho_{\nu\lambda} \Gamma^\lambda_{\mu\sigma}. \quad (1.3)$$

Other useful curvature tensors are the Ricci tensor  $R_{\mu\nu} = R^\rho_{\mu\rho\nu}$  and the Ricci scalar  $R = g^{\mu\nu} R_{\mu\nu}$ . Finally, as understood by Hilbert, Einstein's theory of gravitation can be

completely derived from a Lagrangian theory with an action defined as

$$\mathcal{I}_{EH} = \frac{1}{16\pi G} \int d^4x \sqrt{-g} [R - 2\Lambda] + \mathcal{I}_{mat}, \quad (1.4)$$

where  $G$  is the Newton constant,  $\Lambda$  is another constant relevant at cosmological scales and  $\mathcal{I}_{mat}$  contains all the matter and radiation fields populating the spacetime. To give an intuitive understanding of why there is no consensus on a quantum version of (1.4), let us consider a small perturbation  $h_{\mu\nu}$  around the Minkowski metric  $\eta_{\mu\nu} = \text{diag}(-1, 1, 1, 1)$  as  $g_{\mu\nu} = \eta_{\mu\nu} + \sqrt{G}h_{\mu\nu}$ . Not considering the constant  $\Lambda$  and the matter fields, the action (1.4) becomes

$$\mathcal{I}_{EH} \sim \int d^4x \left[ (\partial h)^2 + \sqrt{G}h(\partial h)^2 + Gh^2(\partial h)^2 + \dots \right], \quad (1.5)$$

where we considered having taken all possible covariant contractions of the metric and its derivatives. In a standard Quantum Field Theory description an interaction between two excitations, for example a graviton-graviton scattering, will have loop corrections in a perturbative expansion in the coupling constant  $G$ , as can be seen pictorially in Figure 1. For a renormalizable theory, the divergent contributions of each loop  $\sim \int_0^\infty d^4k k^4$  can be removed by regularizing the theory integrating only up to a scale  $\Lambda_{UV}$ , adding to the action a finite number of counterterms, and then finding a finite value when  $\Lambda_{UV}$  is taken to be infinite again.

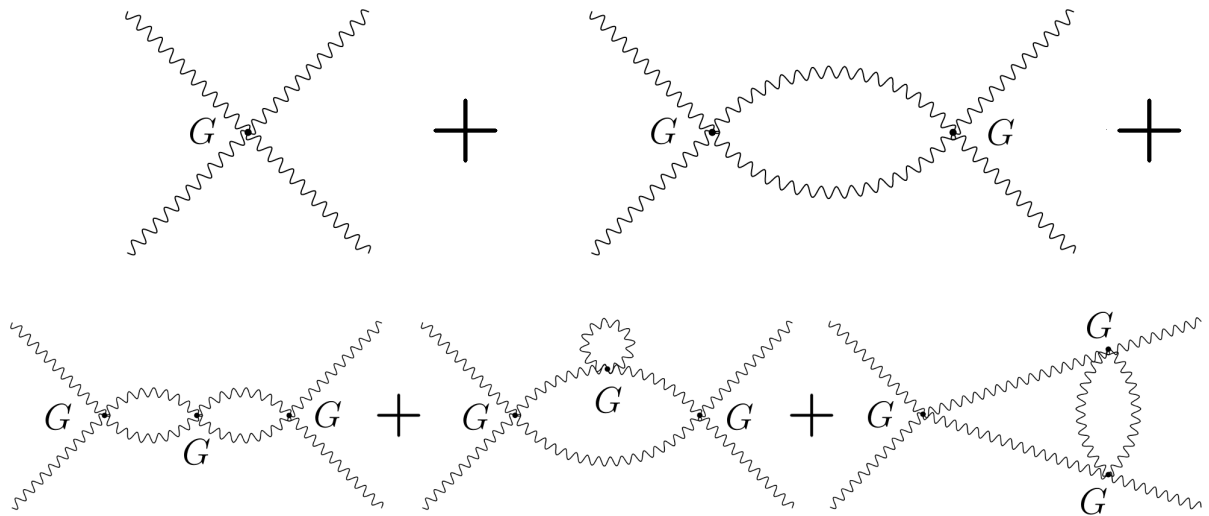


Figure 1: Graviton-graviton scattering at tree level with one-loop and two-loop corrections, where we underlined the dependence from the constant  $G$  of the interaction vertices.

This is not the case for General Relativity, because the coupling constant  $G$  has a dimension of inverse squared energy  $[G] = E^{-2}$ , and to have the same dimension at every loop

order, each diagram will have a dependence from the cutoff scale as

$$(G)_{tree} + (G^2 \Lambda_{UV}^2)_{1-loop} + (G^3 \Lambda_{UV}^4)_{2-loops} + \dots \quad (1.6)$$

Having a dependence from the cutoff different at any loop order, it is necessary to add a different counterterm at each order; in particular, it will be required to add terms with an increasing number of derivatives. The resulting picture is clear: either we add an infinite number of counterterms, or the limit  $\Lambda_{UV} \rightarrow \infty$  of the amplitude will be infinite; in any case, the theory is not renormalizable in the standard sense.

The standard approach to non-renormalizable theories which, nonetheless, are confirmed by low-energy experiments, is to consider them effective theories. For example, let us consider the Fermi model for  $\beta$ -decay shown in Figure 2. The four-point interaction has a coupling constant  $G_F$  of mass dimension  $[G_F] = E^{-2}$ , and the same reasoning made for the graviton-graviton scattering can be applied. Nonetheless, we now know that at energies  $E \sim 1/\sqrt{G_F}$  the  $\beta$ -decay can be described as the emission of a  $W^-$  boson with mass  $m_W \sim 1/\sqrt{G_F}$  in the context of the electroweak theory. The electroweak model, which has a dimensionless coupling constant  $g^*$  is instead renormalizable, while for energy scales  $E \ll m_W$  the Fermi interaction model remains viable and confirmed by experiments.

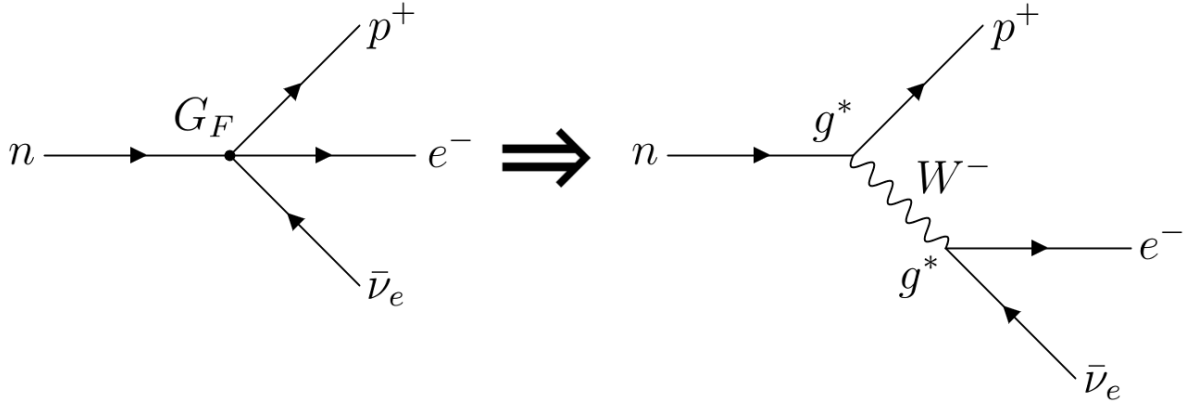


Figure 2:  $\beta$ -decay of a neutron considering Fermi interaction, and considering the exchange of a  $W^-$  boson in the electroweak theory.

This can be stated slightly more formally using the path integral formulation of Quantum Field Theory. If we call all the possible fields of the theory  $\psi$  collectively, and we consider a renormalizable theory with action  $\mathcal{I}(\psi)$ , the partition function of the quantum theory is written as

$$Z = \int D\psi e^{\mathcal{I}(\psi)}. \quad (1.7)$$

Let us now consider the field configurations with momenta below a certain energy scale  $\mu$  and call them  $\bar{\psi}$ , and the field configurations with momenta above the energy scale  $\mu$

called  $\tilde{\psi}$ . The partition function can be rewritten as

$$Z = \int D\psi e^{\mathcal{I}(\psi)} = \int D\bar{\psi} \int D\tilde{\psi} e^{\mathcal{I}(\bar{\psi}, \tilde{\psi})} = \int D\bar{\psi} e^{\mathcal{I}_{eff}(\bar{\psi})}, \quad (1.8)$$

where we defined

$$e^{\mathcal{I}_{eff}(\bar{\psi})} = \int D\tilde{\psi} e^{\mathcal{I}(\bar{\psi}, \tilde{\psi})}. \quad (1.9)$$

The fundamental theory with action  $\mathcal{I}$  is then said to be described at energies  $E < \mu$  by the effective theory with action  $\mathcal{I}_{eff}$ . This theory does not need to be renormalizable, as the loop corrections are integrated in momenta only up to  $k = \mu$  and will not contain fields that are present only at momenta higher than  $\mu$ . In the case of the electroweak interaction, as an example, if the scale  $\mu < m_W$  all the configurations with  $W$  bosons will be integrated and will not be present in  $\mathcal{I}_{eff}$ . The same reasoning has been applied to General Relativity where, however, the scales at which we expect to find new particles are  $E \sim 1/\sqrt{G} = m_P$ , where  $m_P$  is the Planck mass and is of order  $\mathcal{O}(10^{19})$  GeV, which is 15 orders of magnitude above current high energy experiments in Particle Physics. The various proposal of fundamental theories of quantum gravity, such as supergravity or string theory, then predicts particles that are detectable at energies that are completely out of range for current experiments.

Another approach to the problem of non-renormalizability was introduced by Weinberg in the late '70s [1]. The main idea was to focus on the essential properties which a physical quantum theory really needs, which are

- *finiteness*, that is having finite predictions for the results of scattering experiments;
- *predictivity*, that is being able to measure all the theory parameters with a finite number of experiments.

To formalize these statements, let us consider a theory at the energy scale  $k$ , described by the action

$$\mathcal{I}_k(\psi) = \int d^D x \sum_i g_i(k) k^{D-d_i} O_i(\psi), \quad (1.10)$$

where the  $O_i(\psi)$  are all possible operators constructed with the fields  $\psi$  with mass dimension  $[O_i(\psi)] = E^{d_i}$  and the  $g_i(k)$  are dimensionless coupling constants. The two conditions are then guaranteed if and only if

- *finiteness*: the dimensionless coupling constants go to a finite value in the ultraviolet limit  $\lim_{k \rightarrow \infty} g_i(k) = g_i^* < \infty$  for all  $i$ ;
- *predictivity*: at any scale  $k$  there is a finite number of coupling constants  $g_i(k)$  which have the  $g_i^*$  as ultraviolet limit.

Standard renormalization is found simply whenever the limit, called ultraviolet fixed point, is  $g_i^* = 0$  and then perturbative methods can be used. A theory with a finite fixed point different from zero and a finite number of coupling constants attracted to the fixed point is called *asymptotically safe*. Weinberg then applied this definition to General Relativity and argued that could be asymptotically safe [2]; however, its derivation was based on calculations made in dimension  $D = 2 + \epsilon$  with  $\epsilon \ll 1$ , but the proposed limit  $\epsilon \rightarrow 2$  spoiled the required smallness of the  $\epsilon$  parameter. More refined methods have been developed in the '90s, and the asymptotic safety conjecture for quantum gravity has found more evidence (for a review see [3, 4]). However, while these results are intriguing, the techniques used in this context rely on assuming the form in terms of operators of the fundamental action  $\mathcal{I}_{UV} = \lim_{k \rightarrow \infty} \mathcal{I}_k$  and then can be applied to a potentially infinite number of theories.

While all these different approaches have their negative sides, they generally agree that the first-order corrections to General Relativity have to be in the form of the addition of terms quadratic in the curvature tensors to the action (1.4). The one-loop counterterms to the graviton-graviton scattering have been rigorously derived by 't Hooft and Veltmann [5], and they are proportional to

$$R^2, \quad R^{\mu\nu} R_{\mu\nu}, \quad (1.11)$$

where a term proportional to  $R^{\mu\nu\rho\sigma} R_{\mu\nu\rho\sigma}$  was not included because in four dimensions it can be removed by a total derivative. Quadratic terms appear also in the effective theory in the low energy limit of probably the most studied fundamental theory of quantum gravity, that is string theory. The presence of quadratic terms as first corrections was already supposed in the early era of string theory [6], and in the '80s it was shown that for the heterotic  $E_8 \times E_8$  string model the low energy gravitational action should be corrected by the inclusion of a term proportional to

$$R^{\mu\nu\rho\sigma} R_{\mu\nu\rho\sigma} \quad (1.12)$$

[7, 8], which was generalized to

$$R^{\mu\nu\rho\sigma} R_{\mu\nu\rho\sigma} - 4R^{\mu\nu} R_{\mu\nu} + R^2 \quad (1.13)$$

in order to remove by hand the presence of ghost particles [9]. Similar corrections also appear in the low energy limit of the bosonic string, as described in the lectures of David Tong [10]. This, however, is no surprise: if we consider a general effective action  $\mathcal{I}_{eff}$ , in principle all terms which are invariants under diffeomorphism could be present, and if only the metric tensor appears as the dynamical field, these terms have to be constructed

from curvature tensors. If we restrict ourselves to a theory where only curvature tensors and not their derivatives are present, we can imagine expanding the action  $\mathcal{I}_{eff}$  in a sort of power series as

$$\mathcal{I}_{eff} = \int d^4x \sqrt{-g} \left[ g_0 m_p^4 + g_1 m_p^2 R + g_2 R^2 + g'_2 R^{\mu\nu} R_{\mu\nu} + g''_2 R^{\mu\nu\rho\sigma} R_{\mu\nu\rho\sigma} + \frac{g_3}{m_p^2} R^3 + \dots \right], \quad (1.14)$$

where increasing powers of the curvature tensors are matched with decreasing power of the energy scale, chosen as  $m_p$ . It is clear that, as the energy scale at which we study the effective action is increased, more terms in the expansion (1.14) will be relevant: starting from

$$\mathcal{I}_{eff} = \int d^4x \sqrt{-g} [g_0 m_p^4 + g_1 m_p^2 R + \dots] = \frac{1}{16\pi G} \int d^4x \sqrt{-g} [R - 2\Lambda \dots], \quad (1.15)$$

where  $g_0 = -\Lambda/8\pi m_p^2$  and  $g_1 = 1/16\pi$ , the first-order corrections will, in general, be given by

$$\mathcal{I}_{eff} = \int d^4x \sqrt{-g} [g_0 m_p^4 + g_1 m_p^2 R + g_2 R^2 + g'_2 R^{\mu\nu} R_{\mu\nu} + g''_2 R^{\mu\nu\rho\sigma} R_{\mu\nu\rho\sigma} + \dots], \quad (1.16)$$

that is, by quadratic terms in the curvature. The inclusion of quadratic terms is also confirmed by the analysis in the context of asymptotically safe gravity [11]: while looking at the number of relevant operators with actions constructed only using the Ricci scalar  $R$ , it has indeed been found that the effective action will behave a

$$\mathcal{I}_{eff} = \int d^4x \sqrt{-g} \left[ A R^2 + \sum_i \epsilon_i \Lambda^{\theta_i} R^{2-\theta_i/2} \right], \quad (1.17)$$

where, considering  $\theta \leq 4$  to avoid terms as  $1/R$ , we get once again General Relativity with the addition of a squared term in the Ricci scalar.

At last, we write the most general correction of the Einstein-Hilbert action containing terms quadratic in the curvature as

$$\mathcal{I}_{qg} = \int d^4x \sqrt{-g} [\gamma (R - 2\Lambda) + a R^2 + b R^{\mu\nu} R_{\mu\nu} + c R^{\mu\nu\rho\sigma} R_{\mu\nu\rho\sigma}], \quad (1.18)$$

where  $\gamma = 1/16\pi G$ . Considering the previous discussion on the quantum origin of quadratic terms, and recalling that the constant  $\Lambda$  is relevant only at cosmological scales, we set  $\Lambda = 0$ . The action (1.18) is then equivalent, up to a total derivative, to

$$\mathcal{I}_{Stelle} = \int d^4x \sqrt{-g} \left[ \gamma R + \left( \beta + \frac{2}{3} \alpha \right) R^2 - 2\alpha R^{\mu\nu} R_{\mu\nu} \right], \quad (1.19)$$

where we simply used different names for the constants. Interestingly, it has been shown by Stelle [12] that whenever the action (1.19) is considered as a fundamental action for

gravity, the propagator goes as

$$D_{\mu\nu\rho\sigma}(k) = \frac{1}{(2\pi)^4 i} \left( \frac{2P_{\mu\nu\rho\sigma}^{(2)}(k)}{k^2(2\alpha k^2 + \gamma)} - \frac{4P_{\mu\nu\rho\sigma}^{(0-s)}(k)}{k^2(6\beta k^2 + \gamma)} + \text{gauge fixing terms} \right), \quad (1.20)$$

where  $P_{\mu\nu\rho\sigma}^{(2)}(k)$  and  $P_{\mu\nu\rho\sigma}^{(0-s)}(k)$  are projectors for symmetric rank-two tensors, and given that the propagator goes as  $k^{-4}$  the divergences are removed, and the theory is renormalizable. However, the propagator (1.20) can be rewritten as

$$D_{\mu\nu\rho\sigma}(k) = \frac{1}{\gamma(2\pi)^4 i} \left( \frac{2P_{\mu\nu\rho\sigma}^{(2)}(k) - 4P_{\mu\nu\rho\sigma}^{(0-s)}(k)}{k^2} - \frac{2P_{\mu\nu\rho\sigma}^{(2)}(k)}{k^2 + m_2^2} + \frac{4P_{\mu\nu\rho\sigma}^{(0-s)}(k)}{k^2 + m_0^2} + \text{g. f. t.} \right), \quad (1.21)$$

where we defined

$$m_2^2 = \frac{\gamma}{2\alpha}, \quad m_0^2 = \frac{\gamma}{6\beta}. \quad (1.22)$$

The first term in (1.21) is the propagator of a massless particle of spin  $S = 2$ , the second term is the propagator of a massive particle of spin  $S = 2$  and mass  $m_2$ , and the third term is the propagator of a massive particle of spin  $S = 0$  and mass  $m_0$ . This propagator, however, has an extremely problematic property, namely the massive particle with spin  $S = 2$  has a propagator with a negative sign, and it is then a propagating ghost particle. The presence of a ghost particle is associated with negative kinetic energy states, and then with an energy unbounded from below and extreme instabilities. From another point of view, ghost particles can be interpreted as having a negative norm, and then negative energy can be traded for the non-unitarity of the theory [13]. While various proposals to deal with ghosts have been done in the past years [14, 15, 16, 17, 18], the general approach of the scientific community is to discard a theory that contains them. If one does not focus too much on the ghost problem, the classical solutions of (1.19) present a large variety of behaviors, opening the possibility of deviating from General Relativity in many different ways. In particular, in the context of cosmology, the action has been used by Starobinski to model the very early times of the universe [19], and in the case of static and spherically symmetric solutions, different families of solutions have been characterized [20, 21, 22]. More in detail, a class of non-Schwarzschild black holes has been discovered [23] and thoroughly investigated [24, 25], and a class of naked singularities has been studied for its “black hole mimicker” nature [26]. A large part of this thesis will start from these works, aiming to complete the global picture of static and spherically symmetric solutions in quadratic gravity.

At very high energies, it is clear that the quadratic terms in the action (1.19) will dominate over the linear one, making the theory effectively scale invariant. This motivated the study of a generalization of (1.19) in which scale invariance is taken as a fundamental

symmetry [27]; this can be employed by substituting the only mass-scale present in the action  $\gamma = 1/16\pi G = m_p^2/16\pi$  by a dynamical scalar field

$$\mathcal{I}_{si} = \int d^4x \sqrt{-g} \left[ \xi \phi^2 R + \left( \beta + \frac{2}{3}\alpha \right) R^2 - 2\alpha R^{\mu\nu} R_{\mu\nu} - \frac{1}{2} \partial^\mu \phi \partial_\mu \phi - \frac{\lambda}{4} \phi^4 \right], \quad (1.23)$$

where  $\alpha$ ,  $\beta$ ,  $\xi$ , and  $\lambda$  are dimensionless arbitrary positive constants. This action has proved itself able to produce a model for inflation which satisfies all current experimental constraints [28], to produce primordial magnetic fields [29], and also to be stable under one-loop quantum corrections [30]. This new additional, and very stringent, symmetry seems to protect the model from some controversial aspects of Stelle's model. Nonetheless, it is still not completely understood if this model can predict detectable deviations from General Relativity. In this thesis we then carried out some preliminary steps in the study of static and spherically symmetric solutions in this scale-invariant model of gravity.

While a consistent description of quadratic terms in a quantum theory of gravity seems an obstacle course, at the same time it is natural to expect that, if some variations from the solutions of General Relativity are present, they can be described at first approximation by a quadratic theory of gravity. Moreover, the impressive results of recent years and the bright short-term perspectives in experimental gravitational physics open, for the first time, the possibility of having an insight into the behavior of gravity at these scales. We live in a scientific era in which results from precision cosmology, gravitational wave measurements, and radio observations with impressive angular resolutions converge. We believe then that aiming to have a complete description of the consequences of quadratic terms in a realistic setting can be more physically instructive in understanding our universe rather than fully describing the quantum nature of spacetime. To set a more realistic goal, we approached this problem starting from the simplest solutions: static, spherically symmetric isolated objects.

## 1.1 Outline of the thesis

In Section 2 we present the actions considered throughout the thesis and their equations of motion both in tensor form and when applied to a static and spherically symmetric metric. In particular, we present in greater detail Stelle's action (1.19) and its “sectors” in which only one of the two additional massive modes is present, and we will present the model of scale-invariant gravity proposed by Rinaldi and Vanzo (1.23) and its scalar sector, in which only the scalar field and the Ricci scalar are present. We will also present some no-hair-like theorems which, under some general requirements as the metric to be static, constraints the Ricci scalar to be zero in Stelle's theory, and a combination of the

Ricci scalar and the scalar field to be constant in the scale-invariant theory.

In Section 3 we present all the analytical approximations and numerical methods required to find exotic solutions in Stelle’s quadratic theory of gravity. In particular, the solutions at large distances can be found in the linearized theory, and are in the form of the Schwarzschild metric corrected by two Yukawa terms associated with the two massive modes of the theory. The solutions can also be found in terms of power series close to the origin or a metric singularity, and different families are found: there is a family which is regular in the origin and two which describe singularities, and there is the possibility of having either an event horizon or a wormhole throat. We also present the possibility of a solution that is asymptotically vanishing at large distances, as they will be relevant in the subsequent discussions. At last, we present the shooting method used to find solutions, in which we numerically match the behavior at large distances with different possible series expansions.

In Section 4 we present the so-called “phase diagram” of the theory, a diagram in which in all points in the space defined by the asymptotic parameters at large distances we indicate the type of global solution associated. We present the phase diagram in the case of the two sectors of Stelle’s theory, and attempt to extract the relevant information from the phase diagram of the full theory without having a complete description. We will also show the location of non-vacuum solutions in the phase diagram of vacuum solutions to understand which can model the external potential of compact stars.

In Section 5 we describe in detail the metric and the geometrical properties of all the solutions found in the phase diagram. There are Schwarzschild and non-Schwarzschild black holes, naked singularities with an attractive and repulsive gravitational field in the origin, and non-symmetric wormholes. In the last subsection, we present the known analytical static and spherically symmetric solutions of scale-invariant gravity, which are the ones also present in General Relativity. We also present briefly the cosmological model, in which there is a spontaneous transition between two de Sitter configurations, as one of the goals of this thesis was to find a similar transition in the case of isolated objects.

In Section 6 we study dynamical perturbations in Stelle’s theory and scale-invariant gravity. We directly integrated the wave-like equations of perturbations, in order to find both the insurgence of instabilities and the time dependence of the perturbations at large distances simultaneously. In Stelle’s theory most of the solutions result to be unstable, and, in particular, there is a minimum stable radius for the event horizon of black holes. In

the scale-invariant model we show the results of Simon Boudet, who proved that there are two Schwarzschild-de Sitter solutions, of which one is stable and the other is unstable.

In Section 7 we first investigated the evaporation process of black holes in Stelle's theory. In particular, it has been possible to find the dependence between the evaporating total mass and time using the adiabatic approximation, in which black holes evaporate slowly. It is argued that either evaporation has to lead black holes into unstable configurations, or the predictions of quadratic gravity are inconsistent with the existence of our universe. In the scale-invariant model, we focused on the Euclidean action of the two Schwarzschild-de Sitter solutions. It is possible indeed to argue from a semiclassical analysis of the theory that the difference between the two actions leads to a transition between the unstable and the stable solutions. In order to evaluate the Euclidean action we had to develop a technique to avoid the insurgence of conical singularities.

In Section 8 we tried to extract some simple phenomenological predictions from the solutions of Stelle theory. We present the difference between the shadow predicted by General Relativity and the one produced by the exotic solutions, finding a direct relationship between the different families of solutions and the shadow being larger or smaller than the one of the classical case. We also argue that different definitions for the mass measured at a finite radius from the object have different predictions in quadratic gravity, and then that this fact can be exploited to measure deviations from General Relativity. In particular, we will show that the difference in the mass definitions depends on the equation of state describing the microscopical nature of the fluid in the case of compact stars.

After the conclusions, in Appendix A we present black hole solutions in the case of  $\alpha < 0$  (motivated by the results found in the context of asymptotically safe gravity), that have characteristic oscillations at all distances, are not asymptotically flat, and are always unstable. In Appendix B, we will instead tackle the problem of rotating solutions and prove that in quadratic gravity it is not possible to use the Newman-Janis algorithm to directly derive a rotating solution from a static and spherically symmetric seed.

## 1.2 Notes on units and adimensionalization

The presence of massive modes naturally introduces mass scales in quadratic gravity. After imposing natural units as  $c = \hbar = k_B = 1$ , a mass scale is the only quantity needed to determine a set of units to characterize the solutions completely. Choosing a mass scale is also necessary to perform numerical integrations, in which all quantities must be dimensionless. Throughout this thesis, we decided to use as mass scale the one of the

massive tensor modes  $m_2 = \sqrt{\gamma/2\alpha}$ . This choice has been made to be consistent with the simplified case with  $\beta = 0$ , in which many results of this thesis have been derived; in the very few instances in which we considered the case with  $\alpha = 0$ , we used as mass scale the one of the massive scalar  $m_0 = \sqrt{\gamma/6\beta}$ . With some exceptions, which will always be specified in advance, the results of this thesis will all be in these “ $m_2$  units”, to which we also refer as numerical units being the units used in our codes. The exceptions will be the results on compact stars solutions, for which we opted to use more common units such as solar masses and kilometers, and the final results on the evaporation of black holes. If we denote adimensionalized quantities with a subscript “ $a$ ”, we can write down the table of conversion for the mass of the solutions, the radial coordinate, two charges  $S_2^-$  and  $S_0^-$  which will characterize the strength of the contribution to the asymptotic gravitational interactions of the massive tensor and scalar modes, the temperature of black holes, the entropy of black holes, and the energy density and pressure of a perfect fluid:

Physical quantity	$m_2$ units	Plank units	Physical units
$M$	$\frac{16\pi\gamma}{m_2} M_a$	$4\sqrt{2\pi\alpha} M_a m_p$	$\sim M_a 10^{\delta-37} M_\odot$
$r$	$\frac{1}{m_2} r_a$	$4\sqrt{2\pi\alpha} r_a l_p$	$\sim r_a 10^{\delta-37} \text{Km}$
$S_2^-$	$\frac{1}{m_2} S_{2,a}^-$	$4\sqrt{2\pi\alpha} S_{2,a}^- l_p$	$\sim S_{2,a}^- 10^{\delta-37} \text{Km}$
$S_0^-$	$\frac{1}{m_2} S_{0,a}^-$	$4\sqrt{2\pi\alpha} S_{0,a}^- l_p$	$\sim S_{0,a}^- 10^{\delta-37} \text{Km}$
$T_{BH}$	$m_2 T_{BH,a}$	$\frac{1}{4\sqrt{2\pi\alpha}} T_{BH,a} m_p$	$\sim T_{BH,a} 10^{31-\delta} K$
$S_{Wald}$	$\frac{16\pi\gamma}{m_2^2} S_{Wald,a}$	$32\pi\alpha S_{Wald,a}$	$\sim S_{Wald,a} 10^{2\delta-21} J/K$
$\rho$	$\gamma m_2^2 \rho_a$	$\frac{1}{2^9\pi^2\alpha} \rho_a \frac{m_p}{l_p^3}$	$\sim \rho_a 10^{93-2\delta} \text{Kg/m}^3$
$p$	$\gamma m_2^2 p_a$	$\frac{1}{2^9\pi^2\alpha} p_a \frac{m_p}{l_p^3}$	$\sim p_a 10^{110-2\delta} \text{Pa}$

Table 1: Table of conversion for the quantities which can characterize various solutions; in the first column we indicate the physical quantities, in the second their expressions using the “ $m_2$  units”, in the third one using Planck natural units and in the fourth one using the most common physical units in Astrophysics.

In the second and third columns we express the physical quantities using both the  $m_2$  units and Planck units, in which the dependence from the free parameter  $\alpha$  is manifest. In the fourth column of Table 1 we also considered the expressions of the various quantities using the most common units of Astrophysics and expressing the free parameter as  $\alpha = 10^{2\delta}$  to have a direct relationship between the order of magnitude of  $\alpha$  and the physical units of our results. It is clear that using natural values of  $\alpha$  of order of unity, and then with  $\delta = 0$ , the unity of adimensionalized quantities will correspond to almost Planckian values; using a parameter of the order predicted by Cosmic Microwave Background (CMB) anisotropies for Starobinski’s model (that is (1.19) with  $\alpha = 0$ ), we would have  $\alpha = 10^8$  and  $\delta = 4$  [19], and all the quantities will be still above the range

of high energy particle physics; using the maximum values of the parameters allowed by constraints [31], that is  $\alpha = 10^{60}$  and  $\delta = 30$ , we would have masses in the range of the ones of asteroids, which are indeed possible for primordial black holes, but not for the observed astrophysical ones or neutron stars; finally, in order to have physical quantities of the order of magnitude observed we would need  $\alpha = 10^{74}$  and  $\delta = 37$ , which however would lead to measurable but unobserved deviations from General Relativity.

In the case of scale-invariant gravity, clearly, there is no preferred mass scale, and units are entirely arbitrary. To adimensionalize the physical quantities, we then choose units related to the specific solutions considered; in particular, in the case of linear perturbations, we adimensionalized in terms of the mass parameter  $M$  present in the Coulombian part of the potential  $-\frac{2M}{r}$ , and in the case of the Euclidean action, in which we want to be able to vary this parameter  $M$ , we adimensionalized in terms of the product  $M\sqrt{\Lambda}$  where  $\Lambda$  is an effective cosmological constant.

## 2 Quadratic gravity

While many different quadratic theories of gravity share the same physical motivation, and can also present some similarities in the predicted corrections to the solutions of General Relativity, each theory has its own physical and technical properties, varying greatly from one to the other. As said in the introduction, we will focus only on local theories with quadratic invariants constructed by the curvature tensors and not their derivatives. In particular, we will consider including a scalar field only to remove the dependence from the mass scale set by the Planck mass and render the theory scale invariant. In this section we will show the equations of motion and some general properties of quadratic gravity, its non-trivial sectors, and scale-invariant gravity.

This section is divided in two parts:

- in the first subsection we analyze quadratic gravity, in particular Stelle's action, of which we will present the equations of motion both in tensor form and in the case of static and spherically symmetric metrics, and we will also present a theorem which imposes a zero Ricci scalar under simple and generic conditions. We will also show the equations of motion for the two non-trivial reductions of quadratic gravity, namely Einstein-Weyl gravity, in which the Einstein-Hilbert action is corrected by the addition of a squared contraction of the Weyl tensor, and Starobinski's action, in which the Einstein-Hilbert action is corrected by the addition of a squared Ricci scalar term; in particular, of this latter reduction, we will show its interpretation as a simple case of the more general  $f(R)$  class of theories of gravity and its reformulation in the so-called Einstein frame, that is as Einstein gravity with a scalar field;
- in the second subsection we analyze scale-invariant gravity, in which a dynamical scalar field substitutes the Planck mass, and we will present both the equations of motion and a theorem that states that a combination of the Ricci scalar and the scalar field is constant under some generic and simple assumptions; we will also show for scale-invariant gravity that the scalar sector, in which all the terms proportional to curvature tensors different from the Ricci scalar are suppressed, can be reformulated in the Einstein frame as General Relativity with two scalar fields, of which however thanks to scale invariance only one is non-trivial.

The equations of this section are somehow common knowledge, and we refer as partial bibliography to [32, 20, 33, 24] for quadratic gravity, and to [27, 34, 28, 35] for scale-invariant gravity.

## 2.1 General quadratic gravity and Stelle's action

The most general correction of the Einstein-Hilbert action containing only quadratic contractions of the curvature tensors can be simply written as

$$\mathcal{I}_{qg} = \int d^4x \sqrt{-g} [\gamma (R - 2\Lambda) + a R^2 + b R^{\mu\nu} R_{\mu\nu} + c R^{\mu\nu\rho\sigma} R_{\mu\nu\rho\sigma}] ; \quad (2.1)$$

however, for reasons that will be clear shortly, we prefer to recast it as

$$\mathcal{I}_{qg} = \int d^4x \sqrt{-g} [\gamma (R - 2\Lambda) + \beta R^2 - \alpha C^{\mu\nu\rho\sigma} C_{\mu\nu\rho\sigma} + \chi \mathcal{G}] , \quad (2.2)$$

where  $C_{\mu\nu\rho\sigma}$  is the Weyl tensor, defined as

$$C_{\mu\nu\rho\sigma} = R_{\mu\nu\rho\sigma} + \frac{1}{2} (R_{\mu\sigma}g_{\nu\rho} + R_{\nu\rho}g_{\mu\sigma} - R_{\mu\rho}g_{\nu\sigma} - R_{\nu\sigma}g_{\mu\rho}) + \frac{1}{6} (g_{\mu\rho}g_{\nu\sigma} - g_{\mu\sigma}g_{\nu\rho}) , \quad (2.3)$$

which is traceless under any possible contraction of the indices, and  $\mathcal{G}$  is the Gauss-Bonnet combination

$$\mathcal{G} = R^{\mu\nu\rho\sigma} R_{\mu\nu\rho\sigma} - 4R^{\mu\nu} R_{\mu\nu} + R^2 , \quad (2.4)$$

which in four dimensions is a total derivative and its integral is a topological term; for this reason, it *does not contribute* to the equations of motion. As stated in the introduction, we are interested in the short-scale corrections to the solutions of General Relativity, and then we can safely consider  $\Lambda = 0$ , taking into account that in our universe the cosmological constant is relevant only at very large scales; we specify here that this will be the case for all the solutions of quadratic gravity studied in this thesis. Not considering, for now, the Gauss-Bonnet term that, however, will come back in the Thermodynamics of black holes, the action can be written in the form studied by Stelle

$$\mathcal{I}_{Stelle} = \int d^4x \sqrt{-g} [\gamma R + \beta R^2 - \alpha C^{\mu\nu\rho\sigma} C_{\mu\nu\rho\sigma}] . \quad (2.5)$$

While we will not indulge in the quantum description of this theory, we remember that the action has been proven to be renormalizable [12], and at the quantum level three fundamental excitations are present, namely

- a massless tensor particle with spin  $S = 2$ , which can be interpreted as the standard graviton;
- a massive scalar particle with spin  $S = 0$  and mass  $m_0^2 = \gamma/6\beta$ , which is associated with the  $R^2$  term;
- a massive tensor particle with spin  $S = 2$  and mass  $m_2^2 = \gamma/2\alpha$ , which is associated with the  $C^{\mu\nu\rho\sigma} C_{\mu\nu\rho\sigma}$  term and is the ghost particle we discussed in the introduction.

It is then clear why we choose to express the action as (2.2), as those specific combinations of the curvature invariants are indeed the ones with a physical meaning. If we want to include a classical matter component, the action becomes

$$\mathcal{I}_{Stelle,mat} = \int d^4x \sqrt{-g} [\gamma R + \beta R^2 - \alpha C^{\mu\nu\rho\sigma} C_{\mu\nu\rho\sigma} + \mathcal{L}_{mat}] \quad (2.6)$$

and the equations of motion can be derived from the minimization of (2.6); in particular, they are

$$\begin{aligned} \mathcal{G}_{\mu\nu} = & \gamma \left( R_{\mu\nu} - \frac{1}{2} R g_{\mu\nu} \right) + 2\beta \left( R_{\mu\nu} - \frac{1}{4} R g_{\mu\nu} - \nabla_\mu \nabla_\nu + g_{\mu\nu} \square \right) R + \\ & - 4\alpha \left( \nabla^\rho \nabla^\sigma + \frac{1}{2} R^{\rho\sigma} \right) C_{\mu\rho\nu\sigma} = \frac{1}{2} T_{\mu\nu}, \end{aligned} \quad (2.7)$$

where clearly the equations for (2.5) are found by setting  $T_{\mu\nu} = 0$ , and the one for (2.2) are found by setting  $T_{\mu\nu} = 2\Lambda g_{\mu\nu}$ . It can be proven using the definition of the Riemann tensor and the second Bianchi identity

$$\begin{aligned} (\nabla_\rho \nabla_\mu - \nabla_\mu \nabla_\rho) R^\rho_\nu &= R^\rho_{\sigma\rho\mu} R^\sigma_\nu - R^\sigma_{\nu\rho\mu} R^\rho_\sigma = R^\sigma_\nu R_{\sigma\mu} - R^{\rho\nu} R_{\sigma\nu\rho\mu}, \\ \nabla^\rho \nabla^\sigma R_{\mu\rho\nu\sigma} &= \nabla^\rho \nabla_\mu R^\rho_\nu - \square R_{\mu\nu}, \\ \nabla_\rho R^\rho_\mu &= \frac{1}{2} \nabla_\mu R, \end{aligned} \quad (2.8)$$

that the equations (2.7) are equal to

$$\begin{aligned} \mathcal{G}_{\mu\nu} = & \gamma \left( R_{\mu\nu} - \frac{1}{2} R g_{\mu\nu} \right) + 2\beta \left( R_{\mu\nu} - \frac{1}{4} R g_{\mu\nu} - \nabla_\mu \nabla_\nu + g_{\mu\nu} \square \right) R + \\ & - \alpha \left( 4R^{\rho\sigma} R_{\mu\rho\nu\sigma} - R^{\rho\sigma} R_{\rho\sigma} g_{\mu\nu} - \frac{4}{3} R R_{\mu\nu} + \frac{1}{3} R^2 G_{\mu\nu} + 2\square R_{\mu\nu} - \frac{1}{3} \square R g_{\mu\nu} + \right. \\ & \left. - \frac{2}{3} \nabla_\mu \nabla_\nu R \right) = \frac{1}{2} T_{\mu\nu}, \end{aligned} \quad (2.9)$$

and now it is trivial to see that all the vacuum solutions of General Relativity  $T_{\mu\nu} = R_{\mu\nu} = 0$  are also vacuum solutions of this theory. It will not be the case for non-vacuum solutions because the additional terms will couple non-minimally with the stress-energy tensor, and the solutions of General Relativity *will not* be solutions of the quadratic theory. Thanks to the traceless nature of the Weyl tensor, the trace of the equations of motion takes the very simple form

$$6\beta \left( \square - \frac{\gamma}{6\beta} \right) R = 6\beta (\square - m_0^2) R = \frac{1}{2} T, \quad (2.10)$$

where  $T = T^\mu_\mu$  and we used the definition of the mass of the scalar particle present at quantum level  $m_0^2 = \gamma/6\beta$ . As described in [36, 23], from (2.10) it is possible to prove the following theorem:

**Theorem 1.** *Let's consider a static spacetime  $(M, g)$  which is a solution of the vacuum equations of motion of quadratic gravity and a spacelike hypersurface  $\Sigma$ ; if the spacetime satisfies either*

- $g_{\mu\nu}\kappa^\mu\kappa^\nu \rightarrow 0$  at the boundary of  $\Sigma$ , with  $\kappa^\mu$  being the timelike Killing vector,
- $R \rightarrow 0$  at the boundary of  $\Sigma$ ,
- $D_a R \rightarrow 0$  at the boundary of  $\Sigma$ , with  $D_a$  being the covariant derivative on  $\Sigma$ ,

then  $R = 0$  in all  $\Sigma$ .

**Proof.** Considering the ansatz for a generic static metric

$$ds^2 = -\tau^2(x)dt^2 + \xi_{ij}(x)dx^i dx^j. \quad (2.11)$$

Equation (2.10) in the vacuum becomes

$$\square R - m_0^2 R = D^i D_i R + \frac{1}{\tau} D^i \tau D_i R - m_0^2 R = 0, \quad (2.12)$$

where  $D_i$  is the covariant derivative defined by the  $\xi_{ij}$  metric. Multiplying everything by  $\tau R$  and integrating over a spacelike hypersurface  $\Sigma$  we get

$$\begin{aligned} & \int_{\Sigma} d^3x \sqrt{\xi} [\tau R D^i D_i R + R D^i \tau D_i R - m_0^2 \tau R^2] = \\ & = [\tau R D_i R]_{\partial\Sigma} - \int_{\Sigma} d^3x \sqrt{\xi} \tau [D^i R D_i R + m_0^2 R^2] = 0, \end{aligned} \quad (2.13)$$

where we integrated by parts in the second line. If the boundary term goes to zero, the integral term in the second line has to go to zero as well; being that with a static metric its spatial projection  $\xi_{ij}$  is positive definite, the integrand is the sum of two terms which are always non-negative, and then they have to be both identically zero in order to have a zero integral. In particular,  $m_0^2 R^2 = 0 \implies R = 0$ .  $\square$

From theorem 1 the two following corollaries can be trivially derived:

**Corollary 1.** *All the static and asymptotically flat black hole solutions of quadratic gravity have  $R = 0$  outside the event horizon.*

This corollary is proven by the fact that  $\partial\Sigma$ , in this case, is constituted by the event horizon, for which  $\tau = 0$ , and by spatial infinity, for which  $R \rightarrow 0$  for an asymptotically flat solution.  $\square$

**Corollary 2.** *All the solutions of quadratic gravity which satisfy the requirements of theorem 1 are also solutions of a theory with action (2.5) with  $\beta = 0$ .*

In this case, we remember that the terms of the equations of motion which are proportional to  $\beta$  are

$$\left( R_{\mu\nu} - \frac{1}{4}R g_{\mu\nu} - \nabla_\mu \nabla_\nu + g_{\mu\nu} \square \right) R, \quad (2.14)$$

and are always zero for  $R = 0$ ; setting  $\beta = 0$  at the level of the action then does not affect the solutions.  $\square$

As already stressed, the main goal of this thesis will be to characterize static and spherically symmetric spacetimes, for which we choose the ansatz for the metric in Schwarzschild form

$$ds^2 = -h(r)dt^2 + \frac{dr^2}{f(r)} + r^2d\Omega^2, \quad (2.15)$$

and the stress-energy tensor of a perfect fluid with form

$$T_{\mu\nu} = (\rho(r) + p(r)) u_\mu u_\nu + p(r)g_{\mu\nu}, \quad (2.16)$$

where  $u^\mu$  is a timelike unit vector. In principle the equations of motion (2.7) should become a system of two fourth-order ordinary differential equations, however  $\mathcal{G}_{rr}$  depends only on derivatives up to  $h^{(3)}(r)$  and  $f''(r)$ , and  $\mathcal{G}_{tt}$  depends only on derivatives up to  $h^{(4)}(r)$  and  $f^{(3)}(r)$ . It is then possible to use the suitable combination

$$\mathcal{G}_{tt} - X(r) \left( \mathcal{G}_{rr} - \frac{1}{2}T_{rr} \right) - Y(r) \partial_r \left( \mathcal{G}_{rr} - \frac{1}{2}T_{rr} \right) = \frac{1}{2}T_{tt}, \quad (2.17)$$

in order to find an equation dependent only on terms up to  $f^{(3)}(r)$  and  $h''(r)$ . Using

$$X(r) = \frac{f(r)h(r)}{(9\beta rh(r)f'(r) - 2r(\alpha - 3\beta)f(r)h'(r) + 4(\alpha + 6\beta)f(r)h(r))^2} \left( 54\beta r^2(\alpha + -3\beta)h(r)^2f'(r)^2 + rf(r)h(r)(r(-8\alpha^2 + 48\alpha\beta - 153\beta^2)f'(r)h'(r) + 4(\alpha + -3\beta)h(r)((4\alpha + 42\beta)f'(r) - 9\beta rf''(r))) + 2f(r)^2(-r^2(2\alpha - 15\beta)(\alpha + -3\beta)h'(r)^2 - 2r(4\alpha^2 - 15\alpha\beta + 90\beta^2)h(r)h'(r) + 24(\alpha - 3\beta)(\alpha + 6\beta)h(r)^2) \right) \quad (2.18)$$

and

$$Y(r) = -\frac{4r(\alpha - 3\beta)f(r)^2h(r)^2}{2f(r)(r(\alpha - 3\beta)h'(r) - 2(\alpha + 6\beta)h(r)) - 9\beta rh(r)f'(r)}, \quad (2.19)$$

we find the two third-order equations

$$\begin{aligned} \mathcal{G}_{rr} = & -\frac{h^{(3)}(r)(9\beta rh(r)f'(r) - 2r(\alpha - 3\beta)f(r)h'(r) + 4(\alpha + 6\beta)f(r)h(r))}{6rh(r)^2} + \\ & -\frac{h''(r)^2(\alpha - 3\beta)f(r)}{6h(r)^2} + \frac{h''(r)}{12r^2f(r)h(r)^3} \left( 4rf(r)h(r)h'(r)(r(\alpha + 6\beta)f'(r) + 6(\alpha + 3\beta)f(r)) + h(r)^2(-27\beta r^2f'(r)^2 + 4r(2\alpha + 21\beta)f(r)f'(r) + 16(\alpha + 6\beta)f(r)^2) \right) + \end{aligned}$$

$$\begin{aligned}
& -6r^2(\alpha - 3\beta)f(r)^2h'(r)^2\Big) + \frac{7(\alpha - 3\beta)f(r)h'(r)^4}{24h(r)^4} - \frac{h'(r)^3}{12rh(r)^3}\Big(3r(\alpha + 3\beta)f'(r) + \\
& + 2(5\alpha + 12\beta)f(r)\Big) + \frac{h'(r)^2}{24r^2f(r)h(r)^2}\Big(-r^2(\alpha - 39\beta)f'(r)^2 + 4rf(r)(r(\alpha + \\
& - 3\beta)f''(r) + 4(\alpha + 6\beta)f'(r)) - 4(\alpha - 48\beta)f(r)^2\Big) + \frac{h'(r)}{12r^3f(r)h(r)}\Big(r^2f'(r)(2(\alpha + \\
& - 12\beta)f'(r) - 9\beta rf''(r)) - 4rf(r)(2r(\alpha + 6\beta)f''(r) + (\alpha + 15\beta)f'(r) - 3\gamma r) + \\
& + 16(\alpha + 6\beta)f(r)^2\Big) - \frac{1}{6r^4f(r)}\Big(-4\alpha + 12\beta - 4r^2(\alpha - 12\beta)f(r)f''(r) + \\
& - 6f(r)(-12\beta + 6\beta rf'(r) + \gamma r^2) + rf'(r)(18\beta(r^2f''(r) + 2) + r(\alpha - 12\beta)f'(r)) + \\
& + 4(\alpha - 21\beta)f(r)^2 + 6\gamma r^2\Big) = \frac{p(r)}{2f(r)} = \frac{1}{2}T_{rr},
\end{aligned} \tag{2.20a}$$

$$\mathcal{G}_{tt} - X(r)\mathcal{G}_{rr} - Y(r)\partial_r\mathcal{G}_{rr} =$$

$$\begin{aligned}
& = \frac{1}{8r^4h(r)^3(9\beta rh(r)f'(r) + f(r)(4(\alpha + 6\beta)h(r) - 2r(\alpha - 3\beta)h'(r)))^2}\Bigg(144\alpha\beta r^3(rf'(r) + \\
& + 4f(r))f(r)h(r)^5\Big(9\beta rh(r)f'(r) - 2r(\alpha - 3\beta)f(r)h'(r) + 4(\alpha + \\
& + 6\beta)f(r)h(r)\Big)f^{(3)}(r) - 288\alpha\beta r^4(\alpha - 3\beta)f(r)^2h(r)^5(rh'(r) - 2h(r))f''(r)^2 + \\
& - 12\beta r^2h(r)^2\Big(f(r)h(r)^2(r^4(\alpha - 3\beta)^2f'(r)^2h'(r)^2 - 2r^3(2\alpha^2 + 33\alpha\beta + \\
& - 36\beta^2)h(r)f'(r)^2h'(r) + 4h(r)^2(r^2(\alpha^2 - 150\alpha\beta + 36\beta^2)f'(r)^2 - 2(\alpha - 3\beta)(2\alpha + \\
& - 6\beta - 3\gamma r^2))\Big) - 2f(r)^2h(r)\Big(r^4(\alpha - 3\beta)^2f'(r)h'(r)^3 + r^3h(r)f'(r)h'(r)((-20\alpha^2 + \\
& + 21\alpha\beta + 36\beta^2)h'(r) - 2r(\alpha - 3\beta)^2h''(r)) + 2rh(r)^2(2r^2(\alpha - 3\beta)(\alpha + 6\beta)f'(r)h''(r) + \\
& + h'(r)(-8(\alpha - 3\beta)^2 + 3\alpha r(51\beta - 2\alpha)f'(r) + 6\gamma r^2(\alpha - 3\beta))\Big) + 4h(r)^3(24\alpha r(\alpha + \\
& + 6\beta)f'(r) + (\alpha - 3\beta)(8\alpha + 12\beta + 3\gamma r^2))\Big) - 54\alpha\beta r^3h(r)^4f'(r)^3 + f(r)^3(r^4(\alpha + \\
& - 3\beta)^2h'(r)^4 - 16r(11\alpha^2 + 42\alpha\beta + 18\beta^2)h(r)^3h'(r) - 4r^3(\alpha - 3\beta)h(r)h'(r)^2(r(\alpha + \\
& - 3\beta)h''(r) + 6\alpha h'(r)) + 4r^2h(r)^2(r^2(\alpha - 3\beta)^2h''(r)^2 + (41\alpha^2 - 57\alpha\beta + \\
& - 36\beta^2)h'(r)^2) - 16(7\alpha^2 + 84\alpha\beta + 9\beta^2)h(r)^4\Big)f''(r) + 3\beta r^4h(r)^4\Big(r^2(\alpha + \\
& - 3\beta)(2\alpha + 3\beta)h'(r)^2 - 4r(\alpha - 12\beta)(2\alpha + 3\beta)h(r)h'(r) + 4(2\alpha - 15\beta)(\alpha + \\
& - 12\beta)h(r)^2\Big)f'(r)^4 + 3\beta r^3h(r)^3\Big(-r^3(\alpha - 3\beta)(8\alpha + 3\beta)f(r)h'(r)^3 + \\
& + 4r^2f(r)h(r)h'(r)(r(\alpha - 3\beta)(2\alpha + 3\beta)h''(r) + (4\alpha^2 - 105\alpha\beta - 126\beta^2)h'(r)) + \\
& + 4rf(r)h(r)^2((4\alpha^2 + 273\alpha\beta + 36\beta^2)h'(r) - 2r(\alpha - 12\beta)(2\alpha + 3\beta)h''(r)) + \\
& - 8h(r)^3(4(\alpha - 3\beta)(\alpha + 33\beta)f(r) + 9\beta(-4\alpha + 12\beta + 3\gamma r^2))\Big)f'(r)^3 + \\
& + 3\beta r^2h(r)^2\Big(3r^4(\alpha - 3\beta)(4\alpha - 3\beta)f(r)^2h'(r)^4 + 4r^3f(r)^2h(r)h'(r)^2((11\alpha^2 +
\end{aligned}$$

$$\begin{aligned}
& + 6\alpha\beta + 126\beta^2)h'(r) - 6\alpha r(\alpha - 3\beta)h''(r) + 16rf(r)h(r)^3(4r(2\alpha^2 + 24\alpha\beta + \\
& - 9\beta^2)f(r)h''(r) + h'(r)((7\alpha + 6\beta)(5\alpha + 12\beta)f(r) - 3\gamma r^2(\alpha - 3\beta)) + \\
& + 4r^2f(r)^2h(r)^2(r^2(\alpha - 3\beta)(2\alpha + 3\beta)h''(r)^2 - (76\alpha^2 + 831\alpha\beta + 468\beta^2)h'(r)^2 + \\
& - 4r(2\alpha^2 - 3\alpha\beta + 72\beta^2)h'(r)h''(r)) - 8h(r)^4(f(r)(36\beta(21\beta - 4\alpha) + 2(26\alpha^2 + \\
& + 411\alpha\beta - 657\beta^2)f(r) + 3\gamma r^2(14\alpha + 39\beta)) + (2\alpha + 3\beta)(2\alpha - 6\beta - 3\gamma r^2))\Big)f'(r)^2 + \\
& + rf(r)h(r)\Big(-3\beta r^5(3\beta - \alpha)(15\beta - 8\alpha)f(r)^2h'(r)^5 + 12\beta r^4f(r)^2h(r)h'(r)^3(3r(\alpha + \\
& - 3\beta)(2\alpha - 3\beta)h''(r) + (-2\alpha^2 + 39\alpha\beta - 18\beta^2)h'(r)) + 8rh(r)^4h'(r)\Big(f(r)(-12\beta(4\alpha^2 + \\
& - 78\alpha\beta + 117\beta^2) + 6\beta(76\alpha^2 - 141\alpha\beta + 225\beta^2)f(r) + \gamma r^2(8\alpha^2 - 48\alpha\beta + 153\beta^2)) + \\
& + 3\beta(3\beta - 4\alpha)(-2\alpha + 6\beta + 3\gamma r^2)\Big) - 36\beta rf(r)h''(r)(4\alpha(\alpha + 6\beta)f(r) - \gamma r^2(\alpha + \\
& - 3\beta)) + 8r^2f(r)h(r)^3(108\beta^2r^2(\alpha - 3\beta)f(r)h''(r)^2 + h'(r)^2((2\alpha + 3\beta)(\gamma r^2(2\alpha + \\
& + 3\beta) - 12\beta(\alpha - 3\beta)) - 12\beta(32\alpha^2 + 231\alpha\beta + 153\beta^2)f(r)) - 12\beta r(\alpha + 6\beta)(8\alpha + \\
& + 21\beta)f(r)h'(r)h''(r)) + 12\beta r^3f(r)^2h(r)^2h'(r)(-r^2(\alpha - 3\beta)(4\alpha - 3\beta)h''(r)^2 + \\
& + (124\alpha^2 + 327\alpha\beta + 252\beta^2)h'(r)^2 + 4r(\alpha - 12\beta)(\alpha - 3\beta)h'(r)h''(r)) + \\
& - 64h(r)^5(f(r)(12\beta(-2\alpha^2 + 12\alpha\beta + 63\beta^2) + 6\beta(16\alpha^2 + 39\alpha\beta - 99\beta^2)f(r) + \\
& + \gamma r^2(\alpha + 6\beta)(4\alpha + 15\beta)) - 9\beta(\gamma r^2(\alpha + 6\beta) - 6\beta(\alpha - 3\beta))\Big)f'(r) + \\
& + 2f(r)^2\Big(3\beta r^6(\alpha - 3\beta)^2f(r)^2h'(r)^6 - 6\beta r^5(\alpha - 3\beta)f(r)^2h(r)h'(r)^4(2r(\alpha + \\
& - 3\beta)h''(r) + (11\alpha - 6\beta)h'(r)) + 8r^2h(r)^4(12\beta r^2(\alpha - 3\beta)(\alpha + 6\beta)f(r)^2h''(r)^2 + \\
& + 3h'(r)^2(f(r)(4\beta(3\beta - \alpha)(8\alpha + 3\beta) - 2\beta(-7\alpha^2 + 132\alpha\beta + 153\beta^2)f(r) + \\
& + \gamma r^2(4\alpha^2 + 3\alpha\beta + 9\beta^2)) - \beta(\alpha - 3\beta)(2\alpha - 6\beta - 3\gamma r^2)) + \\
& + 4rf(r)h'(r)h''(r)(\gamma r^2(\alpha - 3\beta)^2 - 6\beta(\alpha + 6\beta)(7\alpha + 6\beta)f(r)) + \\
& + 12\beta r^4f(r)^2h(r)^2h'(r)^2(r^2(\alpha - 3\beta)^2h''(r)^2 - 27\alpha(\alpha - 5\beta)h'(r)^2 + 2r(5\alpha - 6\beta)(\alpha + \\
& - 3\beta)h'(r)h''(r)) + 8r^3f(r)h(r)^3h'(r)(-3\beta r^2(5\alpha - 6\beta)(\alpha - 3\beta)f(r)h''(r)^2 + \\
& + h'(r)^2(3\beta(43\alpha^2 + 318\alpha\beta + 36\beta^2)f(r) + (\alpha - 3\beta)(12\beta(\alpha - 3\beta) - \gamma r^2(2\alpha + 3\beta))) + \\
& + 72\alpha\beta r(\alpha - 3\beta)f(r)h'(r)h''(r)) - 16rh(r)^5\Big(4\gamma r^3(\alpha - 3\beta)(\alpha + 6\beta)f(r)h''(r) + \\
& + h'(r)(6\beta(\alpha - 3\beta)(6\beta - 5\alpha) + f(r)(12\beta(2\alpha + 3\beta)(6\beta - 5\alpha) - 6\beta(5\alpha + 3\beta)(6\beta + \\
& - 5\alpha)f(r) + \gamma r^2(4\alpha - 21\beta)(\alpha + 6\beta)) + \gamma r^2(4\alpha - 3\beta)(\alpha + 6\beta)\Big) + 64(\alpha + 6\beta)(f(r) + \\
& - 1)h(r)^6(6\beta(\alpha - 3\beta) + 6\beta(5\alpha + 3\beta)f(r) + \gamma r^2(-(2\alpha + 3\beta)))\Big)\Big) = -\frac{1}{2}h(r)\rho(r) + \\
& = \frac{h(r)p(r)}{2(9\beta rh(r)f'(r) - 2r(\alpha - 3\beta)f(r)h'(r) + 4(\alpha + 6\beta)f(r)h(r))^2}\Big(18\beta r^2(\alpha + \\
& - 3\beta)h(r)^2f'(r)^2 + 9\beta rf(r)h(r)(4(\alpha - 3\beta)h(r)(2f'(r) - rf''(r)) - 9\beta rf'(r)h'(r)) +
\end{aligned}$$

$$\begin{aligned}
& + 2f(r)^2 \left( -r^2(2\alpha - 15\beta)(\alpha - 3\beta)h'(r)^2 - 2r(4\alpha^2 - 15\alpha\beta + 90\beta^2)h(r)h'(r) + \right. \\
& \left. + 24(\alpha - 3\beta)(\alpha + 6\beta)h(r)^2 \right) + \\
& - \frac{2r(\alpha - 3\beta)f(r)h(r)^2}{2f(r)(r(\alpha - 3\beta)h'(r) - 2(\alpha + 6\beta)h(r)) - 9\beta rh(r)f'(r)} p'(r) = \\
& = \frac{1}{2} (T_{tt} - X(r)T_{rr} - Y(r)\partial_r T_{rr}),
\end{aligned} \tag{2.20b}$$

which are the only independent equations of motion. To have a complete set of differential equations, we also have to consider the only non-zero component of the conservation of the stress-energy tensor

$$\nabla_\mu T^{\mu\nu} = 0 \quad \rightarrow \quad p'(r) + \frac{h'(r)}{2h(r)} (\rho(r) + p(r)) = 0, \tag{2.21}$$

and an equation of state

$$p(r) = \mathcal{P}(\rho(r)). \tag{2.22}$$

Unsurprisingly, no analytical solutions of (2.20)-(2.21), except for the vacuum solutions of General Relativity, are known, and solutions must be studied numerically or under approximations. We expect six free parameters for static and spherically symmetric solutions as they solve two third-order ordinary differential equations. However, we can remove two free parameters requiring the spacetime to be asymptotically flat and another one with a gauge fixing of the rescaling of the time coordinate, which is always possible in static spacetimes. The solutions of quadratic gravity we will analyze are then described only by three free parameters.

### 2.1.1 Starobinski action and $f(R)$ theories

Despite its general nature, Stelle's quadratic theory of gravity (2.5) received relatively little attention in the study of classical solutions, especially with respect to its simplified version

$$\mathcal{I}_{Starobinski} = \int d^4x \sqrt{-g} [\gamma R + \beta R^2]. \tag{2.23}$$

For this choice there are three main reasons:

- a theoretical reason, that is that the action (2.23) does not contain ghost particles at quantum level;
- a phenomenological reason, that is that with a Friedmann-Lemaître-Robertson-Walker (FLRW) ansatz for the metric the Weyl term is identically zero, and therefore at background level the two actions are the same. We remember that the cosmological model derived from the action (2.23) has been studied by Starobinski

in [19], and it is one of the models which survived the recent constraints on inflation coming from CMB anisotropies [37, 38]; this is indeed the reason for which we refer to the action (2.23) as Starobinski's action.

- a technical reason, that is that it is possible to rewrite the action in the so-called Einstein frame, that is Einstein gravity minimally coupled with a scalar field, in an easy and manageable way.

While the theoretical reason is intriguing, quadratic terms are expected to be generated by quantum corrections, and there is no natural way to avoid generating terms proportional to the squared Ricci and Riemann tensors. In the absence of such a mechanism, we believe that quadratic gravity remains more solid at the theoretical level.

Regarding the phenomenological reason, it is a peculiarity of the cosmological ansatz for the metric, and we believe that applying it to isolated objects is an excessive extrapolation; moreover, we also recall that the tensor perturbations, which, however, have not been detected yet, have different behaviors in the two theories [39].

To discuss the technical reason, let us briefly describe the actual reformulation of the theory in the Einstein frame. We start introducing the auxiliary field  $\chi$

$$\mathcal{I}'_{Starobinski} = \int d^4x \sqrt{-g} [\gamma R + \beta R^2 - \beta (\chi - R)^2] = \int d^4x \sqrt{-g} [(\gamma + 2\beta\chi) R - \beta\chi^2], \quad (2.24)$$

where the original action is found solving the equations of motion of  $\chi$ . Applying the Weyl rescaling to the metric  $\tilde{g}_{\mu\nu} = (1 + 2\beta\chi/\gamma)g_{\mu\nu}$ , the action becomes

$$\mathcal{I}''_{Starobinski} = \int d^4x \sqrt{-\tilde{g}} \left[ \gamma \tilde{R} - \frac{6\beta^2/\gamma}{(1 + 2\beta\chi/\gamma)^2} \partial^\rho \chi \partial_\rho \chi - \frac{\beta}{(1 + 2\beta\chi/\gamma)^2} \chi^2 \right], \quad (2.25)$$

that with the redefinition  $\phi = \sqrt{3\gamma} \ln(1 + 2\beta\chi/\gamma)$ , dropping the tildes and the superscripts, and renaming  $\gamma = M_p^2/2$ , becomes

$$\mathcal{I}_{Starobinski} = \int d^4x \sqrt{g} \left[ \frac{M_p^2}{2} R - \frac{1}{2} \partial^\rho \phi \partial_\rho \phi - \frac{M_p^4}{16\beta} \left( 1 - e^{-\sqrt{\frac{2}{3}} \frac{\phi}{M_p}} \right)^2 \right], \quad (2.26)$$

which is General Relativity with a minimally coupled scalar field with the potential

$$V(\phi) = \frac{M_p^4}{16\beta} \left( 1 - e^{-\sqrt{\frac{2}{3}} \frac{\phi}{M_p}} \right)^2. \quad (2.27)$$

In particular, the specific form of the potential (2.27) naturally describes a slow-roll inflationary phase. We also note that an infinitesimal field will be described by the Lagrangian density

$$-\frac{1}{2} \partial^\rho \phi \partial_\rho \phi - \frac{M_p^4}{16\beta} \left( 1 - e^{-\sqrt{\frac{2}{3}} \frac{\phi}{M_p}} \right)^2 \sim -\frac{1}{2} \partial^\rho \phi \partial_\rho \phi - \frac{M_p^2}{24\beta} \phi^2 = -\frac{1}{2} (\partial^\rho \phi \partial_\rho \phi + m_0^2 \phi^2), \quad (2.28)$$

which is exactly the action of a free scalar field with mass  $m_0^2 = \gamma/6\beta$ . The formulation in the Einstein frame acquires much more strength whenever we consider Starobinski's action (2.23) in the context of the  $f(R)$  class of theories of gravity. Indeed, it is possible to describe a large variety of models with an action expressed as

$$\mathcal{I}_{f(R)} = \int d^4x \sqrt{-g} f(R), \quad (2.29)$$

of which Starobinski's model is the simplest case that deviates from General Relativity. A property of the  $f(R)$  class is that all models can be mapped to an Einstein theory with a minimally coupled scalar field with a procedure similar to the one shown for Starobinski's model. The potential of the scalar field can be found by solving the equations

$$\begin{aligned} f'(R) &= \frac{M_p^2}{2} e^{\sqrt{\frac{2}{3}} \frac{\phi}{M_p}}, \\ e^{-\sqrt{\frac{2}{3}} \frac{\phi}{M_p}} V'(\phi) &= \frac{M_p}{\sqrt{6}} R, \end{aligned} \quad (2.30)$$

and fixing the constants of integration with the equations of motion. Nonetheless, while the Einstein frame is extremely useful in some cases, it is not optimal to study isolated objects. This is due to the transformation  $\tilde{g}_{\mu\nu} = (1 + 2\beta\chi/\gamma)g_{\mu\nu}$  which, to be a conformal map, has to satisfy  $1 + 2\beta\chi/\gamma > 0$  and then, considering the equation of motion of  $\chi$  means  $R > -m_0^2/3$ , which however can be a strict requirement for isolated objects. In addition, a cosmological constant naturally appears in the Einstein frame, and while it is of fundamental importance in a cosmological context, it might render the discussion of isolated objects much more complicated.

Considering also the possibility of having a non-zero stress-energy tensor, the equations of motion for the action (2.23) are

$$\mathcal{F}_{\mu\nu} = \gamma \left( R_{\mu\nu} - \frac{1}{2} R g_{\mu\nu} \right) + 2\beta \left( R_{\mu\nu} - \frac{1}{4} R g_{\mu\nu} - \nabla_\mu \nabla_\nu + g_{\mu\nu} \square \right) R = \frac{1}{2} T_{\mu\nu}, \quad (2.31)$$

that become a set of fourth-order ordinary differential equations whenever the static and spherically symmetric ansatz (2.15) is considered. However, if we consider the Ricci scalar  $R$  as an independent variable it is possible to rewrite the system as one second-order equation in  $R$  and two first-order equations in  $h(r)$  and  $f(r)$  as

$$\begin{aligned} \mathcal{F}_\mu^\mu &= \frac{9}{2} \beta f'(r) R'(r) + \frac{9\beta f(r) h'(r) R'(r)}{2h(r)} + 6\beta f(r) R''(r) + \frac{18\beta f(r) R'(r)}{r} - \gamma R(r) = \\ &= \frac{1}{2} (-\rho(r) + 3p(r)) = \frac{1}{2} T, \end{aligned} \quad (2.32a)$$

$$\begin{aligned}
\mathcal{F}_{tt} + \frac{h(r)}{3} \mathcal{F}^\mu_\mu &= -\frac{h(r)}{6r^2} (6\gamma r f'(r) - 6\gamma - 3\beta r^2 f'(r) R'(r) + 12\beta r R(r) f'(r) + 2\gamma r^2 R(r) + \\
&\quad + 6f(r) (\gamma - 2\beta r R'(r) + 2\beta R(r)) + 3\beta r^2 R(r)^2 - 12\beta R(r)) = \\
&= \frac{h(r)}{3} (2\rho(r) + 3p(r)) = \frac{1}{2} \left( T_{tt} + \frac{h(r)}{3} T \right), \\
\end{aligned} \tag{2.32b}$$

$$\begin{aligned}
\mathcal{F}_{rr} &= \frac{-2\gamma + 3\beta r^2 f'(r) R'(r) + \beta r^2 R(r)^2 - 4\beta R(r)}{2r^2 f(r)} + \\
&\quad + \frac{r h'(r) (\gamma + \beta r R'(r) + 2\beta R(r)) + h(r) (\gamma + 4\beta r R'(r) + 2\beta R(r))}{r^2 h(r)} = \frac{p(r)}{2f(r)} = \frac{1}{2} T_{rr}.
\end{aligned} \tag{2.32c}$$

Having one second-order and two first-order equations, the solutions of the action (2.23) will have only four free parameters, which will be reduced to two free parameters whenever asymptotic flatness is imposed and a time parametrization is fixed.

### 2.1.2 Einstein-Weyl gravity

As opposed to the case of Starobinski's action (2.23), Einstein-Weyl gravity studies the sector of quadratic gravity where only the squared Weyl tensor is present

$$\mathcal{I}_{EW} = \int d^4x \sqrt{-g} [\gamma R - \alpha C^{\mu\nu\rho\sigma} C_{\mu\nu\rho\sigma}]. \tag{2.33}$$

It has been relatively less studied than Starobinski's action, having all the complications of the full theory, namely having a ghost at the quantum level, having no cosmological model associated, and having a non-manageable Einstein frame counterpart. In particular, to be more specific on the third point, we recall the Einstein frame formulation of Einstein-Weyl gravity derived in [40] as

$$\begin{aligned}
\mathcal{I}_{EW} &= \int d^4x \sqrt{-g} \frac{M_p^2}{2} \left[ \tilde{R} - \tilde{g}^{\mu\nu} (\Delta^\rho_{\mu\sigma}(\phi_{\alpha\beta}) \Delta^\sigma_{\nu\rho}(\phi_{\alpha\beta}) - \Delta^\rho_{\mu\nu}(\phi_{\alpha\beta}) \Delta^\sigma_{\sigma\rho}(\phi_{\alpha\beta})) + \right. \\
&\quad \left. + \frac{m_2^2}{4} \frac{\phi^{\mu\nu} \phi_{\mu\nu} - \phi^2}{\sqrt{\det A(\phi_{\alpha\beta})}} \right], \\
\end{aligned} \tag{2.34}$$

where

$$\begin{aligned}
\Delta^\rho_{\mu\nu}(\phi_{\alpha\beta}) &= \frac{1}{2} (g^{-1})^{\rho\sigma}(\phi_{\alpha\beta}) \left( \tilde{\nabla}_\mu g_{\sigma\nu}(\phi_{\alpha\beta}) + \tilde{\nabla}_\nu g_{\mu\sigma}(\phi_{\alpha\beta}) - \tilde{\nabla}_\sigma g_{\mu\nu}(\phi_{\alpha\beta}) \right), \\
g_{\mu\nu}(\phi_{\alpha\beta}) &= \frac{A_\mu^\rho(\phi_{\alpha\beta}) \tilde{g}_{\rho\nu}}{\sqrt{\det A(\phi_{\alpha\beta})}}, \\
A_\mu^\rho(\phi_{\alpha\beta}) &= \left( 1 + \frac{1}{2} \phi \right) \delta_\mu^\rho - \phi_\mu^\rho, \\
(g^{-1})^{\nu\rho} \phi_{\mu\rho} &= \tilde{g}^{\nu\rho} \pi_{\mu\rho},
\end{aligned} \tag{2.35}$$

the non-tilded quantities are the ones of the original action (2.33), and  $\pi_{\mu\nu}$  is an auxiliary field which satisfies the equations of motion  $\pi_{\mu\nu} = 2m_2^{-2} (R_{\mu\nu} - \frac{1}{6}Rg_{\mu\nu})$ . While it is interesting that the Einstein-Weyl action can be recast in the form of General Relativity with a minimally coupled massive tensor field with spin  $S = 2$ , the form of the action (2.34) does not really simplify the study of solutions, and we will never use the Einstein frame formulation.

However, the most interesting point of Einstein-Weyl gravity is precisely the presence of this additional massive tensor mode with negative energy states. While the  $R^2$  term of (2.5) can be related to the presence of a massive scalar, whose effects are standard in some sense, the action (2.33) contains the more peculiar aspects of the full quadratic theory. In particular, thanks to the second lemma 2 of the theorem 1, Einstein-Weyl gravity describes all the Ricci scalar flat solutions of the full quadratic theory; more specifically, all the static and asymptotically flat black hole solutions of quadratic gravity are solutions also of the Einstein-Weyl theory. Nonetheless, as we will show shortly, the equations of motion are much simpler than the ones of the full quadratic case.

The tensorial form of the equations of motion for the Einstein-Weyl action (2.33) are

$$\mathcal{H}_{\mu\nu} = \gamma \left( R_{\mu\nu} - \frac{1}{2}Rg_{\mu\nu} \right) - 4\alpha \left( \nabla^\rho \nabla^\sigma + \frac{1}{2}R^{\rho\sigma} \right) C_{\mu\rho\nu\sigma} = \frac{1}{2}T_{\mu\nu}, \quad (2.36)$$

with the trace being

$$\mathcal{H}^\mu_\mu = -\gamma R = \frac{1}{2}T, \quad (2.37)$$

which is the same as in General Relativity due to the traceless nature of the Weyl term. Substituting the metric (2.15) results once again in a system of four fourth-order equations. However,  $\mathcal{H}^\mu_\mu$  has only terms up to  $h''(r)$  and  $f'(r)$  and  $\mathcal{H}_{rr}$  only up to  $h^{(3)}(r)$  and  $f''(r)$ . To find another second-order equation we can then use the convenient combination

$$\begin{aligned} \mathcal{H}_{rr} - \tilde{X}(r) \left( \mathcal{H}^\mu_\mu - \frac{1}{2}T \right) - Y(r) \left( \mathcal{H}^\mu_\mu - \frac{1}{2}T \right)^2 - Z(r) \partial_r \left( \mathcal{H}^\mu_\mu - \frac{1}{2}T \right) = \\ = \mathcal{H}_{rr} - X(r) \left( \mathcal{H}^\mu_\mu - \frac{1}{2}T \right) - Y(r) \left( (\mathcal{H}^\mu_\mu)^2 - \frac{1}{4}T^2 \right) - Z(r) \partial_r \left( \mathcal{H}^\mu_\mu - \frac{1}{2}T \right), \end{aligned} \quad (2.38)$$

which has terms only up to  $f''(r)$  and  $h'(r)$ . Using the factors

$$\begin{aligned} \tilde{X}(r) &= \frac{\alpha (2rf(r)h'(r) + h(r)(3rf'(r) + 2f(r) - 2))}{3\gamma r^2 h(r)f(r)}, \\ X(r) &= \frac{\alpha (2rf(r)h'(r) + h(r)(3rf'(r) + 2f(r) - 2))}{3\gamma r^2 h(r)f(r)} - \frac{\alpha}{6\gamma^2 f(r)}T, \\ Y(r) &= -\frac{\alpha}{6\gamma^2 f(r)}, \\ Z(r) &= \frac{\alpha (rh'(r) - 2h(r))}{3\gamma r h(r)}, \end{aligned} \quad (2.39)$$

we have then, finally, the two second-order equations

$$\begin{aligned} \mathcal{H}^\mu_\mu &= \frac{\gamma}{2r^2h(r)^2} \left( rh(r) \left( rh'(r)f'(r) + 2f(r)(rh''(r) + 2h'(r)) \right) - r^2f(r)h'(r)^2 + \right. \\ &\quad \left. + 4h(r)^2(rf'(r) + f(r) - 1) \right) = \frac{1}{2}(-\rho(r) + 3p(r)) = \frac{1}{2}T, \end{aligned} \quad (2.40a)$$

$$\begin{aligned} \mathcal{H}_{rr} - X(r)\mathcal{H}^\mu_\mu - Y(r)(\mathcal{H}^\mu_\mu)^2 - Z(r)\partial_r\mathcal{H}^\mu_\mu &= \frac{1}{2r^4h(r)^3f(r)} \left( \alpha r^3f(r)^2h'(r)^3 + \right. \\ &\quad - \alpha r^2h(r)f(r)h'(r)^2(rf'(r) + 3f(r)) - 2r^2h(r)^2f(r)h'(r)(\alpha rf''(r) + \alpha f'(r) + \right. \\ &\quad \left. - \gamma r) + h(r)^3 \left( r(4\alpha f'(r) - 3\alpha rf'(r)^2 - 2\gamma r) + 2f(r)(4\alpha + 2\alpha r^2f''(r) + \gamma r^2 + \right. \right. \\ &\quad \left. \left. - 2\alpha rf'(r)) - 8\alpha f(r)^2 \right) \right) = \frac{1}{24\gamma^2r^2f(r)h(r)} \left( h(r)(\alpha(4\gamma\rho(r)(3rf'(r) + 2f(r) - 2) + \right. \right. \\ &\quad + 8\gamma rf(r)(3p'(r) - \rho'(r)) + r^2\rho(r)^2) - 6p(r)(\alpha r(6\gamma f'(r) + r\rho(r)) + 4\alpha\gamma f(r) + \right. \\ &\quad \left. - 2\gamma(2\alpha + \gamma r^2)) + 9\alpha r^2p(r)^2) + 4\alpha\gamma rf(r)h'(r)(-3rp'(r) - 6p(r) + r\rho'(r) + 2\rho(r)) \right) = \\ &= \frac{1}{2} \left( T_{rr} - X(r)T - \frac{1}{2}Y(r)T^2 - Z(r)\partial_rT \right), \end{aligned} \quad (2.40b)$$

where in the last equivalence of (2.40b) we used (2.40a) to remove the term proportional to  $Y(r)\mathcal{H}^\mu_\mu T$ . Having two second-order equations, we expect four free parameters for the solutions, which will become two after imposing asymptotic flatness and having fixed a time parametrization, exactly as in the case of Starobinski's action. Finally, we note that, even if the equations are much simpler than (2.20), no analytical solutions are known, except for the vacuum solutions of General Relativity, and it is necessary to resort to numerical integration or approximations.

## 2.2 Scale-invariant gravity

A very simple but very intriguing extension of the quadratic action (2.2) can be found by substituting the Planck mass parameter  $\gamma = M_p^2/2$  with a dynamical scalar field. If we introduce only a quartic self-interaction of the field and no mass term, we find a generalization of the action studied by Rinaldi and Vanzo in [27, 34, 28]

$$\mathcal{I}_{si} = \int d^4x \sqrt{-g} \left[ \xi\phi^2 R + \beta R^2 - \alpha C^{\mu\nu\rho\sigma} C_{\mu\nu\rho\sigma} + \chi\mathcal{G} - \frac{1}{2}\partial^\mu\phi\partial_\mu\phi - \frac{\lambda}{4}\phi^4 \right], \quad (2.41)$$

where  $\alpha$ ,  $\beta$ ,  $\chi$ ,  $\xi$ , and  $\lambda$  are dimensionless arbitrary positive constants, and we specify that we used a different notation than the original authors to be consistent with the parameters used for the action (2.2). This action possesses the dilatation, or scale, symmetry

$$g'_{\mu\nu}(x) = g_{\mu\nu}(\ell x), \quad \phi'(x) = \ell\phi(\ell x), \quad (2.42)$$

for any constant  $\ell$ . It also possesses a rigid Weyl symmetry

$$g'_{\mu\nu}(x) = L^2 g_{\mu\nu}(x), \quad \phi'(x) = L^{-1} \phi(x), \quad (2.43)$$

for any constant  $L$ , and the composite symmetry

$$g'_{\mu\nu}(x) = L^2 g_{\mu\nu}(\ell x), \quad \phi'(x) = L^{-1} \ell \phi(\ell x), \quad (2.44)$$

which is clearly a diffeomorphism transformation in the case  $L = \ell$ . However, the theory's scale-invariant nature was already manifested by the presence of dimensionless constant only, which forces any mass scale in the theory to be generated dynamically. The metric field equations of (2.41) read

$$\begin{aligned} (2\beta R + \xi \phi^2) G_{\mu\nu} - 4\alpha \left( \nabla^\rho \nabla^\sigma + \frac{1}{2} R^{\rho\sigma} \right) C_{\mu\rho\nu\sigma} - \frac{1}{2} \left( \nabla_\mu \phi \nabla_\nu \phi - \frac{1}{2} g_{\mu\nu} \nabla_\rho \phi \nabla^\rho \phi \right) + \\ - (\nabla_\mu \nabla_\nu - g_{\mu\nu} \square) (2\beta R + \xi \phi^2) + \frac{1}{2} \left( \beta R^2 + \frac{\lambda}{4} \phi^4 \right) g_{\mu\nu} = 0, \end{aligned} \quad (2.45)$$

where  $G_{\mu\nu} = R_{\mu\nu} - \frac{1}{2} R g_{\mu\nu}$  is the Einstein tensor, while varying the action with respect to the scalar field yields

$$\square \phi + (2\xi R - \lambda \phi^2) \phi = 0. \quad (2.46)$$

If we restrict ourselves to solutions with constant  $\phi$  and  $R$ , it is trivial to see that (2.45) reduce to the equations of Einstein-Weyl gravity with a cosmological constant. Finally, using the scalar equation (2.46), the trace of the metric equations of motion can be written as

$$\square \left( R + \frac{1+12\xi}{24\beta} \phi^2 \right) = 0. \quad (2.47)$$

This specific form of the trace of the equation of motion suggests that it is possible to derive a no-hair-like theorem as theorem 1. It is indeed possible to derive two theorems:

**Theorem 2.** *Let's consider a static spacetime  $(M, g)$  which is a solution of the vacuum equations of motion of scale-invariant gravity and a spacelike hypersurface  $\Sigma$ ; if the spacetime satisfies either*

- $g_{\mu\nu} \kappa^\mu \kappa^\nu \rightarrow 0$  at the boundary of  $\Sigma$ , with  $\kappa^\mu$  being the timelike Killing vector,
- $D_a \left( R + \frac{1+12\xi}{24\beta} \phi^2 \right) \rightarrow 0$  at the boundary of  $\Sigma$ , with  $D_a$  being the covariant derivative on  $\Sigma$ ,

*then  $\left( R + \frac{1+12\xi}{24\beta} \phi^2 \right) = \text{const.}$  in all  $\Sigma$ .*

**Theorem 3.** *Let's consider an isotropic and homogeneous spacetime  $(M, g)$  which is a solution of the vacuum equations of motion of scale-invariant gravity and a time interval  $\Delta t$ ; if the spacetime satisfies either*

-  $g_{\mu\nu}\kappa^\mu\kappa^\nu \rightarrow 0$  at the boundary of  $\Delta t$ , with  $\kappa^\mu$  being one of the spacelike Killing vectors,

-  $D_t \left( R + \frac{1+12\xi}{24\beta} \phi^2 \right) \rightarrow 0$  at the boundary of  $\Delta t$ , with  $D_t$  being the covariant derivative on  $\Delta t$ ,

then  $\left( R + \frac{1+12\xi}{24\beta} \phi^2 \right) = \text{const. in all } \Delta t$ .

**Proof.** It is possible to prove both theorems simultaneously; let us consider a metric in the form

$$ds^2 = \tau(x)^2 \sigma_{ab}(y) dy^a dy^b + \xi_{ij}(x) dx^i dx^j, \quad (2.48)$$

where  $\sigma_{ab}(y)$  is the metric of a maximally symmetric manifold with dimension  $d_y < 4$  and  $\xi_{ij}(x)$  is the metric of a generic manifold of dimension  $4 - d_y$ . If we impose that the scalar field has the same symmetries of the spacetime, *i.e.* that it depends only on the  $x$  variables, equation (2.10) becomes

$$D^i D_i \left( R + \frac{1+12\xi}{24\beta} \phi^2 \right) + \frac{d_y}{\tau} D^i \tau D_i \left( R + \frac{1+12\xi}{24\beta} \phi^2 \right) = 0, \quad (2.49)$$

where the  $D_i$  are the covariant derivatives defined by the metric  $\xi_{ij}(x)$ . Multiplying by  $\tau^{d_y} \left( R + \frac{1+12\xi}{24\beta} \phi^2 \right)$  and integrating over a submanifold  $\Sigma$  defined by the  $x$  coordinates we get

$$\begin{aligned} \int_{\Sigma} d^{4-d_y} x \sqrt{|\xi|} & \left[ \tau^{d_y} \left( R + \frac{1+12\xi}{24\beta} \phi^2 \right) D^i D_i \left( R + \frac{1+12\xi}{24\beta} \phi^2 \right) \right. \\ & \left. + d_y \tau^{d_y-1} \left( R + \frac{1+12\xi}{24\beta} \phi^2 \right) D^i \tau D_i \left( R + \frac{1+12\xi}{24\beta} \phi^2 \right) \right] = 0, \end{aligned} \quad (2.50)$$

that, integrated by parts, leads to

$$\begin{aligned} & \left[ \tau^{d_y} \left( R + \frac{1+12\xi}{24\beta} \phi^2 \right) D^i \left( R + \frac{1+12\xi}{24\beta} \phi^2 \right) \right]_{\partial\Sigma} \\ & - \int_{\Sigma} d^{4-d_y} x \sqrt{|\xi|} \left[ \tau^{d_y} D^i \left( R + \frac{1+12\xi}{24\beta} \phi^2 \right) D_i \left( R + \frac{1+12\xi}{24\beta} \phi^2 \right) \right] = 0. \end{aligned} \quad (2.51)$$

If the metric  $\xi_{ij}(x)$  is either positive or negative definite in  $\Sigma$  and the boundary term is vanishing, then the combination  $R + \frac{1+12\xi}{24\beta} \phi^2$  is constant in all  $\Sigma$ .  $\square$

To have a better physical understanding of this result, we make explicit the specific cases: with a static metric

$$ds^2 = -\tau^2(x) dt^2 + \xi_{ij}(x) dx^i dx^j, \quad (2.52)$$

the boundary term vanishes whenever the boundary is taken on event horizons ( $\tau^2 = 0$ ) or on hypersurfaces of constant scalar curvature and scalar field, and it leads to

$$R + \frac{1 + 12\xi}{24\beta} \phi^2 = \text{const. (in space)}; \quad (2.53)$$

with a FLRW metric

$$ds^2 = -\xi(t)dt^2 + \tau(t)^2\sigma_{ab}(y)dy^a dy^b, \quad (2.54)$$

the boundary term vanishes whenever the boundary is taken on cosmological singularities ( $\tau^2 = 0$ ), or on times at which the scalar curvature and scalar field are constant, and it leads to

$$R + \frac{1 + 12\xi}{24\beta} \phi^2 = \text{const. (in time)}. \quad (2.55)$$

The spatial constraint (2.53) is then ensured for the external region of black holes, which are either asymptotically flat or asymptotically anti-de Sitter, and in the region between the black hole and cosmological horizon whenever both are present. The time constraint (2.55) is instead ensured if the cosmological evolution is between two fixed points, and can be used to keep track of the value of the effective cosmological constant throughout a cosmological evolution.

### 2.2.1 Scalar sector and Einstein frame formulation

We present here a simplified version of (2.41), which is exactly the one proposed and studied by Rinaldi and Vanzo [27, 28], that is

$$\mathcal{I}_{RV} = \int d^4x \sqrt{-g} \left[ \xi\phi^2 R + \beta R^2 - \frac{1}{2}\partial^\mu\phi\partial_\mu\phi - \frac{\lambda}{4}\phi^4 \right], \quad (2.56)$$

where the Weyl and Gauss-Bonnet terms are suppressed. The equations of motion for the metric are clearly

$$\begin{aligned} (2\beta R + \xi\phi^2) G_{\mu\nu} - \frac{1}{2} \left( \nabla_\mu\phi\nabla_\nu\phi - \frac{1}{2}g_{\mu\nu}\nabla_\rho\phi\nabla^\rho\phi \right) + \\ - (\nabla_\mu\nabla_\nu - g_{\mu\nu}\square) (2\beta R + \xi\phi^2) + \frac{1}{2} \left( \beta R^2 + \frac{\lambda}{4}\phi^4 \right) g_{\mu\nu} = 0, \end{aligned} \quad (2.57)$$

and the one for the scalar field does not change. In this case, the solutions with constant  $\phi$  and  $R$  are simply the ones of General Relativity with a cosmological constant. The main reason for which it is useful to consider this less general case is that it is possible to rewrite the system in the Einstein frame by introducing another scalar field, and without having to introduce a very involved massive tensor field as done in Subsubsection 2.1.2. Similarly to what has been done in (2.24) and (2.25) for Starobinski's action, we can add

an auxiliary field  $\varphi$  as

$$\begin{aligned}\mathcal{I}'_{RV} &= \int d^4x \sqrt{-g} \left[ \xi\phi^2 R + \beta R^2 - \beta(\varphi - R)^2 - \frac{1}{2}\partial^\mu\phi\partial_\mu\phi - \frac{\lambda}{4}\phi^4 \right] = \\ &= \int d^4x \sqrt{-g} \left[ (\xi\phi^2 + 2\beta\varphi) R - \frac{1}{2}\partial^\mu\phi\partial_\mu\phi - \frac{\lambda}{4}\phi^4 - \beta\varphi^2 \right].\end{aligned}\quad (2.58)$$

With the conformal transformation  $\tilde{g}_{\mu\nu} = 2(\xi\phi^2 + 2\beta\varphi)g_{\mu\nu}/M_{SI}^2$  and introducing the variable  $\psi = \xi\phi^2 + 2\beta\varphi$  and the constant  $\Omega = \beta\lambda + \xi^2$  the action becomes

$$\mathcal{I}''_{RV} = \int d^4x \sqrt{-\tilde{g}} \left[ \frac{M_{SI}^2}{2}\tilde{R} - \frac{M_{SI}^2}{4\psi}\partial^\mu\phi\partial_\mu\phi - \frac{3M_{SI}^2}{4\psi^2}\partial^\mu\psi\partial_\mu\psi - \frac{M_{SI}^4(\Omega\phi^4 + \psi^2 - 2\xi\phi^2\psi)}{16\beta\psi^2} \right].\quad (2.59)$$

Here,  $M_{SI}$  is an arbitrary parameter with mass dimensions which, however, turns out to be a so-called redundant parameter (see discussion in [27]), leaving the action scale invariant. While it is not possible to perform a scalar field redefinition for which both kinetic terms have a canonical form, it is possible to redefine them in order to have one scalar field with a canonical kinetic term. In particular, with the scalar field redefinition

$$\begin{aligned}\zeta &= \sqrt{6}M_{SI}\operatorname{arcsinh}\left(\frac{\phi}{2\sqrt{3}\psi}\right), \\ \rho &= \frac{M_{SI}}{2}\ln\left(\frac{\phi^2 + 12\psi}{2M_{SI}^2}\right),\end{aligned}\quad (2.60)$$

dropping the tildes and superscripts, we obtain the expression for the action

$$\mathcal{I}_{RV} = \int d^4x \sqrt{-g} \left[ \frac{M_{SI}^2}{2}R - 3\cosh^2\left(\frac{\zeta}{\sqrt{6}M_{SI}}\right)\partial^\mu\rho\partial_\mu\rho - \frac{1}{2}\partial^\mu\zeta\partial_\mu\zeta - U(\zeta) \right],\quad (2.61)$$

where

$$U(\zeta) = \frac{M_{SI}^4}{\beta} \left( \frac{1}{16} - \frac{3\xi}{2}\sinh^2\left(\frac{\zeta}{\sqrt{6}M_{SI}}\right) + 9\Omega\sinh^4\left(\frac{\zeta}{\sqrt{6}M_{SI}}\right) \right).\quad (2.62)$$

The action's specific form has made the potential dependent only on the field with a canonical kinetic term. Moreover, if we consider the definition of the field  $\rho$  and the equation of motion for the auxiliary field  $\varphi = R$ , we can express this spectator field as

$$\rho = \frac{M_{SI}^2}{2}\ln\left(\frac{12\beta}{M_{SI}^2}\left(R + \frac{1+12\xi}{24\beta}\phi^2\right)\right),\quad (2.63)$$

and then, whenever the theorems 2, 3 are satisfied, this scalar field has zero contribution to the action. Finally, the field equations for the metric and scalar fields in the Einstein frame are

$$\begin{aligned}M_{SI}^2G_{\mu\nu} &= 6\cosh^2\left(\frac{\zeta}{\sqrt{6}M_{SI}}\right)\left(\partial_\mu\rho\partial_\nu\rho - \frac{1}{2}g_{\mu\nu}\partial_\lambda\rho\partial^\lambda\rho\right) + \\ &\quad + \partial_\mu\zeta\partial_\nu\zeta - \frac{1}{2}g_{\mu\nu}\partial_\lambda\zeta\partial^\lambda\zeta - g_{\mu\nu}U(\zeta), \\ \square\zeta &= \frac{\sqrt{6}}{M_{SI}}\cosh\left(\frac{\zeta}{\sqrt{6}M_{SI}}\right)\sinh\left(\frac{\zeta}{\sqrt{6}M_{SI}}\right)\partial_\mu\rho\partial^\mu\rho + \frac{dU}{d\zeta}, \\ \square\rho &= -\frac{2}{\sqrt{6}M_{SI}}\tanh\left(\frac{\zeta}{\sqrt{6}M_{SI}}\right)\partial_\mu\rho\partial^\mu\rho.\end{aligned}\quad (2.64)$$

Note that  $\rho = \text{const.}$  (not necessarily vanishing) is a trivial solution of the system precisely because the potential depends on  $\zeta$  only. As we will show in Subsection 6.3, the Einstein frame formulation of scale-invariant gravity will be fundamental when considering the dynamical stability of black holes, as the perturbed equation will be slight variations from the ones of General Relativity.

### 3 Analytical approximations and numerical methods

As discussed in the previous section, quadratic gravity solutions must be studied using numerical integration or some approximations. In this technical section, we will first describe the various regimes under which it is possible to have analytical approximations, and we will briefly discuss the main properties at the mathematical level of the different behaviors found. We will also describe in detail the numerical methods used to link the various analytical approximations and fully describe the solutions in the non-linear regime.

This section is divided in four parts:

- in the first subsection we will study the linearized equations of motion and use them to describe asymptotically flat solutions at large distances. The metric in this regime results to be the Schwarzschild one with exponentially suppressed corrections; in particular, in the Newtonian limit, the gravitational potential will have two Yukawa corrections, each of them associated with one of the two massive modes which appear together with the standard massless graviton in quadratic gravity. We will also show that, in the presence of a perfect fluid, the stress-energy tensor will fix both the total mass and the strength of the Yukawa corrections, and the Yukawa terms will be dependent on the equation of state of the fluid;
- in the second subsection we will study solutions close to the origin or a finite non-zero radius with a variation of the Frobenius method; with this technique, the metric is expanded in a power series with integer or fractional exponents and is possible to classify the solutions in different families characterized by the first powers of the series. In particular, close to the origin the metric can be either regular, with a curvature singularity generated by a divergent metric, or with a curvature singularity generated by a vanishing metric; at a finite radius is instead possible to have either an event horizon or a wormhole throat. We will also show how the different families of solutions at the origin appear as the fixed points of dynamical system analysis;
- in the third subsection we will study a metric that is asymptotically vanishing at large distances; while there is not a theoretical reason to introduce this type of solution, the non-linear analysis of a type of wormhole solutions indicates that this is indeed the behavior of the metric in the second patch of the spacetime;
- in the fourth section we will present the numerical methods used to study the solutions in the non-linear regime; in particular, we will present the shooting method,

which is a procedure used to solve boundary value problems that can be, and have been, used to study in detail specific types of solutions. We will show in detail also how to apply this method to black holes, compact stars, and wormhole solutions.

Most of the results presented in this section are common knowledge; we refer to [32, 20, 33, 24, 41] for the discussion on the linearized equations of motion, to [32, 20, 33, 21, 22, 42] for the discussion on the different families of solutions, to [24] for the dynamical system analysis, to [43] for the discussion on asymptotically vanishing solutions and to [24, 41, 43] for the numerical methods.

### 3.1 Linear regime and linearized equations of motion

The linear regime is crucial both for understanding the physics of the solutions and for setting the numerical integration used to study the non-linear regime. The weak field limit is fundamental from a phenomenological point of view, as it has all the information on the Newtonian and post-Newtonian limit of the gravitational interaction in this theory. It is fundamental also from a particle physics point of view, as it includes the classical limit of the particles which mediate the interaction, and from a geometrical point of view, as it includes the information about the global properties of the solutions as their total energy. From a numerical point of view, the weak field limit will be used as the initial condition for the integrations of the parameter space of the theory and as one of the boundaries when studying particular types of solutions.

To derive the linearized equations of motion we consider a perturbation around a flat metric as

$$h(r) = 1 + \epsilon V(r), \quad f(r) = 1 + \epsilon W(r), \quad (3.1)$$

and expand the vacuum equations of motion at linear order in  $\epsilon$ . Setting  $\epsilon = 1$  after the expansion, we get

$$\begin{aligned} \mathcal{G}_\mu^\mu &= - (6\beta\nabla^2 - \gamma) (\nabla^2 V(r) + 2Y(r)) = 0 \\ \mathcal{G}_i^i - \mathcal{G}_t^t &= -4 \left( \beta - \frac{1}{3}\alpha \right) \nabla^2 Y(r) - 2 \left( \beta + \frac{2}{3}\alpha \right) \nabla^2 \nabla^2 V(r) + \gamma \nabla^2 V(r) = 0, \end{aligned} \quad (3.2)$$

where  $Y(r) = r^{-2} (rW(r))'$  and  $\nabla^2$  denotes the three-dimensional Laplace operator. These equations, however, form a first-order equation for  $\mathcal{G}_{rr}$ , namely  $\frac{1}{2} (\mathcal{G}_\mu^\mu + (\mathcal{G}_i^i - \mathcal{G}_t^t)) = 3\mathcal{G}_{rr} + r\mathcal{G}'_{rr}$ ; refining the solutions of (3.2) with  $\mathcal{G}_{rr} = 0$  solves this issue. Having reformulated the equations as combinations of Laplace and Helmholtz operators, it is possible to use standard Fourier transform techniques to solve them analytically. The equations

(3.2) can be partially solved as

$$\begin{aligned} Y(r) &= -\frac{1}{2}\nabla^2 V(r) + \frac{3}{2}m_0^2 \left( S_0^- \frac{e^{-m_0 r}}{r} + S_0^+ \frac{e^{m_0 r}}{r} \right), \\ (\nabla^2 - m_2^2) \nabla^2 V(r) &= (m_0^2 - m_2^2) m_0^2 \left( S_0^- \frac{e^{-m_0 r}}{r} + S_0^+ \frac{e^{m_0 r}}{r} \right), \end{aligned} \quad (3.3)$$

where  $m_2^2 = \gamma/2\alpha$  and  $m_0^2 = \gamma/6\beta$  are the masses of the tensor and scalar modes of the quantum theory. The solutions of (3.3) have long been known [32, 20, 24], and are quite trivial to find, and are

$$\begin{aligned} h(r) &= 1 + C_t - \frac{2M}{r} + 2S_2^- \frac{e^{-m_2 r}}{r} + 2S_2^+ \frac{e^{m_2 r}}{r} + S_0^- \frac{e^{-m_0 r}}{r} + S_0^+ \frac{e^{m_0 r}}{r} \\ f(r) &= 1 - \frac{2M}{r} + S_2^- \frac{e^{-m_2 r}}{r} (1 + m_2 r) + S_2^+ \frac{e^{m_2 r}}{r} (1 - m_2 r) \\ &\quad - S_0^- \frac{e^{-m_0 r}}{r} (1 + m_0 r) - S_0^+ \frac{e^{m_0 r}}{r} (1 - m_0 r). \end{aligned} \quad (3.4)$$

We note that, due to our different ansatz for the metric, we have different signs in the radial component of the metric than in [32, 20] and, in particular, we get corrections to the exact Schwarzschild solution. Imposing asymptotic flatness and fixing a time parametrization (*i.e.* imposing  $h(r) \rightarrow 1$  for  $r \rightarrow \infty$ ), that is setting  $C_t, S_2^+, S_0^+ = 0$  leads to the solution in the weak field regime at large distances

$$\begin{aligned} h(r) &= 1 - \frac{2M}{r} + 2S_2^- \frac{e^{-m_2 r}}{r} + S_0^- \frac{e^{-m_0 r}}{r} \\ f(r) &= 1 - \frac{2M}{r} + S_2^- \frac{e^{-m_2 r}}{r} (1 + m_2 r) - S_0^- \frac{e^{-m_0 r}}{r} (1 + m_0 r), \end{aligned} \quad (3.5)$$

that is the Schwarzschild solution with the addition of exponentially suppressed corrections; the corrections take a Yukawa expression in the Newtonian potential  $\phi(r) \sim \frac{1}{2}(h(r) - 1)$  and, for this reason, we will refer to  $S_2^-$  and  $S_0^-$  as Yukawa charges. The sign of these charges determines if their contribution to the potential is either attractive (whenever they are negative) or repulsive (whenever they are positive). Moreover, the presence of Yukawa terms in the gravitational potential perfectly agrees with the presence of massive modes in the quantum theory and is a cross-check for the calculation. We specify here that the mass parameter  $M$  truly represents the mass of the solutions. Let us consider the total energy of the solution as defined by Arnowitt, Deser and Misner (ADM) [44], which is defined in terms of a 3+1 foliation of an asymptotically flat spacetime, and it is usually written as

$$E = 2\gamma \lim_{\partial\Sigma \rightarrow \infty} \sum_{i,j} \int_{\partial\Sigma} dA n_i (\partial_j g_{ij} - \partial_i g_{jj}), \quad (3.6)$$

with  $n_i$  the unit normal vector to a two-dimensional surface  $\partial\Sigma$  of which the limit at spatial infinity is considered, and the indices  $i, j$  run in the directions orthogonal to this

surface. In our case, we can safely use the weak field limit and then (3.6) is easily evaluated as

$$E \sim 2\gamma \lim_{r \rightarrow \infty} 4\pi r^2 \left( \frac{2M}{r^2} - 2m_2 S_2^- e^{-m_2 r} - m_0 S_0^- e^{-m_0 r} \right) \rightarrow 16\pi\gamma M, \quad (3.7)$$

and then the mass parameter  $M$  is indeed the solution's total energy in the case  $\gamma = 1/16\pi \implies G = 1$ . This also agrees with the Komar definition for spacetimes with asymptotic timelike Killing vectors [45], which is defined as

$$E = -4\gamma \lim_{\partial\Sigma \rightarrow \infty} \int_{\partial\Sigma} dA n_\mu \frac{\kappa^\nu \nabla_\nu \kappa^\mu}{\sqrt{-\kappa_\rho \kappa^\rho}}, \quad (3.8)$$

where  $n_\mu$  the unit normal vector to the surface  $\partial\Sigma$ , and  $\kappa^\mu$  is the asymptotic timelike Killing vector. With no surprise, also this definition becomes in the weak field limit

$$E \sim 4\gamma \lim_{r \rightarrow \infty} 4\pi r^2 \frac{1}{2} \left( \frac{2M}{r^2} - 2m_2 S_2^- e^{-m_2 r} - m_0 S_0^- e^{-m_0 r} \right) \rightarrow 16\pi\gamma M, \quad (3.9)$$

confirming once again that the Yukawa terms do not contribute to the total energy, and the parameter  $M$  really represents the mass of the solutions.

### 3.1.1 Non-vacuum case

To linearize the non-vacuum equations, we consider an energy density and pressure linear in  $\epsilon$ , that is

$$\rho(r) = \epsilon\rho(r), \quad p(r) = \epsilon p(r). \quad (3.10)$$

The equations are then simply

$$\begin{aligned} \mathcal{G}_\mu^\mu &= -\left(6\beta\nabla^2 - \gamma\right)\left(\nabla^2 V(r) + 2Y(r)\right) = \frac{1}{2}\left(-\rho(r) + 3p(r)\right) = \frac{1}{2}T \\ \mathcal{G}_i^i - \mathcal{G}_t^t &= -4\left(\beta - \frac{1}{3}\alpha\right)\nabla^2 Y(r) - 2\left(\beta + \frac{2}{3}\alpha\right)\nabla^2 \nabla^2 V(r) + \gamma\nabla^2 V(r) \\ &= \frac{1}{2}\left(\rho(r) + 3p(r)\right) = \frac{1}{2}\left(T_i^i - T_t^t\right), \end{aligned} \quad (3.11)$$

and can be solved with Fourier transform methods as the vacuum case. The equations (3.11) in Fourier modes look like

$$\begin{aligned} 6\beta\left(k^2 + m_0^2\right)\left(-k^2 \tilde{V}(\vec{k}) + 2\tilde{Y}(\vec{k})\right) &= -\frac{1}{2} \int d^3x' e^{-i\vec{k}\cdot\vec{x}'} \left(\rho(\vec{x}') - 3p(\vec{x}')\right), \\ 4\left(\beta - \frac{1}{3}\alpha\right)k^2 \tilde{Y}(\vec{k}) - 2\left(\beta + \frac{2}{3}\alpha\right)k^4 \tilde{V}(\vec{k}) - \gamma k^2 \tilde{V}(\vec{k}) &= \\ &= \frac{1}{2} \int d^3x' e^{-i\vec{k}\cdot\vec{x}'} \left(\rho(\vec{x}') + 3p(\vec{x}')\right), \end{aligned} \quad (3.12)$$

and are formally solved by

$$\begin{aligned}
V(r) &= -\frac{1}{16\pi^3\gamma} \iint d^3k d^3x' e^{i\vec{k}\cdot(\vec{x}-\vec{x}')} \left[ m_2^2 \frac{\rho(\vec{x}') + 3p(\vec{x}')}{k^2(k^2+m_2^2)} + \right. \\
&\quad \left. + \frac{1}{3} (m_2^2 - m_0^2) \frac{\rho(\vec{x}') - 3p(\vec{x}')}{(k^2+m_2^2)(k^2+m_0^2)} \right], \\
Y(r) &= -\frac{1}{32\pi^3\gamma} \iint d^3k d^3x' e^{i\vec{k}\cdot(\vec{x}-\vec{x}')} \left[ m_2^2 \frac{\rho(\vec{x}') + 3p(\vec{x}')}{k^2+m_2^2} + m_0^2 \frac{\rho(\vec{x}') - 3p(\vec{x}')}{k^2+m_0^2} + \right. \\
&\quad \left. + \frac{1}{3} (m_2^2 - m_0^2) k^2 \frac{\rho(\vec{x}') - 3p(\vec{x}')}{(k^2+m_2^2)(k^2+m_0^2)} \right].
\end{aligned} \tag{3.13}$$

In order to find an asymptotically flat solution, we choose an integration path in momentum space that considers only the  $i m_2$  and  $i m_0$  poles. The remaining spatial integrals take the form of

$$\int d^3x' \frac{f(\vec{x}')}{|\vec{x} - \vec{x}'|}, \quad \int d^3x' \frac{e^{-m|\vec{x} - \vec{x}'|} f(\vec{x}')}{|\vec{x} - \vec{x}'|}, \tag{3.14}$$

and can be partially solved considering  $\rho(\vec{x}') = \rho(s)$  and  $p(\vec{x}') = p(s)$ , where  $s$  is the radial coordinate in the  $\vec{x}'$  variables, and positioning ourselves on the outside of the star where we can safely consider  $r > s$ . We then find as final expression for  $V(r)$  and  $Y(r)$

$$\begin{aligned}
V(r) &= -\frac{1}{r} \int_0^\infty ds 4\pi s^2 \frac{\rho(s) + 3p(s)}{8\pi\gamma} + \frac{e^{-m_2 r}}{r} \int_0^\infty ds 4\pi s^2 \frac{(e^{m_2 s} - e^{-m_2 s})}{24\pi\gamma m_2 s} (2\rho(s) + \\
&\quad + 3p(s)) - \frac{e^{-m_0 r}}{r} \int_0^\infty ds 4\pi s^2 \frac{(e^{m_0 s} - e^{-m_0 s})}{48\pi\gamma m_0 s} (\rho(s) - 3p(s)), \\
Y(r) &= -\frac{e^{-m_2 r}}{r} \int_0^\infty ds 4\pi s^2 \frac{m_2 (e^{m_2 s} - e^{-m_2 s})}{48\pi\gamma s} (2\rho(s) + 3p(s)) + \\
&\quad - \frac{e^{-m_0 r}}{r} \int_0^\infty ds 4\pi s^2 \frac{m_0 (e^{m_0 s} - e^{-m_0 s})}{48\pi\gamma s} (\rho(s) - 3p(s)).
\end{aligned} \tag{3.15}$$

Using the definition  $Y(r) = r^{-2} (r W(r))'$  we find  $W(r)$  as

$$\begin{aligned}
W(r) &= -\frac{C}{r} + \frac{e^{-m_2 r}}{r} (1 + m_2 r) \int_0^\infty ds 4\pi s^2 \frac{(e^{m_2 s} - e^{-m_2 s})}{48\pi\gamma m_2 s} (2\rho(s) + 3p(s)) + \\
&\quad + \frac{e^{-m_0 r}}{r} (1 + m_0 r) \int_0^\infty ds 4\pi s^2 \frac{(e^{m_0 s} - e^{-m_0 s})}{48\pi\gamma m_0 s} (\rho(s) - 3p(s)).
\end{aligned} \tag{3.16}$$

From the remaining equations of motion we can prove that  $C = \int_0^\infty ds 4\pi s^2 \frac{\rho(s) + 3p(s)}{8\pi\gamma}$ . We also note that the integral

$$\int_0^\infty ds 4\pi s^2 p(s) \tag{3.17}$$

represents the total work of the system, that in our case is zero, and we get again as the final result

$$\begin{aligned} h(r) &= 1 - \frac{2M}{r} + 2S_2^- \frac{e^{-m_2 r}}{r} + S_0^- \frac{e^{-m_0 r}}{r} \\ f(r) &= 1 - \frac{2M}{r} + S_2^- \frac{e^{-m_2 r}}{r} (1 + m_2 r) - S_0^- \frac{e^{-m_0 r}}{r} (1 + m_0 r), \end{aligned} \quad (3.18)$$

with, however, an expression for the free parameters in terms of the stress-energy tensor properties

$$\begin{aligned} M &= \frac{1}{16\pi\gamma} \int_0^\infty ds 4\pi s^2 \rho(s) \\ S_{2-} &= \frac{1}{16\pi\gamma} \int_0^\infty ds 4\pi s^2 \frac{\sinh(m_2 s)}{3m_2 s} (2\rho(s) + 3p(s)) \\ S_{0-} &= \frac{1}{16\pi\gamma} \int_0^\infty ds 4\pi s^2 \frac{\sinh(m_0 s)}{3m_0 s} (-\rho(s) + 3p(s)), \end{aligned} \quad (3.19)$$

where the definition of  $M$  agrees with the one found solving the Tolman-Oppenheimer-Volkoff (TOV) equations in General Relativity, and the result agrees with the one found by Stelle in [32] with  $\rho(s) = M\delta(s)/4\pi s^2 = M\delta^3(\vec{x})$  and  $p(s) = 0$ . While this result is valid only in the low energy density and pressure limit, it exhibits an extremely interesting feature: the presence of both the energy density and pressure in the expressions for  $S_2^-$  and  $S_0^-$  renders the gravitational potential sensitive to the physical nature of the fluid, namely to its equation of state. It is indeed manifest that fluids with a traceless stress-energy tensor will have no scalar Yukawa contribution, while to have a zero contribution from the tensor Yukawa term it is necessary to have either a negative energy density or a negative pressure, in agreement with the pure trace nature of the  $R^2$  term and the ghost nature of the  $C^{\mu\nu\rho\sigma}C_{\mu\nu\rho\sigma}$  term.

## 3.2 Series expansion at fixed radius

While the linear theory is crucial to determine the asymptotic gravitational properties of the solutions, their specific physical nature can be categorized by analyzing their behavior close to the origin or a metric singularity (as an event horizon). As extensively explained in [20, 22], it is possible to use a variation of the Frobenius method to find the possible behaviors and to determine different families of solutions. Taking an expansion of the metric functions in the form

$$\begin{aligned} h(r) &= (r - r_0)^t \left[ \sum_{n=0}^N h_{t+n/\Delta} (r - r_0)^{\frac{n}{\Delta}} + \mathcal{O}\left((r - r_0)^{\frac{N+1}{\Delta}}\right) \right] \\ f(r) &= (r - r_0)^s \left[ \sum_{n=0}^N f_{s+n/\Delta} (r - r_0)^{\frac{n}{\Delta}} + \mathcal{O}\left((r - r_0)^{\frac{N+1}{\Delta}}\right) \right], \end{aligned} \quad (3.20)$$

with  $h_0, f_0 \neq 0$ , it is possible to solve the equations of motion order by order in  $(r - r_0)$ . The lowest order equations are called *indicial equations* because, considering that  $h_0$  and  $f_0$  are different from zero by definition, they become equations for the indices  $t$  and  $s$  and determine their admissible values. The higher orders determine the number of the free parameters of the solution for a given set of indices instead. On the contrary, the choice of having whether  $r_0 = 0$  or  $r_0 \neq 0$  and of the value of  $\Delta$  have to be chosen arbitrarily at the beginning of the calculation. Finally, it is possible to classify the solutions as  $(s, t)_{r_0}^\Delta$ . At the present time, the known families are:

Family	Nº of free parameters	Interpretation
$(0, 0)_0^1$	$3 (\rightarrow 0)$	Vacuum
$(-1, -1)_0^1$	$4 (\rightarrow 1)$	Naked singularity/Schwarzschild interior
$(-2, 2)_0^1$	$6 (\rightarrow 3)$	Naked singularity (Holdom star)
$(0, 0)_{r_0}^1$	$6 (\rightarrow 3)$	Generic solution
$(1, 1)_{r_0}^1$	$4 (\rightarrow 1)$	Black hole
$(1, 0)_{r_0}^1$	$3 (\rightarrow 0)$	Symmetric wormhole
$(1, 0)_{r_0}^2$	$6 (\rightarrow 3)$	Non-symmetric wormhole
$(3/2, 1/2)_{r_0}^2$	$3 (\rightarrow 0)$	Unusual black hole
$(4/3, 0)_{r_0}^3$	$4 (\rightarrow 1)$	Unusual wormhole

Table 2: Families of solutions around finite and zero radii in quadratic gravity.

where in the second column we made manifest the number of free parameters after imposing asymptotic flatness, a specific time parametrization, and a zero stress-energy tensor. In this thesis we did not analyze the last two families of solutions, being both particularly exotic and present only in a zero measure region of the parameter space, and we will not put any emphasis on the  $(0, 0)_{r_0}^1$  family, as it represents a generic point of the spacetime with no particular properties.

**$(0, 0)_0^1$  family.** This family in the vacuum has the general form

$$\begin{aligned} h(r) &= h_0 \left( 1 + h_2 r^2 + h_4(h_2, f_2) r^4 + \mathcal{O}(r^6) \right) \\ f(r) &= 1 + f_2 r^2 + f_4(h_2, f_2) r^4 + \mathcal{O}(r^6), \end{aligned} \tag{3.21}$$

with free parameters  $h_0, h_2$  and  $f_2$ , and includes all the solutions with regular curvature in the origin. As shown in [33], we can express all the non-zero terms of the Riemann

tensor on a local orthonormal frame  $R_{abcd} = R_{\mu\nu\rho\sigma} e_a^\mu e_b^\nu e_c^\rho e_d^\sigma$  as

$$\begin{aligned} R_{yzyz} &= \frac{1 - f(r)}{r^2}, \\ R_{xyxy} = R_{xzxz} &= -\frac{f'(r)}{2r}, \\ R_{tyty} = R_{tztz} &= \frac{f(r)h'(r)}{2rh(r)}, \\ R_{txtx} &= \frac{h(r)f'(r)h'(r) - f(r)h'(r)^2 + 2f(r)h(r)h''(r)}{4h(r)^2}, \end{aligned} \tag{3.22}$$

where the other non-zero terms are related by symmetries and  $t, x, y$  and  $z$  are the coordinates in the orthonormal frame, and it can be shown that they are not divergent in the origin if and only if the metric behaves like (3.21). In the vacuum, this family's only asymptotically Minkowski solution is the Minkowski spacetime itself, with  $h_2 = f_2 = 0$ . In the context of compact stars, we want solutions that are regular everywhere, and then the metric in the origin will belong to the  $(0, 0)_0^1$  family. Together with the stress-energy tensor, the metric functions will have the form

$$\begin{aligned} h(r) &= h_0 (1 + h_2 r^2 + h_4(h_2, f_2, \rho_0, p_0) r^4 + \mathcal{O}(r^6)) \\ f(r) &= 1 + f_2 r^2 + f_4(h_2, f_2, \rho_0, p_0) r^4 + \mathcal{O}(r^6), \\ \rho(r) &= \rho_0 + \rho_2(h_2, f_2, \rho_0, p_0) r^2 + \mathcal{O}(r^4), \\ p(r) &= p_0 + p_2(h_2, f_2, \rho_0, p_0) r^2 + \mathcal{O}(r^4), \end{aligned} \tag{3.23}$$

where the parameters  $\rho_0$  and  $p_0$  will be related by the equation of state of the fluid.

**$(-1, -1)_0^1$  family.** This family has the general form

$$\begin{aligned} h(r) &= h_{-1} \left( r^{-1} + \frac{1}{f_{-1}} + h_2 r^2 + h_3(f_{-1}, h_2, f_2) r^3 + \mathcal{O}(r^4) \right), \\ f(r) &= f_{-1} r^{-1} + 1 + f_2 r^2 + f_4(f_{-1}, h_2, f_2) r^3 + \mathcal{O}(r^4), \end{aligned} \tag{3.24}$$

with free parameters  $h_{-1}$ ,  $f_{-1}$ ,  $h_2$  and  $f_2$ . The Schwarzschild metric is found setting  $h_{-1} = f_{-1} = -r_s$  and  $h_2 = f_2 = 0$ , for which also all the terms  $f_n$  and  $h_n$  with  $n > 2$  are equal to zero. This family is singular in the origin, with the curvature invariants going as

$$\begin{aligned} R^2 &\sim C(f_{-1}, h_2, f_2) + \mathcal{O}(r), \\ R^{\mu\nu} R_{\mu\nu} &\sim C(f_{-1}, h_2, f_2) + \mathcal{O}(r), \\ R^{\mu\nu\rho\sigma} R_{\mu\nu\rho\sigma} &\sim r^{-6} + \mathcal{O}(r^{-5}), \end{aligned} \tag{3.25}$$

where the constant  $C$  goes to zero for the Schwarzschild metric. This family of solutions from parameter counting should be present in a zero-measure region of the parameter space, but, as we will see later, this is not the case.

$(-2, 2)_0^1$  **family.** This family has the general form

$$\begin{aligned} h(r) &= h_2 \left( r^2 - \frac{f_{-1}}{f_{-2}} r^3 + h_4 r^4 + h_5 (f_{-2}, f_{-1}, h_4, f_0, f_1) r^5 + \mathcal{O}(r^6) \right), \\ f(r) &= f_{-2} r^{-2} + f_{-1} r^{-1} + f_0 + f_1 r + f_2 (f_{-2}, f_{-1}, h_4, f_0, f_1) r^2 + \mathcal{O}(r^2). \end{aligned} \quad (3.26)$$

with free parameters  $h_2$ ,  $f_{-2}$ ,  $f_{-1}$ ,  $h_4$ ,  $f_0$  and  $f_1$ . The metric in the origin is extremely singular, with curvature invariants going as

$$\begin{aligned} R^2 &\sim r^{-4} + \mathcal{O}(r^{-3}), \\ R^{\mu\nu} R_{\mu\nu} &\sim r^{-8} + \mathcal{O}(r^{-7}), \\ R^{\mu\nu\rho\sigma} R_{\mu\nu\rho\sigma} &\sim r^{-8} + \mathcal{O}(r^{-7}). \end{aligned} \quad (3.27)$$

While it is possible to find a combination of the free parameters for which the Ricci scalar is not diverging, namely the combination for which the solution is a solution of the equations of motion of the Einstein-Weyl sector of the theory, the squared Ricci tensor will always be singular as well as the Riemann tensor squared. This family has the total number of free parameters admissible by the equations, and therefore it is expected to represent a type of solution that populates a large area of the parameter space.

$(1, 1)_{r_0}^1$  **family.** This family has the general form

$$\begin{aligned} h(r) &= h_1 ((r - r_0) + h_2 (f_1, f_2, r_0) (r - r_0)^2 + \mathcal{O}((r - r_0)^3)), \\ f(r) &= f_1 (r - r_0) + f_2 (r - r_0)^2 + f_3 (f_1, f_2, r_0) (r - r_0)^3 + \mathcal{O}((r - r_0)^4), \end{aligned} \quad (3.28)$$

with free parameters  $h_1$ ,  $f_1$ ,  $f_2$  and  $r_0$ . In this case, the Schwarzschild solution simply requires  $h_1 = f_1 = 1/r_0$  and  $f_2 = -1/r_0^2$ , and the curvature invariants are all regular at  $r = r_0$ . The hypersurface defined by  $r = r_0$  is then clearly an event horizon, and the  $(1, 1)_{r_0}^1$  family is the family of black hole solutions. As previously said, black holes are present only in the Einstein-Weyl sector of the theory, and the parameter  $f_2$  can be expressed in terms of  $f_1$  and  $r_0$ . From the number of free parameters, it is already manifest that either an additional requirement forces the presence of a horizon or black holes will not be generic vacuum solutions, having only one free parameter after imposing asymptotic flatness and fixing the time parametrization. Thanks to the corollary 1, this family of solutions is present only in the Einstein-Weyl sector of the theory.

$(1, 0)_{r_0}^1$  **and**  $(1, 0)_{r_0}^2$  **families.** These two families of solutions have the form

$$\begin{aligned} h(r) &= h_0 (1 + h_1 (f_1, r_0) (r - r_0) + \mathcal{O}((r - r_0)^2)), \\ f(r) &= f_1 (r - r_0) + f_2 (f_1, r_0) (r - r_0)^2 + \mathcal{O}((r - r_0)^3), \end{aligned} \quad (3.29)$$

with free parameters  $h_0$ ,  $f_1$  and  $r_0$  for the  $(1, 0)_{r_0}^1$  family, and

$$\begin{aligned} h(r) &= h_0(1 + h_{1/2}(r - r_0)^{1/2} + h_1(r - r_0) + h_{3/2}(h_{1/2}, f_1, h_1, f_{3/2}, r_0)(r - r_0)^{3/2} + \\ &\quad + \mathcal{O}((r - r_0)^2)), \\ f(r) &= f_1(r - r_0) + f_{3/2}(r - r_0)^{3/2} + f_2(h_{1/2}, f_1, h_1, f_{3/2}, r_0)(r - r_0)^2 + \mathcal{O}((r - r_0)^{5/2}), \end{aligned} \quad (3.30)$$

with  $h_0$ ,  $h_{1/2}$ ,  $f_1$ ,  $h_1$ ,  $f_{3/2}$  and  $r_0$  as free parameters for the  $(1, 0)_{r_0}^2$  family. While it is manifest that the  $(1, 0)_{r_0}^1$  family is a subset of the  $(1, 0)_{r_0}^2$  family, it is not trivial that it is not sufficient to require  $h_{1/2} = f_{3/2} = 0$  to derive one family from the other; an additional constraint can be derived by their interpretation as wormholes. Curvature invariants are regular at  $r = r_0$ , and then it is sensible to expect the spacetime to continue after this point. Extending the spacetime to the region  $r < r_0$ , we have the expansions

$$\begin{aligned} h(r) &= h_0 \left( 1 + \tilde{h}_1(\tilde{f}_1, r_0)(r_0 - r) + \mathcal{O}((r_0 - r)^2) \right), \\ f(r) &= \tilde{f}_1(r_0 - r) + \tilde{f}_2(\tilde{f}_1, r_0)(r_0 - r)^2 + \mathcal{O}((r_0 - r)^3), \end{aligned} \quad (3.31)$$

for the  $(1, 0)_{r_0}^1$  family, and

$$\begin{aligned} h(r) &= h_0(1 + \tilde{h}_{1/2}(r_0 - r)^{1/2} + \tilde{h}_1(r_0 - r) + \tilde{h}_{3/2}(\tilde{h}_{1/2}, \tilde{f}_1, \tilde{h}_1, \tilde{f}_{3/2}, r_0)(r_0 - r)^{3/2} + \\ &\quad + \mathcal{O}((r_0 - r)^2)), \\ f(r) &= \tilde{f}_1(r_0 - r) + \tilde{f}_{3/2}(r_0 - r)^{3/2} + \tilde{f}_2(\tilde{h}_{1/2}, \tilde{f}_1, \tilde{h}_1, \tilde{f}_{3/2}, r_0)(r_0 - r)^2 + \mathcal{O}((r_0 - r)^{5/2}), \end{aligned} \quad (3.32)$$

for the  $(1, 0)_{r_0}^2$  family. However, the choice  $f_1 = \tilde{f}_1$  leads to a spacetime with two time coordinates, and the choice  $f_1 \neq \tilde{f}_1$  leads to jumps in the curvature invariants. The only possible choice is then connecting one sheet of spacetime with  $r > r_0$  to another sheet of spacetime with  $r > r_0$ , and the solution is then interpreted as a wormhole. To express manifestly the wormhole nature, we can change the radial coordinate as

$$r = r_0 + \frac{1}{4}\rho^2, \quad (3.33)$$

for which the metric of the two families looks like

$$ds^2 = \left( h_0 + \frac{h_1}{4}\rho^2 + \mathcal{O}(\rho^4) \right) dt^2 + \frac{dr^2}{f_1 + \frac{f_2}{4}\rho^2 + \mathcal{O}(\rho^4)} + \left( r_0 + \frac{1}{4}\rho^2 \right)^2 d\Omega^2 \quad (3.34)$$

for the  $(1, 0)_{r_0}^1$  family, and

$$\begin{aligned} ds^2 &= \left( h_0 + \frac{h_{1/2}}{2}\rho + \frac{h_1}{4}\rho^2 + \mathcal{O}(\rho^3) \right) dt^2 + \frac{dr^2}{f_1 + \frac{f_{3/2}}{2}\rho + \frac{f_2}{4}\rho^2 + \mathcal{O}(\rho^3)} + \\ &\quad + \left( r_0 + \frac{1}{4}\rho^2 \right)^2 d\Omega^2, \end{aligned} \quad (3.35)$$

for the  $(1, 0)_{r_0}^2$  family. Both metrics are manifestly well-behaved around  $\rho = 0$ , and the second sheet of spacetime with  $r > r_0$  is defined by the region  $\rho < 0$ . While the metric in (3.34) is symmetric with respect to the transformation  $\rho \rightarrow -\rho$ , the one in (3.35) is not manifestly symmetric. The  $(1, 0)_{r_0}^2$  family is, however, really not symmetric because requiring a symmetry with  $\sqrt{r - r_0} = \frac{1}{2}|\rho|$  leads once again to jumps in the curvature invariants. The symmetry of the  $(1, 0)_{r_0}^1$  family, finally, adds the additional constraint on the free parameters of the solutions. Fixing a time parametrization and imposing asymptotic flatness then leads to only a single symmetric wormhole solution and to a large area of the parameter space populated by non-symmetric wormholes.

### 3.2.1 Behavior close to the origin and autonomous dynamical system

We include here a parallel analysis done in Einstein-Weyl gravity to assess the behavior of the metric close to the origin. Let us consider a redefinition of the metric functions as

$$h(r) = c_h e^{\eta(r)}, \quad f(r) = c_f e^{\lambda(r)}, \quad (3.36)$$

and, taking into consideration that for both the  $(-1, -1)_0^1$  and the  $(-2, 2)_0^1$  families the function  $f(r)$  diverges in the origin, approximate the equations (2.40) at leading order in  $e^{\lambda(r)}$

$$\begin{aligned} 4 + r((4 + r\eta'(r))(\eta'(r) + \lambda'(r)) + 2r\eta''(r)) &= 0, \\ -8 + r(-4\lambda'(r) + r(\eta'(r) + \lambda'(r))(\lambda'(r) + \eta'(r)(-3 + r\eta'(r) - 2r\lambda'(r))) + \\ &\quad -2r(-2 + r\eta'(r))\lambda''(r) = 0. \end{aligned} \quad (3.37)$$

With a redefinition of the independent variable  $x = -\ln(r)$  and of the metric functions as  $t(x) = \eta'(r)$  and  $s(x) = \lambda'(r)$ , the equations form the autonomous dynamical system

$$\begin{aligned} \frac{ds}{dx} &= -\frac{-2s^2t + s^2 - st^2 - 8s + t^3 - 3t^2 - 8}{2(t-2)}, \\ \frac{dt}{dx} &= -\frac{1}{2}(-st - 4s - t^2 - 2t - 4). \end{aligned} \quad (3.38)$$

The functions  $t(x)$  and  $s(x)$  are expressed in terms of the original metric functions as

$$t = \frac{r h'(r)}{h(r)}, \quad s = \frac{r f'(r)}{f(r)}, \quad (3.39)$$

and they clearly go to the leading exponents of a series expansion close to the origin in the limit  $x \rightarrow \infty$ . The dynamical system indeed has two fixed points, that are  $(t, s) = (-1, -1)$  and  $(2, -2)$ , which correspond to the first exponents of the two non-trivial families of solutions close to the origin. The linear analysis shows that the fixed point  $(-1, -1)$  has one attractive and one marginal direction, while the fixed point  $(2, -2)$

has two attractive directions. The non-linear analysis shown in Fig. 3 confirms that the  $(2, -2)$  fixed point is indeed attractive, while the  $(-1, -1)$  one is attractive for only half of the perturbations.

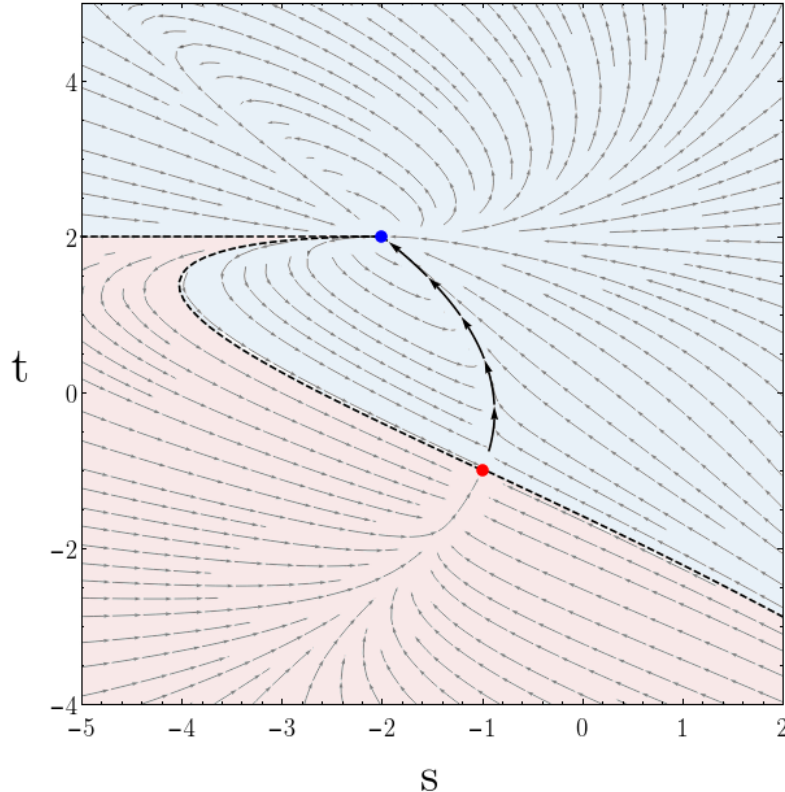


Figure 3: Flow of the running exponents  $t, s$  under the dynamical system (3.38); the arrows point in the direction of decreasing radius. The fixed point  $(-1, -1)$  is in red, while the  $(2, -2)$  is in blue, and the red/blue regions indicate the points that are attracted either to  $(-1, -1)$  or  $(2, -2)$ .

Together with confirming that the  $(-1, -1)_0^1$  and the  $(-2, 2)_0^1$  families are indeed favored as the behavior in the origin for solutions of the theory, the marginally stable nature of the  $(-1, -1)$  fixed point opens the possibility of having logarithmic corrections to the  $(-1, -1)_0^1$  family, which might solve the problem of the number of free parameters of the family that do not agree with the results of the phase diagram.

### 3.3 Non-asymptotically flat solutions

Having introduced in the previous subsection non-symmetric wormhole solutions, it becomes necessary to analyze the possibility of having non-asymptotically flat solutions. In this section we will focus on solutions which are *asymptotically vanishing*, that is where the metric goes as  $h(r) \rightarrow 0$  and  $f(r) \rightarrow \infty$  with  $r \rightarrow \infty$ , and then both the time and radial components of the metric goes to zero at large distances. To study this type of

solution, we write the metric functions as

$$\begin{aligned} h(r) &= \epsilon h_1(r) (1 + \epsilon h_2(r) + \mathcal{O}(\epsilon^2)), \\ f(r) &= \frac{1}{\epsilon f_1(r) (1 + \epsilon f_2(r) + \mathcal{O}(\epsilon^2))}, \end{aligned} \quad (3.40)$$

and expand the equations in powers of  $\epsilon$  starting from  $\mathcal{O}(\epsilon^{-1})$ . Unfortunately, the equations are still not manageable and it is impossible to find a general solution. However, it has been discovered by Alessandro Zuccotti that the functions

$$\begin{aligned} h_1(r) &= C_h r^2 e^{-ar}, \\ f_1(r) &= C_f r^2 e^{-ar}, \end{aligned} \quad (3.41)$$

with  $a$  positive, solve the equations at order  $\mathcal{O}(\epsilon^{-1})$ . This specific form has been found realizing that the metric of non-symmetric wormholes at large distances satisfies with good approximation the equations

$$\begin{aligned} \frac{d}{dr} \left( \frac{h'(r)}{h(r)} \right) &= \frac{2}{r^2}, \\ \frac{d}{dr} \left( \frac{f'(r)}{f(r)} \right) &= -\frac{2}{r^2}. \end{aligned} \quad (3.42)$$

The expression (3.41), moreover, is in agreement at the first order with the one in (3.26) if expanded around a small radius. To go beyond the first order, it is convenient to consider the ansatz for the functions  $h_2(r)$  and  $f_2(r)$

$$\begin{aligned} h_2(r) &= \tilde{h}_2(r) e^{-ar}, \\ f_2(r) &= \tilde{f}_2(r) e^{-ar}, \end{aligned} \quad (3.43)$$

where the expansion in  $\epsilon$  is guaranteed to be well-defined at large distances thanks to the additional powers of  $e^{-ar}$ . The equations of motion at order  $\mathcal{O}(1)$  then become a system of third-order linear differential equations in  $\tilde{h}_2(r)$  and  $\tilde{f}_2(r)$ . The solution can be found in a polynomial form

$$\begin{aligned} \tilde{h}_2(r) &= \tilde{h}_0 + \tilde{h}_1 r + \tilde{h}_2 r^2 + \tilde{h}_3 r^3, \\ \tilde{f}_2(r) &= \tilde{f}_0 + \tilde{f}_1 r + \tilde{f}_2 r^2 + \tilde{f}_3 r^3, \end{aligned} \quad (3.44)$$

where  $\tilde{h}_0$ ,  $\tilde{f}_0$  and  $\tilde{f}_1$  result to be other free parameters, and the other coefficients are completely determined by the six free parameters ( $C_f$ ,  $C_h$ ,  $a$ ,  $\tilde{f}_0$ ,  $\tilde{h}_0$ ,  $\tilde{f}_1$ ). Similarly, it is possible to continue the expansion as

$$\begin{aligned} h(r) &= C_h r^2 e^{-ar} \left( 1 + \tilde{h}_2(r) e^{-ar} + \tilde{h}_3(r) e^{-2ar} + \mathcal{O}(e^{-3ar}) \right), \\ f(r) &= \frac{1}{C_f r^2 e^{-ar} \left( 1 + \tilde{f}_2(r) e^{-ar} + \tilde{f}_3(r) e^{-2ar} + \mathcal{O}(e^{-3ar}) \right)}, \end{aligned} \quad (3.45)$$

where we changed the expansion in  $\epsilon$  in an expansion in  $e^{-ar}$ , which however is well-defined in the large radii limit. The functions  $\tilde{h}_3(r)$  and  $\tilde{f}_3(r)$  at order  $\mathcal{O}(e^{-3ar})$  can be found in a similar way as  $\tilde{h}_2(r)$  and  $\tilde{f}_2(r)$  in terms of six order polynomials, but with no other free parameters appearing. The total number of free parameters of these solutions then results to be six, the correct number needed to connect these solutions with the  $(1,0)_{r_0}^2$  family. Although we do not discuss the convergence of this expansion, we believe that a certain convergence radius  $r^*$  exists, such that for  $r \gg r^*$ , the solution is well approximated by (3.45). The solutions have a curvature singularity at spatial infinity, having curvature invariants going as

$$\begin{aligned} R &\sim C(C_f, a, \tilde{f}_0, \tilde{h}_0, \tilde{f}_1) + \mathcal{O}(e^{-ar}), \\ R^{\mu\nu}R_{\mu\nu} &\sim \mathcal{O}\left(\frac{e^{2ar}}{r^6}\right), \\ R^{\mu\nu\rho\sigma}R_{\mu\nu\rho\sigma} &\sim \mathcal{O}\left(\frac{e^{2ar}}{r^6}\right), \end{aligned} \tag{3.46}$$

where the constant  $C$  goes to zero in the Einstein-Weyl limit. Interestingly, if we look at the squared Weyl tensor, the divergent part of the squared Ricci and Riemann tensors compensate, and we get

$$C^{\mu\nu\rho\sigma}C_{\mu\nu\rho\sigma} \sim 3 \left( \frac{\beta}{\alpha} R + m_2^2 \right)^2 + \mathcal{O}(e^{-ar}) = 3 \left( \frac{\beta}{\alpha} C(C_f, a, \tilde{f}_0, \tilde{h}_0, \tilde{f}_1) + m_2^2 \right)^2 + \mathcal{O}(e^{-ar}) \tag{3.47}$$

which reduces to  $3m_2^4$  in the Einstein-Weyl limit. While it might be simply an interesting curiosity, we believe that it could be relevant for the application of the finite action principle [46], which is getting much attention in recent times for its applications in quadratic theories of gravity [47, 48, 49]

### 3.4 Numerical methods

Having shown in the previous subsections the approximations used to describe the metric in various regimes, we present here the main numerical tools used to investigate the non-linear regime and the global structure of the solutions. Having as one of the main goals the study of isolated objects without a cosmological constant, all the solutions will be described at large distances by the weak field expansion shown in (3.5). To study the solutions qualitatively or to study the phase diagram of the theory, it is sufficient to integrate the equations using (3.5) as initial conditions at a large radius  $x_\infty$ . The integration has been done using the adaptive step size Runge-Kutta integrator D02PDF developed by the N.A.G. group (see <https://www.nag.com> for details) with a tolerance of  $10^{-12}$  for vacuum solutions and of  $10^{-9}$  for non-vacuum solutions. The large radius has then been chosen as  $x_\infty = 18$  in numerical units in order to have Yukawa corrections

larger than the tolerance threshold. The solutions at the origin are classified in terms of the values of the running exponents (3.39) evaluated at a small radius  $r_o = 10^{-3}$ ; this is particularly useful for solutions without no metric singularity for  $r > 0$ , and for the interior of black holes. To study solutions in greater detail, however, it is necessary to use a more refined method, described in the following paragraphs. The method described is also necessary to study black hole solutions, considering that they populate a zero-measure region of the parameter space and, therefore, cannot be analyzed using a simple initial value integration.

### 3.4.1 Shooting method

Choosing a specific type of solution to investigate means choosing one of the behaviors in Table 2 *a priori*, and then specifying an internal boundary. At the numerical level, choosing a specific type of solution to investigate then means solving a boundary value problem for a system of ordinary differential equations. To describe the general procedure, we can recast the equations of motion as a set of  $N$  first-order ordinary differential equations with dependent variables  $\vec{y}$  and independent variable  $x$

$$\frac{d\vec{y}(x)}{dx} = \vec{f}(x, y_1, y_2, \dots, y_N), \quad (3.48)$$

and impose Dirichlet boundary conditions at a certain point  $x_1$ , characterized by  $n_1$  parameters  $V_j$  with  $j = 1, \dots, n_1$

$$\vec{y}(x_1) = \vec{B}_1(x_1, V_1, \dots, V_{n_1}); \quad (3.49)$$

we then impose Dirichlet boundary condition also at another point  $x_2$ , characterized by  $n_2 = N - n_1$  parameters  $V_k$  with  $k = 1, \dots, n_2$

$$\vec{y}(x_2) = \vec{B}_2(x_2, V_1, \dots, V_{n_2}). \quad (3.50)$$

To solve this problem, the shooting method solves exactly (within the numerical integration accuracy) the equations and *then* makes the solution satisfy the boundary conditions, as opposed to the relaxation method in which the boundary conditions are satisfied by a solution which *then* is required to solve the differential equations. To implement the shooting method, we start by defining an  $N$ -dimensional vector  $\vec{V}$  that can be thought as

$$\vec{V} = \begin{pmatrix} \vec{V}_1 \\ \vec{V}_2 \end{pmatrix}$$

where  $\vec{V}_1$  and  $\vec{V}_2$  are respectively an  $n_1$  and  $n_2$ -dimensional vectors with the parameters' values defining the boundary conditions at  $x_1$  and  $x_2$ . We now define two distinct loading subroutine `LOAD1(x1,v1,y)` and `LOAD2(x2,v2,y)` that generate the starting vectors

$\vec{B}(x_1)$  and  $\vec{B}(x_2)$ , and integrate the system (3.48) up to an intermediate point  $x_f$  from both boundaries, using a subroutine `ODEINT(N,yi,y1,xi,xf,derivs)`, defining the vectors  $\vec{y}_L(x_f)$  and  $\vec{y}_R(x_f)$ , where the subscripts  $L$  and  $R$  indicate if the integration has been done from left or right boundary. Finally, the subroutine `SCORE(xf,y1,yr,f)` define a discrepancy vector  $\vec{F}$  as

$$\vec{F} = \vec{y}_L(x_f) - \vec{y}_R(x_f).$$

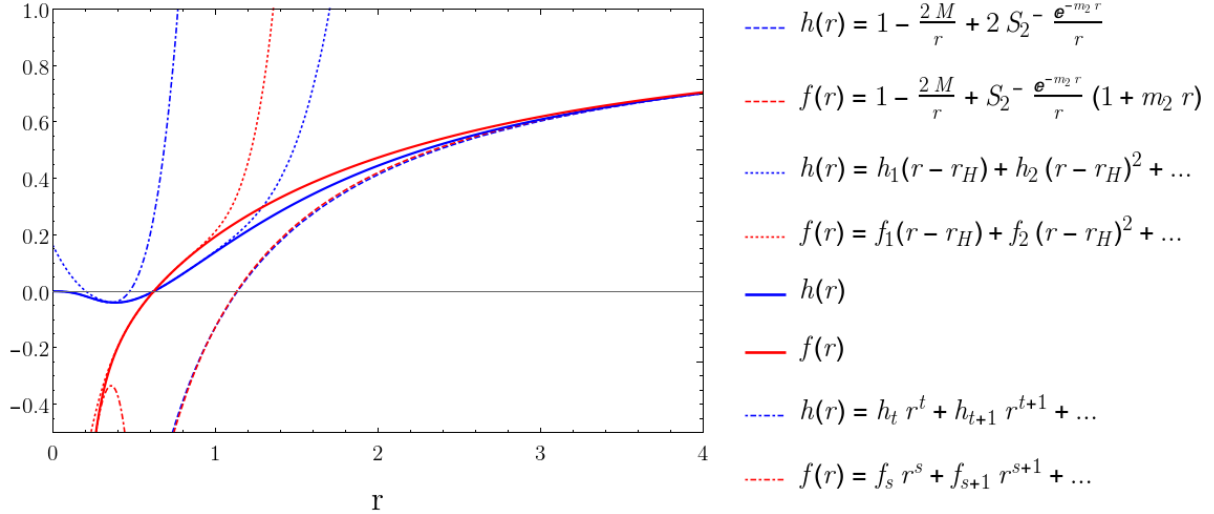
Collecting everything in the subroutine

```
subroutine FUNCV(N,v,f)
    call LOAD1(x1,v,yi)
    call ODEINT(N,yi,y1,x1,xf,derivs)
    call LOAD2(x2,v(n2+1),y)
    call ODEINT(N,yi,yr,x2,xf,derivs)
    call SCORE(xf,y1,yr,f)
    return
end
```

the boundary value problem is reduced to a root-finding problem for the function  $\vec{F}(\vec{V})$  defined by the subroutine `FUNCV(N,v,f)`. Within the work made for this thesis, the subroutine `ODEINT(N,yi,y1,xi,xf,derivs)` has still been defined using the `DO2PDF` integrator, while, for the root-finding algorithm, it has been used the `BROYDN` subroutine found in the `Fortran` version of Numerical Recipes [50], which implements the Broyden's method.

**Shooting method for black holes.** To study black hole solutions we impose, together with the boundary (3.5) at large distances, that the metric satisfies the boundary condition (3.28) at fourth order at a radius  $r_b = r_H + 10^{-3}$ , where  $r_H$  is the radius at which the event horizon is located and is an external parameter. Having specified the value of  $r_H$ , the shooting method then finds the values of  $M$ ,  $S_2^-$ ,  $f_1$  and  $h_1$  for which the boundary value problem is solved with a precision of the root-finding algorithm of  $10^{-6}$  (remember that thanks to the corollary 1 black holes are present only in the Einstein-Weyl sector of the theory); the fitting radius  $r_f$  at which the two integrations are matched does not change the results and have been fixed at  $r_f = r_H + 0.5$  for optimal convergence. The family of black holes is found by varying the value of  $r_H$ , which is the only free parameter left. The series expansion (3.28) can then be extended to the other side of the horizon and be used as the initial value for an additional integration towards the origin. The metric at the origin is then classified using the running exponents (3.39). In Figure 4, finally, we show how the numerical integration interpolates between the various analytical

approximations for a non-Schwarzschild black hole.



**Shooting method for compact stars.** In order to study compact star solutions the boundary (3.5) at large distances is imposed together with the conditions  $\rho(r_\infty) = p(r_\infty) = 0$ , and the other boundary is fixed using the expansion (3.23) at fourth order at a small radius  $r_o = 10^{-3}$ . From the internal boundary the *non-vacuum* equations are integrated up to a radius  $R_*$ , which is an external parameter specified before the integration, while from the external boundary the *vacuum* equations of motion are solved up to the same radius. Matching the vacuum and non-vacuum equations of motion at the radius  $r = R_*$  fixes the star surface precisely at that radius. As in the case of black holes, the parameters  $M$ ,  $S_2^-$ ,  $S_0^-$ ,  $h_0$ ,  $\rho_0$ ,  $p_0$ ,  $h_2$  and  $f_2$  are completely fixed by the integration and the radius  $R_*$  is the only free parameter of the solution, which can be varied to explore the family of solution. Each family is also specified by an equation of state  $p = \mathcal{P}(\rho)$ , which, being an equation with dimensionful parameters, fixes the energy scales of the fluid. As we will discuss in more detail in Subsection 5.4, this will impose some restriction on either the free parameters of the action  $\alpha$  and  $\beta$  or the parameters present in the equation of state. We also note that, in general, the equations of state of physical fluids assume that the energy density is always positive; the shooting method, however, will often produce negative values for the energy density in the integrations before convergence. We specify here that all the equations of state will be in terms of the energy density modulus, which guarantees a well-defined pressure but can slow down the convergence process. In Figure 5, finally, we show how the numerical integration interpolates between the various ana-

lytical approximations for a compact star with the polytropic equation of state  $p = 0.2 \rho^2$  in numerical units.

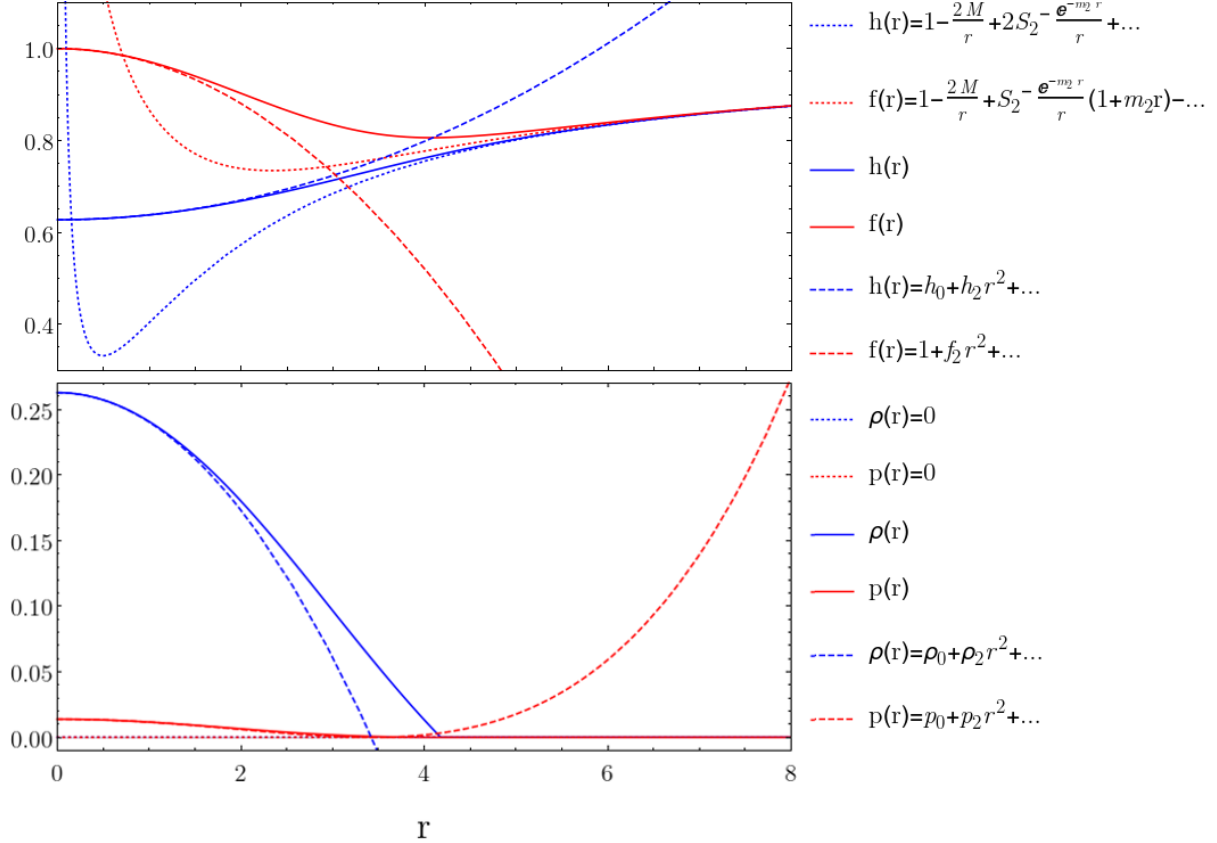


Figure 5: Analytical approximations and the shooting method for a compact star; the non-linear solutions in solid lines interpolates between the asymptotic values (in dotted lines) and the series expansion at the origin (in dashed lines).

**Shooting method for wormholes.** The general procedure for applying the shooting method to wormhole solutions is the same as the one for black holes, that is, a shooting method between the linearized expansion (3.5) at large distances and the series expansion (3.30) close to the metric singularity, and then a further integration with initial conditions set by the boundary at the metric singularity. Applying this method to wormholes, however, requires some additional care due to the presence of three free parameters and a divergent first derivative of the time component of the metric at the throat. We then present the procedure in the case of Einstein-Weyl gravity, where the presence of only two free parameters dramatically simplifies the discussion. The first point of caution is that it is much more convenient to fix the external parameters  $M$  and  $S_2^-$  to have faster convergence in the codes. This required a previous parameter space analysis to find the area where an integration from large radii leads to a metric singularity at a finite radius. After this preliminary scan of the parameter space, using this external integration to

formulate an educated guess for the parameters at the throat is also helpful. Having a divergent derivative of the time component of the metric, the integration from the throat is very sensitive to the specific values of the parameters, in particular to the throat radius and the parameter  $b_{1/2}$  in (3.30). Nonetheless, taking into account these precautions, the shooting method results to be quite efficient also in this case, as can be seen in the example of a wormhole with  $M = 0.6$  and  $S_2^- = -0.2$  in Figure 6.

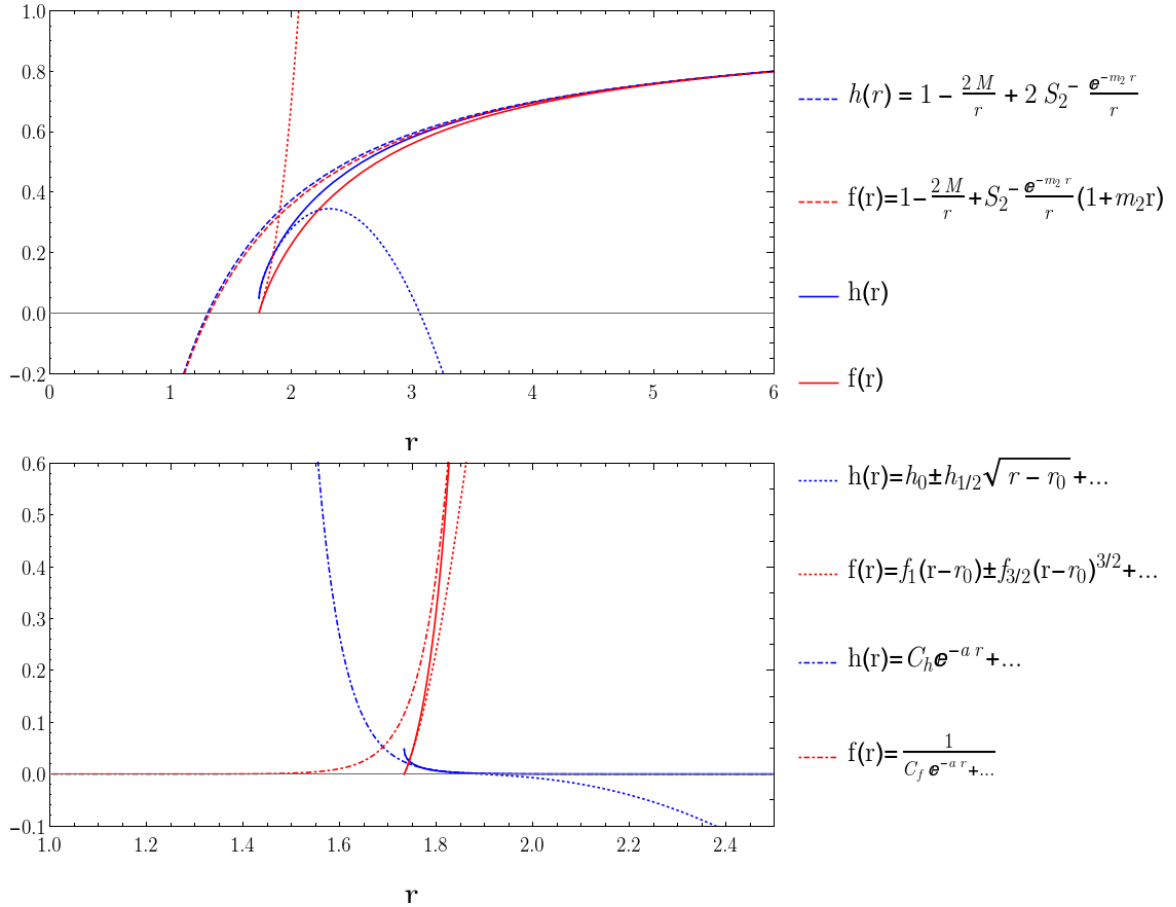


Figure 6: Analytical approximations and the shooting method for wormholes, with the asymptotically flat patch in the top panel and the asymptotically vanishing in the bottom panel; the non-linear solutions in solid lines interpolates between the asymptotic values (in dashed lines) and the series expansion at the throat (in dotted lines), and at the end is fitted by the asymptotically vanishing metric at large distances in the second patch (in dotted-dashed lines).

## 4 The phase diagram of quadratic gravity

As extensively discussed in the previous section, there are many possible behaviors for the metric around the origin or a metric singularity in quadratic gravity. This large variety of short-scale behaviors is contrasted with the single, but very simple and physically intuitive, form of the metric at large distances. The weak field expansion at large distances is indeed characterized by the total mass and the strength of the interactions mediated by the additional massive modes, which characterize the gravitational interaction at large distances. It is then of fundamental relevance to understand how these parameters affect the short-scale behavior of the solutions. To indicate the diagram in which different types of solutions are associated with specific regions of the parameter space, we borrowed the term “phase diagram” from classical Thermodynamics to highlight the fact that we are associating a “microscopical” property of solutions to the parameters describing their “global” external properties.

This section is divided in three parts:

- in the first subsection we will present the phase diagram of vacuum solutions in Einstein-Weyl gravity, which is the most informative two-dimensional reduction of the full quadratic theory. There will be four different types of solutions: black holes with Schwarzschild or non-Schwarzschild nature, naked singularities which are gravitationally repulsive in the origin, naked singularities which are gravitationally attractive in the origin and non-symmetric wormholes; we will show that black holes populate only a zero-measure region of the parameter space and that for large masses most of the solutions will be either wormholes if the Yukawa contribution to the gravitational potential is attractive, or repulsive naked singularities if the Yukawa contribution is repulsive;
- in the second subsection we will present the main issues emerging in the evaluation of the phase diagram of vacuum solutions in the full quadratic theory, namely an inconsistency in the link between the linear and non-linear regimes in the case the masses of the two additional modes are different, and try to extract some physical information nonetheless. The families of solutions will be the same as in Einstein-Weyl gravity and, in this case, also attractive naked singularities will have a relevant role in the region of the phase diagram with solutions with large masses; in particular repulsive singularities will be favored by a repulsive contribution of the massive tensor particle, attractive naked singularities by an attractive contribution of the massive scalar particle, and wormholes by a simultaneous attractive contribution of the tensor particle and a repulsive contribution of the scalar particle;

- in the third subsection we will show the location of non-vacuum solutions in the phase diagram of vacuum solutions; in particular, in Einstein-Weyl gravity they will populate only the region where repulsive naked singularities are present, while in the full quadratic theory they will populate the surface which separates attractive and repulsive naked singularities. In all the cases considered, there will be two points in the phase diagrams which emerge as triple points for all the different types of solutions, of which one of them is Minkowski, and the other represents a solution with a small and positive mass;

The results on the phase diagram of Einstein-Weyl gravity, both for vacuum and non-vacuum solutions, have been published in [51], while the ones on the phase diagram of the full quadratic theory have only been anticipated in [52], but not fully published yet.

## 4.1 The phase diagram of Einstein-Weyl gravity

The phase diagram of vacuum solutions of Einstein-Weyl gravity is depicted in Figure 7. The parameter space is mapped by the values of the mass  $M$  and the Yukawa charge  $S_2^-$ , which characterize the gravitational potential at large distances; we will show here also the part of the phase diagram with  $M < 0$ , and postpone to the following sections the discussion on the possible phenomenological reductions of the diagram. To describe this diagram we will use the term “repulsive mass” for negative values of the parameter  $M$  and attractive or repulsive Yukawa charge for negative or positive values of the parameters  $S_2^-$  respectively; once specified the attractive or repulsive nature of the parameters we will use “large” and “small”, or similar terms, always referring to their modulus. The solutions will be characterized either by the presence of a metric singularity or by the value of the running exponents (3.39)

$$t = \frac{d \log(h(r))}{d \log(r)} = \frac{r h'(r)}{h(r)}, \quad s = \frac{d \log(f(r))}{d \log(r)} = \frac{r f'(r)}{f(r)} \quad (4.1)$$

at a small radius set to  $r_o = 10^{-3}$ . The integration of the equations has been done with a **Fortran** code as described in Section 3.4, and later cross-checked with a code written using the **Wolfram Mathematica** language by Alessandro Zuccotti. The phase diagram is divided into five main regions populated by three different types of solutions:

- Type I solutions: they are characterized by values of the running exponents between  $-0.8$  and  $-1.4$ ;
- Type II solutions: they are characterized by values of the running exponent  $t$  very close to 2 and of the running exponent  $s$  very close to  $-2$ ;

- Type III solutions: they are characterized by a metric singularity at a radius different from zero in which there is a zero of the function  $f(r)$  which *is not* a zero of the function  $h(r)$ .

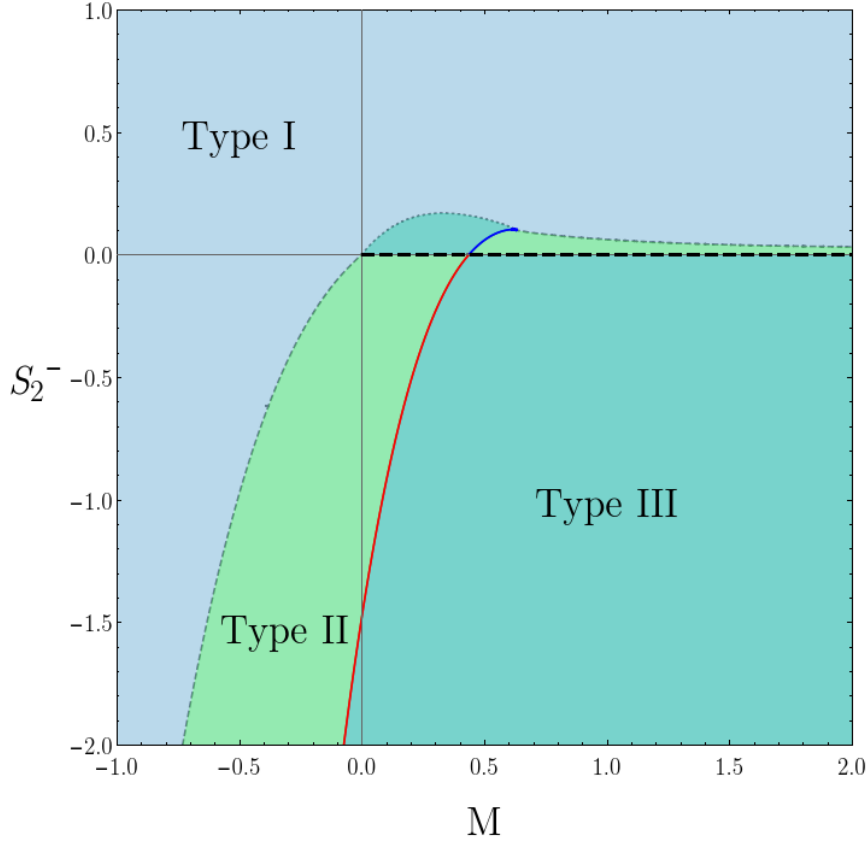


Figure 7: Phase diagram of vacuum solutions of the Einstein-Weyl theory; the dashed black line indicates Schwarzschild black holes, while the solid red and blue lines indicate non-Schwarzschild black holes.

We postpone to Section 5 a detailed description of these solutions; however, now we will sketch their main properties and the relation of their location in the phase diagram with the asymptotic parameters.

**Type I.** The first type of solution seems to belong to the  $(-1, -1)_0^1$  family; however, we have found relevant discrepancies from the expected value  $t = s = -1$  even at radii smaller than  $r_o = 10^{-3}$ . Moreover, these solutions cover an area of the phase diagram, while the number of free parameters of the  $(-1, -1)_0^1$  family suggests that they should occupy a one-dimensional region. These considerations make evident that type I solutions should belong to some correction of the  $(-1, -1)_0^1$  family, but with the same leading order. In [33] a non-Frobenius family that shares the same leading order of the  $(-1, -1)_0^1$  family but with logarithmic corrections and with one additional free parameter has been found in the full quadratic theory, but in Einstein-Weyl gravity none of such family has been discovered. Sharing the leading behavior of  $(-1, -1)_0^1$  solutions, however, we can still infer

that they are naked singularities with a repulsive gravitational force close to the origin, and we will refer to them as “repulsive naked singularities”. Indeed, they populate the area where both the mass and the Yukawa charge are repulsive, the area where the mass is repulsive and the Yukawa charge is attractive but with a repulsive mass larger than the attractive Yukawa charge, and the area where the mass is attractive and the Yukawa charge is repulsive but with a repulsive Yukawa charge larger than the attractive mass.

**Type II.** The second type of solutions instead truly belong to the  $(-2, 2)_0^1$  family, having found no relevant discrepancies from  $(s, t) = (-2, 2)$  (except for the regions close to the transition with other families) and, in contrast with type I solutions, the area populated by these solutions agrees with the number of free parameters of the  $(-2, 2)_0^1$  family. Belonging to this family, they also represent naked singularities, but with an attractive gravitational force close to the origin, and we will refer to them as “attractive naked singularities”. As opposed to their repulsive counterparts, they populate a region with an attractive mass and repulsive Yukawa charge but with a mass much larger than the Yukawa charge, a region with repulsive mass and attractive Yukawa charge but with a Yukawa charge much larger than the repulsive mass, and finally a small region with an attractive mass and an attractive Yukawa charge, but where both take small values.

**Type III.** The third type of solutions, in principle, might belong to the  $(1, 0)_{r_0}^1$  or the  $(1, 0)_{r_0}^2$  families, but the number of the free parameters eliminates the possibility of having an area populated by  $(1, 0)_{r_0}^1$  solutions. Finally, the code which implements the shooting method with a  $(1, 0)_{r_0}^2$  boundary converges in all the regions shown populated by type III solutions in Figure 7, confirming that this is indeed their behavior close to the metric singularity. We will refer to these solutions as either wormholes, non-symmetric wormholes, or the contracted form no-sy WHs. They populated almost all the areas where both the mass and the Yukawa charge are attractive, with the exception of a region where both are small (occupied by type II solutions), a small region with attractive mass and repulsive Yukawa charge, but with small values of both parameters, and a region with repulsive mass and attractive Yukawa charge, but with the Yukawa charge being significantly larger than the repulsive mass.

**Black holes.** Black holes populate only zero-measure regions of the phase diagram and then cannot be found by a simple scan of the parameter space, but it is necessary to use the shooting method. Schwarzschild black holes are shown in the dashed black line in Figure 7, while non-Schwarzschild black holes are shown with the solid red and blue lines, where the two different colors indicate whether they have negative or positive

Yukawa charge and will be useful in the discussion of Section 6 and 7. Their specific location is on the lines which separate attractive naked singularities (type II) and non-symmetric wormholes (type III), and stressing the phase diagram analogy they represent the phase transition between the two different types of solutions. Being on this separation lines, Schwarzschild black holes always have an attractive mass and zero Yukawa charge, and non-Schwarzschild black holes have either an attractive mass and repulsive Yukawa charge, but both being small, an attractive mass and attractive Yukawa charge, but still both being small, or a repulsive mass and attractive Yukawa charge, but with no bounds for both of them and with a Yukawa charge always larger than the repulsive mass.

Let us now focus on the most interesting part of the phase diagram from a phenomenological point of view, which is the one where solutions have a large attractive mass. The first point emerging is that black holes can have only Schwarzschild nature, they are present only in a zero-measure region of the parameter space and therefore are not expected to be the general vacuum solutions of Einstein-Weyl gravity, unless specific arguments are taken into account to require the existence of a horizon. For an attractive contribution of the Yukawa term in the asymptotic potential, the solutions will always be non-symmetric wormholes while, for a repulsive contribution, they will always be naked singularities; the main difference here is that for very small values of the repulsive Yukawa charge the naked singularity will be attractive and in the other cases it will be repulsive.

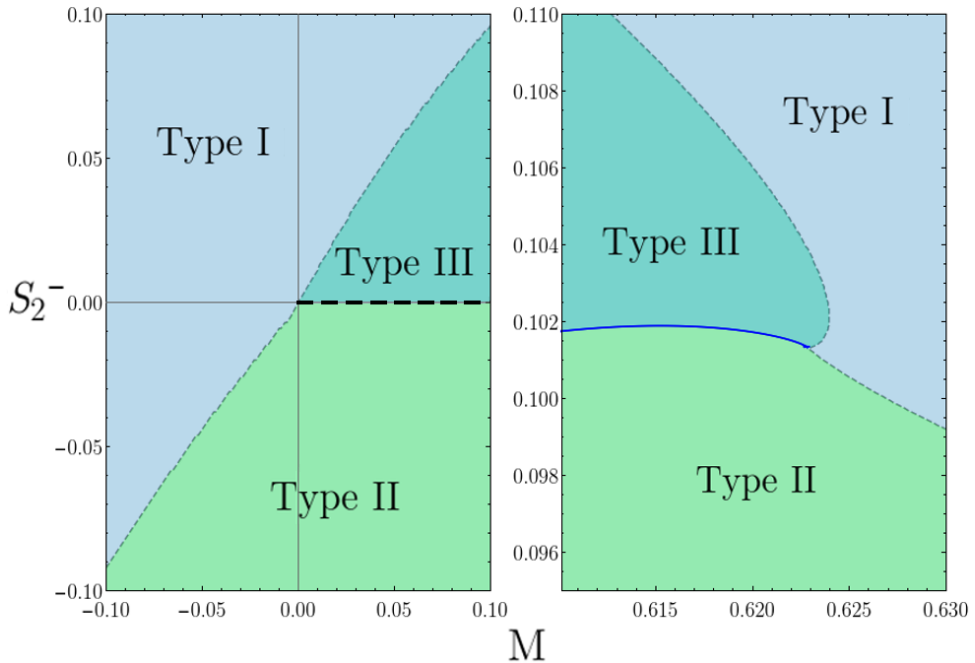


Figure 8: Triple points in the phase diagram of vacuum solutions of the Einstein-Weyl theory; the dashed black line indicates Schwarzschild black holes, while the solid red and blue lines indicate non-Schwarzschild black holes.

Stressing a little bit more the phase diagram analysis, there are two “triple points” in the diagram, shown in detail in Figure 8. The first corresponds to the Minkowski spacetime  $M = 0, S_2^- = 0$ , while the second one, which we will call massive triple point from now on, is located at  $M \simeq 0.623, S_2^- \simeq 0.102$  in our numerical units. Both triple points are at the border of the areas populated by type I, type II, black hole, and wormhole solutions; moreover, the Minkowski one corresponds to the point where the horizon of Schwarzschild black holes goes to zero, while the massive triple point is where the horizon of non-Schwarzschild black holes goes to zero. Taking into account these properties, it seems that the Minkowski flat space is not unique as it is in General Relativity and could be not the only “true vacuum” of the theory; the presence of this massive triple point suggests that there might be a sort of ghost condensate vacuum, that might have relevant consequences on the study of quantum fluctuations.

## 4.2 The phase diagram of quadratic gravity

Finding the phase diagram for the full quadratic theory was one of the objectives of this thesis. Unfortunately, as mentioned at the beginning of this section, an inconsistency in the link between the linear and non-linear regimes in the full theory appeared. In the weak field limit for the metric (3.5), two different Yukawa terms with two different masses are present; having two different masses results in an ill definition of the linear solution, opening possibilities as

$$\frac{e^{-m_0 r}}{r} < \frac{e^{-m_2 r}}{r^2} \quad (4.2)$$

for  $m_0 > m_2$  and  $r$  large enough, which means having

$$\mathcal{O}(\epsilon) < \mathcal{O}(\epsilon^2). \quad (4.3)$$

We specify here that even if in principle it could have been possible also to have a situation as

$$\frac{e^{-m_2 r}}{r} < \frac{1}{r^2} \quad (4.4)$$

for  $r$  large enough, a term with no exponentials would be proportional only to the  $M$  parameter and then, being equal to a non-linear contraction of the Schwarzschild metric, will have a vanishing contribution to the Ricci tensor and will not appear in the equations of motion. Nonetheless, the ill behavior of the linearized metric with two exponentials persists. The most immediate consequence of this inconsistency is that, for  $m_0 > m_2$ , it is not possible to find a phase diagram where the section  $S_0^- = 0$  is equal to the phase diagram of Einstein-Weyl gravity. As a first step in the discussion, we present in 9 the phase diagram of the  $R + R^2$  theory, which is much simpler than the one of Einstein-Weyl gravity. Type I solutions, which are repulsive naked singularities, populate

the majority of the area with a repulsive mass, with the exception of an attractive Yukawa charge larger than the repulsive mass, and are present only in a small portion of the area with an attractive mass and only if a much larger repulsive Yukawa charge is present. Type II solutions, which are attractive naked singularities, still populate the area with a repulsive mass and an attractive Yukawa charge but with a mass smaller than the Yukawa charge, and all the areas with an attractive mass and an attractive Yukawa charge. Type III solutions, which are non-symmetric wormholes, instead populate almost all the area with an attractive mass and a repulsive Yukawa charge, in contrast to what happens in Einstein-Weyl gravity. In agreement with theorem 1 there are only Schwarzschild black holes, which are on the  $S_0^- = 0$  line that is the intersection with the Einstein-Weyl theory. Also in this case, black holes appear only as transitions between wormholes and attractive naked singularities, and the only triple point of the diagram is the Minkowski spacetime. It is interesting to note that, as in Einstein-Weyl gravity, in the large mass limit half of the phase diagram is populated by non-symmetric wormholes, while in contrast to Einstein-Weyl gravity, the other half is populated by attractive naked singularities instead of repulsive ones.

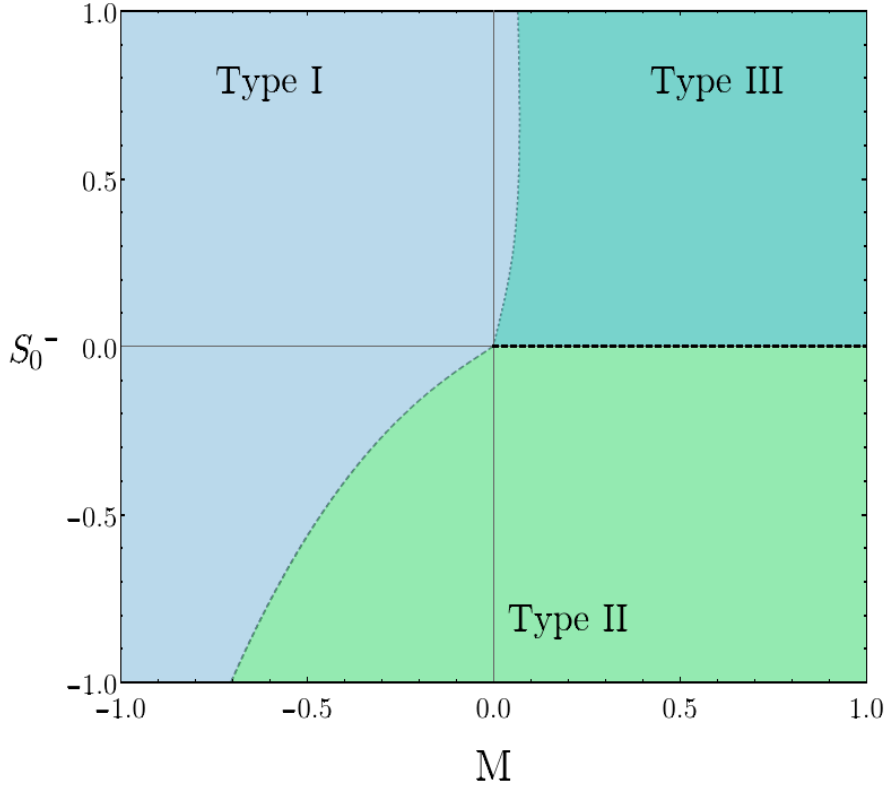


Figure 9: Phase diagram of vacuum solutions of  $R + R^2$  gravity; the three types of solutions are the same as in Einstein-Weyl gravity and the dashed black line indicates Schwarzschild black holes.

To understand how the scalar and tensor Yukawa terms interact one with the other, we can analyze the phase diagram of the full quadratic theory in the specific case  $m_0 = m_2$

where the linearized metric is well-defined, that we present in Figure 10. To clarify the discussion, we superimposed the phase diagram of Einstein-Weyl gravity over the  $S_0^- = 0$  sector of the parameter space and the one of  $R + R^2$  gravity over the  $S_2^- = 0$  sector, with a perfect agreement. Similarly to the previous cases, the three main volumes of the diagram are populated by the same types of solutions, namely attractive and repulsive naked singularities, and non-symmetric wormholes. Black holes are still present only in one-dimensional lines on the  $S_0^- = 0$  section of the surface which separate attractive naked singularities and non-symmetric wormholes.

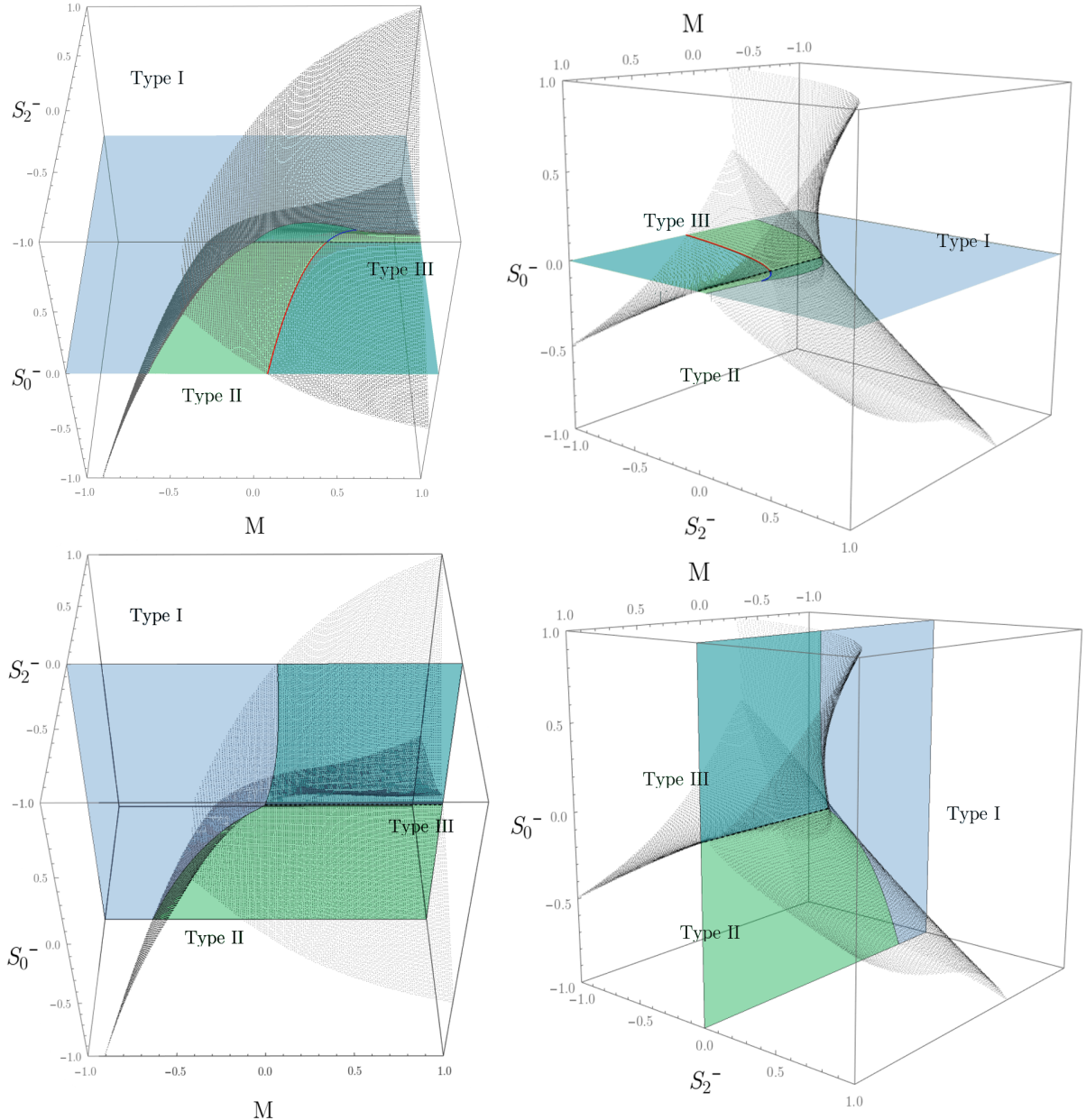


Figure 10: Phase diagram of vacuum solutions of quadratic gravity in the case  $m_0 = m_2$  with superimposed the phase diagram of the Einstein-Weyl and the  $R + R^2$  sectors; the three types of solutions are the same of Einstein-Weyl gravity, the dashed black line indicates Schwarzschild black holes and the solid red and blue lines indicate the non-Schwarzschild ones.

The phase diagram is then populated as follows:

- Type I solutions are still the solutions more present in the area with a repulsive mass; in particular, they are more present whenever also the Yukawa charges have a repulsive contribution; for an attractive mass, they are present only if the tensor Yukawa charge  $S_2^-$  is repulsive, while the scalar charge  $S_0^-$  can be either attractive or repulsive but with an intensity always smaller than the tensor charge;
- Type II solutions mainly populate the area where both the mass and the scalar charge are attractive, while for them to be repulsive they have to be contrasted by a stronger attractive contribution of the tensor Yukawa charge; as the mass increase, if the tensor charge is attractive the scalar charge has to be larger, while if the tensor charge is repulsive the scalar charge can be smaller;
- Type III solutions mainly populate the area where both the mass and the tensor charge are attractive, but the scalar charge is repulsive, while for them to be repulsive they have to be compensated by a much stronger repulsive contribution of the scalar charge; as the mass increase, they can be present both for attractive and repulsive scalar and tensor Yukawa charges, especially in the regions where the repulsive scalar charge is larger than the repulsive tensor charge, or the attractive tensor charge is larger than the attractive scalar charge.

To focus once again on the part of the phase diagram with a large attractive mass, repulsive naked singularities are present approximately when  $-S_2^- \lesssim S_0^- \lesssim S_2^-$ , attractive naked singularities when  $S_0^- \lesssim \min(-S_2^-, S_2^-)$  and non-symmetric wormholes whenever  $S_0^- \gtrsim S_2^-$ . The triple points of the phase diagram of Einstein-Weyl gravity are now the intersections with the surface of zero scalar Yukawa charge of conjunction line of the surfaces that separate the three types of solutions; they still are the only points where the three generic vacuum solutions also meet with black holes. Regardless of the specific behavior of this phase diagram, we can track down some common behavior of the effects of the three asymptotic parameters, that is:

- a repulsive mass  $M < 0$  will always favor repulsive naked singularities, and the values of the Yukawa charges have little effect;
- with an attractive mass, a repulsive tensor charge  $S_2^- > 0$  favors repulsive naked singularities while an attractive tensor charge  $S_2^- < 0$  favors non-symmetric wormholes;
- with an attractive mass, a repulsive scalar charge  $S_0^- > 0$  favors non-symmetric wormholes while an attractive scalar charge  $S_0^- < 0$  favors attractive naked singularities.

From a physical point of view, we expect that changing the ratio between the two masses  $m_0$  and  $m_2$ , the Yukawa with a bigger mass should have less effect, and the phase diagram should become more similar to one of the two bi-dimensional cases 7 or 9; as an example, if we consider the case  $m_2 \gg m_0$  we expect that varying the tensor charge  $S_2^-$  will have little effect and the phase diagram will become the translation solid generated by the phase diagram 9 on the  $S_2^-$  direction. Unfortunately, this is not the case: as we can see in Figure 11, where we show the phase diagram in the case  $m_0 = \frac{2}{3}m_2$ , the tensor charge has less effect indeed, and the families of solutions are not influenced that much by the values of  $S_2^-$ , but the phase diagram is not a translation of the one of  $R + R^2$  gravity.

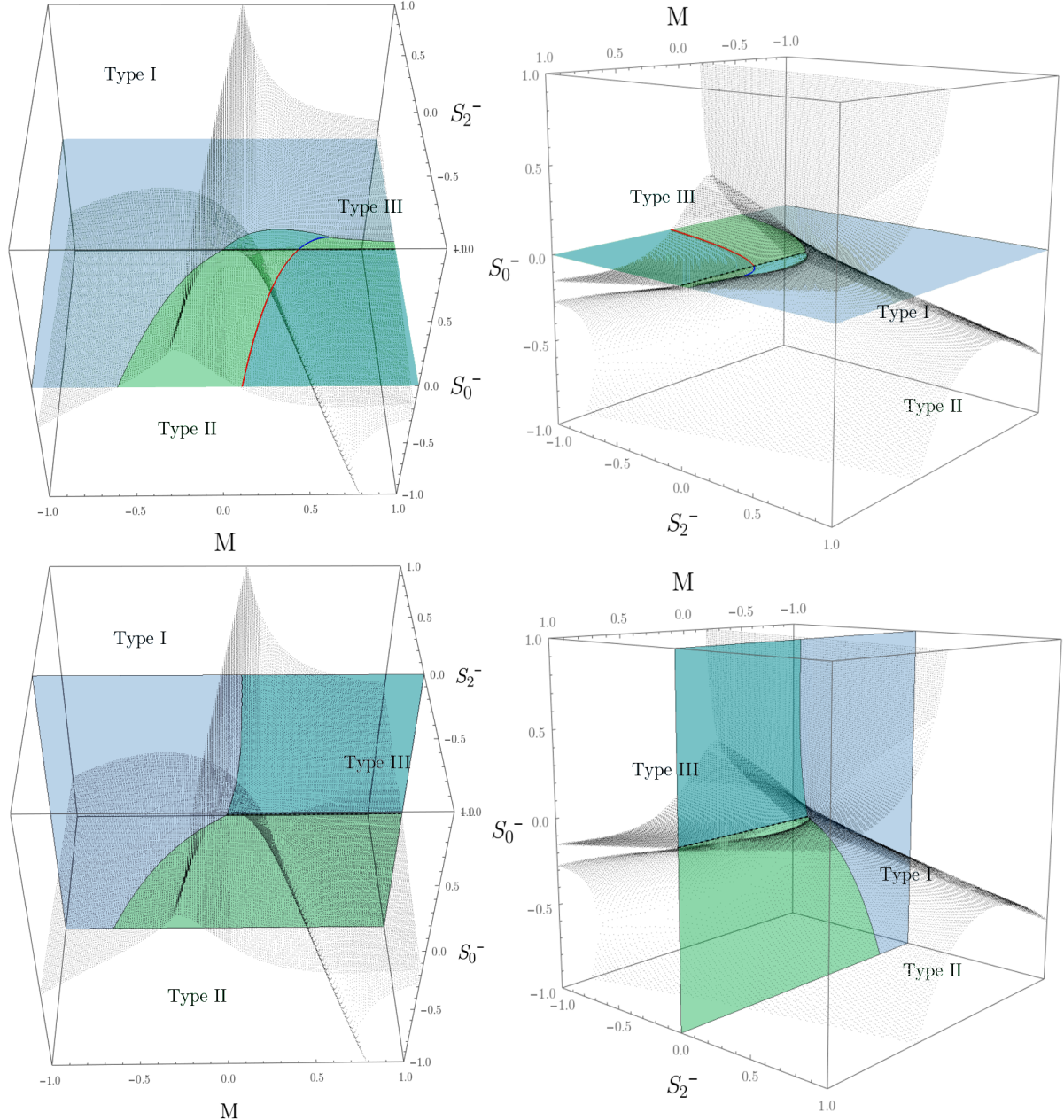


Figure 11: Phase diagram of vacuum solutions of quadratic gravity in the case  $m_0 = \frac{2}{3}m_2$  with superimposed the phase diagram of the Einstein-Weyl and  $R + R^2$  sectors.

Moreover, the sector  $S_2^- = 0$  does not coincide anymore with the one of  $R + R^2$  gravity. The sector  $S_0^- = 0$ , instead, still coincides with the Einstein-Weyl gravity phase diagram. In particular, what happens is that for an attractive scalar charge, repulsive and attractive naked singularities change their places in the phase diagram. Something similar happens in the case of  $m_0$  larger than  $m_2$ , as can be seen in Figure 12, where we present the phase diagram in the case  $m_0 = \frac{3}{2}m_2$ .

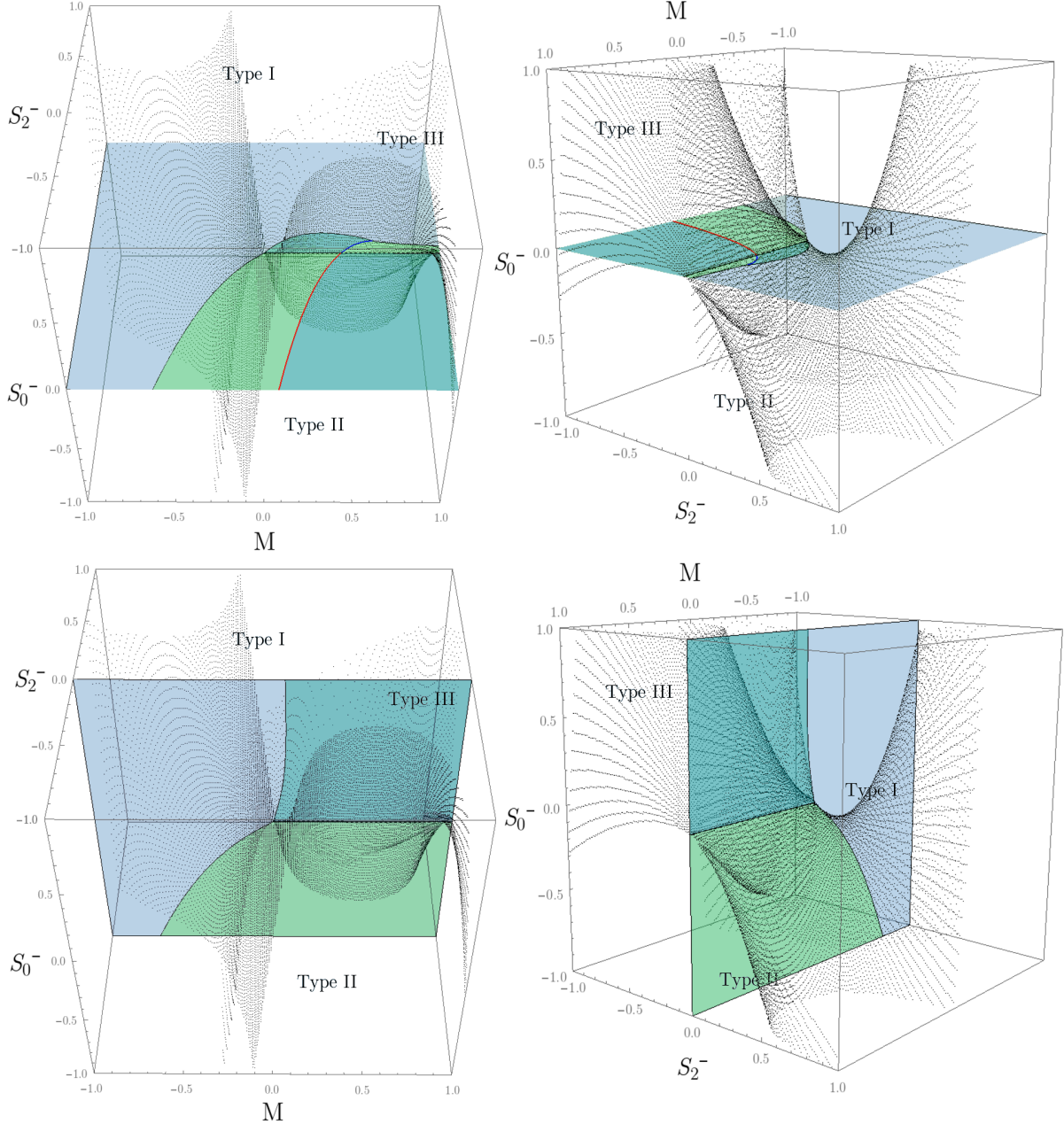


Figure 12: Phase diagram of vacuum solutions of quadratic gravity in the case  $m_0 = \frac{3}{2}m_2$  with superimposed the phase diagram of the Einstein-Weyl and  $R + R^2$  sectors.

Here the values of the scalar charge  $S_0^-$  have little effect on the families of solutions; still, we are not able to find the phase diagram of Einstein-Weyl gravity in the  $S_0^- = 0$  sector,

while we find (approximately) the phase diagram of  $R + R^2$  gravity in the  $S_2^- = 0$  sector. The phase diagram, in this case, has a quite complicated structure that we believe is not particularly insightful to investigate deeply. As previously said at the beginning of this section, we believe these inconsistencies are due to the ill definition of the linear theory in the case of different masses. While having the phase diagram in the Einstein-Weyl, the  $R + R^2$ , and  $m_0 = m_2$  cases can shed light on the phase diagram of the full theory in the generic case, this ill-definition of the linearized theory has to be solved.

### 4.3 Non-vacuum solutions in the phase diagram

Leaving the safe place of General Relativity, where the only vacuum solution is the Schwarzschild metric and non-vacuum solutions also appear as Schwarzschild solutions outside their surface, it becomes a non-trivial and crucial point to understand which type of vacuum solutions describes the exterior of compact stars. We remember that while the vacuum solutions of General Relativity, *i.e.* with  $R_{\mu\nu} = 0$ , are also vacuum solutions of quadratic gravity, the non-vacuum solutions of General Relativity, *i.e.* with  $R_{\mu\nu} = \frac{1}{2}(T_{\mu\nu} - \frac{1}{2}Tg_{\mu\nu})$ , are *not* solutions of quadratic gravity. For the same reason, we do not expect the non-vacuum solution of Einstein-Weyl gravity to be related to the ones of the full theory. Nonetheless, we will present both cases as they complete the discussion made in the previous subsections.

**Einstein-Weyl gravity.** The location of some families of non-vacuum solutions in Einstein-Weyl gravity is shown in Figure 13; in particular, we present solutions generated by self-gravitating fluids with polytropic equations of state

$$p = k_0 \rho^\Gamma, \quad (4.5)$$

with different values of  $k_0$  and  $\Gamma$ . In particular, changing the polytropic exponent  $\Gamma$  changes the shape of the relation between the  $M$  and  $S_2^-$  parameters while changing  $k_0$ , being related to the physical energy scales of the fluid, has a scaling effect on this relation. Nonetheless, there are some important common features:

- the non-vacuum solutions are present only in the area populated by repulsive naked singularities;
- as the star radius decreases, the solutions converge to the massive triple point of the phase diagram.

The main qualitative difference is that the solutions with  $\Gamma = 2$ , for which a vanishing central pressure is reached at a finite radius and with vanishing mass, also converge to

the Minkowski triple point, while the solutions with  $\Gamma = 4/3, 5/3$ , for which a vanishing central pressure instead is reached in the large star radius limit and with a constant mass, seem to have a divergent value of the Yukawa charge. However, we have to note that for very large star radii, the integration becomes unstable because the weak field limit is not reliable anymore.

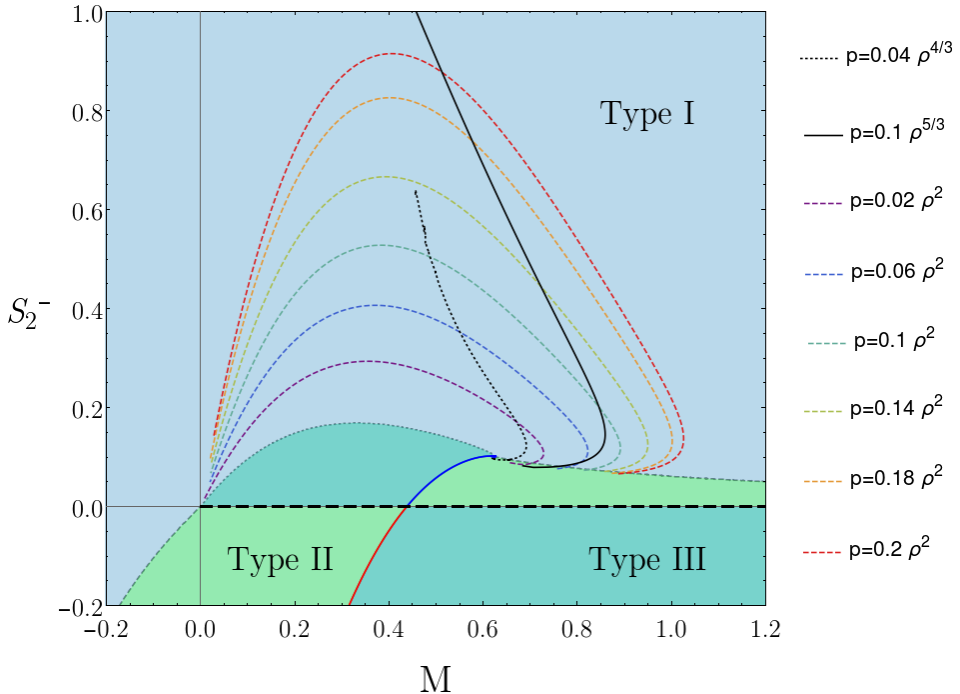


Figure 13: Location of non-vacuum solutions on the phase diagram of Einstein-Weyl gravity; all the fluid equations of state have been modeled using polytropic equations, the dashed colored lines indicate e.o.s. with  $\Gamma = 2$  and different  $k_0$ , while the solid and dotted black lines indicate e.o.s. with  $\Gamma \neq 2$ .

The location of the non-vacuum solution in the phase diagram sheds new light on type I solutions that did not have a physical interpretation until now. They appear, in fact, as the external field of compact objects and are a candidate to be the generic observed solution in a quadratic theory of gravity. The second important aspect emerging from Figure 13 is that the two triple points of vacuum solutions play a special role also for non-vacuum solutions. While the Minkowski flat space remains an attractive point for solutions that vanish for vanishing energy density (a property which is not valid for all the equations of state also in General Relativity), the massive triple point is an attractor for stars with a divergent central energy density independently of the equations of state of the fluid.

**Full quadratic theory.** We show the location of non-vacuum solutions in quadratic gravity only in the specific case  $m_0 = m_2$  in Figure 14. With respect to the Einstein-Weyl theory, there are one major difference and one major similarity:

- *in contrast to* Einstein-Weyl gravity, non-vacuum solutions do not have a corresponding vacuum solution family, as they are constrained to the surface which separates attractive and repulsive naked singularities;
- *similarly as in* Einstein-Weyl gravity, the solutions converge to the massive triple point of the phase diagram as the star radius decreases.

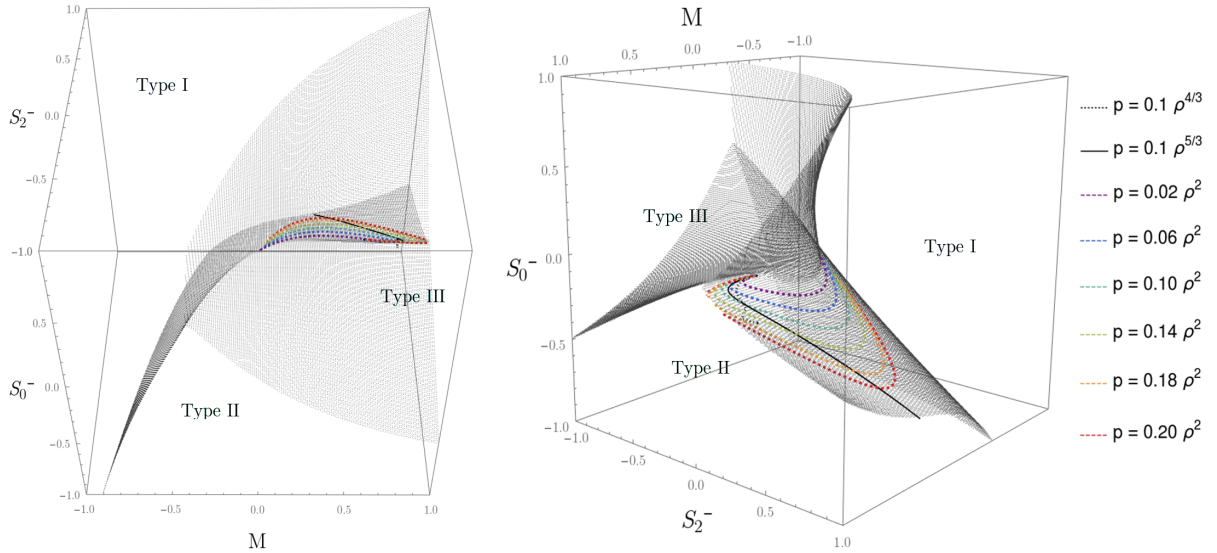


Figure 14: Location of non-vacuum solutions on the phase diagram of quadratic gravity in the case  $m_0 = m_2$ ; all the fluid equations of state have been modeled using polytropic equations, the dashed colored lines indicate e.o.s. with  $\Gamma = 2$  and different  $k_0$ , while the solid and dotted black lines indicate e.o.s. with  $\Gamma \neq 2$ .

The interpretation of repulsive naked singularities as the vacuum solutions representing the asymptotic field of a compact star has been quite short-lived, as now no family has this role. It is still interesting to note that the types of solutions present also in General Relativity, that is, black holes and compact stars, are present only in the surfaces that separate different solutions.

## 5 Solutions of quadratic gravity

In the previous section, we showed how the asymptotic gravitational properties affect the metric in the short-scale regime. However, we just sketched the properties of the different solution types without going into detail. In this section, instead, we will try to give a complete overview of the global properties of the metric for various solutions of quadratic gravity, leaving some specific topics to the following sections. These solutions are collected in Figure 15 in the particular case of Einstein-Weyl gravity, where we also stressed the relevance of the Yukawa charges on the solutions setting the same mass  $M$  for all the types of solutions. In the last subsection we will also present the specific properties of analytical solutions of General Relativity whenever they are considered as solutions of scale-invariant gravity.

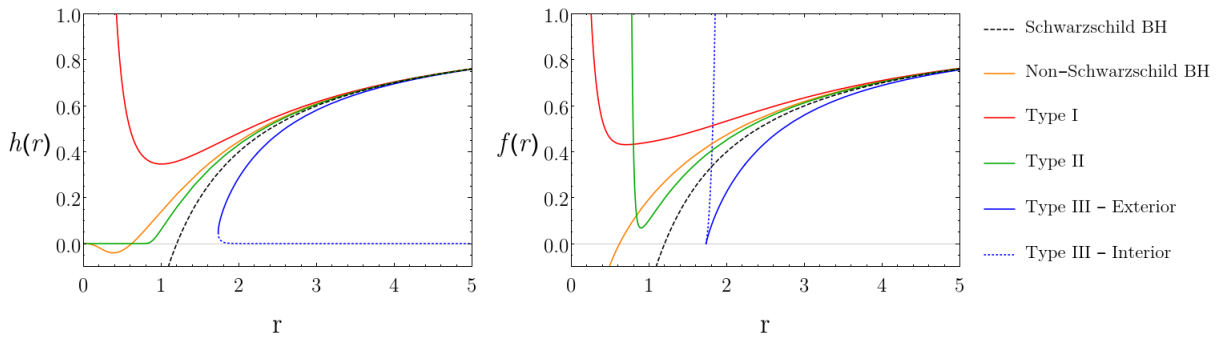


Figure 15: Vacuum solutions in the case of Einstein-Weyl gravity with mass  $M = 0.6$ . The Schwarzschild BH in dashed black has  $S_2^- = 0$ , the non-Schwarzschild BH in orange has  $S_2^- = 0.101$ , the type I solution in red has  $S_2^- = 0.2$ , the type II solution in green has  $S_2^- = 0.075$ , and the type III solution in dotted and solid blue has  $S_2^- = -0.2$ .

This section is divided in five parts:

- in the first subsection we will present black hole solutions, with a focus on the non-Schwarzschild black holes present in quadratic gravity; we will show that it is possible to have black holes for which the Yukawa term in the potential is attractive and black holes for which it is repulsive, which have respectively a divergent and a vanishing metric in the origin. The most interesting characteristic of this type of black hole, however, is that the mass decreases and the surface gravity increases as the horizon radius increases, precisely the opposite of what happens in General Relativity;
- in the second subsection we will describe the two types of naked singularities present in the theory, showing some generic metric forms, their causal structure and discussing the behavior of geodesics. Repulsive naked singularities present an infinite potential barrier that prevents geodesics from reaching it; nonetheless, this means

also that outgoing geodesics will get to spatial infinity with an extreme amount of energy. Attractive naked singularity, on the contrary, can be reached by all ingoing geodesics; outgoing geodesics, instead, need an extreme amount of energy to escape the singularity;

- in the third subsection we will describe non-symmetric wormholes, showing also in this case some generic metric forms, their causal structure and discussing the behavior of geodesics. We will show that these wormholes connect an asymptotically flat spacetime with another one that is asymptotically singular; geodesics will reach this singularity in a finite amount of proper time but in an infinite time for an external observer. We will also discuss that an infinite amount of energy is required to leave the singularity, and that these types of wormholes appear as a good example of black hole mimickers;
- in the fourth subsection we will consider the case of non-vacuum solutions, where a perfect fluid with either a polytropic or a realistic equation of state is self-gravitating. We will show how the presence of the Weyl term in the action has a significant repulsive contribution to the gravitational interaction, opening the possibility of having standard fluids which can sustain compact stars with very large masses. In this subsection we will restore physical units using very unnatural values of  $\alpha$  and  $\beta$  in (2.5), which, however, are helpful to illustrate more clearly the effects of the quadratic terms;
- in the fifth subsection we will present the known analytical solutions of scale-invariant gravity, namely Schwarzschild, (anti-)de Sitter and Schwarzschild-(anti-)de Sitter; in particular, we will show that it is possible to have two Schwarzschild-de Sitter solutions, one with a zero scalar field and the other with a non-zero scalar field, which are also the only solutions present in the Einstein frame. We will also briefly present some results of the theory in a cosmological setting, namely a transition between two asymptotically de Sitter spacetimes, which motivated the analysis of a transition between the two Schwarzschild-de Sitter black holes.

Black hole solutions have been presented for the first time in [23], and later investigated in [20, 25] and in [24] we completely characterized their metric; naked singularities have been studied in [20], and the asymptotically vanishing one have been investigated in detail in [26]; non-symmetric wormholes have been first presented in [20] and then we presented the global properties shown in this section in [43]; we studied compact stars in quadratic gravity for the first time in [43], and most of the results shown in this section will be taken from that paper. Finally, black hole solutions in scale-invariant gravity have been

studied in [53, 54, 55] and we review them in [35], while the cosmological case has been investigated in various paper, of which we point out [27, 34, 28].

## 5.1 Black holes

One of the first results of the study of solutions of quadratic gravity has been the discovery of a class of non-Schwarzschild black hole solutions [23] which, for the corollary 1, are present only in the Einstein-Weyl sector of the theory. These solutions have an event horizon, described by the behavior of the  $(1,1)_{r_0}^1$  family in Subsection 3.2, but have a non-zero value of the Yukawa charge  $S_2^-$  in the asymptotic expansion (3.5) and then the two metric functions  $h(r)$  and  $f(r)$  are different one from the other. In terms of the sign of the Yukawa charge, we can define two different branches of non-Schwarzschild solutions: a Yukawa attractive and Yukawa repulsive branches that connect at a crossing point with the Schwarzschild solutions (which have zero Yukawa charge). As described in Subsection 3.4.1, we find black hole solutions specifying an event horizon radius and deriving all the other parameters using the shooting method technique. In Figure 16 we finally show the parameters characterizing the black hole metrics in function of the horizon radius.

**At large distances** we can immediately see from the top panels that Yukawa repulsive black holes are present only for small horizon radius and small positive masses, while Yukawa attractive black holes have unbounded horizon radii and unbounded *negative* masses. These properties already set some constraints on the presence of non-Schwarzschild black holes in our universe, as they are either large but gravitationally repulsive or small both in size and mass, and then they cannot model astrophysical black holes.

**Close to the horizon** the parameters  $h_1$  and  $f_1$  in the middle panels, which are the values of the first derivatives of  $h(r)$  and  $f(r)$  at the horizon, show another striking difference from Schwarzschild black holes, namely that the strength of the gravitational interaction at the horizon increases for increasing horizon radius. To quantify this statement, we can consider the surface gravity at the horizon

$$\kappa = \sqrt{-\frac{1}{2} (\nabla^\mu K^\nu) (\nabla_\mu K_\nu)} \Big|_{r=r_H} = \frac{1}{2} \sqrt{h_1 f_1}, \quad (5.1)$$

where  $K^\mu$  is the timelike Killing field, which clearly increases as the horizon radius grows with the behavior of  $h_1$  and  $f_1$  shown in Figure 16. This increase leads to an indefinite growth in the tidal forces that, as we will see later, is directly translated to the temperature. Nonetheless, the geometry close to the horizon will have no distinct differences

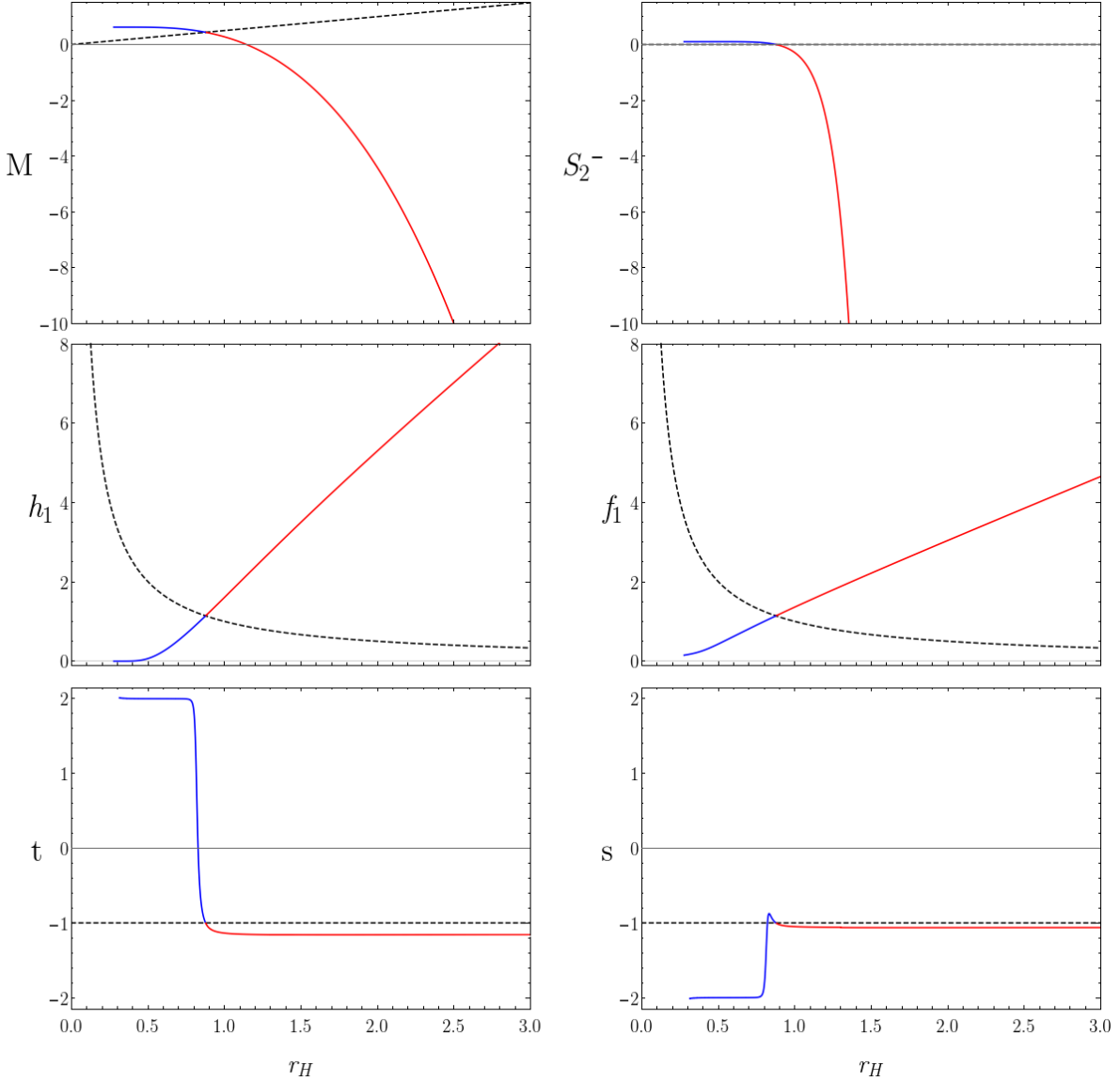


Figure 16: Parameters of black hole solutions in terms of the horizon radius; the black dashed line indicates Schwarzschild black holes, while the solid red and blue lines indicate the two branches of non-Schwarzschild black holes. In the top panels are shown the asymptotic field parameters, in the middle panels are shown the parameters that describe the metric close to the horizon, and in the bottom panels the running exponents which characterize the metric close to the origin.

from the one of a Schwarzschild metric, and there will be no qualitative differences in geodesics dynamics. Let us indeed consider a generic geodesic which, in a static spherically symmetric spacetime, can be defined as the integral line of the vector field  $V^\mu$  with components

$$\begin{aligned}
 V^t &= \frac{dt}{d\tau} = \frac{E}{h(r)}, \\
 V^r &= \frac{dr}{d\tau} = \pm \sqrt{f(r) \left( \frac{E^2}{h(r)} - \frac{L^2}{r^2} + \epsilon \right)}, \tag{5.2}
 \end{aligned}$$

$$V^\theta = \frac{d\theta}{d\tau} = 0,$$

$$V^\phi = \frac{d\phi}{d\tau} = \frac{L}{r^2},$$

with  $\epsilon = -1$  and  $\tau$  the proper time for a timelike geodesic, or  $\epsilon = 0$  and  $\tau$  an affine parameter for a null geodesic, and where we considered  $\theta = \pi/2$  without loss of generality; the  $\pm$  in front of the radial component indicate whether the geodesic is *ingoing* to smaller radii or *outgoing* to larger radii. Close to the horizon, the geodesic will behave as

$$V^t = \frac{dt}{d\tau} \sim \frac{E}{h_1(r - r_H)},$$

$$V^r = \frac{dr}{d\tau} \sim \pm \sqrt{\frac{f_1}{h_1}} E,$$

$$V^\theta = \frac{d\theta}{d\tau} = 0,$$

$$V^\phi = \frac{d\phi}{d\tau} \sim \frac{L}{r_H^2},$$
(5.3)

and then we recover the usual coordinate time and proper time behaviors close to the horizon

$$\tau \sim - \int_{r_{\tau=0}}^{r_H} \frac{dr}{\sqrt{\frac{f_1}{h_1} E}} = \sqrt{\frac{h_1}{f_1}} \frac{r_{\tau=0} - r_H}{E},$$

$$t \sim - \int_{r_{t=0}}^{r_H} \frac{dr}{\sqrt{h_1 f_1} (r - r_H)} = \lim_{r \rightarrow r_H} \frac{\log(r_{t=0} - r_H) - \log(r - r_H)}{\sqrt{h_1 f_1}} = +\infty,$$
(5.4)

in which choosing a Schwarzschild metric has the only effect of setting  $h_1 = f_1 = 1/r_H$ .

**At the origin** in the last panels we show the values of the running exponents (3.39) measured at  $r_o = 10^{-3}$ , which explicitly show that the two branches are indeed different in nature. While the properties at large distances and close to the horizon are physically different but follow a sort of continuity, there is clearly a transition between the  $(-1, -1)_0^1$  and the  $(-2, 2)_0^1$  families as we pass from the Yukawa attractive black holes to the Yukawa repulsive ones, which is faster as we evaluate the running exponents closer to the origin. These two possible behaviors at the origin, however, are not relevant in the context of geodesics dynamics, as the presence of the event horizon guarantees that all of them will reach the singularity.

To conclude, the two branches of black holes have very qualitatively different behaviors, as shown manifestly in Figure 17. All the general properties described above can be directly seen in this figure: for the Yukawa repulsive black hole we note the stronger attractive force at large distances, the weaker tidal forces close to the horizon, and the vanishing of

the time component of the metric at the origin, and for the Yukawa attractive black hole the repulsive gravitational force at large distances, the strong and attractive force close to the horizon, and the divergence of the time component of the metric at the origin.

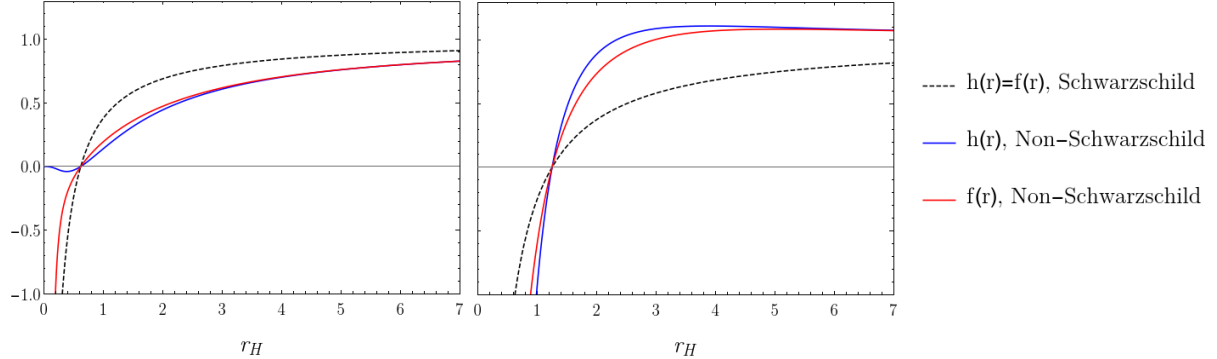


Figure 17: Metric of non-Schwarzschild black holes, with a Yukawa repulsive black hole in the left panel and a Yukawa attractive black hole in the right one; both are compared with a Schwarzschild metric with the same horizon radius.

While they have different metrics, and then different physical properties, having a single horizon and a singularity in the origin, all the three different types of black holes considered have the causal structure depicted in Figure 18, with the singularity being the future endpoint of all the geodesics intersecting the event horizon.

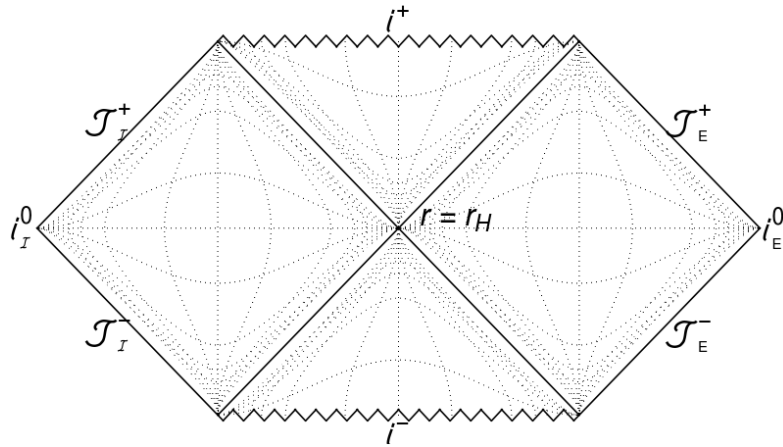


Figure 18: Penrose diagram for all the types of black hole solutions considered.

We also note that in [24] we found a class of non-Schwarzschild black holes in the case of  $\alpha < 0$ , that is a tachyonic mass  $m_2^2 < 0$ ; we will present this type of black holes in Appendix A.

## 5.2 Naked singularities

One of the most immediate results of the study of solutions of quadratic gravity is that naked singularities populate the majority of the parameter space. As previously said,

the first type of naked singularities has a divergent time component of the metric at the origin, and it might coincide with a logarithmic correction of the  $(-1, -1)_0^1$  family; nonetheless, the dominant contribution close to the origin will be given by the  $r^{-1}$  terms in the metric. The second type of naked singularity has a vanishing time component of the metric close to the origin, and it truly coincides with the  $(-2, 2)_0^1$  family of solutions. For both types of solutions, if we consider the  $(-1, -1)_0^1$  as the leading order behavior of type I solutions, the Kretschmann scalar  $R^{\mu\nu\rho\sigma}R_{\mu\nu\rho\sigma}$  diverge, as  $r^{-6}$  for type I and  $r^{-8}$  for type II solutions; also for both solutions the tortoise coordinate

$$r^* = \int \frac{dr}{\sqrt{h(r)f(r)}} \quad (5.5)$$

goes to zero as  $r \rightarrow 0$ , and therefore both types of solutions have the causal structure pictured in the Penrose diagram in Figure 19. It is then manifest that these spacetimes represent naked singularities, having all the light cones intersecting the singular origin at a finite time.

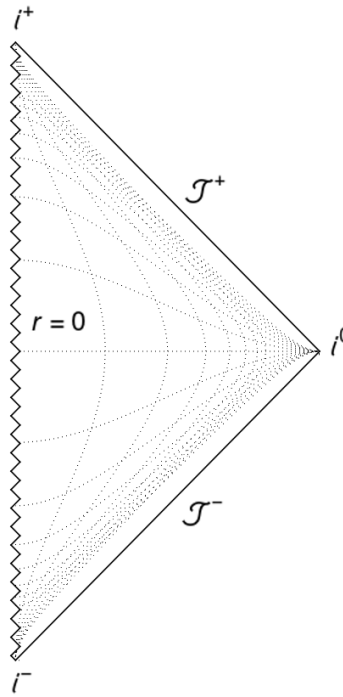


Figure 19: Penrose diagram for both types of naked singularities considered.

While they share the same causal structure, these two types of naked singularities have very different properties that will be described in detail in the following paragraphs.

### 5.2.1 Repulsive naked singularities

From the analysis of the phase diagram in Figure 10, they are linked with the presence of a repulsive gravitational force at large distances, *i.e.* to a negative mass  $M < 0$ , or

to an attractive gravitational force at large distances with a repulsive contribution of the Yukawa term associated with the spin-2 particle whenever it dominates over the contribution of the scalar particle. In other words, to have a repulsive naked singularity is necessary to have a relevant repulsive contribution of a tensor mode, whether massive or massless. In Figure 20 there are two examples of this type of solution, one with positive and one with negative mass. In the second case is clear that the attractive contribution of a Yukawa term is not sufficient to contrast the repulsive contribution of a negative mass. In the first case, the repulsive contribution instead becomes relevant only close to the origin, giving rise to a minimum in the gravitational potential at some radius  $r \neq 0$ .

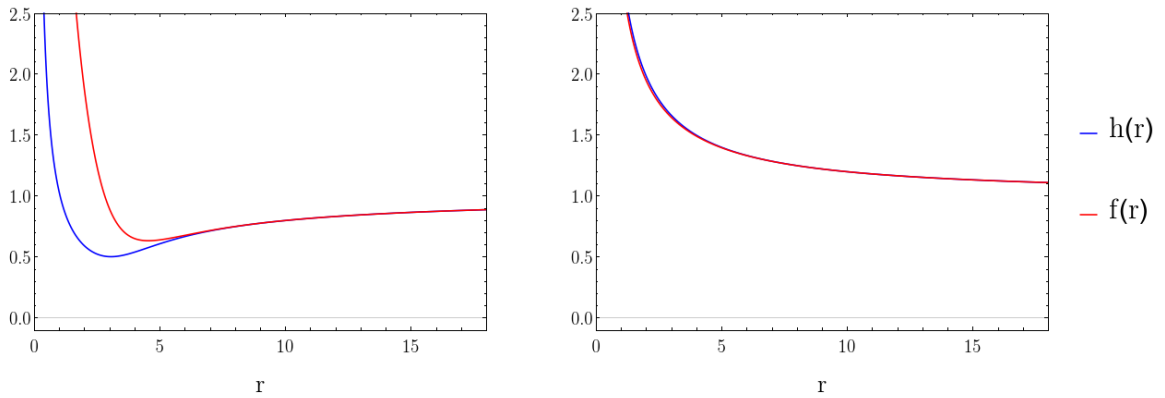


Figure 20: Metric functions for a repulsive naked singularity with positive mass, in particular with  $(M, S_2^-, S_0^-) = (1, 1, -0.3)$  (on the left), and one with negative mass, in particular with  $(M, S_2^-, S_0^-) = (-1, -1, 0.3)$  (on the right).

To recall what was said in Section 4, this type of solution is characterized by a divergent behavior of the time component of the metric  $g_{tt} = -h(r)$  and by a vanishing behavior of the radial component  $g_{rr} = 1/f(r)$ ; from the Frobenius analysis collected in Table 3, the only family of solution which has this behavior at the origin is the  $(-1, -1)_0^1$  family. Unfortunately, there are two main points of caution: the first is that the analysis of the running exponents (3.39) *does not* have  $(-1, -1)$  as a result, but there are discrepancies of the order of some percentage points, the second is that the number of free parameters of that family suggests that these solutions should be present on a line only. Looking at the detail of the running exponents for two repulsive naked singularities in Figure 21, it is clear that it is not a matter of how close to the origin the exponents are evaluated, but it is truly a deviation from the  $(-1, -1)_0^1$  behavior. However, the Frobenius analysis and the dynamical system analysis confirm that the first exponents of a metric that diverges in the origin have to be  $(-1, -1)$ , and the corrections have to be of higher order.

In [33] a family of logarithmic corrections of the Frobenius  $(-1, -1)_0^1$  family exists. However, such a family has not been found in the Einstein-Weyl case where we still find numerically the same behavior. The possibility of logarithmic corrections can be seen

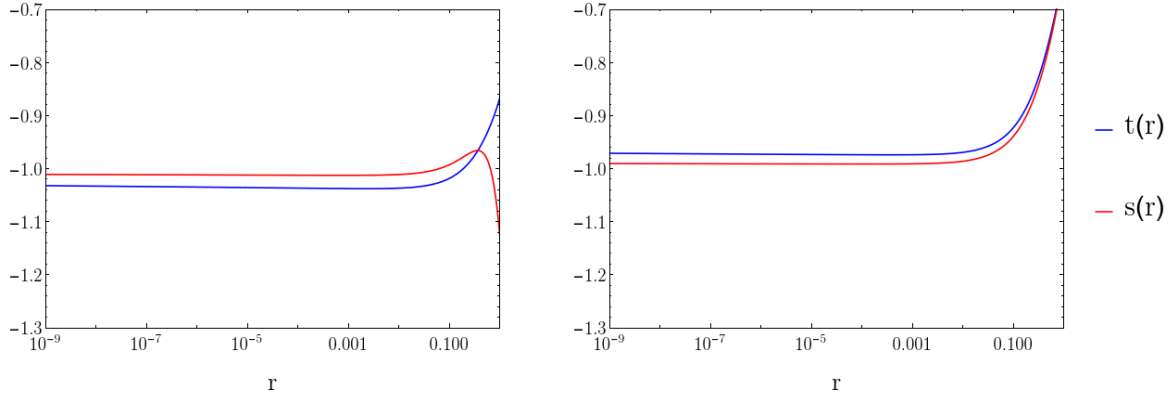


Figure 21: Trend of the running exponents  $t(r)$  and  $s(r)$  defined in (3.39) for a repulsive naked singularity with positive mass (on the left) and one with negative mass (on the right).

in Figure 22, where the log-linear plot of the functions  $r h(r)$  and  $r f(r)$  are shown. In contrast with a pure Frobenius family, where the functions should flatten to a constant, it is clear that they have a logarithmic behavior at small radii.

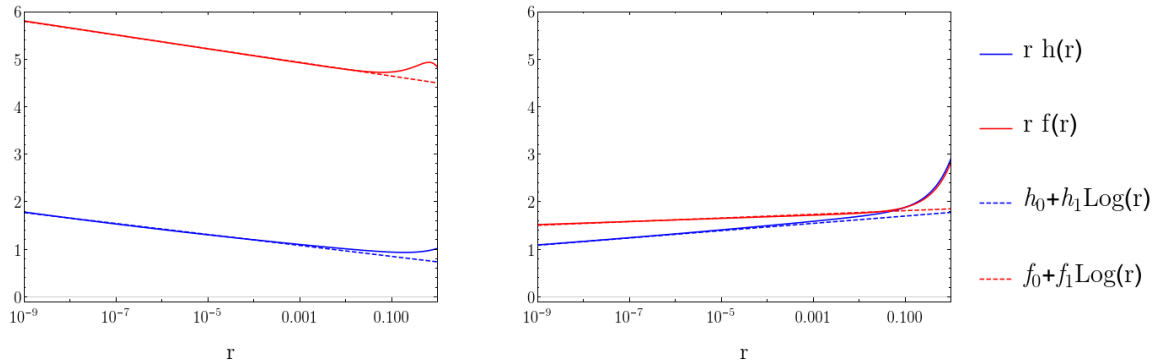


Figure 22: Logarithmic corrections of the  $(-1, -1)_0^1$  family for a repulsive naked singularity with positive mass (on the left) and one with negative mass (on the right).

While the actual behavior of the metric at the origin remains a problem to be solved, most of the relevant physical information can be extracted nonetheless. Let us consider the general geodesic defined by the integral lines of the vector (5.2); if we consider the  $(-1, -1)_0^1$  as the first approximation of the metric, and a timelike radial geodesic with  $L = 0$ , this vector takes the form

$$\begin{aligned}
 V^t &= \frac{dt}{d\tau} \sim \frac{E}{h_{-1}} r, \\
 V^r &= \frac{dr}{d\tau} \sim \pm \sqrt{\frac{f_{-1}}{h_{-1}} (E^2 - h_{-1} r^{-1})}, \\
 V^\theta &= \frac{d\theta}{d\tau} = 0, \\
 V^\phi &= \frac{d\phi}{d\tau} = 0,
 \end{aligned} \tag{5.6}$$

which is clearly defined only up to  $r = \frac{h_{-1}}{E^2}$ . It is then manifest the repulsive nature of this singularity, as a massive particle with starting energy  $\bar{E}$  at spatial infinity can reach only up to the limiting radius  $r_l = \frac{h_{-1}}{E^2}$ , and at the same time a particle emitted at a radius  $\bar{r}$  will reach spatial infinity with an energy  $E_i = \sqrt{\frac{h_{-1}}{\bar{r}}}$ . The particle emitted close to the singularity will then have a huge amount of energy, but, to reach the singularity, it is necessary to have an infinite amount of energy. It is clear that having logarithmic corrections, or simply having an exponent  $t \sim -1$  does not change this property of the singularity. It is instead possible to reach the singularity for null geodesics, for which the argument of the square root is always positive. It is also possible to evaluate the total proper time and coordinate time that is required to reach the singularity, which both result to be finite

$$\begin{aligned}\tau &= - \int_{r_{\tau=0}}^0 \frac{dr}{\sqrt{f(r)\left(\frac{E^2}{h(r)}\right)}} \sim - \int_{r_{\tau=0}}^0 \sqrt{\frac{h_{-1}}{f_{-1}}} \frac{dr}{E} = \sqrt{\frac{h_{-1}}{f_{-1}}} \frac{r_{\tau=0}}{E}, \\ t &= - \int_{r_{t=0}}^0 \frac{E dr}{h(r)\sqrt{f(r)\left(\frac{E^2}{h(r)}\right)}} \sim - \int_{r_{t=0}}^0 \frac{r dr}{\sqrt{f_{-1}h_{-1}}} = \frac{r_{t=0}^2}{2\sqrt{f_{-1}h_{-1}}}.\end{aligned}\tag{5.7}$$

We can have an insight into the nature of the singularity by studying a congruence of infalling geodesics with tangent vector (5.2). Following the discussion in chapter 4 of [56], we can define the vector field  $Z^\mu$ , which represents the separation of points in nearby geodesics, that satisfies the equation

$$\frac{d}{d\tau} Z^\mu = B^\mu_\nu Z^\nu, \tag{5.8}$$

where we have defined the deviation tensor

$$B_{\mu\nu} = h^\rho_\mu h^\sigma_\nu \nabla_\rho V_\sigma \tag{5.9}$$

with  $h_{\mu\nu}$  being the metric of either the hypersurface orthogonal to the geodesic in the timelike case or the surface transverse to the geodesic in the null case. For the timelike case it is not possible to reach the singularity, while for the null case the equation (5.8) close to the singularity can be rewritten in terms of the radial coordinate as

$$\frac{d\tau}{dr} \frac{d}{d\tau} \begin{pmatrix} Z^t(r) \\ Z^r(r) \\ Z^\theta(r) \\ Z^\phi(r) \end{pmatrix} = \frac{d}{dr} \begin{pmatrix} Z^t(r) \\ Z^r(r) \\ Z^\theta(r) \\ Z^\phi(r) \end{pmatrix} \sim \begin{pmatrix} 0 & 0 & 0 & 0 \\ 0 & 0 & 0 & 0 \\ 0 & 0 & \frac{1}{r} & 0 \\ 0 & 0 & 0 & \frac{1}{r} \end{pmatrix} \begin{pmatrix} Z^t(r) \\ Z^r(r) \\ Z^\theta(r) \\ Z^\phi(r) \end{pmatrix}, \tag{5.10}$$

with the geodesics keeping a constant distance in the time and radial directions and converging in the angular directions as  $Z^\theta \sim Z^\phi \sim r \rightarrow 0$  purely for geometrical aspects

(that is, they follow radial directions which converge to the origin), exactly as in the case of Minkowski space. The repulsive naked singularity, therefore, seems to have no physical problems for everything concerning *ingoing* geodesics, while its singular nature is present in the high energy of the *outgoing* geodesics.

### 5.2.2 Attractive naked singularities

The second type of naked singularities, as shown in Figure 10, is associated with the presence of a positive mass and an attractive contribution of the Yukawa term associated with the scalar particle, whenever it dominates over the contribution of the tensor particle. However, it is possible to find this type of singularity also in the region of negative mass, but only if there is a strongly attractive contribution of the Yukawa term associated with the tensor particle. In other words, it is a type of solution that requires a strong attractive gravitational force. In Figure 23 we show two examples of this type of solution, one with an attractive gravitational potential at large distances, on the left, and one with a repulsive gravitational potential at large distances, on the right. In the second case, the repulsive behavior at large distances and the attractive behavior close to the origin give rise to a potential barrier at some radius  $r \neq 0$ , which can be more and more accentuated as we get closer to the family of repulsive naked singularities.

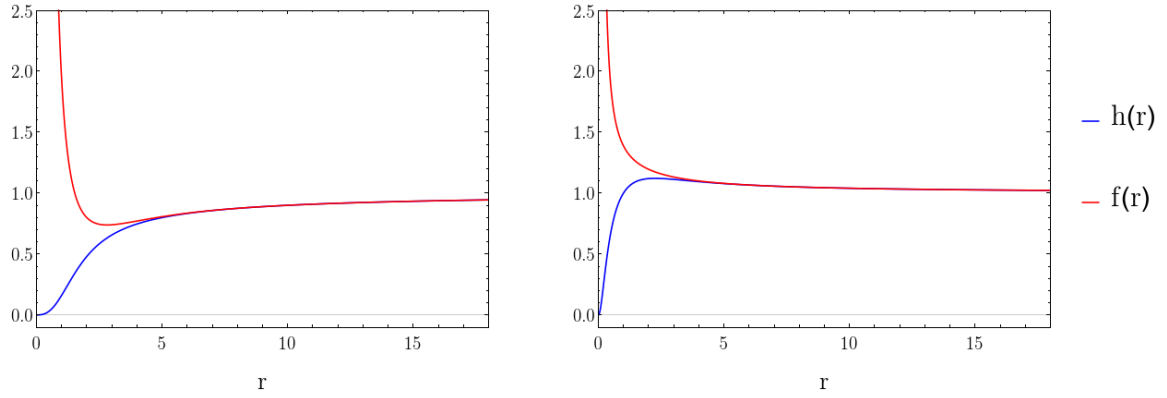


Figure 23: Metric functions for an attractive naked singularity with positive mass, in particular with  $(M, S_2^-, S_0^-) = (0.5, -0.1, -0.5)$  (on the left), and one with negative mass, in particular with  $(M, S_2^-, S_0^-) = (-0.2, -0.5, -0.5)$  (on the right).

As previously said, this type of solution is characterized by both the time component of the metric  $g_{tt} = -h(r)$  and the radial one  $g_{rr} = 1/f(r)$  going to zero at the origin, and from the analysis done in Subsection 3.2 we expect it to coincide with the  $(-2, 2)_0^1$  Frobenius family of solutions. In contrast to what happens for repulsive naked singularities, the running exponents (3.39) converge precisely on the  $(-2, 2)$  values, as can be seen in Figure 24.

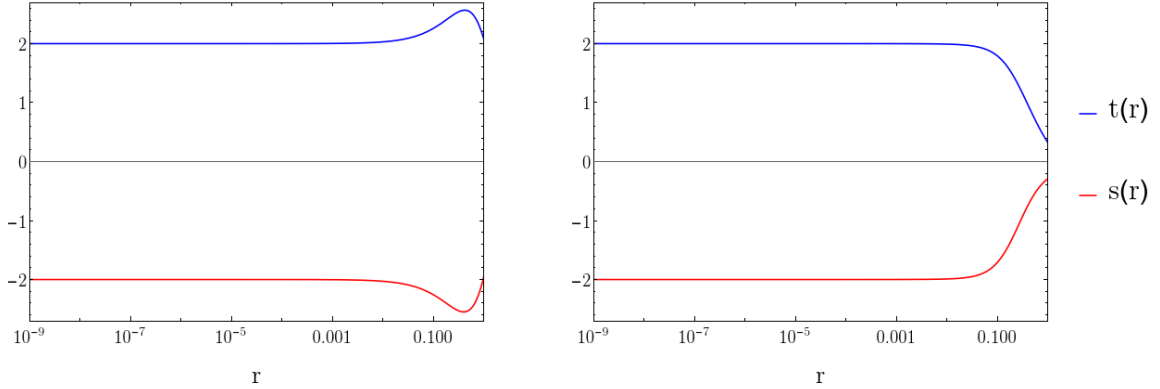


Figure 24: Trend of the running exponents  $t(r)$  and  $s(r)$  defined in (3.39) for an attractive naked singularity with positive mass (on the left) and one with negative mass (on the right).

As an additional cross-check, we can also perform an analysis similar to the one done for repulsive naked singularities, and study the behavior of the functions  $r^{-2}h(r)$  and  $r^2f(r)$  close to the origin. We show as an example the behavior of such functions for the same two solutions in Figure 25, where it is clear that there are no logarithmic corrections to the Frobenius family. It is however important to specify that, while the value of the  $h_2$  parameter on the left and of the  $f_{-2}$  parameter on the right are quite small, they are of order  $\mathcal{O}(10^{-2})$  and have to be considered as small parameter *different from zero*.

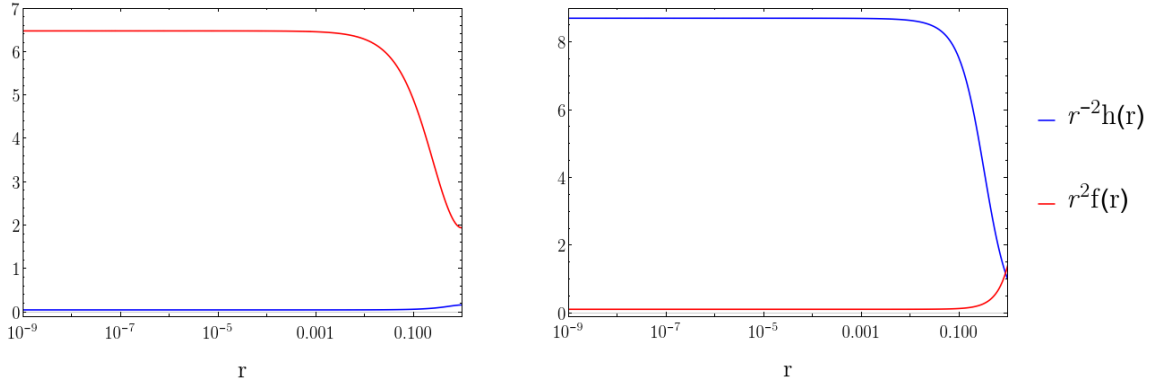


Figure 25: No logarithmic corrections of the  $(-2, 2)_0^1$  family for an attractive naked singularity with positive mass (on the left) and one with negative mass (on the right).

If we now look at the geodesic (5.2), there is no infinite potential barrier, and it can be extended up to the origin. In the case  $L = 0$  the geodesic takes the form

$$\begin{aligned} V^t &= \frac{dt}{d\tau} \sim \frac{E}{h_2 r^2}, \\ V^r &= \frac{dr}{d\tau} \sim \pm \frac{1}{r^2} \sqrt{f_{-2} \left( \frac{E^2}{h_2} + \epsilon r^2 \right)} \sim \pm \frac{1}{r^2} E \sqrt{\frac{f_{-2}}{h_2}}, \end{aligned} \tag{5.11}$$

$$V^\theta = \frac{d\theta}{d\tau} = 0,$$

$$V^\phi = \frac{d\phi}{d\tau} = 0,$$

and there is no difference between a timelike and a null geodesic. From 5.11 we can then immediately evaluate the proper and coordinate time required to reach the singularity as

$$\begin{aligned} \tau &= - \int_{r_{\tau=0}}^0 \frac{dr}{\sqrt{f(r)\left(\frac{E^2}{h(r)} + \epsilon\right)}} \sim - \int_{r_{\tau=0}}^0 \sqrt{\frac{h_2}{f_{-2}}} \frac{r^2 dr}{E} = \sqrt{\frac{h_2}{f_{-2}}} \frac{r_{\tau=0}^3}{3E}, \\ t &= - \int_{r_{t=0}}^0 \frac{E dr}{h(r)\sqrt{f(r)\left(\frac{E^2}{h(r)} + \epsilon\right)}} \sim - \int_{r_{t=0}}^0 \frac{dr}{\sqrt{f_{-2}h_2}} = \frac{r_{t=0}}{\sqrt{f_{-2}h_2}}, \end{aligned} \quad (5.12)$$

which are both finite. It is now possible also to solve the differential equation (5.8) for the deviation vector  $Z^\mu$  of a congruence of geodesics both in the timelike and in the null cases. The null congruence follows the same equation as in (5.10), with different geodesics keeping a constant distance in the time and radial direction and converging on the angular directions for geometrical aspects. The timelike congruence instead has to satisfy the equation

$$\frac{d\tau}{dr} \frac{d}{d\tau} \begin{pmatrix} Z^t(r) \\ Z^r(r) \\ Z^\theta(r) \\ Z^\phi(r) \end{pmatrix} = \frac{d}{dr} \begin{pmatrix} Z^t(r) \\ Z^r(r) \\ Z^\theta(r) \\ Z^\phi(r) \end{pmatrix} \sim \begin{pmatrix} \frac{1}{r} & \frac{1}{\sqrt{h_2 f_{-2} r}} & 0 & 0 \\ -\frac{\sqrt{h_2 f_{-2}}}{r} & -\frac{1}{r} & 0 & 0 \\ 0 & 0 & \frac{1}{r} & 0 \\ 0 & 0 & 0 & \frac{1}{r} \end{pmatrix} \begin{pmatrix} Z^t(r) \\ Z^r(r) \\ Z^\theta(r) \\ Z^\phi(r) \end{pmatrix}, \quad (5.13)$$

which is solved by

$$Z^\mu = \begin{cases} Z^t(r) \sim c_1 + c_2 \log(r), \\ Z^r(r) \sim -\sqrt{h_2 f_{-2}} (c_1 + c_2 \log(r)), \\ Z^\theta(r) \sim c^\theta r, \\ Z^\phi(r) \sim c^\phi r. \end{cases} \quad (5.14)$$

While on the angular directions geodesics converge, as usual simply for geometrical reasons, the behavior in the time and radial component is quite peculiar, with different points in the geodesics being separated by an *infinite* amount of time and an *infinite* radial distance. In other words, an object falling into an attractive naked singularity will undergo an extreme spaghettification process. While, at least for solutions with positive mass, geodesics can always reach the singularity, what has to be taken with care is how

geodesics *can leave* the singularity. While the proper and coordinate time required to reach a specific (small) radius  $\bar{r}$  is simply

$$\tau \sim \sqrt{\frac{h_2}{f_{-2}} \frac{\bar{r}^3}{3E}}, \quad t \sim \frac{\bar{r}}{\sqrt{f_{-2} h_2}}, \quad (5.15)$$

as can be seen from (5.12), what is relevant is the time component of the vector  $V^\mu$  in (5.11). From this component is indeed possible to extract the redshift of a photon emitted at radius  $r$  and measured at infinity as

$$z = \sqrt{\frac{h(r_\infty)}{h(r)}} = \frac{1}{\sqrt{h(r)}} \sim \frac{1}{\sqrt{h_2 r}}, \quad (5.16)$$

which clearly diverges as  $r \rightarrow 0$ . As we approach the singularity, the energy required to leave it gets larger and larger, and it becomes infinite precisely at the singularity. Exactly the opposite of what happens for repulsive naked singularities, we can conclude that the singularity cannot communicate with the surrounding spacetime, but all the infalling geodesics can experience the nature of the singularity.

### 5.3 Wormholes

A large area of the phase diagram is populated by type III solutions for which the radial component of the metric diverges, while the time component is finite and different from zero. It is common practice to interpret this behavior as the presence of a wormhole solution [57, 58, 59, 60] and, as already discussed in Subsection 3.2, we believe that this is the case also in quadratic gravity. From now on, we will refer to these solutions as non-symmetric wormholes or using the contracted forms, no-sy wormholes or no-sy WHs. This type of solution seems to be favored by a positive mass and either a repulsive contribution of the massive scalar field or an attractive contribution of the massive tensor field. They are also present in the case of a repulsive negative mass, but in this case a very attractive massive tensor contribution and a very repulsive massive scalar contribution are required. In other words, type III solutions are favored by the competing contributions of the tensors and scalar fields.

Due to the numerical expenses of implementing the shooting method for wormhole solutions, and for the sake of simplicity while presenting the results, we will specify the discussion on this type of solution to the case of the Einstein-Weyl theory. Thanks to this numerical method is indeed possible to confirm that type III solutions of the phase diagram in Figure 7 truly belong to the  $(1, 0)_{r_0}^2$  family, as the shooting method implemented as stated in the paragraph 3.4.1 converges in all and only in the area populated by

wormhole solutions. Moreover, is it possible to show the relations between the asymptotic parameters and the property close to the throat; in Figure 26 we then show the relation between the throat radius  $r_T$  and the parameter  $h_0$ , which can be linked to the redshift of a photon emitted at such distance and measured at infinity by  $z(r_T) = 1/\sqrt{h_0}$ , with the location of the solutions in the phase diagram. It is manifest from the left panel of Figure 26 that the throat radius increases with an increasing mass; and in particular, as the Yukawa charge goes to zero, the throat radius approaches the mass-radius relation of the event horizon of the Schwarzschild metric  $r_H = 2M$ . We note that the throat radius also increases as the Yukawa charge decreases, and then in the large mass limit where no-sy wormholes are present only for negative values of  $S_2^-$ , the throat is always larger than the event horizon of a Schwarzschild black hole with the same mass. It is also important to note that as the gravitational parameters of a wormhole get closer to the ones of a black hole, that is, in the phase diagram we get closer to either the Schwarzschild or non-Schwarzschild black hole lines, the parameter  $h_0$  gets closer to zero, and then the redshift of a photon emitted at the throat increases, and diverges in the limit of black holes. At the physical level, this means that the topological sphere defined by  $r_T$  becomes an infinite redshift surface in this limit or, in other words, it becomes indistinguishable from an event horizon. For large masses then, if the Yukawa charge is sufficiently small, no-sy wormholes are optimal black hole mimickers.

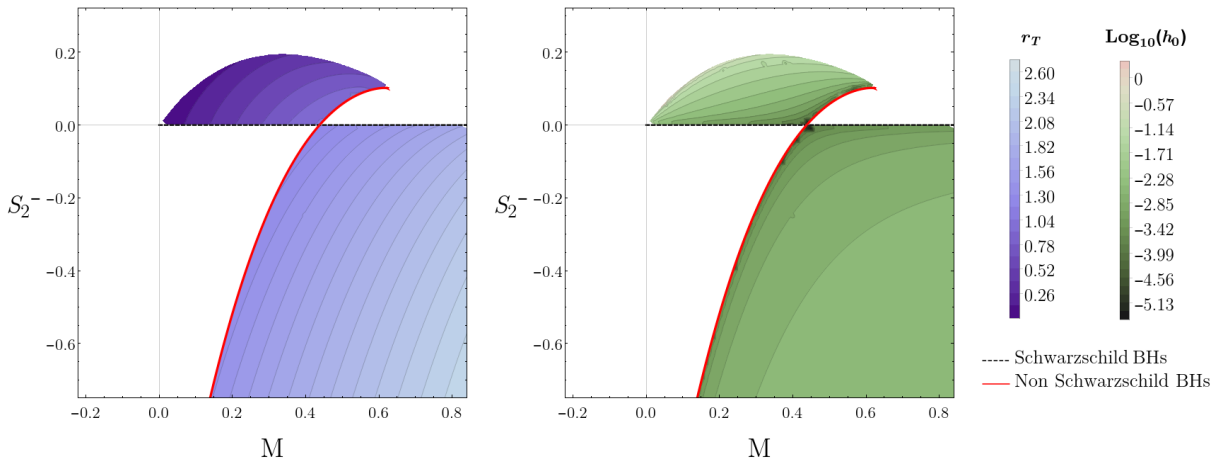


Figure 26: Trend of the two main throat parameters in the phase diagram of Einstein-Weyl gravity. In function of the gravitational parameters  $M$  and  $S_2^-$  we show the throat radius  $r_T$  in the left panel, and the redshift parameter  $h_0$  in the right panel.

As for single solutions, in Figure 27 we present an example of a non-symmetric wormhole spacetime, both in function of the  $r$  coordinate and of the  $\rho$  coordinate defined in (3.33); in particular in function of this latter coordinate, the functions  $h(\rho)$  and  $f(\rho)$ , as well as  $g_{\rho\rho}(\rho)$  are smoothly matched from both the patches in  $\rho = 0$ . The time component of the metric in this coordinate frame  $h(\rho)$  is monotonic, meaning that an observer would

feel a gravitational force always in the direction of decreasing  $\rho$ . This corresponds to an attractive central force in the asymptotically flat patch and a repulsive central force in the second patch, considering as attractive or repulsive whether it attracts objects towards small or large values of the  $r$  coordinate, respectively.

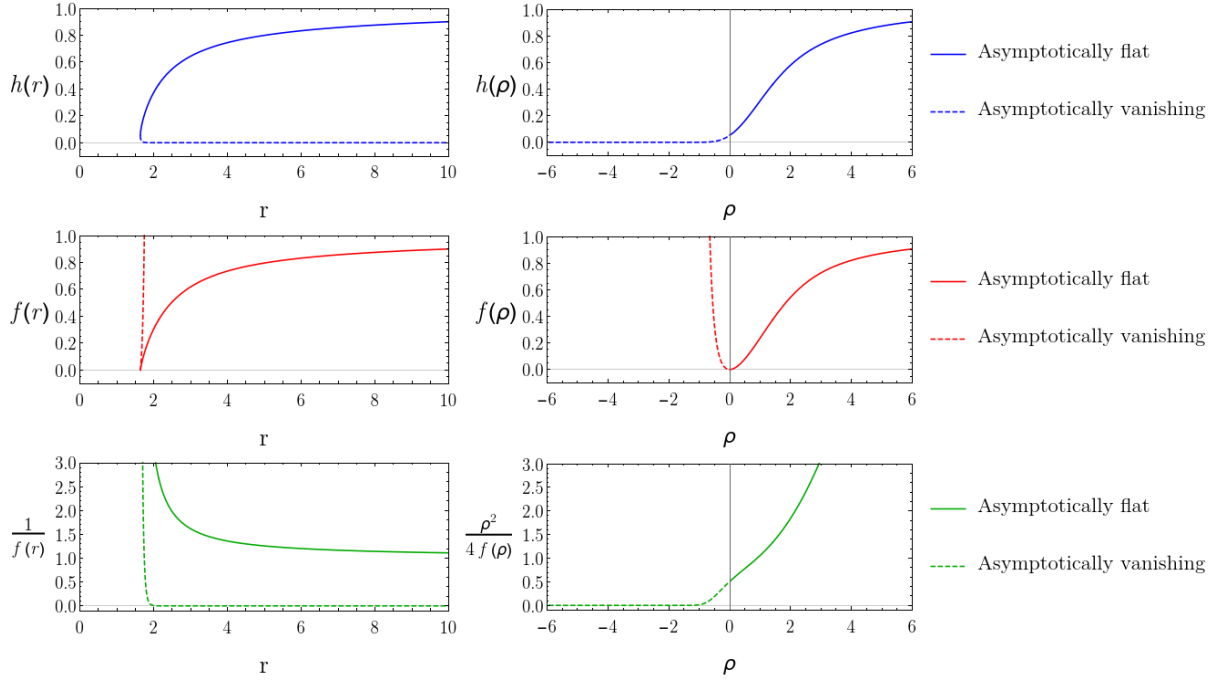


Figure 27: Metric of a no-sy WH solution with  $M = 0.5$ ,  $S_2^- = -0.3$  and  $S_0^- = 0$ : in the panels on the left the metric is in function of the  $r$ -coordinate, while in the panels on the right is in function of the  $\rho$ -coordinate; solid and dashed lines indicate whether we are in the asymptotically flat or in the asymptotically vanishing patch, respectively.

The wormhole nature is manifest in the geodesic dynamics around the throat. Indeed, recalling the transformation (3.33), the radial component in (5.2) can be written in terms of  $\rho$  as

$$\frac{d\rho}{d\tau} = \pm \sqrt{\frac{f(r)}{(r - r_T)} \left( \frac{E^2}{h(r)} - \frac{L^2}{r^2} + \epsilon \right)}. \quad (5.17)$$

If we consider the specific form of  $f(r)$  around the throat (3.30), equation (5.17) can be integrated, obtaining a smooth geodesic that goes from positive to negative  $\rho$ . On the contrary, it is not possible to build a differentiable geodesic that goes from  $r > r_T$  to  $r < r_T$  with a metric as (3.32), confirming once again the interpretation of the  $(1, 0)_{r_0}^2$  as a wormhole solution family. It is trivial to see that geodesics will reach the throat in a

finite amount of proper and coordinate time

$$\begin{aligned}
\tau &= - \int_{r_{\tau=0}}^{r_T} \frac{dr}{\sqrt{f(r) \left( \frac{E^2}{h(r)} - \frac{L^2}{r^2} + \epsilon \right)}} \sim - \int_{r_{\tau=0}}^{r_T} \frac{dr}{\sqrt{f_1(r - r_T) \left( \frac{E^2}{h_0} - \frac{L^2}{r_T^2} + \epsilon \right)}} = \\
&= \frac{2 \left( \sqrt{r_{\tau=0}} - \sqrt{r_T} \right)}{\sqrt{f_1 \left( \frac{E^2}{h_0} - \frac{L^2}{r_T^2} + \epsilon \right)}}, \\
t &= - \int_{r_{t=0}}^{r_T} \frac{E dr}{h(r) \sqrt{f(r) \left( \frac{E^2}{h(r)} - \frac{L^2}{r^2} + \epsilon \right)}} \sim - \int_{r_{t=0}}^{r_T} \frac{E dr}{h_1(r - r_T)^{3/2} \sqrt{f_1 \left( \frac{E^2}{h_0} - \frac{L^2}{r_T^2} + \epsilon \right)}} = \\
&= \frac{2E \left( \sqrt{r_{t=0}} - \sqrt{r_T} \right)}{h_1 \sqrt{f_1 r_T r_{t=0} \left( \frac{E^2}{h_0} - \frac{L^2}{r_T^2} + \epsilon \right)}}.
\end{aligned} \tag{5.18}$$

From geodesics dynamics close to the throat, it is also possible to infer that a free-falling object entering the wormhole throat from the asymptotically flat patch will always proceed until it reaches the surface  $r \rightarrow \infty$  of the second patch. Taking into account that the radical argument in (5.17) has to be positive, and considering the expansion  $f(r) = f_1(r - r_T) + O((r - r_T)^{\frac{3}{2}})$  and  $h(r) = h_0 + O((r - r_T)^{\frac{1}{2}})$ , for positive  $f_1$  and  $h_0$  we get the condition

$$\frac{E^2}{h_0} > \frac{L^2}{r_T^2} - \epsilon. \tag{5.19}$$

However this means that once entered the second patch,  $\frac{d\rho}{d\tau}$  cannot vanish, indeed we have

$$\frac{E^2}{h(r)} > \frac{E^2}{h_0} > \frac{L^2}{r_T^2} - \epsilon > \frac{L^2}{r^2} - \epsilon, \tag{5.20}$$

since  $h(r)$  decreases in the asymptotically vanishing region. This means that a free-falling object will inevitably reach  $\rho = -\infty$  since the gravitational force attracts it, and the angular momentum conservation contributes in the same direction. This behavior implies that the photon sphere (see *e.g.* [61]) of no-sy wormholes is always located in the asymptotically flat patch.

Finally, we move our analysis to the asymptotic surface  $\rho = -\infty$  in the second patch, which, as can be seen from Figure 27, has both the time component of the metric  $g_{tt} = -h(r)$  and the radial component of the metric  $g_{rr} = 1/f(r)$  going to zero. A common behavior for the metric in this limit emerged during the calculations, namely all the

solutions considered satisfy with good accuracy the relation

$$\begin{aligned}\frac{d}{dr} \left( \frac{h'(r)}{h(r)} \right) &= \frac{h''(r)}{h(r)} - \left( \frac{h'(r)}{h(r)} \right)^2 \rightarrow -\frac{2}{r^2}, \\ \frac{d}{dr} \left( \frac{f'(r)}{f(r)} \right) &= \frac{f''(r)}{f(r)} - \left( \frac{f'(r)}{f(r)} \right)^2 \rightarrow \frac{2}{r^2},\end{aligned}\quad (5.21)$$

at large distances in the second patch; this particular combination is shown in 28.

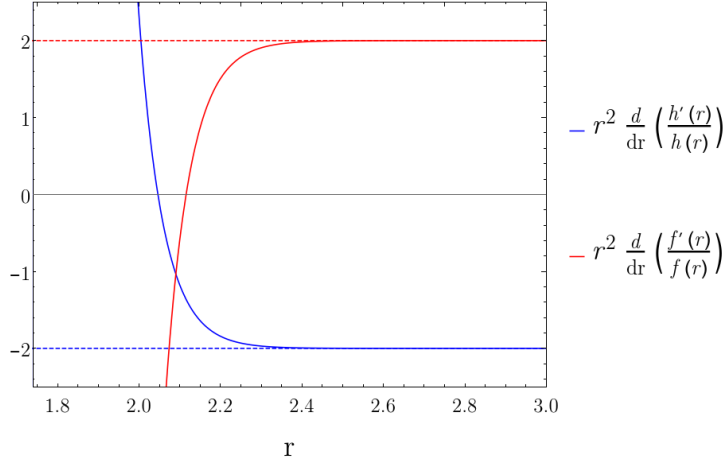


Figure 28: Details of the metric in the asymptotically vanishing region of a no-sy WH solution with  $M = 0.5$ ,  $S_2^- = -0.3$  and  $S_0^- = 0$ .

This asymptotic behavior can be analytically integrated and results in the approximation (3.41), which has been proven to be a solution of the first-order expansion of an asymptotically vanishing solution at large distances. We can then use this approximation of the metric to infer some properties of the spacetime in this limit. At first, it is possible to show that the asymptotic surface  $r \rightarrow \infty$ ,  $\rho \rightarrow -\infty$  is located at a finite proper distance from the wormhole throat. Indeed, the proper radial distance is given by

$$\tilde{r}_{max} = \int_{r_T}^{\infty} \frac{dr}{\sqrt{f(r)}}, \quad (5.22)$$

and this integral converges with  $f(r)$  interpolated between (3.30) and (3.41) as

$$\tilde{r}_{max} = \int_{r_T}^{\infty} \frac{dr}{\sqrt{f(r)}} \sim \tilde{r}_{asy} + \int_{r_{asy}}^{\infty} \sqrt{C_f} r e^{-\frac{a}{2}r} dr = \tilde{r}_{asy} + \frac{2\sqrt{C_f}}{a^2} e^{-\frac{a}{2}r_{asy}} (2 + ar_{asy}), \quad (5.23)$$

where  $r_{asy}$  is a radius at which the metric is well approximated by (3.41) and  $\tilde{r}_{asy}$  is its proper distance from the throat. This means that even the proper volume of the entire  $\rho < 0$  region is finite, as given by

$$V_p = 4\pi \int_{r_T}^{\infty} dr \frac{r^2}{\sqrt{f(r)}} \sim V_{asy} + \frac{8\pi\sqrt{C_f}}{a^4} e^{-\frac{a}{2}r_{asy}} (48 + 24ar_{asy} + 6a^2ar_{asy}^2 + a^3r_{asy}^3), \quad (5.24)$$

where  $V_{asy}$  is the proper volume closed inside the radius  $r_{asy}$ . Moreover, the proper time interval needed to fall into this surface is finite, as it goes as

$$\tau_s = \int_{r_{\tau=0}}^{\infty} \frac{dr}{\sqrt{f(r)\left(\frac{E^2}{h(r)} - \frac{L^2}{r^2} + \epsilon\right)}} \sim \tau_{asy} + \frac{2\sqrt{C_h C_f}}{Ea^3} e^{-ar_{asy}} (2 + 2ar_{asy} + a^2 r_{asy}^2), \quad (5.25)$$

where  $\tau_{asy}$  is the proper time required to reach  $r_{asy}$ . However, for a distant observer in the asymptotically flat patch, a particle falls into the wormhole throat in a finite time interval, but the time needed to reach the surface  $\rho \rightarrow -\infty$  results divergent, as it is given by

$$t = \int_{r_{t=0}}^{\infty} \frac{E dr}{h(r) \sqrt{f(r)\left(\frac{E^2}{h(r)} - \frac{L^2}{r^2} + \epsilon\right)}} \sim \int_{r_{t=0}}^{\infty} \sqrt{\frac{C_f}{C_h}} dr \rightarrow \infty. \quad (5.26)$$

These peculiar properties are in agreement with the fact that the hypersurface defined by  $r \rightarrow \infty$  is indeed singular, as seen by the behavior of the curvature invariants in (3.46) which, however, as said in Subsection 3.3, leave the Ricci scalar and squared Weyl tensor constant (3.47). We also note that, besides the singular nature of the curvature invariants, the fact that a timelike geodesic reaches an infinite radius in a finite proper time is a strong indication that the spacetime is geodesically incomplete. As it is clear that the hypersurface at  $r \rightarrow \infty$  is a singular region, it is a new kind of singularity with unique physical properties. To begin with, the causal structure of this spacetime is radically different from the standard solutions of General Relativity. As shown in the conformal diagram of Figure 29, we see that the causal structure of a no-sy WH is equivalent to the one of a maximally extended Minkowski with a singularity at the “internal”  $\mathcal{J}_I^+$  and  $\mathcal{J}_I^-$ . This is not surprising, considering that the  $t$ - $r$  sector of a no-sy wormhole spacetime is conformally equivalent to the Minkowski one after the coordinate transformation

$$ds^2 = h(r)(-dt^2 + dr^{*2}) + r^2 d\Omega^2, \quad (5.27)$$

where the tortoise coordinate goes to zero at the throat. The relevant information manifestly shown in Figure 29, however, is that the singularity is at the edges of the causal structure. In other words, a distant observer can communicate with the singularity only in an infinite amount of time. Furthermore, recalling the definition of the redshift of a photon emitted at radius  $r$  and measured at infinity  $z(r) = \frac{1}{\sqrt{h(r)}}$ , we see that the singularity is actually on an infinite redshift surface and, as for an event horizon, an infinite amount of energy is required to leave it. The singularity is therefore naked only in its infinite past section, and can be interpreted as the equivalent of a white hole singularity. The problem of dealing with naked singularities in no-sy wormhole spacetimes is then

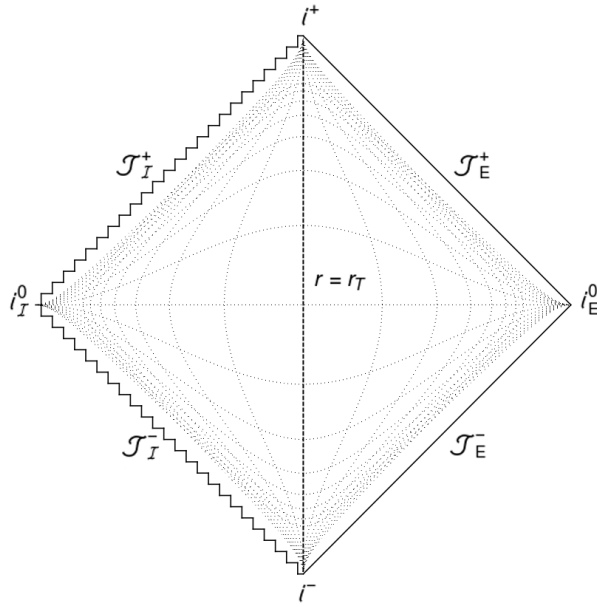


Figure 29: Conformal diagram of a no-sy WH spacetime; the dotted lines indicate surfaces of constant time and radius.

reduced to finding a collapse mechanism for generating such objects.

We now consider the behavior of a congruence of infalling geodesics with tangent vector (5.2), where with infalling we mean that has a negative  $V^r$  in the asymptotically flat patch and a positive  $V^r$  in the asymptotically vanishing one. The first thing we want to highlight is that the expansion scalar

$$\theta = h^{\mu\nu} B_{\mu\nu} \quad (5.28)$$

does not go to a *negative* infinite value at the singularity, as it happens in the Schwarzschild case, but it goes to a *positive* infinite value as in the limit of outgoing geodesics reaching spatial infinity in asymptotically flat solutions. However, the peculiar feature here is that *the expansion scalar goes to infinity in a finite proper time*. It is, in fact, possible to prove that the expansion scalar at large radii satisfies

$$\theta(\tau) > \frac{1}{(\tau_s - \tau)^\alpha}, \quad (5.29)$$

with  $0 < \alpha < 1$  and  $\tau_s$  being the proper time (or the affine parameter) at which the geodesic reaches the singularity, and then that it diverges in the limit  $\tau \rightarrow \tau_s$ . The second thing we want to highlight is the behavior of the deviation vector  $Z^\mu$ . If we restrict ourselves to radial geodesics, using the definition of proper time (5.25) and the asymptotic expansion (3.41), we can solve the differential equations (5.8) close to the

singular surface as

$$Z^\mu = \begin{cases} Z^t(r) \sim c^t r, \\ Z^r(r) \sim c^r r, \\ Z^\theta(r) \sim c^\theta r, \\ Z^\phi(r) \sim c^\phi r, \end{cases} \quad Z^\mu = \begin{cases} Z^t(r) \sim c^t, \\ Z^r(r) \sim c^r, \\ Z^\theta(r) \sim c^\theta r, \\ Z^\phi(r) \sim c^\phi r, \end{cases} \quad (5.30)$$

in the timelike and null cases, respectively. While null geodesics diverge only for geometrical aspects, timelike geodesics experience extreme tidal forces in the radial and temporal directions that actually diverge as they get closer to the singularity. The presence of such disruption of timelike observers at a finite value of the proper time has a remarkable resemblance with the Big Rip cosmological scenario, where the expansion of the universe diverges in a finite amount of cosmological time. However, this Big Rip-like singularity is localized inside a topological sphere of radius  $r = r_T$  for an observer in the asymptotically flat patch, and has an “origin” in the topological sphere of radius  $r = r_T$  for an observer in the asymptotically vanishing one.

With the information at our disposal, we can now have an insight into how observers perceive no-sy wormholes:

- *infalling* observers coming from the asymptotic flat patch are attracted by the no-sy wormhole just as by other compact objects, but after they have reached the radius  $r = r_T$  they start to feel a repulsive force, and tidal forces in all directions: they are quickly pushed away to spatial infinity, and the tidal forces become so strong that can break all the binding energies and completely disrupt the observer in a finite amount of proper time, just like in the Big Rip cosmological scenario; however, in principle observers can always turn on a rocket and escape their fate;
- *distant* observers in the asymptotically flat patch see an attractive object enclosed inside the topological sphere of radius  $r = r_T$ ; the object is smaller than its photon sphere, and the object will absorb the light emitted outside this sphere; however, particles can emit light from inside the object, but this emission is expected at extremely low frequencies: first of all photons are exponentially redshifted, and the temperature of a ball of gas is expected to decrease, as the volume increases as can be seen from (5.30); moreover, distant observers will never see the disruption of the infalling gas, that is instead perceived as “frozen” inside the object.

In conclusion, we can interpret no-sy WHs as black hole mimickers with a “singularity by disruption” instead of a “singularity by compression” that, for this reason, is always avoidable.

## 5.4 Compact stars

We conclude our review of solutions of quadratic gravity with non-vacuum solutions or, using a more astrophysical term, compact stars. This name is guaranteed to have a physical sense by our choice of equations of state, which can be a simple, “scholastic”, polytropic model [62]

$$p = k \rho^\Gamma, \quad (5.31)$$

where in particular we used  $\Gamma = 2, 3, 4/3, 5/3$  while studying the location of non-vacuum solutions in the phase diagram and only the case  $\Gamma = 2$  for the results shown in this subsection, and a realistic SLy equation of state [63, 64] in its analytical representation [65]

$$\begin{aligned} \log_{10} p = & \frac{a_1 + a_2 \log_{10} \rho + a_3 (\log_{10} \rho)^3}{\exp [a_5 (\log_{10} \rho - a_6)] + 1} + \frac{a_7 + a_8 \log_{10} \rho}{\exp [a_9 (a_{10} - \log_{10} \rho)] + 1} + \\ & + \frac{a_{11} + a_{12} \log_{10} \rho}{\exp [a_{13} (a_{14} - \log_{10} \rho)] + 1} + \frac{a_{15} + a_{16} \log_{10} \rho}{\exp [a_{17} (a_{17} - \log_{10} \rho)] + 1}; \end{aligned} \quad (5.32)$$

we have to note, however, that in the analytical representation of the SLy equation of state the pressure and density are expressed respectively in  $dyn/cm^2$  and  $g/cm^3$ , and the  $a_i$  are numerical parameters that can be found in [65]. The analytical representation (5.32) is then consistent only in the range of energy densities of order  $[10^4 - 10^{16}] g/cm^3$ , and it is clear that this sets a constraint on the scales of the solutions that can be described using such an equation of state. The choice of an equation of state indeed, fixing the energy scales of the fluid, renders necessary to make some clarifications on the units used. In particular, in the general quadratic theory, we have that the dimensionful and dimensionless energy densities relate as

$$\rho_{df} \simeq \rho_{dl} \frac{10^{90}}{\alpha} g/cm^3. \quad (5.33)$$

Having the minimum dimensionless value fixed at  $10^{-6}$  by the tolerance threshold of the root-finding algorithm, we have to choose values of  $\alpha$  not greater than  $10^{80}$ . We believe that, having found most of the dimensionless values of the density in the range  $[10^{-6} - 10^0]$ , a value of  $\alpha$  of order  $10^{74}$  might be optimal. For the evaluation of (5.32), and while showing the results, we will restore physical units fixing the length scale  $l_2 = 1/m_2$  equal to the Sun Schwarzschild radius  $r_{s,\odot} = 2G M_\odot$ , in a similar, yet different, fashion to what has been done in [66]. We use the same units, *i.e.* the unit length equals to the Sun Schwarzschild radius, also for the  $R + R^2$  and General Relativity results, in order to have an explicit comparison with the  $R + C_{\mu\nu\rho\sigma} C^{\mu\nu\rho\sigma}$  and full quadratic cases. The numerical value for the parameter  $\alpha$  (or  $\beta$ ) is then actually of order  $10^{74}$ , as required by the SLy equation of state. This value exceeds the  $10^{60}$  laboratory limit obtained for the

Yukawa correction to the gravitational potential [67, 31]. These values are also against “naturalness” principles, considering that they lead to minimal values of the masses  $m_0$  and  $m_2$ , which would be of order  $\mathcal{O}(10^{-9})\text{eV}$ , and an extreme amount of fine-tuning is necessary. Nevertheless, we opted to use these units for two reasons:

- exaggerating the quantitative variations from General Relativity we are able to have a better understanding of the qualitative differences between the different theories;
- most of the results that we will show in this section are sensitive only to the presence of two Yukawa terms in the potential, regardless of their fundamental origin, and then they could model different theories in which could be not necessary to have extremely large dimensionless numbers.

At last, we specify that in this section we fixed the energy scale of the fluid in the case of the polytropic equation of state by fixing  $k = 6.51185 \cdot 10^{-17}\text{cm}^3/\text{g}$ .

To have a better understanding of the role of the two quadratic terms in the action, we will investigate both the case in which a single Yukawa is present, that is, in Starobinski's  $R + R^2$  and Einstein-Weyl  $R + C^{\mu\nu\rho\sigma}C_{\mu\nu\rho\sigma}$  models, and the full quadratic theory. We believe that in this subsection can be instructive to study solutions with a ratio of the masses  $\xi = m_0/m_2$  different from unity in order to try to have an insight into the relative weights of the two terms in the action. In figures 13 and 14 can be indeed seen that non-vacuum solutions in the full quadratic theory and its reductions are qualitatively different; at the physical level, this is understood as a coupling between the fluid and the massive modes of the gravitational theory. We then believe that it is more relevant to study the general theory, and use Starobinski's and Einstein-Weyl models to have clear in mind the different roles of the two quadratic terms, taking into account the problems of using different masses ratios. Nonetheless, both from figures 13 and 14, and from Figure 30, we can try to extrapolate the relation between the Yukawa charges  $S_2^-$  and  $S_0^-$  and

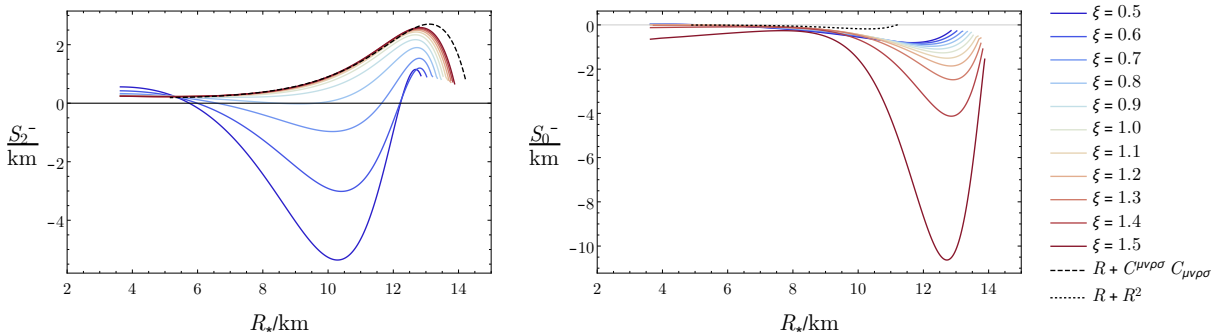


Figure 30:  $S_2^-$  and  $S_0^-$  relation with the radius varying  $\xi$ , and the reference  $R + C_{\mu\nu\rho\sigma}C^{\mu\nu\rho\sigma}$  and  $R + R^2$  solutions.

compact stars. The scalar sector has somehow a predictable trend: it is always attractive, and the associated charge  $S_0^-$  decreases as the value of  $\xi$  is lowered. Here we have to remember that lower values of  $\xi$  mean that the  $R^2$  term is dominant with respect to the  $C_{\mu\nu\rho\sigma}C^{\mu\nu\rho\sigma}$  term in the action (2.5), or, from a particle point of view, the range of the massive scalar contribution to the gravitational interaction is larger than the massive tensorial one. The tensor sector, on the contrary, can be both attractive and repulsive, which, however, is something we have already seen for all the solutions considered. In particular, for values of  $\xi > 1$  the contribution is always repulsive and the precise value has very little impact on the associated charge  $S_2^-$ , while for values  $\xi < 1$  it rapidly becomes attractive for most of the solutions. However, we have to remember that in this case the range of the scalar contribution is larger than the tensor one, and then we can associate the attractive behavior of the Weyl term to the presence of massive scalar particles outside the effective volume where the majority of the repulsive particles are present. As a final remark, we can differentiate the dependence of the solutions of the full quadratic theory from  $\xi = m_0/m_2$  in three classes:

- $m_0 > m_2$  the two Yukawa terms are competing, one being attractive and the other repulsive, and the scalar charge is larger than the tensorial one;
- $m_0 \sim m_2$  the two Yukawa terms are competing, one being attractive and the other repulsive, and the scalar charge is of the same order as the tensorial one;
- $m_0 < m_2$  the two Yukawa terms are both attractive, and the scalar charge is smaller than the tensorial one.

Nonetheless, we specify one more time that the only completely consistent case is the one with  $m_0 = m_2$ , in which then the scalar sector is always attractive and the tensor is always repulsive.

We move now to the analysis of explicit star structure, which we show in Figure 31 in the case of General Relativity, Starobinski's and Einstein-Weyl models, and in Figure 32 in the full quadratic theory. In particular, we opted to show the behavior of the metric functions  $h(r)$  and  $f(r)$ , the scalar curvature  $R$  and the pressure for three stars with the same mass. From Figure 31 it seems that the presence of the massive scalar results in a slight strengthening of gravity, with a deeper non-relativistic gravitational potential  $\phi(r) \propto (h(r) - 1)$  and higher internal pressure. The massive spin-2 particle, on the contrary, leads to a major softening of the gravitational interaction, with much smaller internal pressure and non-relativistic gravitational potential. On the other hand, including both terms results in a decrease in radial distortion and scalar curvature. If, in

the Einstein-Weyl case, we could relate this effect to the decrease in the fluid pressure and energy density, in the  $R + R^2$  case we have to connect this behavior with a specific property of the theory.

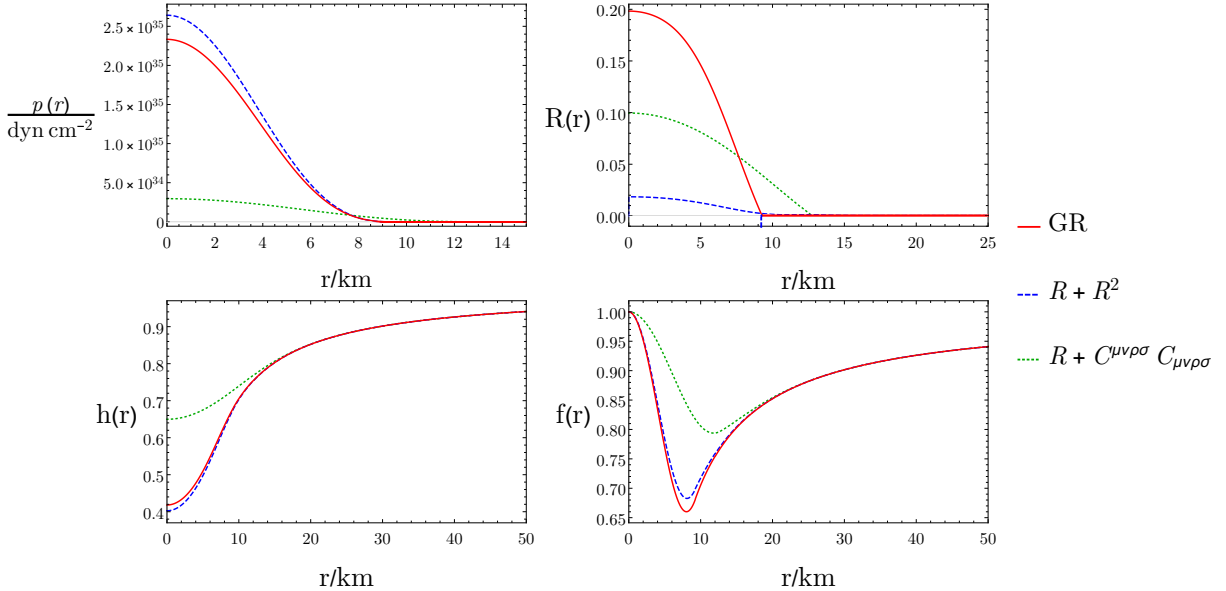


Figure 31: Structure of three  $M = M_{\odot}$  stars for GR,  $R + R^2$ , and  $R + C_{\mu\nu\rho\sigma}C^{\mu\nu\rho\sigma}$  theories; the dashed vertical lines in the top-right panel indicate the star surface in the  $R + R^2$  case. From left to right and top to bottom are: pressure, Ricci scalar, temporal component of the metric and radial component of the metric.

From Figure 32 we see that the full quadratic case is mainly affected by the presence of the Weyl term, with a global softening of gravity, that is less pronounced as the value of  $\xi$  is lowered. Here we have to remember that lower values of  $\xi$  mean that the  $R^2$  term is dominant with respect to the  $C_{\mu\nu\rho\sigma}C^{\mu\nu\rho\sigma}$  term in the action (2.6), or, from a particle point of view, the range of the massive scalar contribution to the gravitational interaction is larger than the massive tensorial one. The impact of the  $R^2$  term on the scalar curvature is also clearer, which is to increase the curvature outside the star and decrease it inside. The  $R^2$  term also contributes to smooth even more the radial component of the metric, decreasing the radial distortion. The behavior of the Ricci scalar is better understood by looking at the trace of the equation of motion (2.10)

$$(6\beta \square - 2\gamma) R = \frac{1}{2}T \quad \Rightarrow \quad \left( \frac{1}{\xi^2} \square - 2 \right) R = \frac{1}{2}T, \quad (5.34)$$

where on the right we made everything dimensionless and introduced the parameter  $\xi$ . For higher values of  $\xi$ , the Ricci scalar gets closer to its form in General Relativity  $R \propto -T$ , which is zero outside and large inside the star. For lower values of  $\xi$ , instead, we have that the presence of the fluid has little effect on scalar curvature that gets closer to being determined by  $\square R = 0$  and then, having imposed regularity in the origin and asymptotic

flatness, flattens out and gets closer to zero. Having a deeper gravitational potential, the flattening of the scalar curvature has to be driven by a more regular behavior of  $f(r)$ , or in other words, by a decrease in the radial distortion.

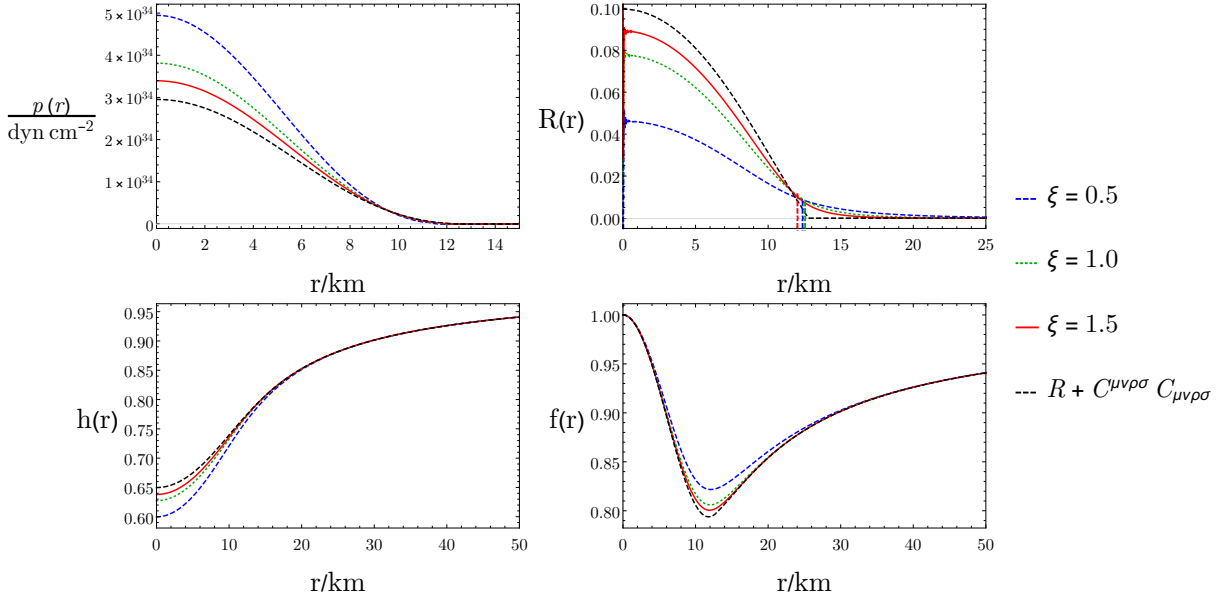


Figure 32: Structure of three  $M = M_{\odot}$  stars with different values of  $\xi$ , and the reference  $R + C_{\mu\nu\rho\sigma}C^{\mu\nu\rho\sigma}$  solution; the dashed vertical lines in the top-right panel indicate the star surfaces in the full quadratic cases. From left to right and top to bottom are: pressure, Ricci scalar, temporal component of the metric and radial component of the metric.

Having now a fluid sustaining our solution, it becomes crucial to understand in which way the properties of the fluid affect the global properties of the compact star. In Figure 33 and 34 we show the asymptotic mass  $M$  relations with the star radius and central pressure, for the restricted theories and for the full quadratic theory, respectively. In Figure 33 the softening effect of the Weyl term is manifest, with the same pressure being able to sustain greater stellar masses, and with the same mass being bounded in larger volumes. We also note that this softening is quite impressive, with an increase in the maximum mass of a factor greater than 1.5.

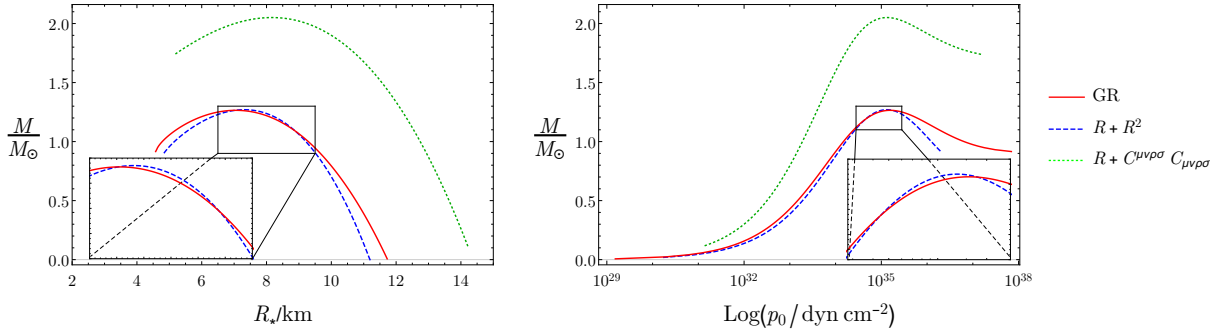


Figure 33: Mass relations with radius and central pressure for GR,  $R + R^2$  and  $R + C_{\mu\nu\rho\sigma}C^{\mu\nu\rho\sigma}$ .

From both Figure 33 and 34, we see that the  $R^2$  term does not always lead to a strengthening of gravity, but there is a trend inversion for higher masses, where the scalar contribution seems to weaken the gravitational interaction, resulting in an increase of the maximum mass. From Figure 34, it also appears that there is a confirmation that the full quadratic theory is mainly affected by the Weyl term, with the scalar mode slightly modifying the parameters found in the  $R + C_{\mu\nu\rho\sigma}C^{\mu\nu\rho\sigma}$  theory.

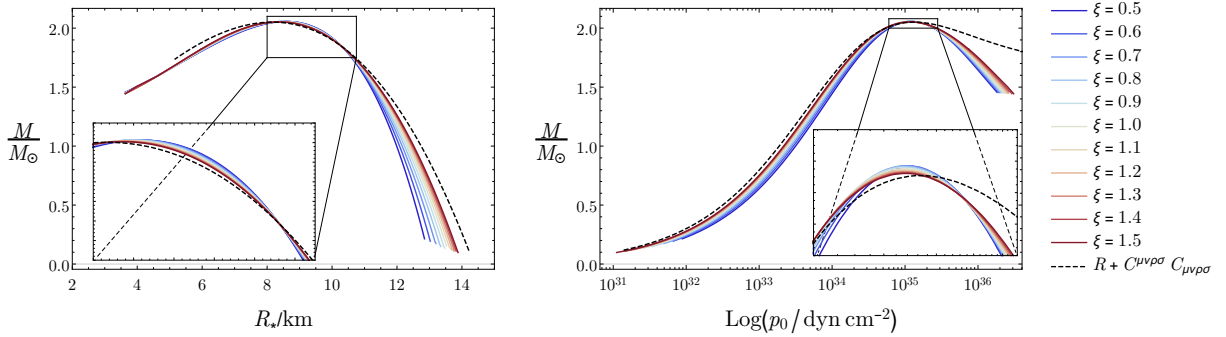


Figure 34: Mass relations with radius and central pressure varying  $\xi$ , and the reference  $R + C_{\mu\nu\rho\sigma}C^{\mu\nu\rho\sigma}$  solutions.

Even if a complete formal description of such effects has yet to be found, we can still associate these behaviors with the nature of the two massive modes. The Weyl term acts through a particle with negative energy states, therefore it is sensible to expect a repulsive contribution to gravity. The  $R^2$  term, instead, acts through a massive scalar that has a more familiar role in gravity. In particular, we expect an attractive contribution to the interaction, but also an increase in stability, considering that the scalar field is also distributed outside the star. It is then sensible to have a strengthening of the gravitational interaction, but also a greater maximum mass.

In all the previous discussions we left unchanged the mass of one of the massive modes or, in other words, the value of either  $\alpha$  or  $\beta$  in the action (2.5). This approach is useful to emphasize the relative effects of the  $R^2$  and Weyl terms, but does not explain the global impact of the quadratic terms in detail. Here we want to give a flavor of the effects of the free parameters; while we are conscious that differences in the internal energy densities and pressures would have important consequences while using a realistic equation of state, we indeed limit ourselves to present the impact of the free parameters only at a qualitative level using the polytropic e.o.s. In Table 3 we show the variation of the maximum mass, the radius and central pressure for stars with mass equal to their maximum in General Relativity, similar to what has been done in [68].

The parameter  $\alpha$  (or  $\beta$  for the  $R + R^2$  theory) is in units of the value  $\alpha_0$  (or  $\beta_0$ ) for which the intrinsic length scale is equal to the Sun Schwarzschild radius. We confirm once again

Theory	$\alpha/\alpha_0$ or $\beta/\beta_0$	$\Delta M_{max}/M_\odot$	$\Delta R_{max}/km$	$\Delta p_{c,max}/dyn\,cm^{-2}$
$R + R^2$	1/2	0.001	0.350	$-0.969 \cdot 10^{35}$
	1	0.005	0.539	$-0.544 \cdot 10^{35}$
	2	0.009	0.665	$0.314 \cdot 10^{35}$
	5	0.013	0.770	$2.897 \cdot 10^{35}$
	10	0.015	0.816	$7.218 \cdot 10^{35}$
$R + C_{\mu\nu\rho\sigma}C^{\mu\nu\rho\sigma}$	1/2	0.472	3.733	$-1.502 \cdot 10^{35}$
	1	0.786	5.112	$-1.505 \cdot 10^{35}$
	2	1.256	6.915	$-1.512 \cdot 10^{35}$
	5	2.225	10.177	$-1.524 \cdot 10^{35}$
	10	3.341	13.585	$-1.531 \cdot 10^{35}$
Full theory, $\xi = 0.5$	1/2	0.477	3.489	$-1.488 \cdot 10^{35}$
	1	0.791	4.549	$-1.481 \cdot 10^{35}$
	2	1.258	5.849	$-1.480 \cdot 10^{35}$
	5	2.209	8.004	$-1.484 \cdot 10^{35}$
	10	3.292	10.030	$-1.490 \cdot 10^{35}$
Full theory, $\xi = 1.0$	1/2	0.472	3.615	$-1.496 \cdot 10^{35}$
	1	0.790	4.808	$-1.495 \cdot 10^{35}$
	2	1.267	6.261	$-1.496 \cdot 10^{35}$
	5	2.243	8.644	$-1.501 \cdot 10^{35}$
	10	3.357	10.853	$-1.506 \cdot 10^{35}$
Full theory, $\xi = 1.5$	1/2	0.474	3.668	$-1.499 \cdot 10^{35}$
	1	0.787	4.936	$-1.450 \cdot 10^{35}$
	2	1.264	6.512	$-1.504 \cdot 10^{35}$
	5	2.247	9.140	$-1.511 \cdot 10^{35}$
	10	3.374	11.608	$-1.517 \cdot 10^{35}$

Table 3: Impact of the free parameters on the solutions; the parameters are taken in units of the length scales discussed in subsection,  $\Delta M_{max}$  is the difference in the maximum mass of the stars,  $\Delta R_{max}$  and  $\Delta p_{c,max}$  are the differences of the radius and central pressure for stars with mass equal to the maximum of General Relativity.

that the Weyl term has an impressive impact on the solutions, with both masses and radii increasing significantly as the value of  $\alpha$  is increased; the  $R^2$  term, instead, only slightly modifies the case of General Relativity and the Einstein-Weyl solutions. We also have a confirmation of the softening effect of the Weyl term, having a decrease in the central pressure, and of the trend inversion of the strengthening effect of the  $R^2$  term close to the maximum mass. We note, however, that the significant differences in the

internal pressures for different values of  $\beta$  might be much more relevant while considering a realistic equation of state. In conclusion, the variation of the free parameters of the theory does not change the behavior of the solutions of quadratic gravity but, as could be expected, has an impact only on the scales of the deviations from General Relativity.

## 5.5 Black holes in scale-invariant gravity

Having a more complex theory, we believe that the first step that can be done to understand the solutions of scale-invariant gravity is to analyze the behavior of the known, analytical solutions of General Relativity whenever they are considered as solutions of this theory. In this subsection we will not indulge in the properties of these solutions because they are common knowledge, having exactly the same geometrical structure as the solutions of General Relativity. The relevant discrepancies will be given by these solutions' dynamical and thermodynamical aspects, which we postpone to the following sections. Considering then the ansatz for the metric

$$ds^2 = -f(r)dt^2 + \frac{dr^2}{f(r)} + r^2d\Omega^2, \quad (5.35)$$

the known analytical solutions are the Schwarzschild metric

$$\begin{aligned} \phi &= 0, \\ R &= 0, \\ f(r) &= 1 - \frac{2M}{r}, \end{aligned} \quad (5.36)$$

where  $M$  is a free length parameter; there is also a Schwarzschild-anti-de Sitter solution

$$\begin{aligned} \phi &= 0, \\ R &= -4|\Lambda|, \\ f(r) &= 1 - \frac{2M}{r} + \frac{|\Lambda|}{3}r^2, \end{aligned} \quad (5.37)$$

where  $\Lambda$  is a free *negative* cosmological constant, and we used its modulus to underline this fact; finally, there are two distinct Schwarzschild-de Sitter solutions

$$\begin{aligned} \phi &= 0, \\ R &= 4\Lambda_u, \\ f(r) &= 1 - \frac{2M_u}{r} - \frac{\Lambda_u}{3}r^2, \end{aligned} \quad (5.38)$$

and

$$\begin{aligned} \phi &= \pm \sqrt{\frac{8\xi\Lambda_s}{\lambda}}, \\ R &= 4\Lambda_s, \\ f(r) &= 1 - \frac{2M_s}{r} - \frac{\Lambda_s}{3}r^2, \end{aligned} \quad (5.39)$$

where  $\Lambda_u$ ,  $\Lambda_s$ ,  $M_u$  and  $M_s$  are free parameters, and the cosmological constants are positive. We can clearly also find (anti-)de Sitter solutions, simply requiring the  $M$  parameters to be zero; then there will be a single anti-de Sitter spacetime and two de Sitter spacetimes, of which one has a zero scalar field and the other a non-zero scalar field. If we look at the theory in the Einstein frame, not all these solutions have a counterpart: the Schwarzschild and Schwarzschild-anti-de Sitter solutions would require an ill-defined conformal transformation  $\tilde{g}_{\mu\nu} = u(x)g_{\mu\nu}$  with a non-positive  $u(x)$ , which however *is not* a conformal map. In the Einstein frame the only solutions with constant curvature and scalar field are indeed two Schwarzschild-de Sitter solutions, namely

$$\begin{aligned}\rho &= \rho_0, \\ \zeta &= 0, \\ \Lambda_u &= \frac{M_{SI}^2}{16\beta}, \\ f(r) &= 1 - \frac{2M_u}{r} - \frac{\Lambda_u}{3}r^2,\end{aligned}\tag{5.40}$$

and

$$\begin{aligned}\rho &= \rho_0, \\ \zeta &= \sqrt{6}M_{SI}\operatorname{arcsinh}\left(\sqrt{\frac{\xi}{12\Omega}}\right), \\ \Lambda_s &= \frac{M_{SI}^2}{16\beta}\left(1 - \frac{\xi^2}{\Omega}\right), \\ f(r) &= 1 - \frac{2M_s}{r} - \frac{\Lambda_s}{3}r^2,\end{aligned}\tag{5.41}$$

where here only  $\rho_0$ ,  $M_u$  and  $M_s$  are free parameters. Scale invariance, however, is recovered if we remember that the effective Planck mass  $M_{SI}$  is a redundant parameter, and it is not fixed by any experiment. To fix a convention for the next sections, we will refer to the horizon of Schwarzschild solutions as

$$r_b = 2M,\tag{5.42}$$

and to the horizon of Schwarzschild-anti-de Sitter as

$$r_b \quad \text{s.t.} \quad r_b - 2M + \frac{|\Lambda|}{3}r_b^3 = 0.\tag{5.43}$$

For the Schwarzschild-de Sitter solution, instead, we remember that whenever the parameters satisfy the relation  $9M^2\Lambda < 1$ , the function  $f(r)$  has three real roots given

by

$$r_b = \frac{2}{\sqrt{\Lambda}} \cos\left(\frac{\pi + \eta}{3}\right), \quad (5.44)$$

$$r_c = \frac{2}{\sqrt{\Lambda}} \cos\left(\frac{\pi - \eta}{3}\right), \quad (5.45)$$

$$r_0 = -\frac{2}{\sqrt{\Lambda}} \cos\left(\frac{\eta}{3}\right), \quad (5.46)$$

where  $\cos \eta = 3M\sqrt{\Lambda}$ . The first two are positive and represent the black hole and cosmological horizons, respectively, while the third will not be considered as it is in the region  $r < 0$ . The main goal in our study of solutions in scale-invariant gravity will be looking for a transition between the two different Schwarzschild-de Sitter solutions. This is motivated by the results in a cosmological setting, which we will shortly present, and will be carried out both at a purely classical and dynamical level in 6.3 and at a semiclassical level in 7.3.

### 5.5.1 Quadratic scale-invariant cosmology

A transition between two cosmological de Sitter spacetimes is known to happen in scale-invariant gravity, as shown in [27, 28] in the simplified theory (2.56). By imposing the flat Friedmann-Lemaître-Robertson-Walker metric

$$ds^2 = -dt^2 + a(t)^2 \delta_{ij} dx^i dx^j \quad (5.47)$$

in the equations of motion, is indeed possible to rewrite the equations of motion (2.57) as two second-order equations in the scalar field  $\phi$  and the Hubble parameter  $H = \dot{a}/a$ , namely

$$\begin{aligned} \ddot{\phi} + 3H\dot{\phi} - 12\xi\phi\dot{H} - \phi(24\xi H^2 - \lambda\phi^2) &= 0, \\ 36\beta\left(2H\ddot{H} - \dot{H}^2 + 6H^2\dot{H}\right) - \frac{1}{2}\dot{\phi}^2 + 12\xi\phi\dot{\phi}H + \frac{\phi^2}{4}(24\xi H^2 - \lambda\phi^2) &= 0, \end{aligned} \quad (5.48)$$

where the  $(\cdot)$  indicates a derivative with respect to the cosmological time coordinate  $t$ . Despite the apparent complicate form, these equations can be reduced to four first-order equations and studied with the means of dynamical system analysis. The result is that the system has two fixed points. The first, at

$$H_u = \sqrt{\frac{\Lambda_u}{3}}, \quad \phi_u = 0, \quad (5.49)$$

where  $\Lambda_u$  is an arbitrary cosmological constant, while the second, at

$$H_s = \sqrt{\frac{\Lambda_s}{3}}, \quad \phi_s = \sqrt{\frac{8\xi\Lambda_s}{\lambda}}, \quad (5.50)$$

where  $\Lambda_s$  is still arbitrary. A linear analysis of the two fixed points shows that the first one (5.49) is unstable, and the second one (5.50) is stable. Numerical integration not only confirms the stability and instability of the two points but shows explicitly that there is a transition between the unstable and the stable points, which we show in Figure 35.

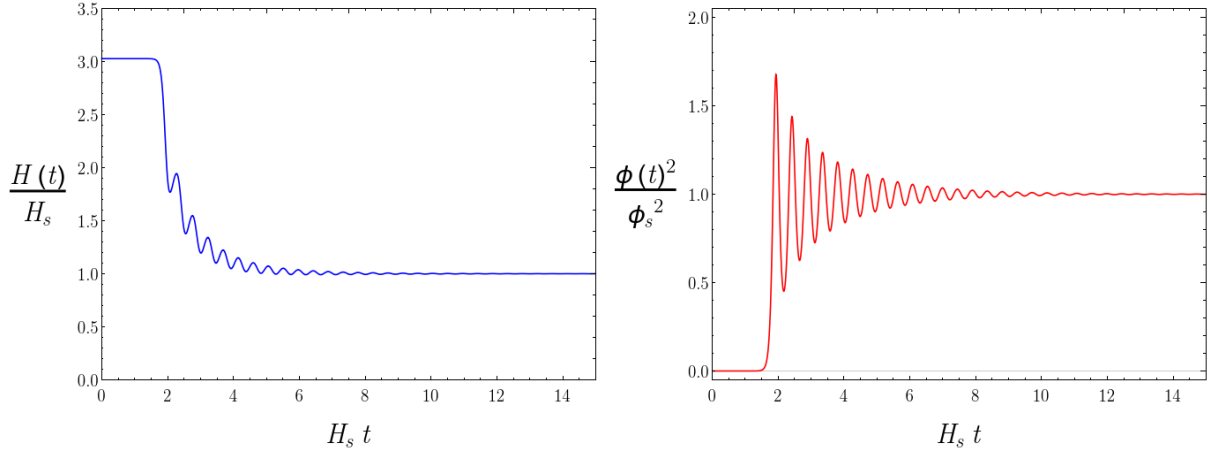


Figure 35: Cosmological evolution of the Hubble parameter  $H(t)$ , on the left, and the scalar field  $\phi(t)^2$ , on the right, in terms of the cosmological time coordinate.

It turns out that the evolution from the unstable to the stable point yields an inflationary phase, thoroughly studied in [28]. In particular, we can use (2.55) to relate the two cosmological constants of the two possible de Sitter solutions with zero and non-zero scalar field:

$$\Lambda_u = \left( 1 + \frac{\xi(1 + 12\xi)}{12\beta\lambda} \right) \Lambda_s. \quad (5.51)$$

The interesting feature is that, at the stable fixed point, the scalar field has a non-trivial value and, as a result, a mass term is spontaneously generated and the scale invariance is spontaneously broken. Together with looking for a similar transition in the case of static and spherically symmetric configurations, one of our goals will be trying to understand whether the presence of black holes will increase the lifetime of the meta-stable phase, and then of inflation, or if it will speed up its decay.

## 6 Quasi-normal modes and stability of the solutions

The stability of solutions against linear perturbations is one of the most important properties to investigate. An unstable solution in general will be in a time-evolving state and, if the time scales of this evolution are much shorter than the ones generally present in Astrophysics, the probability of detecting it could be effectively zero. The phase diagram of solutions of quadratic gravity and the knowledge of their global properties are then only the starting point for the analysis of these solutions in a physical context. In this section, we study the evolution of linear perturbations of quadratic gravity and scale-invariant gravity solutions, with a special focus on black hole solutions.

This section is divided in three parts:

- in the first subsection we present the general procedure used to integrate the equations governing the dynamics of linear perturbations, and we will discuss how it can be used both for assessing the stability of a solution and to recover the frequency of quasi-normal modes, that are the decaying oscillations of perturbations at large distances;
- in the second subsection we apply this procedure to the solutions of Einstein-Weyl gravity: after presenting the equation of motion of tensor perturbation derived in [69], we first show that both Schwarzschild and non-Schwarzschild black holes in quadratic gravity need a minimum radius to be stable, which is precisely the radius at which the two families of solutions crosses each other; we also make a first exploratory study of the stability of exotic solutions, finding that all wormhole solutions are unstable, attractive naked singularities are stable, and repulsive naked singularities are stable only if the Yukawa charge is small;
- in the third subsection we study the evolution of perturbations of the two Schwarzschild-de Sitter solutions present in scale-invariant gravity: we show using both analytical and numerical methods that Schwarzschild-de Sitter black holes with zero scalar field are always unstable, while Schwarzschild-de Sitter solutions with a non-zero value of the scalar field are always stable, in agreement with the results of the theory in a cosmological setting [27].

The results on the stability of solutions of quadratic gravity presented in Subsection 6.2 are not part of any publication yet, while the results on the stability and instability of Schwarzschild-de Sitter black holes in scale-invariant gravity presented in Subsection 7.3, which we specify here that have been found by Simon Boudet, have been published in [35].

## 6.1 Numerical methods for quasi-normal modes

As just anticipated, in this subsection we briefly describe the method used to study perturbations in quadratic gravity and scale-invariant gravity; however, we will not refer to a specific form of the equations used, and the method presented can be applied to quadratic gravity as well as General Relativity or scale-invariant gravity.

Linear perturbations are defined considering the ansatz for the metric

$$g_{\mu\nu} = \bar{g}_{\mu\nu} + \epsilon h_{\mu\nu}, \quad (6.1)$$

where  $\bar{g}_{\mu\nu}$  is the background metric and  $h_{\mu\nu}$  is the perturbation, and the equations of motion are expanded at first order in  $\epsilon$

$$\mathcal{G}_{\mu\nu} = \bar{\mathcal{G}}_{\mu\nu} + \epsilon \mathcal{H}_{\mu\nu} + O(\epsilon^2) = \epsilon \mathcal{H}_{\mu\nu} + O(\epsilon^2), \quad (6.2)$$

where the last equality is given by the fact that the background metric satisfies the background equations of motion. The impressive result of the Regge-Wheeler-Zerilli equation [70, 71] was to reduce the tensor equation (6.2), in the case of a static and spherically symmetric background, to a scalar equation for a function  $\varphi(r, t)$  in the form

$$\left( \frac{d^2}{dt^2} - \frac{d^2}{dr^{*2}} \right) \varphi(r, t) + V(r) \varphi(r, t) = 0, \quad (6.3)$$

where  $V(r)$  is a potential determined by the theory in exam and the background metric, and  $r^*$  is the tortoise coordinate, defined as usual as

$$r^* = \int \frac{dr}{\sqrt{f(r)h(r)}}. \quad (6.4)$$

Many methods to study the stability of the solutions consider the ansatz for the function  $\varphi(r, t) = \psi(r)e^{i\omega t}$  (see for example [72]), to rewrite equation (6.3) as

$$\frac{d^2}{dr^{*2}} \psi(r) - (\omega^2 + V(r)) \psi(r) = 0, \quad (6.5)$$

and to look for a positive or negative value of the imaginary part of  $\omega$  and assess whether the solution is stable or unstable. Our procedure instead directly tackles equation (6.3) using the light-cone coordinates  $v = t + r^*$  and  $u = t - r^*$ , in which the equation takes the form

$$4 \frac{d^2}{dv du} \varphi(u, v) + V(r) \varphi(u, v) = 0 \quad (6.6)$$

which can be integrated numerically. As described in [72, 73, 74, 75, 35], the standard technique is to discretize the coordinates  $u, v$  on a grid with step  $h$  and dimension  $n_{max} \times n_{max}$  and performing the integration as

$$\varphi(N) = \varphi(W) + \varphi(E) - \varphi(S) + \frac{h^2}{8} V(S)(\varphi(W) + \varphi(E)) + O(h^4) \quad (6.7)$$

where the variable is evaluated in the points  $S = (u, v)$ ,  $W = (u + h, v)$ ,  $E = (u + h, v)$  and  $N = (u + h, v + h)$ , as shown in Figure 36. With suitable initial conditions, the integration can be carried on row after row, and the evolution of perturbation is known both in space and in time. There are indeed two fundamental pieces of information that can be extracted with this procedure:

- setting  $v - u = 2r_\infty^*$ , with  $r_\infty^*$  large and fixed, gives us the time evolution of perturbation at large distances, of which the frequencies are the quasi-normal modes of the solution;
- setting  $v + u = 2t_\infty$ , with  $t_\infty$  large and fixed, gives us the radial displacement of perturbations at large times, and the presence of large values of the perturbations at any point is the smoking-gun of the instability of the solution.

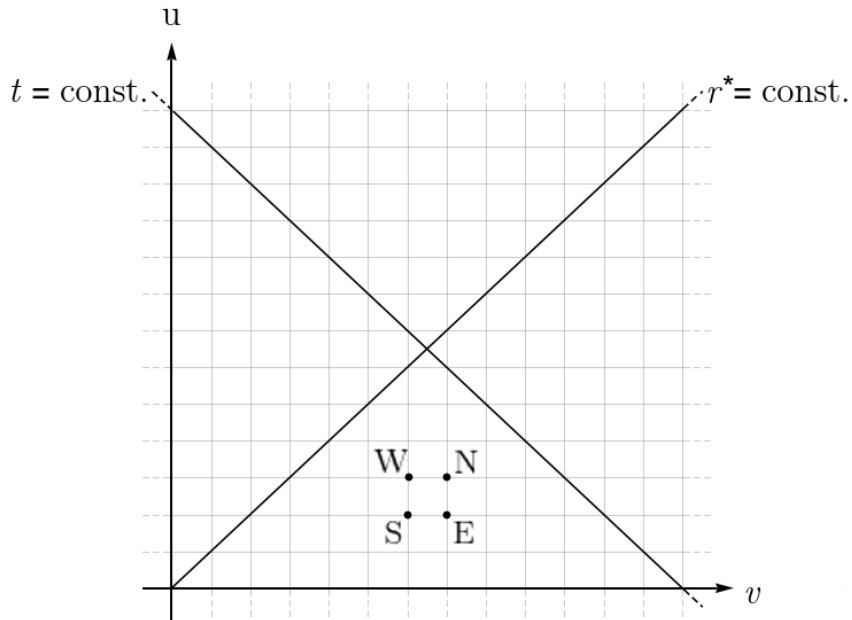


Figure 36: Integration grid for the numerical evolution of the perturbation on light-cone coordinates; the black dots indicate the rhomboid of vertices  $S$ ,  $W$ ,  $E$  and  $N$  used for the integration.

For this integration there are two main points of caution: the first one is numerical, and it is due to the fact that the theory predicts a potential with a dependence from the radial coordinate  $r$ , but the integration is done using the tortoise coordinate  $r^*$ , the second is more fundamental and it is the choice of the initial conditions. Regarding the first point, the inversion of the tortoise coordinate has been done simply by looking at the radius  $\bar{r}(r^*)$  which solves the equation

$$\int \frac{dr}{\sqrt{f(r)h(r)}} - r^* \Big|_{r=\bar{r}(r^*)} = 0. \quad (6.8)$$

While it can be numerically expensive to invert the tortoise coordinate at each point of the grid, having a potential that depends only on the radius allows us to evaluate the potential at the beginning of the integration for all the possible values of  $r^*$  which, being on a diagonal of the grid, will be  $n_{max}$  instead of  $n_{max} \times n_{max}$ , and consider its value at the point  $S$  as

$$V(S) = V(v, u) = V(v - u) = V(r^*) = V(r). \quad (6.9)$$

Regarding the second point of caution, the initial conditions have to be set differently depending on the solutions considered. On the  $u = 0$  axis the standard approach is to consider an initial Gaussian perturbation

$$\varphi(v, 0) = e^{-\frac{(v-v_0)^2}{2\sigma^2}}, \quad (6.10)$$

which represents an initial “impulse” sent into the spacetime, of which, however, the specific form will not be relevant for the late time evolution. For black holes the second standard initial condition is to set to zero the perturbation on the  $v = 0$  axis (see as an example [76]). With this choice of the initial conditions, it is easy to see that the grid can be filled integrating row by row. The same initial condition can be used for wormholes but not for naked singularities, for which the tortoise coordinate is not defined in the range  $(-\infty, \infty)$  but in the range  $(0, \infty)$ . In this case we considered the initial conditions  $\varphi(r^* = 0) = 0$ , as done for example in [77]. While the condition for black holes means setting to zero the perturbation close to the horizon, both the conditions for wormholes and naked singularities imply that we are setting to zero the perturbation close to the singularity. Even if it might be possible to have a non-zero perturbation at the singularity, we will consider only this case as in the most conservative approach the singularity is a point that does not belong to the spacetime, and then considering the perturbation exactly at the singularity has no physical meaning. In the subsequent discussion the perturbation is integrated using a modification of the previous **Fortran** codes, where the inversion of the tortoise coordinate is made using the N.A.G. subroutine C05ADF with the same precision of the integrator. To test the code, we performed some integrations in the case of General Relativity, in which the potential in (6.6) has to be taken to be the Regge-Wheeler one

$$V(r) = h(r) \left( \frac{l(l+1)}{r^2} - \frac{3f(r)}{2r} \left( \frac{h'(r)}{h(r)} + \frac{f'(r)}{f(r)} \right) \right), \quad (6.11)$$

and the metric is the Schwarzschild one, which is

$$h(r) = f(r) = 1 - \frac{2M}{r}. \quad (6.12)$$

We show in Figure 37 both the potential and the quasi-normal modes for a perturbation of a Schwarzschild metric with horizon radius  $r_H = 1$  and multipole  $l = 2$ . This choice

of multipole has been taken because it is the lowest multipole perturbation which cannot be removed with a choice of gauge. Both the potential and the quasi-normal modes agree with the standard results in General Relativity; in particular, we compared the potential found using the shooting method with its analytical form and the power law tail of the quasi-normal modes with the expected analytical one

$$\phi(t, r_\infty) \sim t^{-(2l+3)}. \quad (6.13)$$

We believe then that we can use the code in quadratic gravity with sufficient trust in its results.

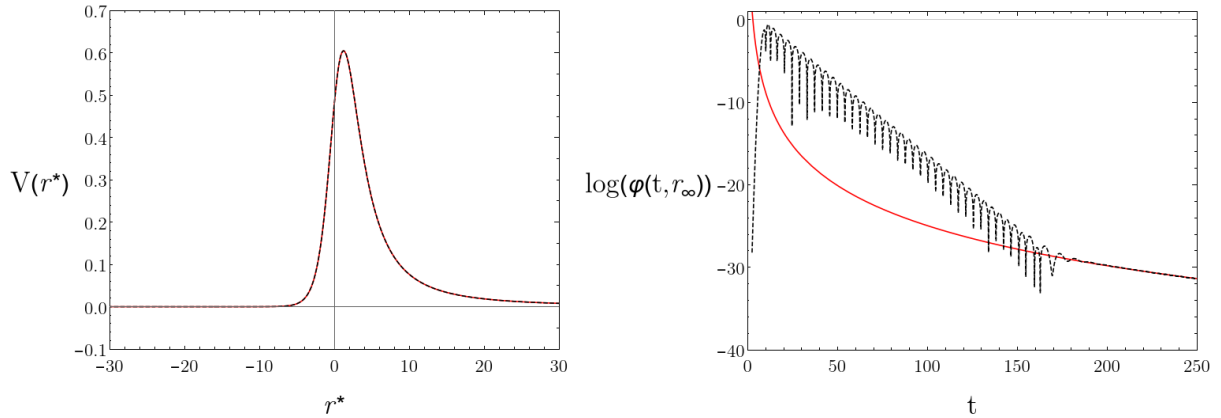


Figure 37: Regge-Wheeler potential in terms of the tortoise coordinate and quasi-normal modes for a Schwarzschild black hole with horizon radius  $r_H = 1$  for a perturbation of multipole  $l = 2$ ; in dashed black there are the numerical results, and in solid red the analytical ones.

## 6.2 Quasi-normal modes of solutions of quadratic gravity

The main obstacle that prevented the study of perturbations in quadratic gravity was the difficulty in finding an equation in the form of (6.3) for tensor perturbation in quadratic gravity. Nonetheless, such an equation was found at the end of 2022 by A. Held and J. Zang in [69]. The first step in the derivation is rewriting the action (2.5) in the Einstein frame, following [40], as

$$\mathcal{I}_{Stelle} = \int d^4x \sqrt{-g} \gamma \left[ R + \frac{3}{2} \psi \square \psi - \frac{3}{2} m_0^2 e^{-2\psi} (e^\psi - 1)^2 + 2f^{\mu\nu} G_{\mu\nu} + m_2^2 (f^{\mu\nu} f_{\mu\nu} - f^2) \right], \quad (6.14)$$

where  $\psi$  is a scalar auxiliary field associated with the massive scalar mode and  $f_{\mu\nu}$  is an auxiliary tensor field associated with the massive tensor mode. If we consider now the perturbation

$$\begin{aligned} g_{\mu\nu} &= \bar{g}_{\mu\nu} + \delta g_{\mu\nu}, \\ \psi &= \bar{\psi} + \delta\psi, \\ f_{\mu\nu} &= \bar{f}_{\mu\nu} + \delta f_{\mu\nu}, \end{aligned} \quad (6.15)$$

and impose the condition of Ricci scalar flat background solutions, which set  $\bar{R} = \bar{\psi} = \bar{f} = 0$ , the linear equations of motion are

$$\begin{aligned} \bar{\square}\delta\psi + m_0^2\delta\psi &= 0, \\ \delta G_{\mu\nu} + m_2^2(\delta f_{\mu\nu} - \bar{g}_{\mu\nu}\delta f) &= 0, \\ \bar{\square}\delta f_{\mu\nu} - \bar{\nabla}_\mu\bar{\nabla}_\nu\delta f + 2\bar{R}_{\mu\rho\nu\sigma}\delta f^{\rho\sigma} + 2\bar{f}^{\rho\sigma}\delta R_{\mu\rho\nu\sigma} + \\ -m_2^2\left(\delta f_{\mu\nu} - \bar{g}_{\mu\nu}\bar{f}^{\rho\sigma}\delta f_{\rho\sigma} - (\bar{g}_{\mu\nu} + \bar{f}_{\mu\nu})\delta f - \frac{1}{2}\bar{f}^{\rho\sigma}\bar{f}_{\rho\sigma}\delta g_{\mu\nu}\right) &= 0, \end{aligned} \quad (6.16)$$

where  $\delta G_{\mu\nu}$  and  $\delta R_{\mu\rho\nu\sigma}$  are the first order variations of the Einstein and Riemann tensor with respect to the metric and  $\bar{\nabla}_\mu$  and  $\bar{\square}$  are the covariant derivative and the d'Alembert operator built with respect to the background metric. The massive scalar mode is completely decoupled, and we will focus solely on the tensor perturbations. We now consider the ansatz for the perturbations

$$\begin{aligned} \delta g_{\mu\nu} &= \begin{pmatrix} -h(r)H_0(r) & H_1(r) & 0 & 0 \\ H_1(r) & \frac{H_2(r)}{f(r)} & 0 & 0 \\ 0 & 0 & r^2\mathcal{K}(r) & 0 \\ 0 & 0 & 0 & r^2\sin^2\theta\mathcal{K}(r) \end{pmatrix} Y_{lm}(\theta, \phi)e^{-i\omega t}, \\ \delta f_{\mu\nu} &= \begin{pmatrix} -h(r)F_0(r) & F_1(r) & 0 & 0 \\ F_1(r) & \frac{F_2(r)}{f(r)} & 0 & 0 \\ 0 & 0 & r^2\mathcal{M}(r) & 0 \\ 0 & 0 & 0 & r^2\sin^2\theta\mathcal{M}(r) \end{pmatrix} Y_{lm}(\theta, \phi)e^{-i\omega t}. \end{aligned} \quad (6.17)$$

As discussed in [69], while monopole and dipole perturbations are pure gauge for massless tensor perturbations, this is not the case for massive ones; taking  $l = m = 0$ , using the constraints  $f = 0$  and  $\nabla_\mu f^{\mu\nu} = 0$ , choosing a gauge such that  $\mathcal{K}(r) = H_0(r) = 0$  and using the two lowest order metric perturbation equations to remove  $H_1(r)$  and  $H_2(r)$  leaves us with the two equations and the constraint

$$\begin{aligned} \phi''(r) + \left(\frac{4}{r} + \frac{3h'(r)}{2h(r)} - \frac{f'(r)}{2f(r)}\right)\phi'(r) + \frac{\omega^2\phi(r)}{h(r)f(r)} + V_{\phi\phi}(r)\phi(r) + V_{\phi\chi}(r)\chi &= 0, \\ \chi''(r) + \left(\frac{2}{r} + \frac{3h'(r)}{2h(r)} + \frac{3f'(r)}{2f(r)}\right)\chi'(r) + \frac{\omega^2\chi(r)}{h(r)f(r)} + V_{\chi\chi}(r)\chi(r) + V_{\chi\phi}(r)\phi &= 0, \\ \phi'(r) + i\frac{2f(r)}{r}\chi'(r) + V_\phi(r)\phi(r) + V_\chi(r)\chi(r) &= 0, \end{aligned} \quad (6.18)$$

where  $\phi(r) = -2\omega\mathcal{M}(r)$ ,  $\chi(r) = F_1(r)$  and the various  $V$ 's are potentials independent of  $\omega$ ; for more details we refer to the original article [69]. Finally, with the ansatz

$$\begin{aligned} \phi(r) &= a(r)\tilde{\psi}(r) + b(r)\tilde{\psi}'(r), \\ \chi(r) &= c(r)\tilde{\psi}(r) + d(r)\tilde{\psi}'(r), \end{aligned} \quad (6.19)$$

where  $a(r)$ ,  $b(r)$  and  $c(r)$  are fixed by the equations and  $b(r) = 0$  for simplicity, and the new variable

$$\varphi(r, t) = r\tilde{\psi}(r)e^{i\omega t}, \quad (6.20)$$

is it possible to write a Zerilli-like equation for the tensor mode of the metric with the potential

$$\begin{aligned} V(r) = & \frac{h(r)f'(r) + h'(r)f(r)}{2r} + m_2^2 h(r) + \\ & + \frac{24m_2^2 f(r)h(r)^2 (rf'(r) + 2f(r))(2h(r) - rh'(r))}{r((h(r)f'(r) + f(r)h'(r))(h(r)(3rf'(r) - 4) + 3rf(r)h'(r)) + 4m_2^2 r(1 - 3f(r))h(r)^2)} + \\ & + \frac{288m_2^4 f(r)^3 h(r)^3 (rh'(r) - 2h(r))^2}{((h(r)f'(r) + f(r)h'(r))(h(r)(3rf'(r) - 4) + 3rf(r)h'(r)) + 4m_2^2 r(1 - 3f(r))h(r)^2)^2}, \end{aligned} \quad (6.21)$$

where the second term indicates that the potential does not go to zero at large radii, as in General Relativity, but goes to the limiting value  $V(r) \rightarrow m_2^2$  as expected by a massive mode. Perturbations have been studied by analyzing the imaginary part of  $\omega$  in (6.5) in the case of Schwarzschild black holes [78] and non-Schwarzschild black holes [69]; in both cases, it has been shown that black holes are stable only up to a minimum radius  $r_{min} = 0.876$  in numerical units, which is exactly the radius where the two families of solutions cross each other. In this subsection we will confirm these results by integrating the wave-like equation (6.6), and show the first step done to understand all the regions of the phase diagram with stable or unstable solutions.

### 6.2.1 Quasi-normal modes of black holes in quadratic gravity

As a first step in studying the stability of black holes, it is necessary to run the shooting code for black holes in order to define the metric functions  $h(r)$  and  $f(r)$  and determine the tortoise coordinate in function of the radial coordinate. Once the background metric is defined, we can invert the tortoise coordinate and find the potential (6.21) in function of  $r^*$ . To explore late times with the method described in Subsection 6.1, however, it is necessary to have the potential defined for very small and very large values of the tortoise coordinate. For this reason, the metric has to be evaluated outside the range  $[r_O, r_\infty] = [10^{-3}, 18]$  used for the shooting method; in particular, we considered the different intervals

$$\begin{aligned} r < r_{\ll 1}, & \quad h(r), f(r) \text{ not defined, } V(r) = 0, \\ r_{\ll 1} < r < r_O, & \quad h(r), f(r) \text{ from the series expansion in (3.28),} \\ r_O < r < r_\infty, & \quad h(r), f(r) \text{ from the shooting method,} \\ r > r_\infty, & \quad h(r), f(r) \text{ from the weak field expansion (3.5),} \end{aligned}$$

where  $r_{\ll 1}$  is the radius at which the potential becomes smaller than the numerical threshold of sensitivity. In Figure 38 we show the potential for two Schwarzschild black holes in the top panels, where the red on the left has  $r_H = 1$  and the blue on the right has  $r_H = 0.8$ , and two non-Schwarzschild black holes in the bottom panels, where the red on the right has  $r_H = 1$ ,  $M = 0.276$ ,  $S_2^- = -0.294$  and the blue on the right has  $r_H = 0.8$ ,  $M = 0.568$ ,  $S_2^- = 0.082$ .

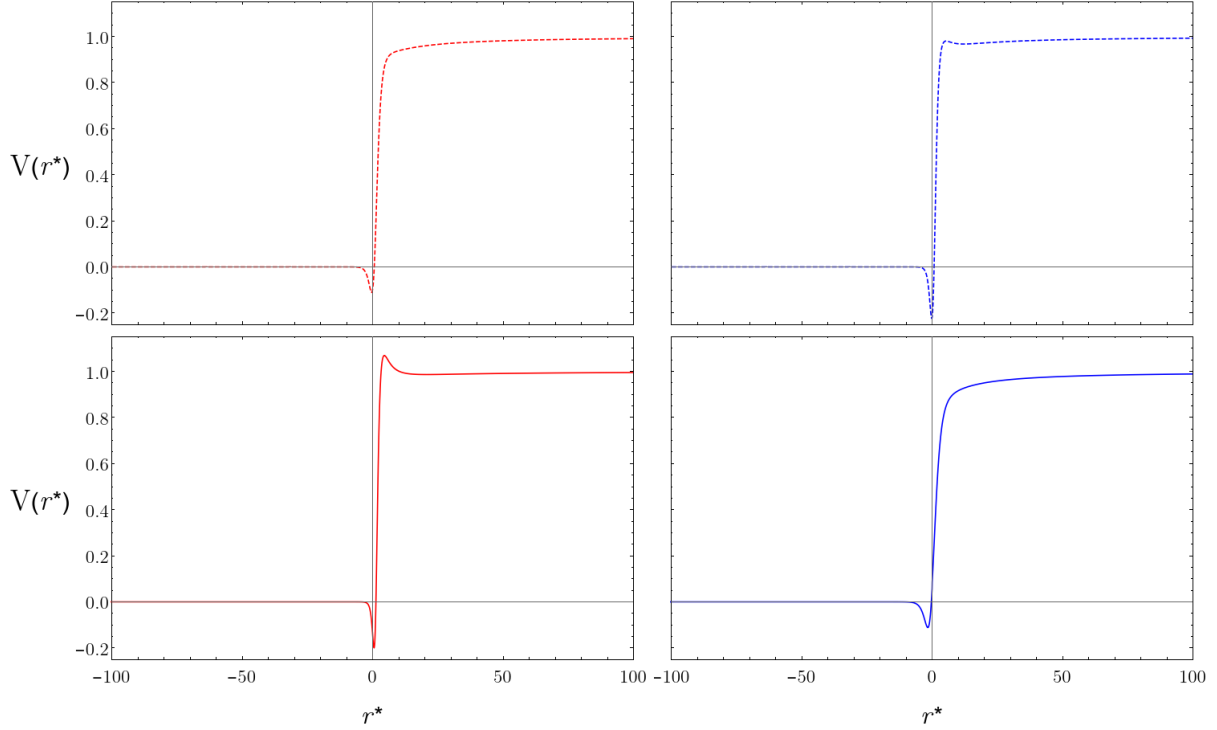


Figure 38: Potential in function of the tortoise coordinate of two Schwarzschild black holes, in the top panels in dashed lines, and two Schwarzschild black holes, in the bottom panels in solid lines; in the left panels, in red, the horizon radius is  $r_H = 1$  and in the right panels, in blue, it is  $r_H = 0.8$ .

At the qualitative level the two solutions with smaller masses, that is, the Schwarzschild with radius  $r_H = 0.8$  and the non-Schwarzschild with radius  $r_H = 1$ , have some similarities, with a deeper but narrower potential well in the small and negative  $r^*$  region and a small potential barrier in the small and positive  $r^*$  region. Nonetheless, the two larger black holes on the left result to be stable, while the two smaller black holes on the right are unstable. To see that we integrate equation (6.6) with the methods described in Subsection 6.1 with the parameters of the initial condition (6.10) set to

$$\sigma = 1, \quad v_0 = 10, \quad h = 0.1, \quad n_{max} = 8000, \quad (6.22)$$

and find the results shown in figures 39, 40. The standard approach of assessing stability by looking at the time evolution of perturbations at large distances, *i.e.* the quasi-normal modes, is not the best way to tackle this problem in this context. If we look at Figure

39, where we show the quasi-normal modes of the solutions with the potentials shown in Figure 38, an instability is present only at very late times for the non-Schwarzschild black hole with radius  $r_H = 0.8$ , while all the other solutions seem to be stable.

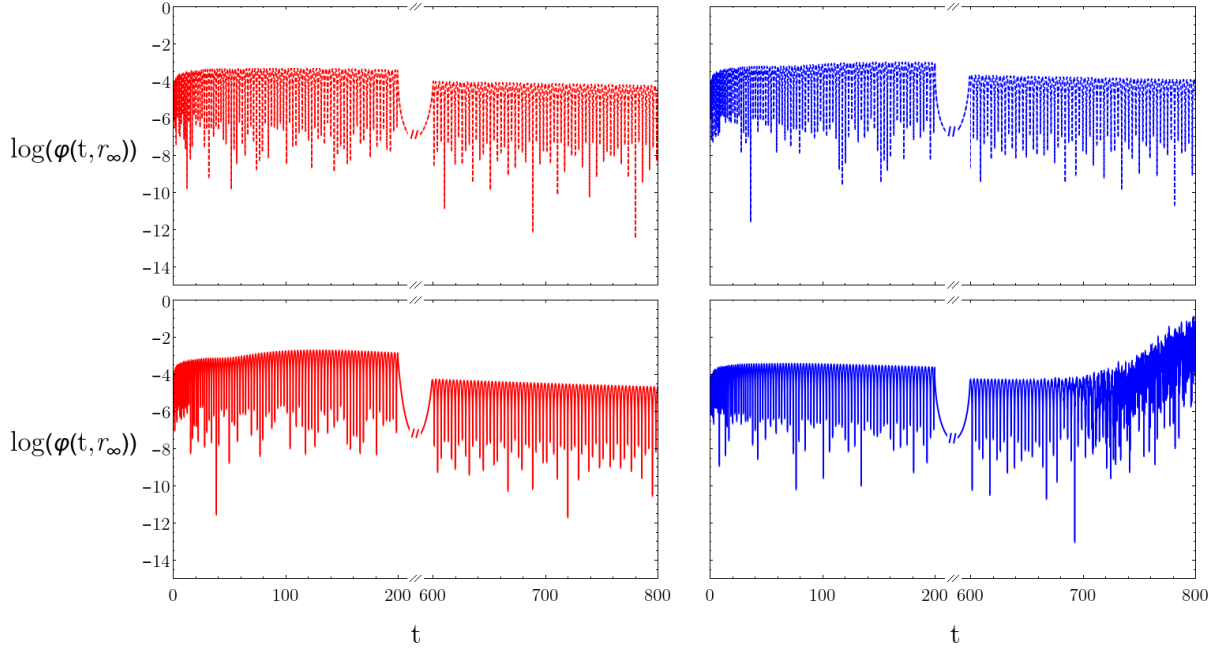


Figure 39: Quasi-normal modes for the black holes of which the potentials are shown in Figure 38; the radius at which we evaluated the time evolution is  $r_\infty = 50$ , and we removed the time interval  $[200 - 600]$  to show both the initial and final evolutions, and to have visible oscillations.

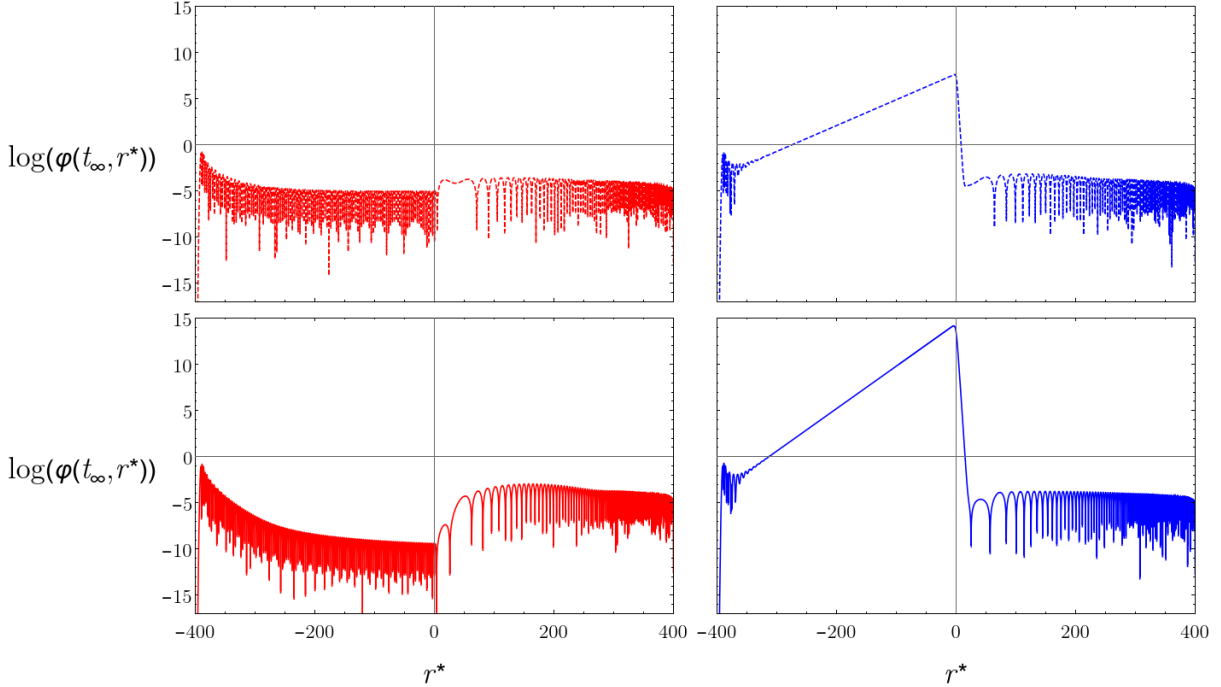


Figure 40: Radial displacement of the perturbations for the black holes of which the potentials are shown in Figure 38; the time at which we evaluated the displacement is  $t_\infty = 400$ .

In Figure 40, we show the radial displacement of the perturbations of the same black holes of the previous figures at time  $t = 400$ . It is clear that the perturbation is much larger in the region close to the horizon rather than at large distances; in particular, it seems to reach its maximum value close to  $r^* = 0$ . The physical reason behind this behavior is that we are looking at *massive* perturbation modes, which can have an effective range in which they propagate efficiently. Eventually, at some point, the perturbation will also reach the larger radii but, for solutions close to the transition point between stable and unstable behaviors, it might be at extremely late times. To investigate the stability is then useful to extract the time evolution of the perturbations at smaller radii; in Figure 41 we show this at  $r^* = 0$  for both Schwarzschild (in the top panels) and non-Schwarzschild (in the bottom panels) black holes close to the transition point  $r_H = 0.876$ . To have a better view of the imaginary part of the frequencies  $\omega$ 's, we have also shown on the right the moving average over a time interval of  $\Delta t = 20$ .

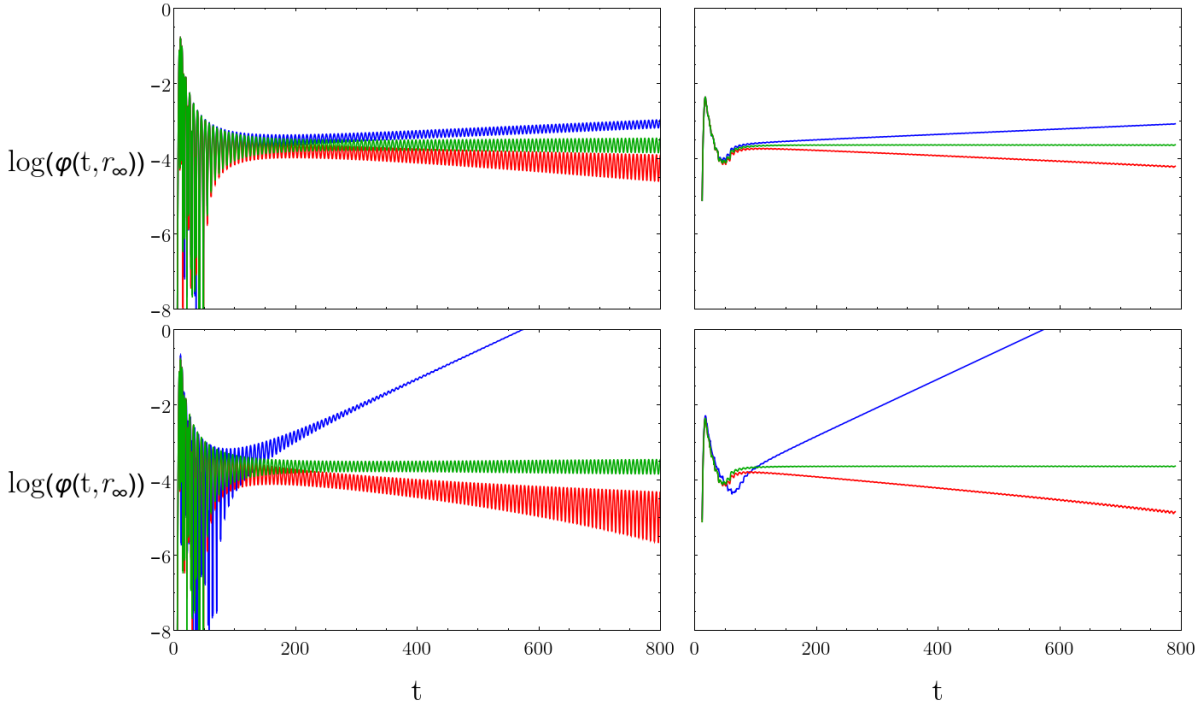


Figure 41: Time evolution of perturbations at  $r^* = 0$  for black holes with horizon radius  $r_H = 0.874$  in blue,  $r_H = 0.876$  in green and  $r_H = 0.878$  in red; in the top panels there are Schwarzschild black holes and in the bottom ones there are non-Schwarzschild black holes. In the right panels are shown the moving average over an interval of  $\Delta t = 20$  of the perturbations shown in the left panels.

It is clear that both for Schwarzschild and non-Schwarzschild black holes, the radius  $r_H = 0.876$  represents a transition point between stability and instability, and that in both cases the smaller black holes are unstable and the larger ones are stable. It is also clear that stable non-Schwarzschild black holes have more damped oscillations than their Schwarzschild counterparts, and a much stronger instability in the case of unstable

solutions. The resulting picture is then clear: the instability of black holes with horizon radius  $r_H < 0.876$  is confirmed, and the only stable non-Schwarzschild black holes are the Yukawa attractive ones. We recall here that, unfortunately, most of the Yukawa attractive black holes have negative mass, and then they are not sensible candidates to be astrophysical objects, unless an unknown mechanism to force them to have positive mass is present.

### 6.2.2 Quasi-normal modes of exotic solutions in Einstein-Weyl gravity

We now move to a first, preliminary, analysis of the perturbations of exotic solutions, that is, wormholes and naked singularities. Considering the complexity of the problem, we decided to investigate only solutions of the Einstein-Weyl sector, for which the equation of the perturbations is exactly the same as for black holes. While for black holes the procedure described in Subsection 6.1 is standard by now, there is no complete consensus on the procedure for solutions without a horizon. In particular, the point of caution is how to deal with initial conditions whenever a singularity is present in the region where the perturbation is evolving. Furthermore, in the case of naked singularities, the tortoise coordinate is defined only in the interval  $[0, \infty)$ , and then to explore in detail the region close to the singularity it is necessary to decrease the step-size of the grid  $h$ ; this is not the case for wormholes, for which it is sufficient to extend the size of the grid  $n_{max}$  to get closer to the singularity. Regarding the first point, as anticipated in Subsection 6.1, we will impose a zero perturbation exactly at the singularity because, with a conservative approach, this point does not belong to the spacetime and considering a perturbation of the metric in that point is then meaningless. Regarding the second point of caution, we used the same grid used for black holes and, for this reason, we specify that the results we will present have to be considered preliminary.

**Wormholes.** For wormhole solutions the tortoise coordinate has the same range of black holes  $(-\infty, \infty)$ , but in this case the surface defined by  $r^* = -\infty$  is a singularity and not a horizon. As in the case of black holes, to study later times it is necessary to increase the grid size, and then we need to be able to explore a region much larger than the one explored simply with the shooting method. In this case, the spacetime has been divided into the following regions

asymptotically vanishing region:

$$\begin{aligned} r > r_{\gg 1}, & \quad h(r), f(r) \text{ not defined, } V(r) = 0, \\ r_O < r < r_{\gg 1}, & \quad h(r), f(r) \text{ from integration starting at } r_O, \\ r_T < r < r_O, & \quad h(r), f(r) \text{ from the series expansion (3.30),} \end{aligned}$$

asymptotically flat region:

$$\begin{aligned}
 r_T < r < r_O, & \quad h(r), f(r) \text{ from the series expansion (3.30),} \\
 r_O < r < r_\infty, & \quad h(r), f(r) \text{ from the shooting method,} \\
 r > r_\infty, & \quad h(r), f(r) \text{ from the weak field expansion (3.5),}
 \end{aligned}$$

where  $r_{\gg 1}$  is the radius at which the potential gets smaller than the numerical tolerance. For the integration, we still considered a zero initial condition at  $v = 0$  and a Gaussian at  $u = 0$ , as in the case of black holes, and performed the integration exactly with the same procedure. We have to note, however, that the code suffers much more from numerical instabilities than the one used for black holes, and retrieving information is more complicated. In Figure 42 we show the potentials for two wormholes: a Yukawa repulsive one (that is, with positive  $S_2^-$ ) in blue on the left, and a Yukawa attractive one (that is, with negative  $S_2^-$ ) in red on the right.

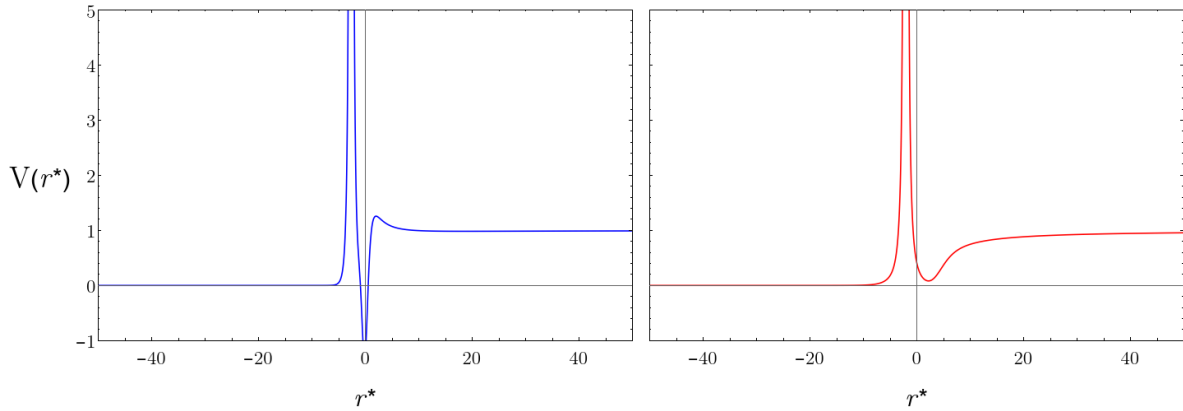


Figure 42: Potential in function of the tortoise coordinate for two wormhole solutions; the blue on the left has  $M = 0.3$  and  $S_2^- = 0.1$  and the red on the right has  $M = 1$  and  $S_2^- = -0.5$ .

The Yukawa attractive one has a potential well before the throat, which in this case is at  $r_T^* \sim 1$ , while before reaching the throat of the Yukawa repulsive one, which is at  $r_T^* \sim -1.3$ , we have to face both a small potential barrier and a deep and negative potential well. Nonetheless, the main feature of both potentials is an extremely high potential barrier just after the throat. Probably due to this barrier, the perturbations increase exponentially in both cases, as can be seen both in the time evolution at radius  $r_\infty = 50$  in Figure 43 and in the radial displacement at  $t_\infty = 250$  in Figure 44. While, as previously said, the code is not completely numerically stable, and it has not been possible yet to explore the phase diagram rigorously, all the wormhole solutions which have been analyzed had the same unstable behavior as the two shown in these figures, and then we are inclined to consider *all wormhole solutions as unstable*.

Finally, Figure 44 underlines that the instability is generated close to the throat, probably either by the potential barrier or the potential wells.

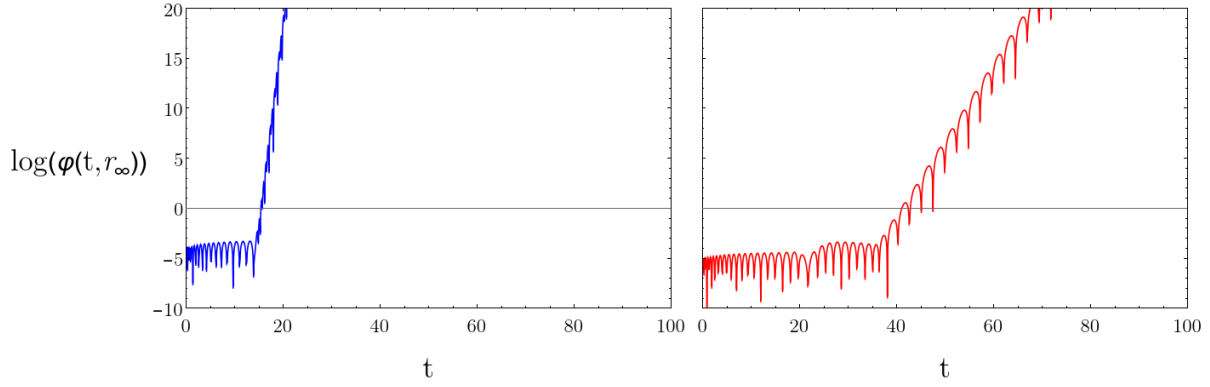


Figure 43: Quasi-normal modes for the wormholes of which the potentials are shown in Figure 42; the radius at which we evaluated the time evolution is  $r_\infty = 50$  in the asymptotically flat patch.

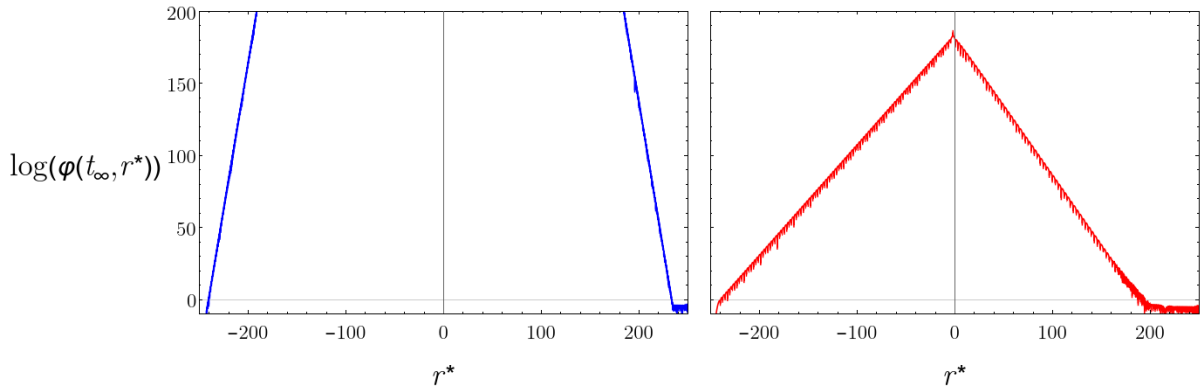


Figure 44: Radial displacement of the perturbations for the wormholes of which the potentials are shown in Figure 42; the time at which we evaluated the displacement is  $t_\infty = 250$ .

In conclusion, this first exploratory analysis confirms that non-symmetric wormholes are unstable, as generally found in alternative theories of gravity.

**Naked singularities.** To study naked singularities we have to slightly adapt the code to the limited range of the tortoise coordinate. The most rigorous way of studying these types of solutions would be to implement the shooting method between a large radius and the origin, and adapt the step size of the grid to the different regions of the spacetime. For this first exploratory scan, we integrated the equations of motion from large radii to the origin and left a fixed step size. The spacetime is then divided simply as

$$\begin{aligned} r_O < r < r_\infty, & \quad h(r), f(r) \text{ from integration starting at } r_\infty, \\ r > r_\infty, & \quad h(r), f(r) \text{ from the weak field expansion (3.5).} \end{aligned} \tag{6.23}$$

While we cannot explore in great detail the area close to the singularity, we believe that most of the information can still be extracted from this analysis. As initial conditions we choose to set the perturbation to zero *at* the singularity. As said before, we made this choice because, with a conservative approach, the singularity does not belong to the

spacetime, and it is also confirmed by the results of General Relativity in the case of Schwarzschild solutions with negative mass [79].

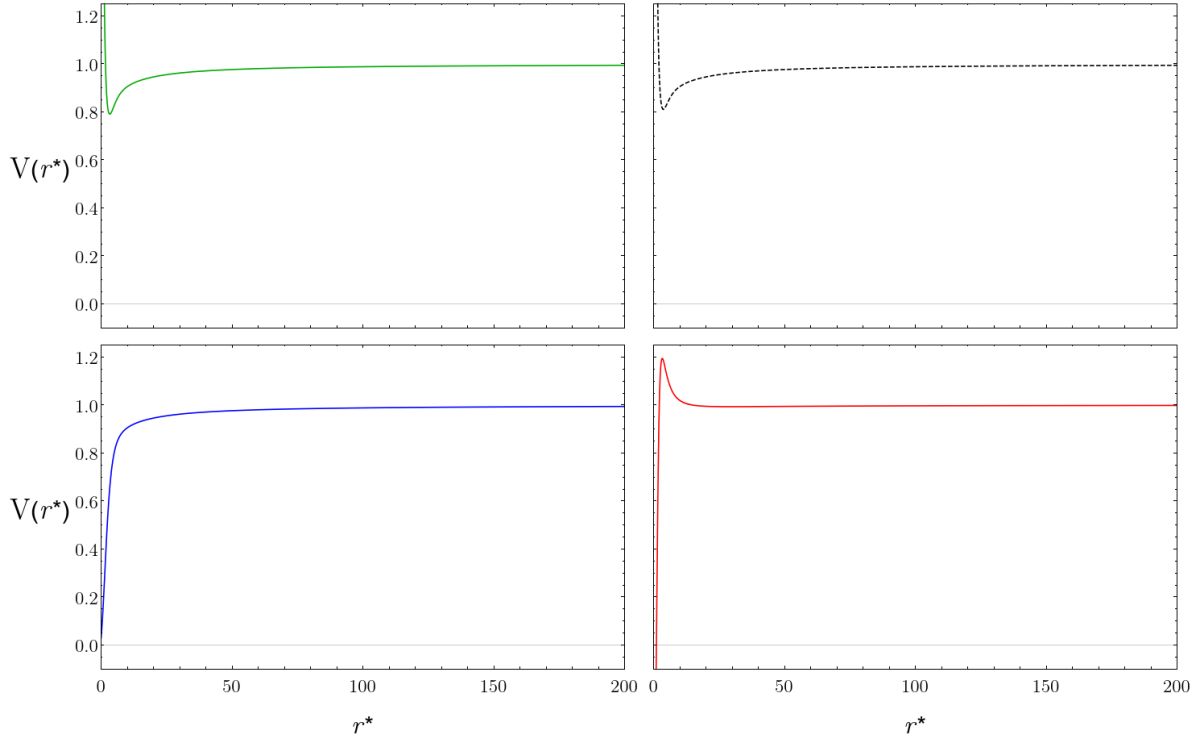


Figure 45: Potential in function of the tortoise coordinate for naked singularities; in the top panels there are repulsive naked singularities, the green on the left has  $M = 0.6, S_2^- = 0.2$  and the dashed black on the right has  $M = 0.6, S_2^- = 0.2239$ , in the bottom panels there are attractive naked singularities, the blue on the left has  $M = 0.6, S_2^- = 0.05$  and the red on the right has  $M = 0.2, S_2^- = -0.2$ .

In Figure 45 we show the potentials of four different naked singularities with positive mass: there are two repulsive naked singularities in the top panels with slightly different positive Yukawa charges, and two attractive naked singularities in the bottom panels of which the blue on the left has a positive Yukawa charge and the red on the right a negative Yukawa charge. The main features are clearly an infinite potential barrier at the origin in the case of repulsive naked singularities and a potential well at the origin in the case of attractive naked singularities. In addition, the repulsive ones have a potential well before the barrier, which gets deeper as the mass is increased and the Yukawa charge is decreased, while the attractive naked singularity with a negative Yukawa charge, on the contrary, presents a small potential barrier just before the potential well, which also decreases as the Yukawa charge gets smaller in modulus. In figures 46 and 47 we show, as usual, the time evolution and radial displacement of the perturbations, where it is clear why we had shown two repulsive naked singularities with slightly different Yukawa charges: the one with a larger value of  $S_2^-$  is indeed unstable, while the other is stable. Investigating other solutions with mass  $M = 0.6$  it is possible to show that all the solutions with  $S_2^-$  smaller

than a certain value are stable, while all the ones with  $S_2^-$  larger are unstable.

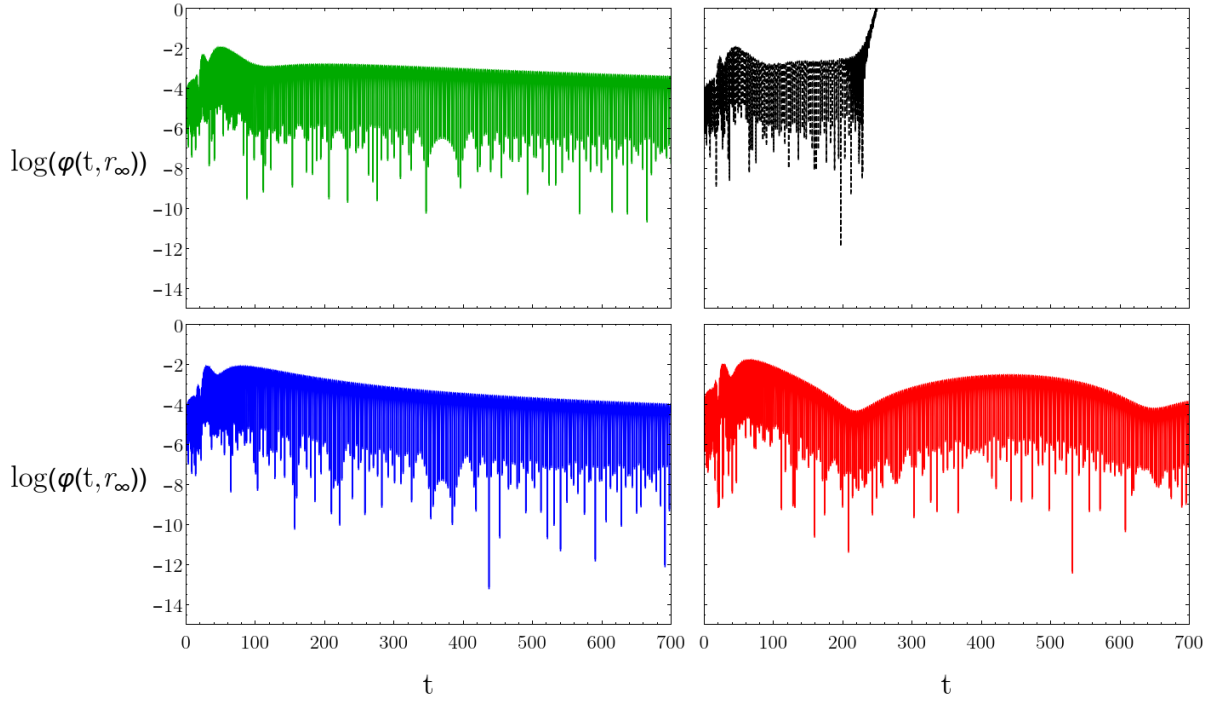


Figure 46: Quasi-normal modes for the naked singularities of which the potentials are shown in Figure 45; the radius at which we evaluated the time evolution is  $r_\infty = 50$ .

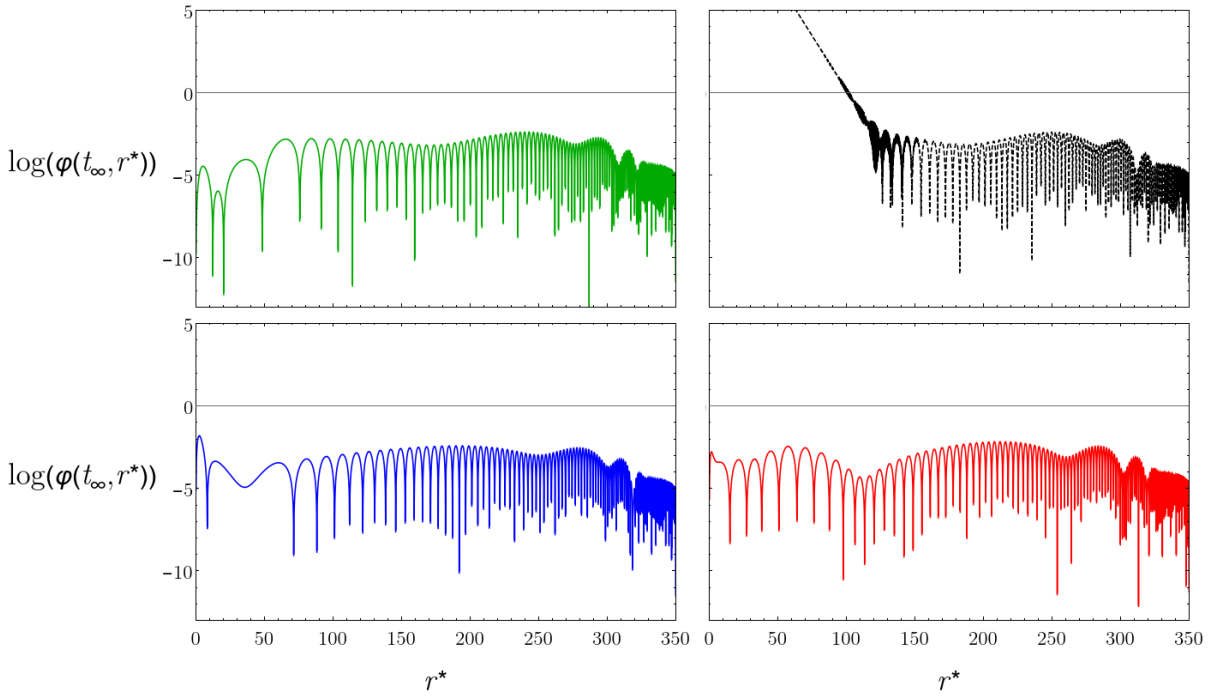


Figure 47: Radial displacement of the perturbations for the naked singularities of which the potentials are shown in Figure 45; the time at which we evaluated the displacement is  $t_\infty = 350$ .

From Figure 47 it is also clear that the instability is generated close to the singularity; therefore, it is fundamental to investigate this region in greater detail. In particular, while

attractive and repulsive naked singularities have a very qualitatively different nature, and then it is sensible to expect them to have different stability properties, the difference between stable and unstable repulsive naked singularities is quantitative, and therefore has to be considered more carefully. In particular, if we look at Figure 48, the transition between stable and unstable behavior is very sharp, with a slight change in the parameter exciting a strong instability.

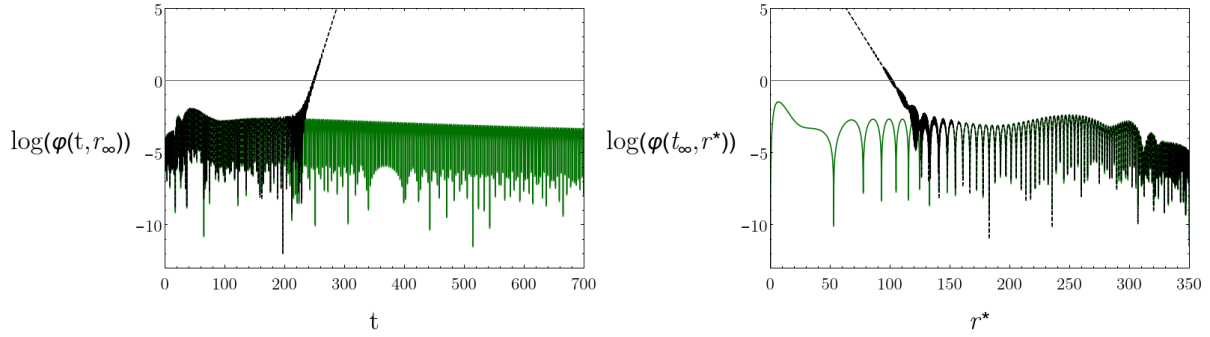


Figure 48: Transition between stable and unstable behavior of repulsive naked singularities; both have  $M = 0.6$ , but the one in darker green has  $S_2^- = 0.2238$  and the one in dashed black has  $S_2^- = 0.2239$ .

Finally, it is interesting to note that the attractive naked singularity with negative Yukawa charge has some sort of “beat” pattern, with an oscillatory change in the intensity of the oscillations, which is a very specific phenomenological signature of this type of solution.

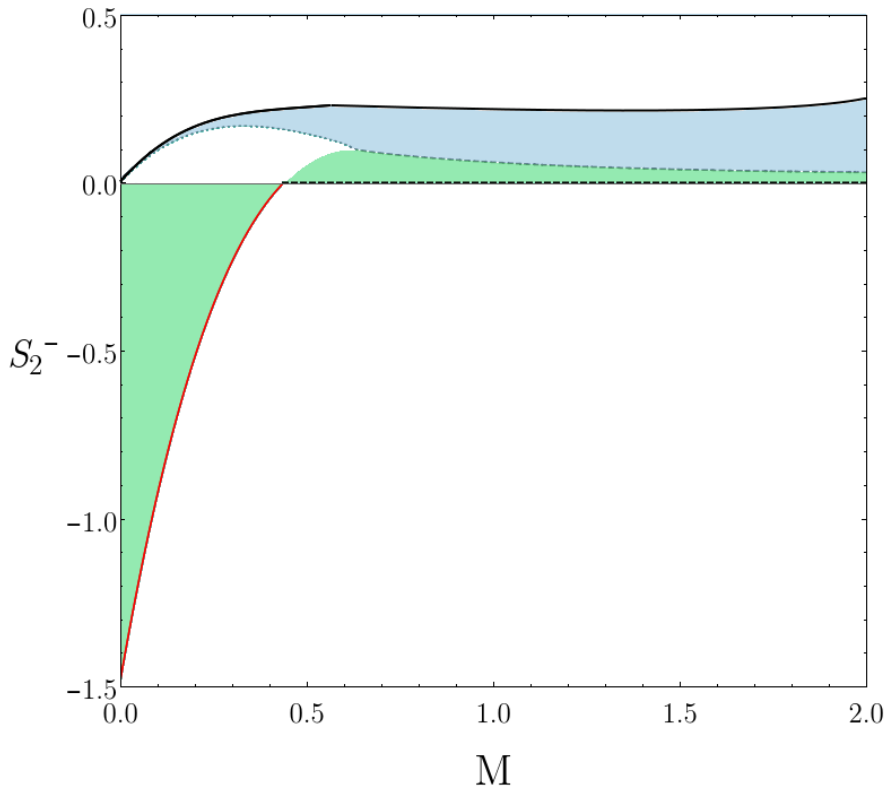


Figure 49: Phase diagram of Einstein-Weyl gravity from which have been removed the unstable solutions.

At last, we collected in Figure 49 the results of this subsection with a first attempt to picture the phase diagram of stable solutions of Einstein-Weyl gravity. We considered only the region with positive mass and removed the solutions which are unstable from the analysis of perturbations: the resulting picture is that small mass stable solutions have to be either attractive naked singularities or Yukawa attractive non-Schwarzschild black holes while, in the large mass limit, we are forced to have either Schwarzschild black holes or naked singularities, that is solutions with  $S_2^- \geq 0$ . It is interesting to note that the maximum value of  $S_2^-$  for which repulsive naked singularities are stable seems to increase with the mass, but we remember that a quantitative discussion has to be postponed to a more detailed analysis of the perturbations close to the singularity.

### 6.3 Quasi-normal modes of black holes in scale-invariant gravity

We now move from quadratic gravity to the scale-invariant theory presented in Subsection 2.2. As said in Subsection 5.5, having a more complex theory, we start from the analysis of known analytical solutions of General Relativity when considered as solutions of the scale-invariant theory. In this subsection, we study the stability against linear perturbation of the two types of Schwarzschild-de Sitter solutions present in the theory. However, we specify that this calculation has been done by Simon Boudet, but we believe it is important to be inserted in this thesis for completeness. All the images (which also have to be credited to Simon Boudet) and part of the discussion are taken from [35]; we recall that having used different notations there could be some slight differences with the formulas and plots of that paper.

To study the dynamical stability of the two Schwarzschild-de Sitter solutions, it is convenient to work in the Einstein frame. To simplify the discussion, we will not study the most general scale-invariant gravity (2.41), but the reduction (2.56) where the tensor perturbations are suppressed and where the Lagrangian density in the Einstein frame is given by (2.61). The fields can be expanded to linear order as

$$\begin{aligned} g_{\mu\nu} &= \bar{g}_{\mu\nu} + h_{\mu\nu}, \\ \rho &= \bar{\rho} + \delta\rho, \\ \zeta &= \bar{\zeta} + \delta\zeta, \end{aligned} \tag{6.24}$$

where barred quantities, as usual, represent the background solution, which will be either the Schwarzschild-de Sitter (5.40) or the Schwarzschild-de Sitter (5.40). At first order,

the system (2.64) gives

$$\begin{aligned} M_{SI}^2 \delta G_{\mu\nu} + U(\bar{\zeta}) h_{\mu\nu} &= 0, \\ \bar{\square} \delta \rho &= 0, \\ \left( \bar{\square} - \frac{d^2 U}{d\zeta^2}(\bar{\zeta}) \right) \delta \zeta &= 0, \end{aligned} \quad (6.25)$$

where, as in quadratic gravity,  $\delta G_{\mu\nu}$  is the first order variation of the Einstein tensor with respect to the metric and  $\bar{\square}$  denotes the d'Alambert operator built with the background metric. We see that, at linear order, the three perturbations are decoupled. Moreover, since  $U(\bar{\zeta}) = M_{SI}^2 \Lambda$ , where  $\Lambda$  denotes (5.40) or (5.40) indifferently, the first equation coincides with the equation for the metric perturbation of General Relativity on a Schwarzschild-de Sitter background with cosmological constant  $\Lambda$ . Hence, the dynamics of  $h_{\mu\nu}$  is not modified. The same happens for the equation for  $\rho$  in (6.25), which is nothing but the usual Klein-Gordon equation on a Schwarzschild-de Sitter background. The mass term's presence modifies the dynamics of  $\delta \zeta$  in the third equation of (6.25). Therefore, in the following, we will only focus on the dynamics of  $\delta \zeta$  since instabilities can only arise from the latter, and then to the equation

$$\left( \bar{\square} - \frac{d^2 U}{d\zeta^2}(\bar{\zeta}) \right) \delta \zeta = 0. \quad (6.26)$$

To proceed, one can exploit the spherical symmetry of the problem, adopting the following harmonic expansion for the scalar perturbation:

$$\delta \zeta = \frac{Z(r)}{r} Y_{lm}(\theta, \varphi) e^{-i\omega t}, \quad (6.27)$$

where  $Y_{lm}$  are the standard spherical harmonics. Substituting into (6.26), one finds

$$\frac{d^2 Z}{dr_*^2} + [\omega^2 - V_\zeta(r)] Z = 0, \quad (6.28)$$

where  $r_*$  is the tortoise coordinate defined by

$$r^* = \int \frac{dr}{f(r)} = \int \frac{dr}{1 - \frac{2M}{r} - \frac{\Lambda}{3} r^2}, \quad (6.29)$$

and, as usual, the argument of the potential must be considered as a function of  $r^*$ . The effective potential featuring (6.28) can be written in terms of a parameter  $\bar{p}$  as

$$V_\zeta(r) = V_{GR}(r) - \frac{4\Lambda}{3} \bar{p} f(r), \quad (6.30)$$

where  $V_{GR}(r)$  represents the effective potential appearing in the case of General Relativity, namely for a Klein-Gordon equation on a Schwarzschild-de Sitter background:

$$V_{GR}(r) = f(r) \left( \frac{l(l+1)}{r^2} + \frac{2M}{r^3} - \frac{2\Lambda}{3} \right). \quad (6.31)$$

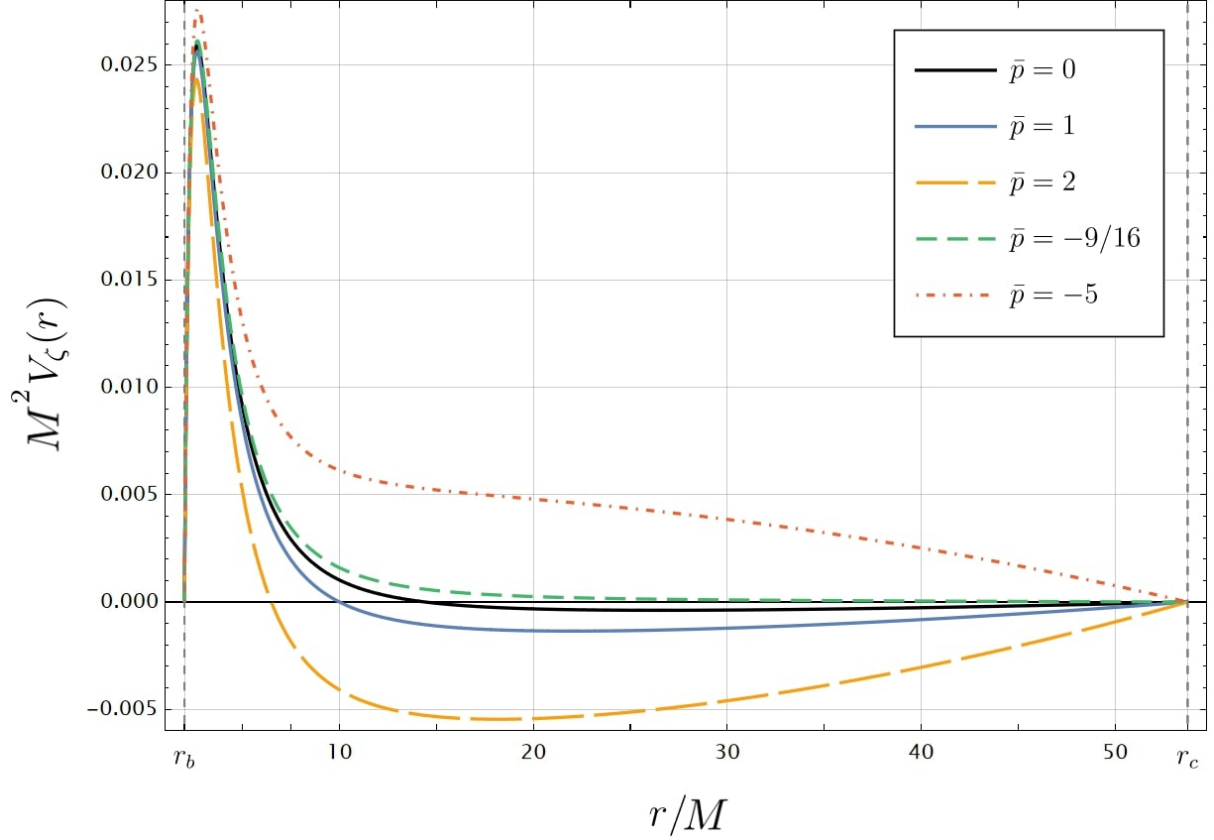


Figure 50: Effective potential within the static region  $r_b < r < r_c$  for  $l = 0$  and different values of  $\bar{p}$ . The cosmological constant is set to  $\Lambda = 0.001/M^2$ . The  $\bar{p} = 0$  curve represents the case of General Relativity.

For  $\bar{p} = 0$  one recovers the case of General Relativity, while deviations for non-vanishing  $\bar{p}$  can be appreciated in Figure 50.

The value of the parameter  $\bar{p}$  depends on the specific solution one is considering. For the unstable solution we have

$$\bar{p} = p_u \equiv 6\xi, \quad (6.32)$$

while the stable one is characterized by

$$\bar{p} = p_s \equiv 1 - \frac{M_{SI}^2}{16\beta\Lambda_s}(1 + 12\xi) = -\frac{\xi(12\beta\lambda + \xi + 12\xi^2)}{\beta\lambda}, \quad (6.33)$$

where in the last step we used (5.41). We will now show that the asymptotic behavior of the perturbation crucially depends on the value of  $\bar{p}$ . The critical value of  $\bar{p}$  separating stable from unstable modes is related to the form of the potential in the pure de Sitter,  $M \rightarrow 0$  limit. This was shown in [80], where the case of a non-minimally coupled scalar field on a Schwarzschild-de Sitter background is considered. It turns out that the effective potential (6.30) is very similar to the one computed in [80]. In that case, starting from

$$(\square - \nu R)\phi = 0, \quad (6.34)$$

one gets

$$V(r) = f(r) \left( \frac{l(l+1)}{r^2} + \frac{2M}{r^3} - \frac{2\Lambda}{3}(1-6\nu) \right). \quad (6.35)$$

Therefore, the two potentials are mapped into each other via the substitution  $\nu \leftrightarrow -\bar{p}/3$ , which allows us to obtain the late time behavior of the scalar perturbation from the results of [80] as

$$\delta\zeta \sim e^{-\mu\kappa_c t}, \quad (6.36)$$

where  $\kappa_c$  is the surface gravity of the cosmological horizon, i.e.

$$\kappa_c = \frac{\Lambda(r_c - r_b)(r_c - r_0)}{6r_c}, \quad (6.37)$$

and

$$\mu = l + \frac{3}{2} - \frac{1}{2}\sqrt{9 + 16\bar{p}} + O\left(\frac{r_b}{r_c}\right). \quad (6.38)$$

We can identify three different behaviors for different values of the parameter  $\bar{p}$ . When  $\bar{p} < -9/16$ ,  $\mu$  becomes complex, and the purely exponential decay is replaced by a damped oscillatory regime, as observed in [80] (see fig. 51):

$$\delta\zeta \sim e^{-(l+\frac{3}{2})\kappa_c t} e^{\frac{i}{2}\sqrt{|9+16\bar{p}|}\kappa_c t}. \quad (6.39)$$

The main difference with respect to [80], is that now  $\mu$  changes sign for  $\bar{p}$  greater than the critical value

$$\bar{p}_c = \frac{(2l+3)^2 - 9}{16}, \quad (6.40)$$

so that we have an exponential decay for  $-9/16 < \bar{p} < \bar{p}_c$ , with no oscillations, while the case  $\bar{p} > \bar{p}_c$  yields unstable diverging modes.

Numerical integrations confirm this: in the results presented in the following, we used the procedure presented in Subsection 6.1 and the initial conditions used for the results shown in Subsection 6.2, that is  $Z(u, 0) = 0$  and  $Z(0, v) = \exp[-(v - v_c)^2/2\sigma]$ . In this particular case, the inversion of the tortoise coordinate can be found by solving numerically in  $r$  the equation

$$r^* = \ln \left( \frac{(r - r_b)^{\beta_b}(r + r_c + r_b)^{\beta_0}}{(r_c - r)^{\beta_c}} \right), \quad (6.41)$$

where

$$\beta_c = \frac{3r_c}{\Lambda(r_c - r_b)(2r_c + r_b)}, \quad (6.42)$$

$$\beta_b = \frac{3r_b}{\Lambda(r_c - r_b)(2r_b + r_c)}, \quad (6.43)$$

$$\beta_0 = \frac{3(r_b + r_c)}{\Lambda(2r_c + r_b)(2r_b + r_c)}. \quad (6.44)$$

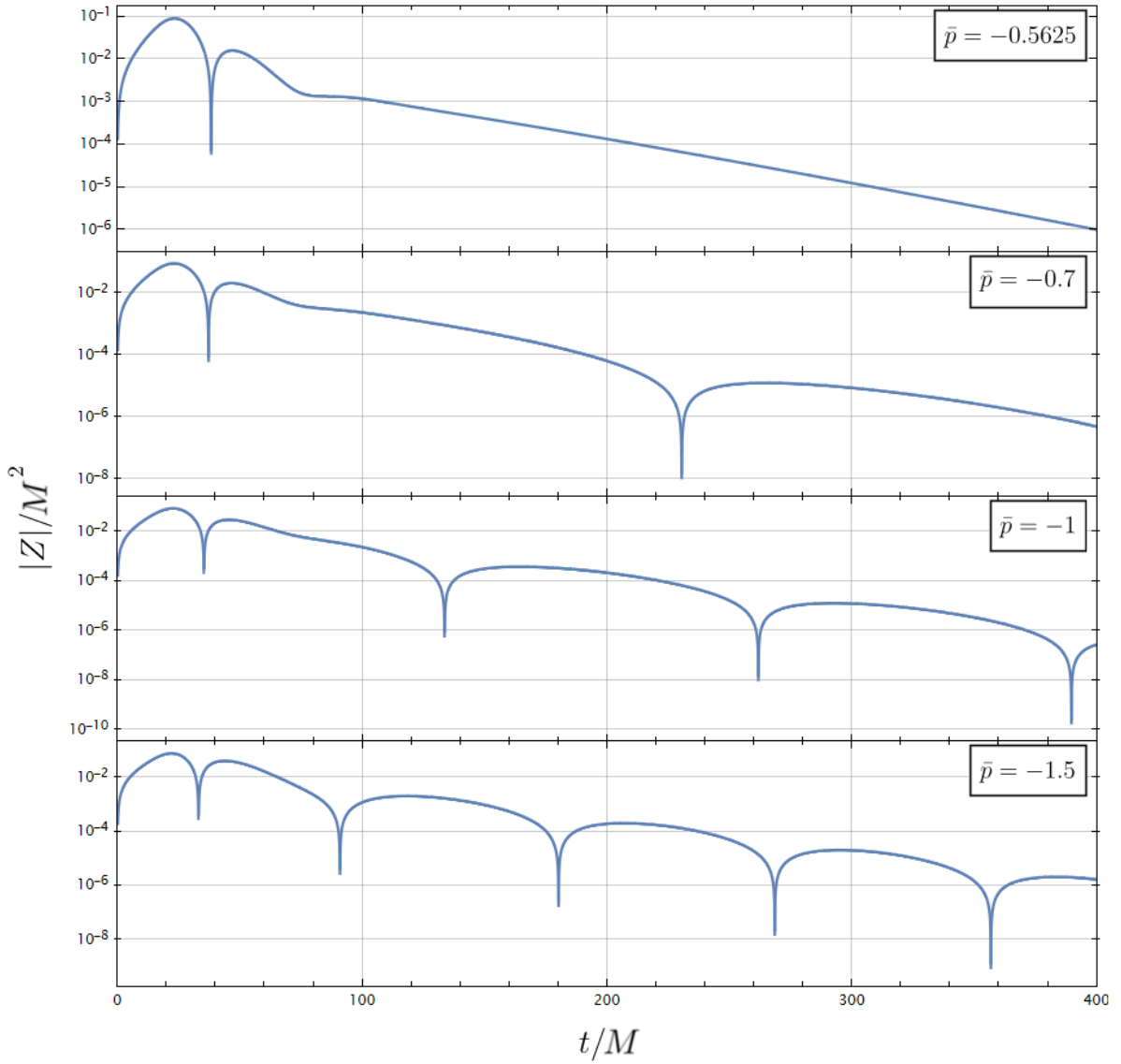


Figure 51: Evolution of  $|Z|/M^2$  as a function of  $t/M$  at a fixed radius, for  $l = 0$  and different values of  $\bar{p}$ , showing the onset of the oscillatory regime in the late-time region for  $\bar{p} < -9/16 = -0.5625$ . The cosmological constant is set to  $\Lambda = 0.001/M^2$ .

The results presented here are obtained setting

$$\sigma = 1, \quad v_0 = 10, \quad h = 0.1, \quad n_{max} = 5000, \quad (6.45)$$

and we extracted the time evolution at  $r_\infty^* = 50M$ ; we note that we worked with dimensionless variables rescaling every quantity by the appropriate black hole mass  $M$  power. The outcome of the numerical integrations is shown in Figure 51 and 52. In particular, Figure 51 shows the transition from an exponential decay to the damped oscillatory regime when  $\bar{p}$  becomes lower than  $-9/16$ . Figure 52 instead confirms the stability behavior discussed above, showing how the perturbations diverge if  $\bar{p} > \bar{p}_c$ , while they are stable and decay exponentially to zero when  $\bar{p} < \bar{p}_c$ .

Let us now apply these results to the two solutions under consideration. Given that  $\bar{p}_c$  is

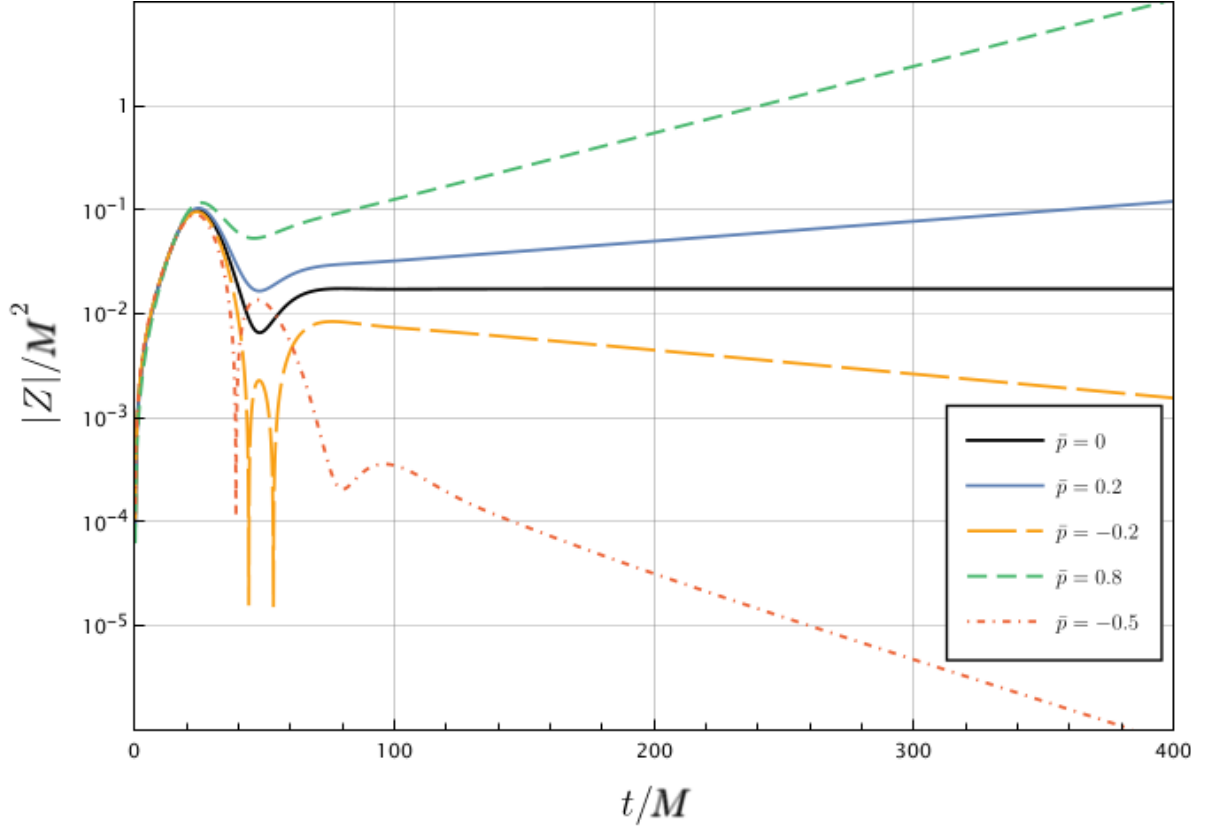


Figure 52: Evolution of  $|Z|/m^2$  as a function of  $t/m$  at fixed radius, for  $\ell = 0$  and different values of  $\bar{p}$ . The cosmological constant is set to  $\Lambda = 0.001/m^2$ .

non-negative, instabilities can never trigger when the stable solution is considered, since the latter has  $\bar{p} = p_s < 0$  (see equation (6.33)). Regarding the other solution instead, since  $p_u = \xi$  the stability condition is provided by

$$\xi < \bar{p}_c. \quad (6.46)$$

The value of  $\bar{p}_c$  increases with the angular momentum number  $l$ , implying that the first multiple suffering from instabilities would be the lowest-lying mode, namely the monopole, identified by  $l = 0$ . Since  $\bar{p}_c(l = 0) = 0$  and being  $\xi$  non-negative, we conclude that the stability condition (6.46) is never satisfied, and the second solution is always unstable. Therefore, the stable character of the two solutions agrees with the one resulting from the investigations pursued in a cosmological setting in [27], and solutions with zero scalar field are unstable and solutions with non-zero scalar field are stable. Nonetheless, these properties are not sufficient to assess whether there is a transition between the unstable Schwarzschild-de Sitter and the stable one; we will tackle this problem in Subsection 7.3, where we will perform a semiclassical analysis of the stability of these solutions.

## 7 Semiclassical quadratic gravity and black hole Thermodynamics

The thermodynamical interpretation of black holes proposed for the first time by Gibbons and Hawking [81, 82, 83] has completely renewed our understanding of this type of solution. First, within such interpretation, black holes appear to have a mutual interaction with the surrounding environment and are, therefore, truly physical objects. Second, the derivation of the thermodynamical properties of black holes is the first robust result of a semiclassical approach to gravity. It is semiclassical in two distinct senses: the original derivation of Hawking radiation is semiclassical in the sense that the gravitational interaction is considered purely classical but the matter (or radiation) fields populating this classical spacetime have quantum nature; it is also semiclassical in the sense that all the thermodynamical properties of black holes can be derived from the mean field approximation of a consistently defined quantum theory of gravity. The two interpretations are, in any case, complementary and consistent one with the other.

This section is divided in three parts:

- in the first subsection we review the main concepts of black hole Thermodynamics, such as Hawking radiation, black hole entropy and black hole evaporation, and sketch the derivation of these properties from the path integral approach to quantum gravity;
- in the second subsection we present the thermodynamical properties of non-Schwarzschild black holes in quadratic gravity and describe the evaporation process in this theory; we will show that the stable black holes with an attractive Yukawa contribution have unphysical thermodynamical properties and that either quadratic gravity is a poor theory of gravity or the evaporation process has to deviate from stable solutions in its final stages;
- in the third subsection we present a technique to evaluate the Euclidean action of a solution with multiple horizons in scale-invariant gravity; we will apply this technique to Schwarzschild-de Sitter black holes and show that, similarly to the cosmological case, there is a phase transition between two asymptotically de Sitter spacetimes in which the scalar field acquire a non-zero expectation value.

The results on the evaporation process of black holes in quadratic gravity presented in Subsection 7.2 are not part of any publication yet, while the results on the phase transition in scale-invariant gravity presented in Subsection 7.3 are corrections of the ones published in [35].

## 7.1 Black hole Thermodynamics and semiclassical gravity

As stated before, in this subsection we will recall the main concepts of black hole Thermodynamics and their semiclassical derivation. There are three main points that we address in as many subsubsections: the first one is the emission of particles from the vacuum close to an event horizon, and the resulting evaporation process of a black hole, the second one is the semiclassical approximation of the path integral approach to quantum gravity, and its use for the derivation of all the thermodynamical properties as energy and entropy, and the third one is the Wald definition of the entropy of a black hole, which can be applied to black holes in quadratic gravity without having to evaluate the Euclidean action of the solutions.

### 7.1.1 Hawking radiation and black hole evaporation

In the first years of the '70s different scientists realized that the presence of a horizon should have consequences on the quantum fields surrounding it, and that it would pose a puzzle to our concepts of information. The first solid statement was formulated by Hawking with the derivation of black hole radiation using Quantum Field Theory on curved spacetime [81]. In this subsubsection we will show the calculation hiding some technical complications, hoping to keep both a substantial level of rigorousness and physical meaning.

The starting point is the non-unique definition for the vacuum in curved spacetimes, quantified for the first time by Bogoliubov in the '50s [84]. Let us consider a free scalar field with action

$$\mathcal{I}_\phi = -\frac{1}{2} \int d^4x \sqrt{-g} [\partial^\mu \phi \partial_\mu \phi + m^2 \phi^2], \quad (7.1)$$

with equations of motion

$$(\square + m^2) \phi = (\nabla^\mu \partial_\mu + m^2) \phi = 0. \quad (7.2)$$

We can expand the field  $\phi$  using a basis  $\{f_i\}$  of solutions of (7.2) as

$$\phi = \sum_i (f_i a_i + f_i^* a_i^\dagger), \quad (7.3)$$

where  $a_i$  and  $a_i^\dagger$  are two sets of operators, that we will call creation and annihilation operators in analogy to what is done in flat spacetimes. Clearly it is possible to expand the field  $\phi$  using a second basis  $\{g_i\}$  of solutions of (7.2) as

$$\phi = \sum_i (g_i b_i + g_i^* b_i^\dagger), \quad (7.4)$$

with creation and annihilation operators  $b_i$  and  $b_i^\dagger$ . These expansions become physically meaningful if we allow the existence of timelike Killing vectors, or at least of asymptotic

ones. If a timelike Killing vector  $\kappa^\mu$  exists, we can define the energy states of the field  $\phi$  as the eigenvalues of the operator  $\kappa^\mu \partial_\mu$ ; in practical terms, these eigenvalues are the conserved charges associated to time translation, as seen by an observer defined by the Killing vector  $\kappa^\mu$ . In particular, it is possible to prove that the Laplace operator  $\square$  and the Killing operator  $\kappa^\mu \partial_\mu$  commute and can be simultaneously diagonalized, and then we can consider the elements of  $\{f_i\}$  to be simultaneously eigenvectors of the two operators

$$\square f_i = -m^2 f_i, \quad i\kappa^\mu \partial_\mu f_i = \omega_i f_i, \quad (7.5)$$

where the  $\omega_i$  are positive and will be called frequencies, and the elements of  $\{g_i\}$  to be eigenvectors of a second timelike Killing vector  $\tilde{\kappa}^\mu$

$$\square g_i = -m^2 g_i, \quad i\tilde{\kappa}^\mu \partial_\mu g_i = \omega'_i g_i, \quad (7.6)$$

with frequencies  $\omega'_i$ . It is now possible also to define an internal product for the basis  $\{f_i\}$  and  $\{g_i\}$ , that now we can safely call ‘‘modes’’, and the elements of the two expansions satisfy the relations

$$\begin{aligned} \left[ a_i, a_j^\dagger \right] &= \delta_{ij}, & (f_i, f_j) &= i \int_{\Sigma} d^3x \sqrt{\gamma} n^\mu (f_i \partial_\mu f_j^* - f_j^* \partial_\mu f_i) = \delta_{ij}, \\ \left[ b_i, b_j^\dagger \right] &= \delta_{ij}, & (g_i, g_j) &= i \int_{\Sigma} d^3x \sqrt{\gamma} n^\mu (g_i \partial_\mu g_j^* - g_j^* \partial_\mu g_i) = \delta_{ij}, \end{aligned} \quad (7.7)$$

where  $\Sigma$  is a spacelike surface,  $\gamma_{ij}$  is its metric and  $n^\mu$  is the unit normal to it. Being both complete sets, we can express a  $f_i$ -mode in terms of the  $g_i$  as

$$f_i = \sum_j (\alpha_{ij} g_j + \beta_{ij} g_j^*), \quad (7.8)$$

where the so-called Bogoliubov coefficients  $\alpha_{ij}$  and  $\beta_{ij}$  are found as

$$\alpha_{ij} = (g_j, f_i), \quad \beta_{ij} = (g_j^*, f_i). \quad (7.9)$$

These coefficients are of fundamental importance because they can be used to define the operators  $b_i$  in terms of the  $a_i$  and  $a_i^\dagger$ ; indeed inserting (7.8) into (7.3) and comparing with (7.4), we get the expression

$$b_i = \sum_j (\alpha_{ij} a_j + \beta_{ij}^* a_j^\dagger). \quad (7.10)$$

Let us now consider the vacuum state for the observer  $\kappa^\mu$ , defined as  $a_i |0_a\rangle = 0$  for all  $a_i$ . The fundamental question is how this state is seen by the second observer  $\tilde{\kappa}^\mu$ ; the second observer can define the number operator  $n_i^{(b)} = b_i^\dagger b_i$ , which has as expectation value the number  $N_i$  of particles with frequency  $\omega'_i$ . However, due to (7.10) the expectation value of

the number operator  $n_i^{(b)}$  of the second observer on the vacuum  $|0_a\rangle$  of the first observer is

$$\begin{aligned}\langle 0_a | n_i^{(b)} | 0_a \rangle &= \langle 0_a | b_i^\dagger b_i | 0_a \rangle = \sum_{j,k} \langle 0_a | \left( a_j^\dagger \alpha_{ji}^* + a_j \beta_{ji} \right) \left( \alpha_{ik} a_k + \beta_{ik}^* a_k^\dagger \right) | 0_a \rangle = \\ &= \sum_{j,k} \langle 0_a | a_j \beta_{ji} \beta_{ik}^* a_k^\dagger | 0_a \rangle = \sum_{j,k} \beta_{ji} \beta_{ik}^* \langle 0_a | \left( a_k^\dagger a_j + \delta_{ij} \right) | 0_a \rangle = \sum_j |\beta_{ji}|^2,\end{aligned}\quad (7.11)$$

and then, if  $\sum_j |\beta_{ji}|^2 \neq 0$ , it is not a vacuum state.

The Hawking radiation process can be derived by looking at the expectation value of the number operator after the creation of the black hole on the vacuum state defined before the creation of the event horizon; in practical terms, this means that an observer will detect particles outside the black hole, while it would have detected nothing before its creation. To quantify these statements, let us consider a massless field expanded in *ingoing* modes before the collapse

$$\begin{aligned}\phi &= \sum_i \left( f_i a_i + f_i^* a_i^\dagger \right), \\ f_i &= \frac{1}{\sqrt{2\pi\omega_i}} \frac{F_i(r)}{r} Y_{lm}(\theta, \phi) e^{i\omega_i v},\end{aligned}\quad (7.12)$$

where  $v = t + r^*$ , and  $r^*$  is the standard tortoise coordinate, and in *ingoing* modes  $q_i$  and *outgoing* modes  $p_i$  after collapse

$$\begin{aligned}\phi &= \sum_i \left( p_i b_i + p_i^* b_i^\dagger + q_i c_i + q_i^* c_i^\dagger \right), \\ p_i &= \frac{1}{\sqrt{2\pi\omega'_i}} \frac{P_i(r)}{r} Y_{lm}(\theta, \phi) e^{i\omega'_i u}, \\ q_i &= \frac{1}{\sqrt{2\pi\omega'_i}} \frac{Q_i(r)}{r} Y_{lm}(\theta, \phi) e^{i\omega'_i v},\end{aligned}\quad (7.13)$$

where  $u = t - r^*$ , and the frequencies are defined using the asymptotic timelike Killing vectors in the past and future null infinities. Hawking radiation is then defined by the Bogoliubov coefficient of outgoing modes  $p_i$  over the ingoing modes  $f_i$ . To do that we have to “track back” an outgoing mode  $p_i$  into the infinite past  $\mathcal{J}^-$  (see Figure 53); here the dotted lines indicate the trajectories of the massless particles coming from infinity before the collapse, going to the origin and re-emerging from the body before the formation of the horizon.

The blue line will re-emerge just before the formation of the event horizon; therefore, we can argue that the exponent of  $e^{i\omega_i u}$  will oscillate extremely fast for the divergence of  $u = t - r^*$  (the tortoise coordinate diverge on the horizon), and the geometrical approximation can be used even in the presence of a collapsing body because a high-frequency mode is expected to have few interactions. The subtlety here is in the definition

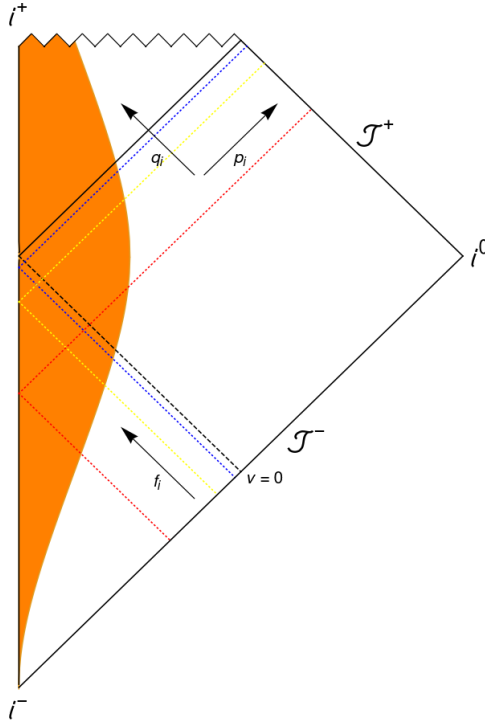


Figure 53: Evaporation of a black hole from a collapsing body, the orange section is the collapsing body, the arrows indicate the different modes used during the expansion, and the dotted lines indicate the trajectories of different modes.

of the proper distance between the geodesics followed by the mode and the null geodesics which enter the body and re-emerge exactly *on* the horizon. After the formation of the black hole, the proper distance  $\lambda$  is defined in terms of the Kruskal-Szekeres coordinate

$$\lambda = -U = C_1 e^{-\kappa u}, \quad (7.14)$$

where  $C_1$  is a generic constant and  $\kappa$  is the surface gravity (5.1). Before the formation of the black hole, the proper distance is instead proportional to the Eddington-Finkelstein coordinate

$$\lambda = -C_2 v, \quad (7.15)$$

where  $C_2$  is another generic constant and we set  $v = 0$  for the null geodesics re-emerging on the horizon. The outgoing mode then can be expressed as

$$p_i = \frac{1}{\sqrt{2\pi\omega'_i}} \frac{P_i(r_H)}{r} Y_{lm}(\theta, \phi) e^{i\omega'_i u} = \frac{1}{\sqrt{2\pi\omega'_i}} \frac{P_i}{r} Y_{lm}(\theta, \phi) \left( \frac{C_1}{C_2} \right)^{\frac{i\omega'_i}{\kappa}} e^{-i\frac{\omega'_i}{\kappa} \log(-v)}, \quad (7.16)$$

where  $P_i = P_i(r_H)$ , and the Bogoliubov coefficient can be found from

$$p_i = \sum_j (\alpha_{ij} f_j + \beta_{ij} f_j^*). \quad (7.17)$$

However, for the subsequent calculation is convenient to pass from a discrete set of modes to a continuum one, where the mode  $p_i$  becomes

$$p_{\omega'} = \int_0^\infty d\omega \frac{1}{\sqrt{2\pi\omega}} \frac{Y_{lm}(\theta, \phi)}{r} (\alpha_{\omega\omega'} e^{i\omega v} + \beta_{\omega\omega'} e^{-i\omega v}), \quad (7.18)$$

where we considered  $\lim_{r \rightarrow \infty} F_\omega(r) = 1$ . The specific form of the integral resembles the one of the Fourier transform

$$p_{\omega'} = \frac{1}{2\pi} \int_{-\infty}^\infty d\omega \tilde{p}_{\omega'}(\omega) e^{i\omega v} = \frac{1}{2\pi} \int_0^\infty d\omega (\tilde{p}_{\omega'}(\omega) e^{i\omega v} + \tilde{p}_{\omega'}(-\omega) e^{-i\omega v}). \quad (7.19)$$

By comparing (7.18) and (7.19), we can then express the Bogoliubov coefficients as

$$\begin{aligned} \alpha_{\omega\omega'} &= \frac{r\sqrt{\omega}}{\sqrt{2\pi}} \tilde{p}_{\omega'}(\omega) = \frac{P_{\omega'}}{2\pi} \sqrt{\frac{\omega}{\omega'}} \left( \frac{C_1}{C_2} \right)^{\frac{i\omega'}{\kappa}} \int_{-\infty}^0 dv e^{-i\frac{\omega'}{\kappa} \log(-v)} e^{-i\omega v}, \\ \beta_{\omega\omega'} &= \frac{r\sqrt{\omega}}{\sqrt{2\pi}} \tilde{p}_{\omega'}(-\omega) = \frac{P_{\omega'}}{2\pi} \sqrt{\frac{\omega}{\omega'}} \left( \frac{C_1}{C_2} \right)^{\frac{i\omega'}{\kappa}} \int_{-\infty}^0 dv e^{-i\frac{\omega'}{\kappa} \log(-v)} e^{i\omega v}, \end{aligned} \quad (7.20)$$

where the boundaries of integration are given by the requirement  $v < 0$  necessary to have a particle outside the horizon at late times. If we rewrite the  $\beta_{\omega\omega'}$  as

$$\begin{aligned} \beta_{\omega\omega'} &= \frac{P_{\omega'}}{2\pi} \sqrt{\frac{\omega}{\omega'}} \left( \frac{C_1}{C_2} \right)^{\frac{i\omega'}{\kappa}} \int_{-\infty}^0 dv e^{-i\frac{\omega'}{\kappa} \log(-v)} e^{i\omega v} = \\ &= \frac{P_{\omega'}}{2\pi} \sqrt{\frac{\omega}{\omega'}} \left( \frac{C_1}{C_2} \right)^{\frac{i\omega'}{\kappa}} \int_0^\infty dv e^{-i\frac{\omega'}{\kappa} \log(v)} e^{-i\omega v} = \\ &= \frac{P_{\omega'}}{2\pi} \sqrt{\frac{\omega}{\omega'}} \left( \frac{C_1}{C_2} \right)^{\frac{i\omega'}{\kappa}} \int_0^\infty dv e^{-i\frac{\omega'}{\kappa} (\log(-v) - i\pi)} e^{-i\omega v} = \\ &= e^{-\frac{\pi\omega'}{\kappa}} \frac{P_{\omega'}}{2\pi} \sqrt{\frac{\omega}{\omega'}} \left( \frac{C_1}{C_2} \right)^{\frac{i\omega'}{\kappa}} \int_0^\infty dv e^{-i\frac{\omega'}{\kappa} \log(-v)} e^{-i\omega v}, \end{aligned} \quad (7.21)$$

we can consider the combination

$$\begin{aligned} \alpha_{\omega\omega'} + e^{\frac{\pi\omega'}{\kappa}} \beta_{\omega\omega'} &= \frac{P_{\omega'}}{2\pi} \sqrt{\frac{\omega}{\omega'}} \left( \frac{C_1}{C_2} \right)^{\frac{i\omega'}{\kappa}} \left( \int_{-\infty}^0 dv e^{-i\frac{\omega'}{\kappa} \log(-v)} e^{-i\omega v} + \right. \\ &\quad \left. + \int_0^\infty dv e^{-i\frac{\omega'}{\kappa} \log(v)} e^{-i\omega v} \right) = \\ &= \frac{P_{\omega'}}{2\pi} \sqrt{\frac{\omega}{\omega'}} \left( \frac{C_1}{C_2} \right)^{\frac{i\omega'}{\kappa}} \int_{-\infty}^\infty dv e^{-i\frac{\omega'}{\kappa} \log(-v)} e^{-i\omega v} = 0, \end{aligned} \quad (7.22)$$

where the last equation is provable by integrating in the complex plane and taking the cut of the logarithm in the lower half-plane. We can now consider the normalization of the modes

$$\begin{aligned} (f_\omega, f_\omega) &= 1, \\ (p_{\omega'}, p_{\omega'}) &= \int dr P_{\omega'}(r)^2 = \Gamma_{\omega'}, \end{aligned} \quad (7.23)$$

where the normalization of the modes  $p_{\omega'}$  is not set to 1 because some modes will generally be scattered inside the black hole (usually the low-frequency ones). Using the continuum version of (7.17) the normalization of the  $p_{\omega'}$  can also be expressed as

$$(p_{\omega'}, p_{\omega'}) = \int d\omega (\alpha_{\omega\omega'}\alpha_{\omega\omega'}^* - \beta_{\omega\omega'}\beta_{\omega\omega'}^*) = \left(e^{\frac{2\pi\omega'}{\kappa}} - 1\right) \int d\omega |\beta_{\omega\omega'}|^2 = \Gamma_{\omega'}, \quad (7.24)$$

where the second equivalence is given by (7.22). Finally, we arrive at the continuum version of (7.11)

$$\langle 0_a | n_{\omega'}^{(b)} | 0_a \rangle = \int d\omega |\beta_{\omega\omega'}|^2 = \frac{\Gamma_{\omega'}}{e^{\frac{\omega'}{\kappa/2\pi}} - 1}, \quad (7.25)$$

which is a thermal distribution with temperature

$$T_{BH} = \frac{\kappa}{2\pi}, \quad (7.26)$$

and a so-called grey body factor  $\Gamma_{\omega'}$ , which is simply a cut-off of the low-frequency modes at the physical level.

While the calculation just presented shows the presence of emission of particles at the horizon, it is still not sufficient to demonstrate the evaporation of a black hole. To do so, it is necessary to understand how the radiation at the horizon affects the time evolution of the metric. The fundamental equation under analysis is then the flux equation

$$\mathcal{G}_{tr} = \frac{1}{2} \langle T_{tr} \rangle, \quad (7.27)$$

where  $\mathcal{G}_{tr}$  is the time-radial component of the equations of motion and  $\langle T_{tr} \rangle$  is the expectation value of the energy flux component of the stress-energy tensor of the particles which are being emitted. For the calculation of (7.27) it is necessary to resort to the so-called *adiabatic approximation*, where we consider the metric to evolve in time slowly and then to be expressible as the static metric with time-dependent parameters. As an example, the Schwarzschild metric becomes the Vaidya metric

$$1 - \frac{2M}{r} \rightarrow 1 - \frac{2M(t)}{r}. \quad (7.28)$$

If we consider a scalar field non-minimally coupled with the Ricci scalar with a term  $\xi\phi^2R$ , the flux component of the stress-energy tensor is [85]

$$T_{tr} = \frac{1}{2(1 - \xi\phi^2)} (\partial_r\phi\partial_t\phi^* + \partial_t\phi\partial_r\phi^* - 2\xi\partial_t\partial_r\phi^2) \sim \frac{1}{2} (\partial_r\phi\partial_t\phi^* + \partial_t\phi\partial_r\phi^* - 2\xi\partial_t\partial_r\phi^2), \quad (7.29)$$

where the approximation is taken because we need a small back-reaction in order to use the adiabatic approximation. Evaluating the expectation value requires some care because

the normal ordering of the operators diverges on the horizon. Nonetheless, it is possible to express the stress-energy tensor in terms of the  $p_\omega$  modes as [82, 85, 86, 87]

$$\begin{aligned} \langle T_{tr} \rangle &= \int d\omega d\omega' |\beta_{\omega\omega'}|^2 \frac{1}{2} (\partial_r p_\omega \partial_t p_\omega^* + \partial_t p_\omega \partial_r p_\omega^* - 2\xi \partial_t \partial_r |p_\omega|^2) = \\ &= - \int d\omega |Y_{lm}(\theta, \phi)|^2 \frac{\omega P_\omega(r)^2}{2\pi r^2} \frac{dr^*}{dr} \frac{\Gamma_\omega}{e^{\frac{\omega}{\kappa/2\pi}} - 1} \rightarrow - \frac{1}{r^2 \sqrt{f(r, t)h(r, t)}} \int d\omega \frac{\omega}{8\pi^2} \frac{\Gamma_\omega}{e^{\frac{\omega}{\kappa/2\pi}} - 1}, \end{aligned} \quad (7.30)$$

where we exploited the conservation of the stress-energy tensor and that  $P(r) \rightarrow 1$  for  $r \rightarrow \infty$  and averaged over the angular directions. The prefactor  $1/\sqrt{f(r, t)h(r, t)}$ , which acts as a redshift factor, can be conveniently moved on the left-hand side of the equation as

$$r^2 \sqrt{f(r, t)h(r, t)} \mathcal{G}_{tr} = - \frac{1}{2} \int d\omega \frac{\omega}{8\pi^2} \frac{\Gamma_\omega}{e^{\frac{\omega}{\kappa/2\pi}} - 1}. \quad (7.31)$$

Since this point, we were never required to consider a specific theory of gravity in our calculations; however, the left-hand side of (7.27) is manifestly dependent on the action under analysis. In the case of General Relativity, it is

$$r^2 \sqrt{f(r, t)h(r, t)} \mathcal{G}_{tr} = -\gamma r \sqrt{\frac{h(r, t)}{f(r, t)}} \frac{df(r, t)}{dt} = 2\gamma \frac{dM(t)}{dt}, \quad (7.32)$$

where in the last line we inserted the Vaidya metric (7.28). In the case of quadratic gravity, it is necessary to stress the adiabatic approximation a bit more and consider only terms linear in the first derivatives in time, and with no higher-order derivatives in time. With this approximation, the flux equation can be studied both at large radii and at the horizon. In the first case we consider the weak field metric (3.5) with time-dependent  $M(t)$  and  $S_2^-(t)$ , and the left-hand side of (7.31) becomes

$$\begin{aligned} r^2 \sqrt{f(r, t)h(r, t)} \mathcal{G}_{tr} &\rightarrow \gamma \left( 2 \frac{dM(t)}{dt} - \frac{dS_2^-(t)}{dt} e^{-m_2 r} (1 + m_2 r) \right) + \\ &\quad + 2\alpha m_2^2 \frac{dS_2^-(t)}{dt} e^{-m_2 r} (1 + m_2 r) = 2\gamma \frac{dM(t)}{dt}, \end{aligned} \quad (7.33)$$

where in the last equality we used  $m_2^2 = \gamma/2\alpha$ . Stressing the adiabatic approximation it is possible to evaluate (7.31) also close to the horizon with the metric expressed by (3.28) with time-dependent  $r_H(t)$ ,  $h_1(t)$  and  $f_1(t)$ , and it takes the form

$$\begin{aligned} r^2 \sqrt{f(r, t)h(r, t)} \mathcal{G}_{tr} &\rightarrow \gamma \sqrt{f_1(t)h_1(t)} r_H(t) \frac{dr_H(t)}{dt} + \\ &\quad - 2\alpha \sqrt{f_1(t)h_1(t)} \left( f_1(t) \frac{dr_H(t)}{dt} + r_H(t) \frac{df_1(t)}{dt} \right) = \\ &= \frac{1}{2} \gamma \sqrt{f_1(t)h_1(t)} \frac{d}{dt} \left( r_H(t)^2 + \frac{2}{m_2^2} (1 - f_1(t)r_H(t)) \right). \end{aligned} \quad (7.34)$$

Remembering the definition of black hole temperature (7.26), we can express the last line of (7.34) as

$$2\gamma T_{BH}(t) \frac{d}{dt} \left( \pi \left( r_H(t)^2 + \frac{2}{m_2^2} (1 - f_1(t)r_H(t)) \right) \right), \quad (7.35)$$

where the argument of the derivative we will show in Subsection 7.1.3 is exactly the Wald definition of entropy. Finally, we can show that the left-hand side of (7.31) can be written as

$$r^2 \sqrt{f(r, t)h(r, t)} \mathcal{G}_{tr} \rightarrow 2\gamma T_{BH}(t) \frac{dS_{Wald}(t)}{dt}, \quad (7.36)$$

and then prove that the two limits satisfy the first law of black hole Thermodynamics

$$\frac{r^2}{2\gamma} \sqrt{f(r, t)h(r, t)} \mathcal{G}_{tr} \Big|_{r \rightarrow \infty} = \frac{dM(t)}{dt} = T_{BH}(t) \frac{dS_{Wald}(t)}{dt} = \frac{r^2}{2\gamma} \sqrt{f(r, t)h(r, t)} \mathcal{G}_{tr} \Big|_{r \rightarrow r_H}. \quad (7.37)$$

Finally, the flux equation can be written as

$$\begin{aligned} \frac{dM(t)}{dt} &= - \int d\omega \frac{\omega}{32\pi^2\gamma} \frac{\Gamma_\omega}{e^{\frac{\omega}{\kappa/2\pi}} - 1}, \\ T_{BH} \frac{dS_{Wald}(t)}{dt} &= - \int d\omega \frac{\omega}{32\pi^2\gamma} \frac{\Gamma_\omega}{e^{\frac{\omega}{\kappa/2\pi}} - 1}. \end{aligned} \quad (7.38)$$

If we concentrate on high-frequency modes, we can take the approximation  $\Gamma_\omega \rightarrow 1$ , in which the right-hand side of (7.38) takes the form

$$\int d\omega \frac{\omega}{32\pi^2\gamma} \frac{\Gamma_\omega}{e^{\frac{\omega}{\kappa/2\pi}} - 1} \sim \frac{\sigma}{m_2^2} T_{BH}^2, \quad (7.39)$$

where  $\sigma = 1/384\alpha$  is an adimensional constant, acting as the Stefan-Boltzmann constant. Taking everything in units of  $m_2$  leads us finally to the equations

$$\begin{aligned} \frac{dM(t)}{dt} &\sim -\sigma T_{BH}^2, \\ \frac{dS_{Wald}(t)}{dt} &\sim -\sigma T_{BH}, \end{aligned} \quad (7.40)$$

that can be easily integrated once  $T_{BH}(M)$  or  $T_{BH}(S_{Wald})$  are known.

### 7.1.2 The path integral approach to quantum gravity and black hole Thermodynamics

In the previous subsubsection we have shown how it is possible to define a temperature associated with a black hole and, by implementing an evaporation mechanism, how it is possible to define, using specific assumptions on the form of the metric, also the energy and the entropy. However, it is possible to define this concept without resorting to a convenient form of the metric, and even without requiring a specific theory of gravity.

As anticipated at the beginning of the subsection, this is possible by applying the path integral approach to quantum gravity [83, 88], which in its semiclassical limits has the same results as the Quantum Field Theory on curved spacetime approach.

Let us consider the partition function of a quantum theory of gravity defined by a bare action  $\mathcal{I}(g)$

$$Z = \int \mathcal{D}g \left[ e^{-\mathcal{I}(g)} \right], \quad (7.41)$$

where the integral  $\int \mathcal{D}g$  has to be intended as an integral over all possible spacetimes. Let us now suppose that the Euclidean time has periodicity  $\beta$  and that it is possible to rewrite the bare action as  $\mathcal{I}(g) = \beta \mathcal{H}(g)$ . The partition function now has the form

$$Z = \int \mathcal{D}g \left[ e^{-\beta \mathcal{H}(g)} \right] \rightarrow \sum_g \langle g | e^{-\beta \mathcal{H}(g)} | g \rangle, \quad (7.42)$$

where in the second step we discretized the sum over all possible spacetimes. The crucial point here is that the partition function now formally has the same expression as a thermodynamical partition function in the canonical ensemble. It is then possible to apply all the machinery of classical Thermodynamics and define the temperature

$$T = \frac{1}{\beta}, \quad (7.43)$$

the expectation value of the energy

$$\langle E \rangle = \frac{1}{Z} \sum_g \langle g | \mathcal{H}(g) e^{-\beta \mathcal{H}(g)} | g \rangle = -\frac{\partial \log(Z)}{\partial \beta}, \quad (7.44)$$

and the entropy

$$S = - \sum_g \langle g | \frac{e^{-\beta \mathcal{H}(g)}}{Z} \log \left( \frac{e^{-\beta \mathcal{H}(g)}}{Z} \right) | g \rangle = \log(Z) + \beta \langle E \rangle. \quad (7.45)$$

These definitions, however, acquire a physical sense in the semiclassical approximation, where the partition function takes the form

$$Z \sim e^{-\mathcal{I}(g_0)}, \quad (7.46)$$

where  $g_0$  is the metric which minimizes the action. The previous definitions now look

$$\begin{aligned} \langle E \rangle &= \frac{\partial \mathcal{I}(g_0)}{\partial \beta}, \\ S &= \beta \frac{\partial \mathcal{I}(g_0)}{\partial \beta} - \mathcal{I}(g_0), \end{aligned} \quad (7.47)$$

and all the thermodynamical information can be extracted from the action evaluated on a specific spacetime. As an example, let us consider the Schwarzschild solution in General Relativity

$$ds_E^2 = \left( 1 - \frac{2GM}{r} \right) dt_E^2 + \frac{dr^2}{1 - \frac{2GM}{r}} + r^2 d\Omega^2. \quad (7.48)$$

It is necessary to add to the action a boundary term which, in the case of General Relativity, completes the action as

$$\mathcal{I} = \frac{1}{16\pi G} \left( \int_{\mathcal{M}} d^4x \sqrt{-g} R + 2 \int_{\partial\mathcal{M}} d^3x \sqrt{-h} (K - K_0) \right), \quad (7.49)$$

where  $\partial\mathcal{M}$  is the boundary of the manifold  $\mathcal{M}$ ,  $h_{\mu\nu}$  is its metric,  $K$  its extrinsic curvature and  $K_0$  the extrinsic curvature of a chosen background metric embedded in the spacetime. The spacetime has a conical singularity at  $r = 2GM$ , which can be removed by choosing a periodic Euclidean time with periodicity  $\beta = 8\pi GM$ . Choosing the Minkowski spacetime as background and the boundary at spatial infinity, the Euclidean action results to be  $\mathcal{I} = 4\pi GM^2$ . The thermodynamical properties then are

$$\begin{aligned} T &= \frac{1}{\beta} = \frac{1}{8\pi GM} = \frac{1}{4\pi r_s}, \\ \langle E \rangle &= \frac{\partial \mathcal{I}(g_0)}{\partial \beta} = 8\pi GM \frac{\partial M}{\partial \beta} = M, \\ S &= \beta \frac{\partial \mathcal{I}(g_0)}{\partial \beta} - \mathcal{I}(g_0) = 8\pi GM^2 - 4\pi GM^2 = 4\pi GM^2 = \frac{\pi r_s^2}{G} = \frac{A}{4G}, \end{aligned} \quad (7.50)$$

where the temperature agrees with the results obtained with Quantum Field Theory in curved spacetime, considering that  $\kappa = 1/r_s$ , the energy agrees with the Newtonian limit and all possible definitions of the energy of Schwarzschild spacetime, and the entropy satisfies the first law of Thermodynamics and agrees with the intuition of Bekenstein that a black hole should have an entropy proportional to its area [89, 90].

### 7.1.3 Wald entropy

While the definition of entropy (7.45) is consistently defined, it requires being able to evaluate both the Euclidean action and its derivative with respect to the Euclidean time periodicity. A different definition of entropy has been proposed by Wald in [91] as the conserved charge associated with diffeomorphism for any theory of gravity which admits a Lagrangian formulation. While the original derivation is somewhat abstract and not extremely simple, we will try to sketch the main idea in a non-rigorous, but hopefully physically meaningful, way. The key point is to define an Hamiltonian density  $H$  starting from the Lagrangian density  $\mathcal{L}$ , and express its variation under diffeomorphism in terms of a current  $\mathbf{j}$  which, however, is a boundary term

$$\delta H = \delta \int_{\mathcal{M}} \mathbf{j} = \delta \int_{\partial\mathcal{M}} \mathbf{b}. \quad (7.51)$$

If the integration has a boundary at infinity and one over an event horizon, requiring the equations of motion to be satisfied, that is,  $\delta H = 0$ , imposes

$$\delta \int_{\partial\mathcal{M}_\infty} \mathbf{b} = -\delta \int_{\partial\mathcal{M}_H} \mathbf{b}. \quad (7.52)$$

It is now sufficient to define the quantity

$$\delta E = \delta \int_{\partial\mathcal{M}_\infty} \mathbf{b}, \quad T\delta S = -\delta \int_{\partial\mathcal{M}_H} \mathbf{b}, \quad (7.53)$$

and the first law of Thermodynamics is satisfied. This definition of energy is consistent with all the possible definitions of the total energy of a spacetime, as the ADM or Bondi one, as could be expected being associated with the flux of the Hamiltonian at infinity. The definition of entropy remains a little bit involved and not very manageable; however, it is possible to express it as [92]

$$S = -\frac{1}{8} \int d\Sigma \sqrt{h} \epsilon^{\mu\nu} \epsilon^{\rho\sigma} \frac{\partial \mathcal{L}}{\partial R^{\mu\nu\rho\sigma}}, \quad (7.54)$$

where  $\Sigma$  is the surface defined by the horizon,  $h_{\mu\nu}$  its metric and  $\epsilon^{\mu\nu}$  is the binormal on the surface. In [93], (7.54) has been evaluated in the case of the action (2.2), and has as result

$$S_{Wald} = 16\pi (\gamma\pi r_H^2 + 4\chi - 4\alpha f_1 r_H), \quad (7.55)$$

where  $f_1 = f'(r)|_{r=r_H}$ . To have  $S \propto A/4$  in the case of Schwarzschild it is necessary to impose  $\chi = \alpha$ , and finally we obtain

$$S_{Wald} = 16\pi^2 \gamma \left( r_H^2 + \frac{2}{m_2^2} (1 - f_1 r_H) \right) \rightarrow \pi \left( r_H^2 + \frac{2}{m_2^2} (1 - f_1 r_H) \right), \quad (7.56)$$

where we gave a dimension to the entropy dividing by  $16\pi\gamma$  in order to have the parameter  $M$  in (3.5), which we recall has the dimension of an inverse energy, to satisfy the first law of Thermodynamics

$$\delta M = T_{BH} \delta S_{Wald}. \quad (7.57)$$

It is now no surprise that this definition satisfies the first law of Thermodynamics, as anticipated in (7.37), because it is defined to do so. What is of great relevance, instead, is that thanks to the Wald formula it is possible to define the entropy of a black hole knowing its behavior at the horizon exclusively. Using the shooting method between a large radius and the horizon to find black hole solutions gave us then a direct link between all the thermodynamical properties of black holes without needing an explicit expression of the metric.

## 7.2 Thermodynamics of black holes in quadratic gravity

As extensively stressed, the thermodynamical properties of black holes are a semiclassical effect relevant at small scales (the temperature of a black hole gets higher than the CMB temperature at masses  $M \lesssim 10^{-8} M_\odot$ , that is, horizon radius  $r_H \lesssim 10^{-5} m$ ). It is then natural to ask what is the impact of higher curvature terms on black hole Thermodynamics. Thanks to the discussion of the previous subsection, we now have at our disposal

a complete set of thermodynamical properties, that is, Hawking temperature (7.26) and Wald entropy (7.56), which can be derived directly from the values of the parameters at the horizon  $h_1$  and  $f_1$  found with the shooting method (and shown in Figure 16), and their link with the total energy  $M$  which can be instead derived by the parameters at large distances. At last, we show the temperature and entropy in terms of the horizon radius and the total mass in Figure 54.

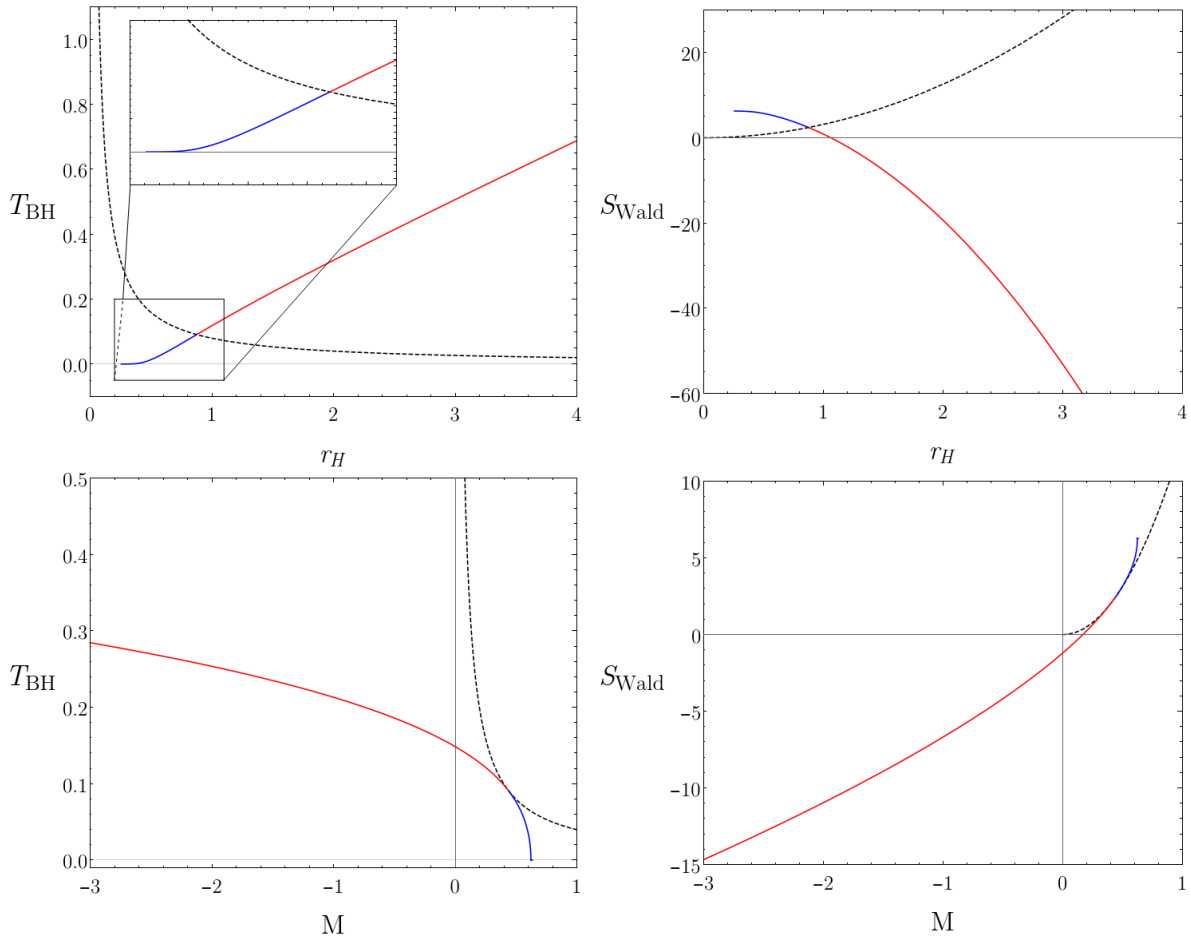


Figure 54: Hawking temperature and Wald entropy for black holes in quadratic gravity in function of the horizon radius (in the top panels) and in function of the total mass (in the bottom panels); as usual, the black dashed line indicates Schwarzschild black holes, the solid red indicates Yukawa attractive black holes and the solid blue the Yukawa repulsive ones. In the plot for the temperature in terms of the horizon radius there is an inset showing the vanishing of the temperature for vanishing radius.

The temperature, which is shown in the left panels of Figure 54, has an opposite behavior for Schwarzschild and non-Schwarzschild black holes when considered in terms of the horizon radius, namely, it decreases for smaller black holes, as already anticipated in Subsection 5.1. Even if it is counter-intuitive, it is clear that the gravitational forces an observer experiences close to the horizon are indeed stronger for a larger black hole, and then the extraction process of particles from the vacuum is more efficient. Nonetheless, the temperature increase for a decreasing mass, as for Schwarzschild black holes, indicat-

ing that the specific heat of the black hole is still negative, and also that these solutions are thermodynamically unstable and will continue evaporating; having the possibility of black holes with negative masses, however, the evaporation seems unbounded. The main critical point of the thermodynamical properties shown in Figure 54 is however given by the entropy. In terms of the horizon radius, it decreases for an increasing radius reversing completely the idea of a concept of entropy associated with the area of the black hole; in terms of the total mass, instead, it decreases for a decreasing mass, signaling that the entropy of Hawking radiation (which is  $S_{rad} = S_{tot} - S_{BH}$ , given that the evaporation process is adiabatic and then the total variation of entropy is zero) is increasing indefinitely. It can be noted, maybe only as a curiosity, that the maximum allowed entropy for a non-Schwarzschild black hole, reached for a vanishing horizon radius, is  $2\pi$ ; restoring the original form of the entropy (7.55) it becomes  $64\pi\alpha$  which is a topological contribution due to the Gauss-Bonnet combination, remembering that we set  $\chi = \alpha$ . However, the most striking feature of the entropy of non-Schwarzschild black holes is that *it gets negative* at some point. If we consider the mechanical statistics definition of entropy

$$S \propto - \sum_i p_i \log(p_i) = -\langle \log(p) \rangle, \quad (7.58)$$

it is clear that a negative entropy means that  $p > 1$ , and then unitarity is violated. It is then manifest that the ghost particle, which is responsible for the violation of unitarity in the quantum version of quadratic gravity, is also responsible for a violation of unitarity at the semiclassical level.

While these considerations already signal an unphysical nature of non-Schwarzschild black holes at the semiclassical level, it is necessary to consider the evaporation process in order to make statements about the effects of these properties in the physical world. Let us then consider equation (7.40): for a Schwarzschild black hole they can be easily integrated considering  $T_{BH} = 1/8\pi M$  as

$$t - t_0 = -\frac{64\pi^2}{\sigma} \int dM M^2 = \frac{64\pi^2}{3\sigma} (M(t_0)^3 - M(t)^3); \quad (7.59)$$

the integration is less immediate in the case of non-Schwarzschild black holes, as there is no analytical relation between mass, entropy and temperature. It is necessary then to either integrate (7.40) numerically, or fit  $-1/T^2$  in terms of the mass, or  $-1/T$  in terms of the entropy. We choose the second option that, while less precise in the result, is more explanatory of the qualitative evaporation trend. We show in Figure 55 the two functions and their fit, which is not optimal but is sufficient for qualitative analysis.

We also specify that it is much more convenient to fit the temperature in terms of mass and entropy and then do the inverse rather than directly fit the inverse temperature. If

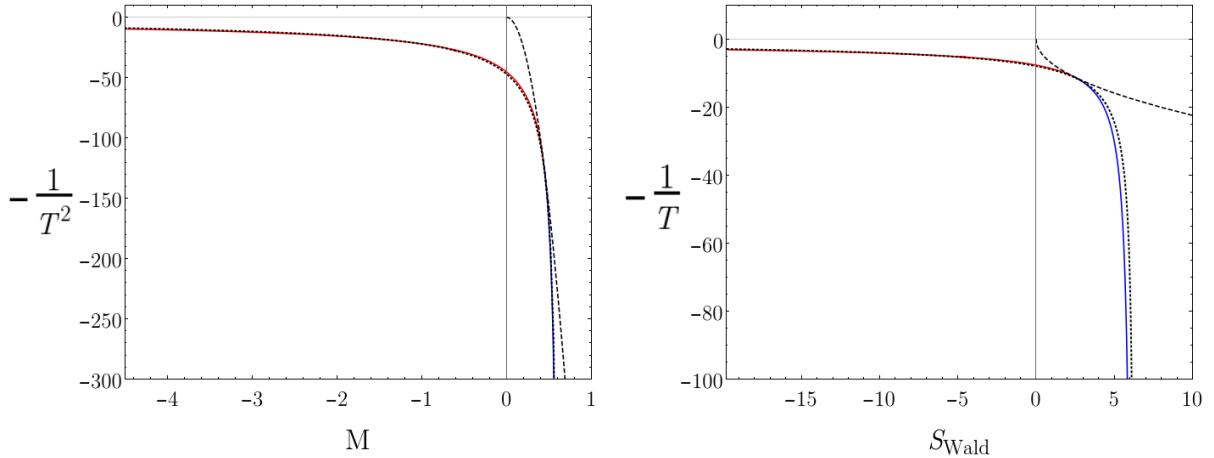


Figure 55: Squared inverse temperature in function of the mass, and inverse temperature in function of Wald entropy; as usual in dashed black there are Schwarzschild black holes, in solid red Yukawa attractive black holes and in solid blue Yukawa repulsive ones. In dotted black is shown the fit for non-Schwarzschild black holes.

we focus on the mass-temperature relation, this is given by

$$-\frac{1}{T_{BH}^2} \sim -A (M_{mtp} - M)^{-\eta} \quad \text{with} \quad \begin{cases} A \sim 32.451 \\ M_{mtp} \sim 0.623 \\ \eta \sim 0.787 \end{cases} \quad (7.60)$$

where  $M_{mtp}$  is the mass of the massive triple point of the phase diagram of Einstein-Weyl gravity, which is the mass of a non-Schwarzschild black hole with a vanishing horizon radius. Integrating (7.40) then has the result

$$t - t_0 \sim \frac{A}{\sigma(1-\eta)} \left( (M_{mtp} - M(t))^{1-\eta} - (M_{mtp} - M(t_0))^{1-\eta} \right), \quad (7.61)$$

and can be inverted as

$$M(t) \sim M_{mtp} - \left( (M_{mtp} - M(t_0))^{1-\eta} + \frac{\sigma(1-\eta)}{A} (t - t_0) \right)^{\frac{1}{1-\eta}}. \quad (7.62)$$

The first thing that can be inferred from (7.61) is that, being a monotonically decreasing function in time, also for non-Schwarzschild black holes the time evolution is in the direction of decreasing mass. The main difference here is that *there is no minimum mass*, and then, as already argued before, the evaporation process is unbounded. Let us be more specific and consider a Schwarzschild black hole of initial mass  $M_0$  created at time  $t = 0$  which evaporates. At the time

$$t_{sns} = \frac{64\pi^2}{3\sigma} (M_0^3 - M_{sns}^3), \quad (7.63)$$

it will have reached the mass  $M_{sns}$  at which Schwarzschild and non-Schwarzschild black holes coincide. At this point, both smaller Schwarzschild and Yukawa repulsive black

holes will be unstable, and then let us assume that it will have a transition into Yukawa attractive black holes. If this is the case, the mass at time  $t$  will be

$$M(t) \sim M_{mtp} - \left( (M_{mtp} - M_{sns})^{1-\eta} - \frac{64\pi^2(1-\eta)}{3A} (M_0^3 - M_{sns}^3) + \frac{\sigma(1-\eta)}{A} t \right)^{\frac{1}{1-\eta}}. \quad (7.64)$$

Remembering that everything has been adimensionalized in terms of the mass  $m_2$ , we can restore units by

$$\begin{aligned} M &\rightarrow \frac{m_2}{16\pi\gamma} M \rightarrow \frac{1}{\sqrt{32\pi\alpha m_p}} M, \\ t &\rightarrow m_2 t \rightarrow \frac{1}{\sqrt{32\pi\alpha t_p}} t, \end{aligned} \quad (7.65)$$

and, in particular, we will give each term the dimensions

$$\begin{aligned} M(t) &\rightarrow \frac{M_\odot}{\sqrt{32\pi\alpha m_p}} \frac{M(t)[M_\odot]}{M_\odot}, \\ M_0 &\rightarrow \frac{Kg}{\sqrt{32\pi\alpha m_p}} \frac{M_0[Kg]}{Kg}, \\ t &\rightarrow \frac{Gy}{\sqrt{32\pi\alpha t_p}} \frac{t[Gy]}{Gy}, \end{aligned} \quad (7.66)$$

and leave the rest without dimensions. Finally, equation (7.64) can be written with dimensions as

$$M(t) \sim \sqrt{\alpha} \left( c_0 10^{-37} - \left( c_1 10^{-8} - \frac{c_2 10^{12}}{\alpha^{3/2}} \left( \frac{M_0[Kg]}{Kg} \right)^3 + \frac{c_3 10^{54}}{\alpha^{3/2}} \frac{t[Gy]}{Gy} \right)^\delta \right) M_\odot, \quad (7.67)$$

where  $c_0$ ,  $c_1$ ,  $c_2$  and  $c_3$  are constants of order  $\mathcal{O}(1)$ , and in particular the parameters are

$$c_0 = 0.684, \quad c_1 = 1.132, \quad c_2 = 1.845, \quad c_3 = 0.997, \quad \delta = 4.704. \quad (7.68)$$

It is now possible to describe the evaporation process of an astrophysical black hole. Let us now consider that in the early universe (let us say  $t \sim 10Gy$ ) a primordial Schwarzschild black hole of mass  $M_0$  has formed and started evaporating. In the General Relativity description is it possible to have black holes of a range of masses that goes from Planckian to thousand of solar masses [94]; however, primordial black holes with masses of order  $M_0 < 10^{11}Kg$  would be completely evaporated at the present time. In quadratic gravity, instead, a black hole with initial mass

$$\begin{cases} M_0 > 10^{11}Kg, & \text{with } \alpha < 10^{37}, \\ M_0 > 10^{-7}\sqrt{\alpha}Kg, & \text{with } \alpha > 10^{37} \end{cases} \quad (7.69)$$

has still not reached the transition point, and it would be a Schwarzschild black hole in the present time. In contrast with General Relativity, primordial black holes with smaller

initial mass are not completely evaporated but would have undergone the transition, and they would evaporate as non-Schwarzschild black holes. However, the present stage of these black holes depends on the value of the free parameter  $\alpha$ . We can summarize this behavior as

- $\alpha > 10^{60}$ : this range of parameter has been excluded by experiments on torsion balance;
- $10^{42} < \alpha < 10^{60}$ : the constant term multiplied by  $c_0$  dominates, and the black hole will have a positive mass of order  $M(t) \sim \sqrt{\alpha} 10^{-37} M_\odot$  and then of order  $10^{-16} M_\odot < M(t) < 10^{-7} M_\odot$ ;
- $\alpha < 10^{42}$ : the term at power  $\delta$  dominates, and the black hole will have a negative mass of order  $M(t) \sim -\alpha^{-6.556} 10^{259} M_\odot$ .

It is then sufficient to have  $\alpha < 10^{39}$  and primordial black holes with initial mass  $M_0 < 10^{11} K g$  to have in the present universe black holes with negative masses larger than a solar mass; with parameters of the order predicted by CMB anisotropies for Starobinsky's model [19], that is  $\alpha \sim 10^8$ , we would have black holes with negative masses of the order of  $M(t) \sim -10^{206} M_\odot$ , which is clearly an absurd, being  $\sim -10^{182}$  times the total energy of the observable universe.

The evaporation process of non-Schwarzschild black holes then leads us to choose between one of these possibilities:

- quadratic gravity is a flawed theory of gravity and has to be discarded;
- black holes are not a physical solution of quadratic gravity, and gravitational collapse ends in an exotic solution;
- our assumption that an evaporating Schwarzschild black hole will undergo a transition into the stable Yukawa attractive solutions is wrong, and at the minimum stable radius is not possible anymore to describe solutions using a quasi-equilibrium description.

The first hypothesis is the most conservative, the second is probably the less conservative, and the third is a good compromise. In particular, in the third case, we can imagine that the black hole will have a non-static metric that, however, maintains its event horizon. If we want to speculate that the endpoint of this unstable phase should be a static spacetime, the only possibility would be the two triple points of the phase diagram, namely Minkowski spacetime and the massive triple point discussed in Section 4. As seen

as the limit of black holes, however, Minkowski spacetime is the limit of a black hole with a vanishing horizon, vanishing mass but *infinite* temperature. The massive triple point, on the contrary, has a vanishing radius, a vanishing temperature, a *finite* mass, and a *finite* entropy. As a concluding remark, we believe that this massive triple point could actually be the final relic of the evaporation process of a black hole.

### 7.3 Semiclassical analysis of black holes in scale-invariant gravity

We now move again to the study of solutions of General Relativity in the context of scale-invariant gravity. We recall that in this theory a transition between two de Sitter solutions is known to happen in a cosmological setting, in which the scalar field of action (2.41) spontaneously acquires a non-zero expectation value. We also know that two distinct Schwarzschild-de Sitter solutions are present in this theory, as discussed in Subsection 5.5, of which we studied in Subsection 6.3 the stability against dynamical perturbation and shown that the solution with zero scalar field is unstable and the one with a non-zero scalar field is stable. While the linear analysis is rigorous proof of the stability or instability of the solutions, what cannot be inferred by that analysis is whether one solution can have a transition into the other or not, and what is the role of black holes in the cosmological evolution shown in Subsection 5.5.1. A non-linear analysis can answer both of these problems and confirm that no strong non-linear effect spoils the results of the linear analysis. Usually, the non-linear stability of black holes is inferred from their Thermodynamics which, however, is not always well defined. The thermodynamical properties of Schwarzschild, de Sitter, and Schwarzschild-anti-de Sitter solutions can be extracted from (7.46), as described in Subsubsection 7.1.2 and as we will show later, but unfortunately, despite the effort of many authors (see as examples [95, 96]), there is still no consensus on how to define a global temperature for the Schwarzschild-de Sitter spacetime, and a thermodynamical description of such type of solution is a much-debated subject. From a thermodynamical point of view, this is because Schwarzschild-de Sitter solutions have two horizons with different temperatures, and the system is not at thermodynamical equilibrium; from a path integral point of view, it is not possible to define a time periodicity, which removes the two conical singularities emerging in the Euclidean action from the presence of two horizons. In this subsection, therefore, we will not indulge in the thermodynamical description of Schwarzschild-de Sitter black holes, and discuss the possible transition between the two solutions using only the semiclassical description of Euclidean quantum gravity. While in a purely classical description any spacetime which is in a stationary point of the action has equivalent relevance, in the

path integral formulation the absolute value of the action determines which solution has a dominant contribution to the partition function, opening the possibility of having meta-stable solutions which will tunnel away with probability

$$\Gamma = A e^{-(\mathcal{I}_{ms} - \mathcal{I}_s)}, \quad (7.70)$$

where  $A$  is a prefactor and  $\mathcal{I}_{ms}$ ,  $\mathcal{I}_s$  are the Euclidean actions of the meta-stable and stable solutions. This approach has been used to derive the Hawking-Page transition for Schwarzschild-anti-de Sitter black holes [97], and we believe it will be of relevance also in our case. As already said at the beginning of this section, the results of this subsection are corrections of the ones published in [35], and part of the discussion has been extracted from that paper.

As anticipated in the case of General Relativity in (7.49), to evaluate the Euclidean action we need to add a suitable boundary term to the action. Taking into account all the different terms in (2.41), the boundary terms for scale-invariant gravity result to be

$$\begin{aligned} \mathcal{I}_{\partial M,1} &= \int d^3x \sqrt{-h} 2\xi \phi^2 K, \\ \mathcal{I}_{\partial M,2} &= \int d^3x \sqrt{-h} 4\beta R K, \\ \mathcal{I}_{\partial M,3} &= - \int d^3x \sqrt{-h} 2\alpha C^{\mu\nu\rho\sigma} (n_\mu n_\rho K_{\nu\sigma} - n_\mu n_\sigma K_{\nu\rho} + n_\nu n_\sigma K_{\mu\rho} - n_\nu n_\rho K_{\mu\sigma}), \quad (7.71) \\ \mathcal{I}_{\partial M,4} &= \int d^3x \sqrt{-h} 2\chi [R^{\mu\nu\rho\sigma} (n_\mu n_\rho K_{\nu\sigma} - n_\mu n_\sigma K_{\nu\rho} + n_\nu n_\sigma K_{\mu\rho} - n_\nu n_\rho K_{\mu\sigma}) + \\ &\quad - 4(R^{\mu\nu} K_{\mu\nu} + R^{\mu\nu} n_\mu n_\nu K - 2R^{\mu\nu} n_\mu n^\rho K_{\rho\nu}) + 2R K], \end{aligned}$$

where  $h_{\mu\nu}$  is the metric of the boundary,  $K_{\mu\nu}$  is its extrinsic curvature,  $K$  its trace,  $n^\mu$  is its unit normal, and where the ones for the Weyl and Gauss-Bonnet combinations are derived from [98].

**Schwarzschild solution.** In this case there is a single horizon, which generates a single conical singularity at  $r = r_b (= 2M)$  in the Euclidean action. This singularity can be removed as in General Relativity requiring a Euclidean time with periodicity  $\beta_S = 4\pi r_b$ , and therefore we can define the temperature as

$$T_S = \frac{1}{\beta_S} = \frac{1}{4\pi r_b}. \quad (7.72)$$

The action is easily evaluated, taking into account that the bulk of the action vanishes, and only the terms proportional to the Riemann tensor in (7.71) survive, and is

$$\mathcal{I}_S = 64\pi^2 (\alpha - \chi). \quad (7.73)$$

In contrast with General Relativity then the thermodynamical energy of the solution is

$$\langle E_S \rangle = \frac{\partial \mathcal{I}_S}{\partial \beta_S} = 0, \quad (7.74)$$

and the entropy is

$$S_S = \beta_S \frac{\partial \mathcal{I}_S}{\partial \beta_S} - \mathcal{I}_S = 64\pi^2 (\chi - \alpha). \quad (7.75)$$

These values are actually very sensible, as scale invariance forces the total energy to zero, and the value of the entropy is precisely the topological contribution of the Gauss-Bonnet term that would also survive in the Wald definition of entropy in the case of the vanishing horizon of a Schwarzschild black hole (and that we removed imposing  $\chi = \alpha$ ).

**de Sitter solution.** In this case there is no boundary term, considering that the de-Sitter solution is a compact manifold and the bulk term gives the Euclidean action completely. In principle is possible to have an ambiguity in the sign of the periodicity, given that the surface gravity (5.1) can, in principle, be negative. However, the Euclidean action of de-Sitter spacetime is proportional to the surface of a four-dimensional sphere with radius  $r_c = \sqrt{\frac{3}{\Lambda}}$ , being defined by  $x_0^2 + x_1^2 + x_2^2 + x_3^2 = r_c^2$ , that is

$$\begin{aligned} \mathcal{I}_{dS} &= - \left( \beta + \frac{\chi}{6} + \epsilon \frac{\xi^2}{\lambda} \right) R^2 \int_{dS} d^4x \sqrt{-g} = - \left( \beta + \frac{\chi}{6} + \epsilon \frac{\xi^2}{\lambda} \right) (4\Lambda)^2 S_4 \left( \sqrt{\frac{3}{\Lambda}} \right) = \\ &= - 384\pi^2 \left( \beta + \frac{\chi}{6} + \epsilon \frac{\xi^2}{\lambda} \right), \end{aligned} \quad (7.76)$$

where  $\epsilon$  is a parameter that can be either 0 or 1 if the expectation value of the scalar field is zero or different from zero. The correct periodicity is then strictly positive  $\beta_{dS} = 2\pi\sqrt{3}/\sqrt{\Lambda}$ , as so it is the temperature

$$T_{dS} = \frac{1}{\beta_{dS}} = \frac{1}{2\pi} \sqrt{\frac{\Lambda}{3}}. \quad (7.77)$$

For later convenience, let us write the Euclidean action as

$$\mathcal{I}_{dS} = -384\pi^2 \left( \beta + \frac{\alpha}{6} + \epsilon \frac{\xi^2}{\lambda} \right) + 64\pi^2 (\alpha - \chi), \quad (7.78)$$

and then the energy as

$$\langle E_{dS} \rangle = \frac{\partial \mathcal{I}_{dS}}{\partial \beta_{dS}} = 0, \quad (7.79)$$

and the entropy as

$$S_{dS} = \beta_{dS} \frac{\partial \mathcal{I}_{dS}}{\partial \beta_{dS}} - \mathcal{I}_{dS} = 384\pi^2 \left( \beta + \frac{\alpha}{6} + \epsilon \frac{\xi^2}{\lambda} \right) + 64\pi^2 (\chi - \alpha). \quad (7.80)$$

As in the Schwarzschild case, scale invariance forces the total energy to be zero, leading to a constant entropy in which the topological contribution of the Gauss-Bonnet term is manifest.

**Schwarzschild-anti-de Sitter solution.** In this case we still have a single horizon, and then a single conical singularity at  $r = r_b$  which can be removed with a periodicity of the Euclidean time  $\beta_{Sads} = 4\pi r_b / (1 + |\Lambda| r_b^2)$ , where  $\Lambda$  is a negative cosmological constant such that  $\Lambda = R/4$ , which defines a temperature for the Schwarzschild-anti-de Sitter

$$T_{Sads} = \frac{1}{\beta_{Sads}} = \frac{1 + |\Lambda| r_b^2}{4\pi r_b}. \quad (7.81)$$

To define a finite Euclidean action is necessary in this case to remove a background anti-de Sitter solution with  $M = 0$  as in the case of General Relativity [97]. The boundary term is then removed by the background, and the remaining finite part of the bulk of the action is

$$\mathcal{I}_{Sads} = -\frac{128}{3}\pi^2 \left( \beta + \frac{\alpha}{6} \right) \frac{|\Lambda| r_b^2 (3 - |\Lambda| r_b^2)}{1 + |\Lambda| r_b^2} + 64\pi^2 (\alpha - \chi). \quad (7.82)$$

Having a non-constant Euclidean action, the total energy is

$$\langle E_{Sads} \rangle = \frac{\partial \mathcal{I}_{Sads}}{\partial \beta_{Sads}} = -128\pi \left( \beta + \frac{\alpha}{6} \right) |\Lambda| M, \quad (7.83)$$

where we removed the explicit dependence from  $r_b$  reintroducing the parameter  $M$ , and we considered  $\Lambda$  as fixed, being the same as the background anti-de Sitter metric. Finally, entropy is

$$S_{Sads} = \beta_{Sads} \frac{\partial \mathcal{I}_{Sads}}{\partial \beta_{Sads}} - \mathcal{I}_{Sads} = -128\pi^2 \left( \beta + \frac{\alpha}{6} \right) |\Lambda| r_b^2 + 64\pi^2 (\chi - \alpha), \quad (7.84)$$

which has a term proportional to the area of the black hole plus the usual topological one. We note that if we remove the topological term by setting  $\chi = \alpha$ , and we rename the parameters as

$$-128\pi \left( \beta + \frac{\alpha}{6} \right) |\Lambda| = 128\pi \left( \beta + \frac{\alpha}{6} \right) \Lambda \rightarrow \frac{1}{G}, \quad (7.85)$$

we recover exactly the same result of General Relativity.

**Schwarzschild-de Sitter solution.** While the Schwarzschild, de Sitter and Schwarzschild-anti-de Sitter cases can be evaluated with the same techniques of General Relativity, the Schwarzschild-de Sitter case requires some care due to the presence of two conical singularities which cannot be simultaneously removed with a suitable period of the Euclidean time. In [99] the Euclidean action for a Schwarzschild-de Sitter black hole in General Relativity has been calculated as

$$\mathcal{I}_{Sds, GR} = -\frac{A_b}{4G} - \frac{A_c}{4G} = -8\pi^2 M_p^2 (r_b^2 + r_c^2), \quad (7.86)$$

where  $M_p$  is the reduced Planck mass, using the explicit expression for the conical singularities found in [100] in terms of Dirac delta functions. In the same paper [100] it is shown

that it is not possible to define quadratic curvature invariants with the same techniques, having to regularize a squared delta function. However, having no physical singularities in the Euclidean sector, it is sensible to expect a finite value of the Euclidean action also in the scale-invariant case. Moreover, in the calculation of the Euclidean action in [99] it is shown that the action does not depend on the periodicity of the Euclidean time, which acts as a tool to derive the action in the standard way and acquires physical meaning only through the thermodynamical interpretation. To evaluate the action we then exploited this fact to have more freedom in the bounds of integration of the Euclidean action. In particular, we considered three manifolds: a Schwarzschild-de Sitter from which we removed by hand the cosmological horizon, a Schwarzschild-de Sitter from which we removed the black hole horizon, and a Schwarzschild-de Sitter from which we removed both horizons. We then assumed that the Euclidean action of Schwarzschild-de Sitter is the sum of the ones of the first two manifolds minus the action of the third

$$\mathcal{I}_{SdS} = \mathcal{I}_{SdS \setminus \{c\}} + \mathcal{I}_{SdS \setminus \{b\}} - \mathcal{I}_{SdS \setminus \{c,b\}}. \quad (7.87)$$

We start from the third manifold, where for now we consider the bulk and the two boundary terms separately as

$$\begin{aligned} \mathcal{I}_{SdS \setminus \{c,b\}}^{bulk} &= -4\pi\beta_p \int_{r_b}^{r_c} dr r^2 \left( \xi\phi^2 R + \beta R^2 - \alpha C^{\mu\nu\rho\sigma} C_{\mu\nu\rho\sigma} + \chi\mathcal{G} - \frac{1}{2}\partial^\mu\phi\partial_\mu\phi - \frac{\lambda}{4}\phi^4 \right) = \\ &= -4\pi\beta_p \left( 16\Lambda \left( \beta + \frac{\chi}{6} + \epsilon\frac{\xi^2}{\lambda} \right) \frac{\Lambda}{3} (r_c^3 - r_b^3) + 16M(\alpha - \chi) \left( \frac{M}{r_c^3} - \frac{M}{r_b^3} \right) \right), \end{aligned} \quad (7.88)$$

where  $\beta_p$  is a generic periodicity of the Euclidean time, and

$$\begin{aligned} \mathcal{I}_{SdS \setminus \{c,b\}}^{b-boundary} &= -8\pi\beta_p \sqrt{g_{tt}} \left( -4\chi(R^{\mu\nu}K_{\mu\nu} + R^{\mu\nu}n_\mu n_\nu K - 2R^{\mu\nu}n_\mu n^\rho K_{\rho\nu}) + \right. \\ &\quad \left. + (\chi R^{\mu\nu\rho\sigma} - \alpha C^{\mu\nu\rho\sigma})(n_\mu n_\rho K_{\nu\sigma} - n_\mu n_\sigma K_{\nu\rho} + n_\nu n_\sigma K_{\mu\rho} - n_\nu n_\rho K_{\mu\sigma}) + \right. \\ &\quad \left. + (\xi\phi^2 + 2(\beta + \chi)R)K \right) \Big|_{r=r_b} = \\ &= 4\pi\beta_p \left( 16\Lambda \left( \beta + \frac{\chi}{6} + \epsilon\frac{\xi^2}{\lambda} \right) (2r_b - 3M - \Lambda r_b^3) + 16M(\alpha - \chi) \frac{r_b - 3M}{r_b^3} \right), \end{aligned} \quad (7.89)$$

$$\begin{aligned} \mathcal{I}_{SdS \setminus \{c,b\}}^{c-boundary} &= -8\pi\beta_p \sqrt{g_{tt}} \left( -4\chi(R^{\mu\nu}K_{\mu\nu} + R^{\mu\nu}n_\mu n_\nu K - 2R^{\mu\nu}n_\mu n^\rho K_{\rho\nu}) + \right. \\ &\quad \left. + (\chi R^{\mu\nu\rho\sigma} - \alpha C^{\mu\nu\rho\sigma})(n_\mu n_\rho K_{\nu\sigma} - n_\mu n_\sigma K_{\nu\rho} + n_\nu n_\sigma K_{\mu\rho} - n_\nu n_\rho K_{\mu\sigma}) + \right. \end{aligned}$$

$$\begin{aligned}
& + (\xi\phi^2 + 2(\beta + \chi)R) K \Bigg) \Bigg|_{r=r_c} = \\
& = -4\pi\beta_p \left( 16\Lambda \left( \beta + \frac{\chi}{6} + \epsilon \frac{\xi^2}{\lambda} \right) (2r_c - 3M - \Lambda r_c^3) + 16M(\alpha - \chi) \frac{r_c - 3M}{r_c^3} \right); \tag{7.90}
\end{aligned}$$

the different signs in the two boundary terms are due to the opposite direction of the normal to the boundary, which is considered to be always outgoing. Finally, the sum of the three terms (7.88), (7.89) and (7.90) is

$$\begin{aligned}
\mathcal{I}_{SdS \setminus \{c,b\}} = & -4\pi\beta_p \left( 32\Lambda \left( \beta + \frac{\chi}{6} + \epsilon \frac{\xi^2}{\lambda} \right) \left( r_c - \frac{\Lambda}{3}r_c^3 - \left( r_b - \frac{\Lambda}{3}r_b^3 \right) \right) + \right. \\
& \left. + 16M(\alpha - \chi) \left( \frac{r_c - 2M}{r_c^3} - \frac{r_b - 2M}{r_b^3} \right) \right) = 0 \tag{7.91}
\end{aligned}$$

where the last equivalence is given by the definitions of the horizons. Thanks to the equivalence in (7.91), and the fact that the spatial part of the bulk action is independent of whether we are removing the boundary or not, we can express the action for the other two spacetimes as

$$\begin{aligned}
\mathcal{I}_{SdS \setminus \{c\}} = & \frac{\beta_b}{\beta_p} \left( \mathcal{I}_{SdS \setminus \{c,b\}}^{bulk} + \mathcal{I}_{SdS \setminus \{c,b\}}^{c-boundary} \right) = -\frac{\beta_b}{\beta_p} \mathcal{I}_{SdS \setminus \{c,b\}}^{b-boundary} = \\
& = -\frac{24\pi^2 r_b^2}{3M - \Lambda r_b^3} \left( 16\Lambda \left( \beta + \frac{\chi}{6} + \epsilon \frac{\xi^2}{\lambda} \right) (2r_b - 3M - \Lambda r_b^3) + 16M(\alpha - \chi) \frac{r_b - 3M}{r_b^3} \right), \\
\mathcal{I}_{SdS \setminus \{b\}} = & \frac{\beta_c}{\beta_p} \left( \mathcal{I}_{SdS \setminus \{c,b\}}^{bulk} + \mathcal{I}_{SdS \setminus \{c,b\}}^{b-boundary} \right) = -\frac{\beta_c}{\beta_p} \mathcal{I}_{SdS \setminus \{c,b\}}^{c-boundary} = \\
& = -\frac{24\pi^2 r_c^2}{3M - \Lambda r_c^3} \left( 16\Lambda \left( \beta + \frac{\chi}{6} + \epsilon \frac{\xi^2}{\lambda} \right) (2r_c - 3M - \Lambda r_c^3) + 16M(\alpha - \chi) \frac{r_c - 3M}{r_c^3} \right), \tag{7.92}
\end{aligned}$$

where  $\beta_b$  and  $\beta_c$  are the periodicities required to remove the black hole and cosmological horizon conical singularities, respectively, and are imposed to be both positive in order to be consistent with the calculations used for the Schwarzschild and pure de Sitter cases. Finally, with some simplifications, the two terms take the form

$$\begin{aligned}
\mathcal{I}_{SdS \setminus \{c\}} = & -128\pi^2 \left( \beta + \frac{\alpha}{6} + \epsilon \frac{\xi^2}{\lambda} \right) \Lambda r_b^2 + 64\pi^2(\alpha - \chi), \\
\mathcal{I}_{SdS \setminus \{b\}} = & -128\pi^2 \left( \beta + \frac{\alpha}{6} + \epsilon \frac{\xi^2}{\lambda} \right) \Lambda r_c^2 + 64\pi^2(\alpha - \chi). \tag{7.93}
\end{aligned}$$

The sum (7.87) then has trivially the result

$$\mathcal{I}_{SdS} = -128\pi^2 \left( \beta + \frac{\alpha}{6} + \epsilon \frac{\xi^2}{\lambda} \right) \Lambda (r_b^2 + r_c^2) + 128\pi^2(\alpha - \chi). \tag{7.94}$$

We note that, when applied to the context of General Relativity, our procedure has the same result of [99]. While it might seem a crude calculation, this result indicates that the Euclidean action of Schwarzschild-de Sitter is given entirely by the conical singularities, exactly as shown for General Relativity in [99]. The main difference here is that the singularity is integrated away while defining the action and not during the volume integration, opening the possibility of using the same technique for all the actions for which the boundary terms are known.

Finally, we note that for Schwarzschild, de Sitter and Schwarzschild-(anti-)de Sitter space-times the Euclidean scale-invariant action  $\mathcal{I}_{SI}$  can be derived directly from the action of General Relativity using the relation

$$\mathcal{I}_{SI} = 16 \left( \beta + \frac{\alpha}{6} + \epsilon \frac{\xi^2}{\lambda} \right) \frac{\Lambda}{M_p^2} \mathcal{I}_{GR} + 64\pi^2 (\alpha - \chi) N_H. \quad (7.95)$$

where  $N_H$  is the number of horizons and  $\mathcal{I}_{GR}$  is the Euclidean action of General Relativity, and we recall that  $M_p$  is the reduced Planck mass,  $\epsilon = 0, 1$  respectively in the  $\phi = 0$  and  $\phi \neq 0$  cases and  $\Lambda = 0$  for Schwarzschild and  $\Lambda = -|\Lambda|$  for Schwarzschild-anti-de Sitter. In particular, with the choice of parameters  $\chi = \alpha$  and

$$128\pi \left( \beta + \frac{\alpha}{6} + \epsilon \frac{\xi^2}{\lambda} \right) \Lambda \rightarrow \frac{1}{G} \quad (7.96)$$

it is possible to recover also the thermodynamical properties in the Schwarzschild and Schwarzschild-anti-de Sitter cases, in which the cosmological constant is truly considered as a constant parameter and does not appear in the variations (as it happens for the de Sitter spacetime).

### 7.3.1 Non-linear stability and transitions of Schwarzschild-de Sitter solutions

We now move to the analysis of the non-linear stability of the two Schwarzschild-de Sitter solutions present in the theory. To better compare the dynamical perturbation discussion, we will analyze the Euclidean version of the simplified action (2.56), where the Euclidean action can be trivially found from the ones of the previous discussion setting  $\alpha = \chi = 0$ . In the case of Schwarzschild-de Sitter, in particular, the action has the form

$$\mathcal{I}_{SdS} = -128\pi^2 \left( \beta + \epsilon \frac{\xi^2}{\lambda} \right) \Lambda (r_b^2 + r_c^2). \quad (7.97)$$

To understand whether an unstable Schwarzschild-de Sitter black hole undergoes a transition into a stable one, we have to understand the most convenient parameters to compare the two solutions. While in principle the Euclidean action of a Schwarzschild-de Sitter black hole is characterized by two parameters, that is, its mass and cosmological constant,

the scale-invariant nature of the theory removes one degree of freedom by making everything dependent only from a dimensionless combination of the two parameters. With the definitions for the black hole and cosmological horizons (5.44), the expression (7.97) becomes

$$\mathcal{I}_{SdS} = -256\pi^2 \left( \beta + \epsilon \frac{\xi^2}{\lambda} \right) \left( 2 - \cos \left( \frac{2\eta}{3} \right) \right), \quad (7.98)$$

where  $\cos \eta = 3M\sqrt{\Lambda}$ , and therefore the difference in the actions with zero and non-zero scalar field is

$$\Delta\mathcal{I}_{SdS} = \mathcal{I}_{SdS,u} - \mathcal{I}_{SdS,s} = 256\pi^2 \left( \frac{\xi^2}{\lambda} \left( 2 - \cos \left( \frac{2\eta_s}{3} \right) \right) + \beta \left( \cos \left( \frac{2\eta_u}{3} \right) - \cos \left( \frac{2\eta_s}{3} \right) \right) \right), \quad (7.99)$$

with  $\cos \eta_u = 3M_u\sqrt{\Lambda_u}$  and  $\cos \eta_s = 3M_s\sqrt{\Lambda_s}$ . The two parameters  $\Lambda_u$  and  $\Lambda_s$ , however, are not independent one from the other. If we consider the black holes as immersed in a large, evolving universe, it is sensible to expect that the value of the effective cosmological constant will be given by the global cosmological evolution, and will not be affected by the presence of the black holes. The relation (5.51) will then link the two parameters, and the two Schwarzschild-de Sitter black holes can be compared using relations between  $\eta_u$  and  $\eta_s$  which will depend only on the free parameters of the theory. We will consider four different relations and show that they all agree on the result.

**Black holes with the same geometry.** In this case we require that the parameters  $M$  and  $\Lambda$  evolve in such a way that the two horizon radii are kept fixed, and then the geometry of the spacetime does not change from one solution to the other. The relation between  $\eta_u$  and  $\eta_s$  is clearly

$$\eta_u = \eta_s = \eta. \quad (7.100)$$

In this case, the difference of the action (7.99) is always positive because only the term multiplied by  $\xi^2/\lambda$ , which is always positive, survives

$$\Delta\mathcal{I}_{SdS} = \mathcal{I}_{SdS,u} - \mathcal{I}_{SdS,s} = 256\pi^2 \frac{\xi^2}{\lambda} \left( 2 - \cos \left( \frac{2\eta}{3} \right) \right) > 0. \quad (7.101)$$

**Black holes with the same mass parameter.** In this case we require the mass parameter  $M$  to be fixed, and then only the cosmological constant  $\Lambda$  changes between one solution and the other. The relation between  $\eta_u$  and  $\eta_s$  is

$$\eta_u = \arccos \left( \sqrt{1 + \frac{\xi(1 + 12\xi)}{12\beta\lambda}} \cos \eta_s \right). \quad (7.102)$$

In this case the positiveness of the difference is assessed simply by requiring  $\beta, \xi, \lambda > 0$  which, however, is a sensible requirement in order to have the terms in the action having

a standard signature. While now in the difference of the actions (7.99) is present also the term multiplied by  $\beta$ , the relation (7.102) guarantees that  $\eta_u < \eta_s$  for  $\sqrt{1 + \xi(1 + 12\xi)/12\beta\lambda} > 1$ , and then that

$$\cos\left(\frac{2\eta_u}{3}\right) > \cos\left(\frac{2\eta_s}{3}\right) \quad \text{for } \eta_u < \eta_s. \quad (7.103)$$

The difference (7.99) is then the sum of two non-negative terms and is always positive.

**Black holes with the same cosmological horizon temperature.** In this case, we allow parameters  $M$  and  $\Lambda$  to change from one solution to the other, but we require that the physical properties at the cosmological horizon remain unchanged. In particular we require the local gravitational force, and then the temperature, to stay fixed, enforcing the relation between  $\eta_u$  and  $\eta_s$

$$\begin{aligned} \eta_u = & \pi - 3 \arccos \left( \left( 1 + \frac{\xi(1 + 12\xi)}{12\beta\lambda} \right)^{-\frac{1}{2}} \frac{1}{8 \cos\left(\frac{\pi - \eta_s}{3}\right)} \left( 4 \cos^2\left(\frac{\pi - \eta_s}{3}\right) - 1 \right. \right. \\ & \left. \left. + \sqrt{\left( 4 \cos^2\left(\frac{\pi - \eta_s}{3}\right) - 1 \right)^2 + 16 \left( 1 + \frac{\xi(1 + 12\xi)}{12\beta\lambda} \right) \cos^2\left(\frac{\pi - \eta_s}{3}\right)} \right) \right). \end{aligned} \quad (7.104)$$

In [35] there was an error in the derivation of this relation; nonetheless the consequences are the same, still having  $\eta_u < \eta_s$  for  $\sqrt{1 + \xi(1 + 12\xi)/12\beta\lambda} > 1$ , and then that

$$\cos\left(\frac{2\eta_u}{3}\right) > \cos\left(\frac{2\eta_s}{3}\right) \quad \text{for } \eta_u < \eta_s. \quad (7.105)$$

Being (7.99) the sum of two non-negative terms is always positive.

**Black holes with the same black hole horizon temperature.** Similarly to the previous case we allow both parameters  $M$  and  $\Lambda$  to change from one solution to the other, but now we require that the physical properties at the black hole horizon remain unchanged. We make this statement formal by requiring that the temperature at the black hole horizon stays fixed, but we note that this also means that the classical absorption cross section [101] is left unchanged. As the previous case there was an error in [35], and the variables  $\eta_u$  and  $\eta_s$  are now linked by

$$\begin{aligned} \eta_u = & 3 \arccos \left( \left( 1 + \frac{\xi(1 + 12\xi)}{12\beta\lambda} \right)^{-\frac{1}{2}} \frac{1}{8 \cos\left(\frac{\pi + \eta_s}{3}\right)} \left( 4 \cos^2\left(\frac{\pi + \eta_s}{3}\right) - 1 \right. \right. \\ & \left. \left. + \sqrt{\left( 4 \cos^2\left(\frac{\pi + \eta_s}{3}\right) - 1 \right)^2 + 16 \left( 1 + \frac{\xi(1 + 12\xi)}{12\beta\lambda} \right) \cos^2\left(\frac{\pi + \eta_s}{3}\right)} \right) \right) - \pi. \end{aligned} \quad (7.106)$$

It is not necessary to analyze numerically the positivity of (7.99) because from this relation is still valid that  $\eta_u < \eta_s$  for  $\sqrt{1 + \xi(1 + 12\xi)/12\beta\lambda} > 1$ , and then that

$$\cos\left(\frac{2\eta_u}{3}\right) > \cos\left(\frac{2\eta_s}{3}\right) \quad \text{for } \eta_u < \eta_s. \quad (7.107)$$

The results shown in [35] are then incorrect from a quantitative point of view but are correct from the more important qualitative point of view, that is in showing that also in the case of black holes with the same temperature at the black hole horizon, the difference in the actions is always positive.

Finally, we can state that in all the cases under consideration

$$\mathcal{I}_{SdS,u} > \mathcal{I}_{SdS,s} \quad \text{for every } M, \Lambda_u \text{ s.t. } 3M\sqrt{\Lambda_u} < 1, \quad (7.108)$$

where the constraint on the parameters is given by  $M < \frac{1}{3} \min\left(\frac{1}{\sqrt{\Lambda_u}}, \frac{1}{\sqrt{\Lambda_s}}\right) = \frac{1}{3\sqrt{\Lambda_u}}$ . Such relation guarantees that any Schwarzschild-de Sitter black hole prefers to be immersed in a de Sitter space with a smaller cosmological constant and, in our specific case, confirms that a Schwarzschild-de Sitter black hole will have a transition from a solution with zero scalar field to a solution with a non-zero scalar field.

Having clarified that the unstable Schwarzschild-de Sitter will have a transition into the stable one, what is left to understand is if the presence of a black hole immersed in the cosmological setting described in (5.5.1) can stabilize the unstable de Sitter space, or aggravates its instability. Taking into account the difference in the Euclidean actions of the two de Sitter spacetimes

$$\Delta\mathcal{I}_{dS} = \mathcal{I}_{dS,u} - \mathcal{I}_{dS,s} = 384\pi^2 \frac{\xi^2}{\lambda}, \quad (7.109)$$

the quantity that we want to analyze now is

$$\Delta\mathcal{I}_{dS} - \Delta\mathcal{I}_{SdS} = 256\pi^2 \left( \frac{\xi^2}{\lambda} \left( \cos\left(\frac{2\eta_s}{3}\right) - \frac{1}{2} \right) - \beta \left( \cos\left(\frac{2\eta_u}{3}\right) - \cos\left(\frac{2\eta_s}{3}\right) \right) \right), \quad (7.110)$$

which quantifies the increase or decrease of tunneling probability. It is clear that, when comparing black holes by their radius, the difference (7.99) is always smaller than (7.109), being

$$\Delta\mathcal{I}_{dS} - \Delta\mathcal{I}_{SdS} = 256\pi^2 \frac{\xi^2}{\lambda} \left( \cos\left(\frac{2\eta_s}{3}\right) - \frac{1}{2} \right), \quad (7.111)$$

which is always positive. The tunneling probability (7.70) will then always be smaller if a black hole is present, and the unstable de Sitter configuration will have a longer life expectancy. The situation is the same for black holes with the same mass parameter or

temperature at the black hole horizon; while an analytical statement cannot be made, considering that (7.110) is the sum of an always positive term and an always negative one, we can assess the positivity of (7.110) numerically. In Figure 56 we show the behavior of (7.110) for black holes with the same mass parameter or temperature at the black hole horizon, varying the parameter  $\beta\lambda$  or  $\xi$  independently; in both cases, the tunneling probability is reduced by the presence of a black hole, as (7.110) is positive in all the cases considered. The difference clearly goes to zero in the case of  $\eta_s \rightarrow \pi/2$ , which corresponds to the case of vanishing  $M$ , and then it is the de-Sitter limit.

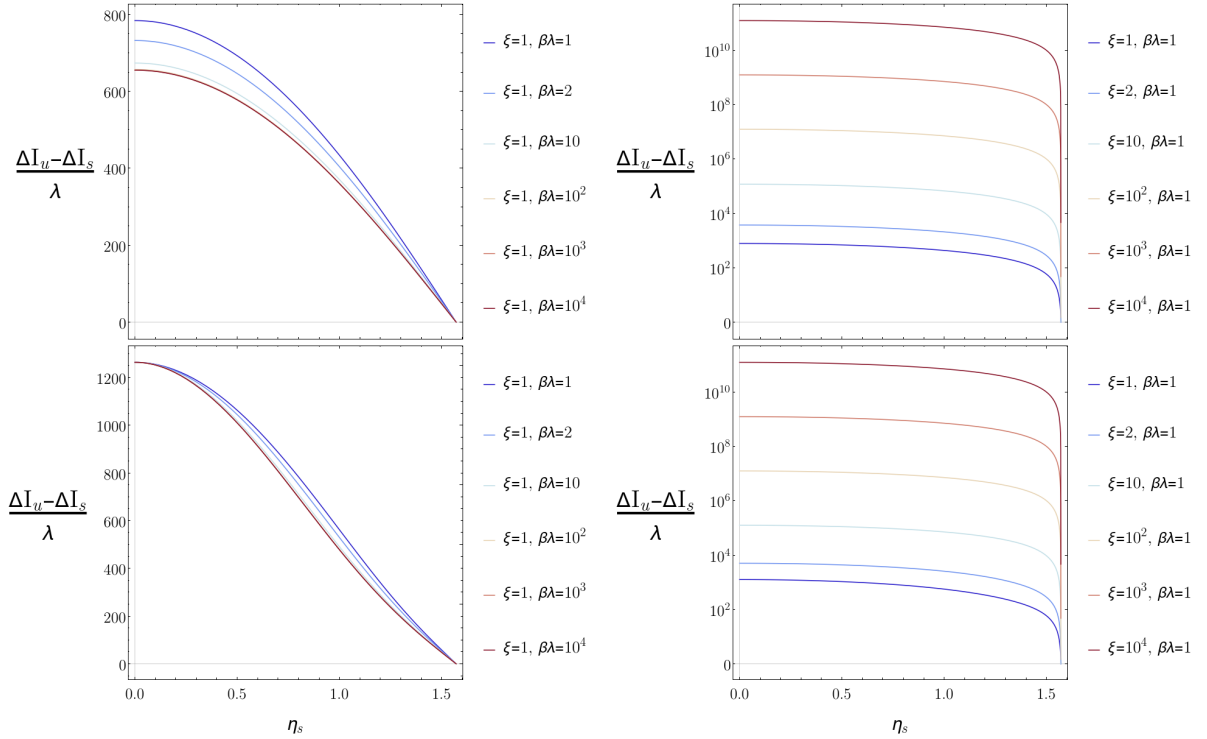


Figure 56: Decrease of the tunneling probability between two Schwarzschild-de Sitter and two de Sitter spacetimes for black holes with the same mass parameter, in the panels on top, or the same temperature at the black hole horizon, in the panels in the bottom, varying separately  $\beta\lambda$ , in the panels on the left, and  $\xi$  in the panels on the right.

Comparing black holes by their temperature at the cosmological horizon renders the discussion more complicated: as we show in Figure 57, the presence of a large black hole will always stabilize the de Sitter solution, while the presence of a small one will always increase its instability. This is because the maximum value of (7.110) is reached in the Nariai limit, in which

$$\Delta\mathcal{I}_{dS} - \Delta\mathcal{I}_{SdS} \rightarrow 128\pi^2 \frac{\xi^2}{\lambda} > 0, \quad \text{for } \eta_s \rightarrow 0, \quad (7.112)$$

while the minimum is reached for a vanishing mass parameter  $M$ , that is the de Sitter

limit, where

$$\Delta\mathcal{I}_{ds} - \Delta\mathcal{I}_{Sds} \rightarrow 128\pi^2 \frac{\xi^2}{\lambda} \left( 1 - 2 \cos \left( \frac{2}{3} \left( \pi - 3 \arccos \left( \frac{2 + \sqrt{16 + \frac{\xi(1+12\xi)}{\beta\lambda}}}{2\sqrt{12 + \frac{\xi(1+12\xi)}{\beta\lambda}}} \right) \right) \right) \right)$$

for  $\eta_s \rightarrow \frac{\pi}{2}$ ,

(7.113)

which is always negative for  $\beta$ ,  $\xi$  and  $\lambda$  larger than zero. This is because the de Sitter limit has to be taken with care in this case because it represents two de Sitter spacetime with different cosmological constants, but with the same properties at the cosmological horizon.

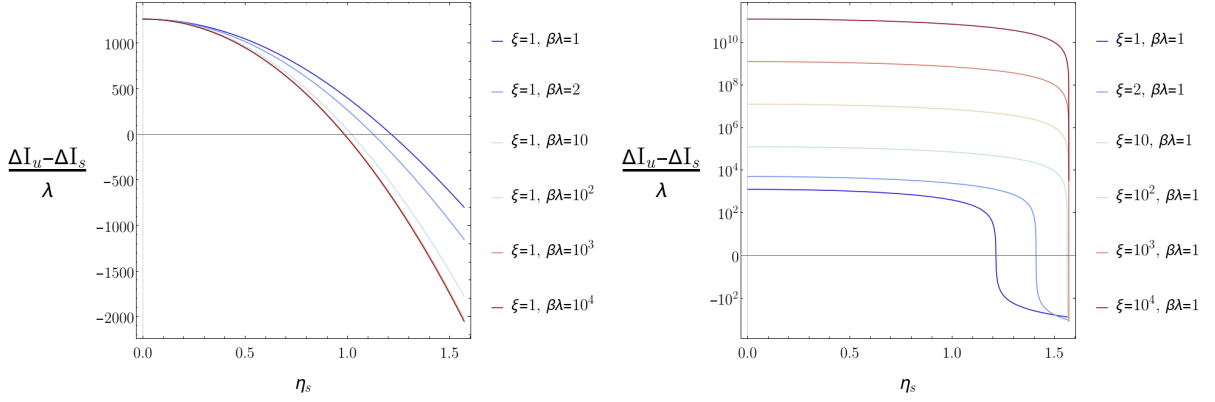


Figure 57: Change of the tunneling probability between two Schwarzschild-de Sitter and two de Sitter spacetimes for black holes with the temperature at the cosmological horizon, varying separately  $\beta\lambda$ , in the panels on the left, and  $\xi$  in the panels on the right.

From Figure 57 it is also clear that the minimum mass to increase the stability of the de Sitter tunneling decreases as the ratio  $\xi^2/\beta\lambda$  decreases. Considering the most recent results obtained in the cosmological setting [28], we expect  $\beta\lambda$  to be much smaller than  $\xi^2$ , and then only microscopical black hole will increase the tunneling probability of the de Sitter spacetimes. We note that all the discussion made in this subsection is still valid in the full scale-invariant case: the constant term  $128\pi^2(\alpha - \chi)$  is indeed equal in both solutions, and the only difference left can be reabsorbed with a redefinition  $\beta \rightarrow \beta + \frac{\alpha}{6}$ .

## 8 Phenomenological signatures of quadratic gravity

The quantum motivation of the inclusion of quadratic terms suggests that the actual variations from General Relativity should be relevant only at extremely small scales, and the results of the previous sections, in particular the one made in the case of compact stars in Subsection 5.4, confirm this suggestion. Most of the work of this thesis is then relevant mainly at the theoretical level, specifically in understanding how much physical sense can have quadratic gravity. Nonetheless, we would like to conclude this thesis by giving a flavor of the possible phenomenological impact of quadratic terms in astrophysical solutions. While with sensible parameters the predicted values of the variations from General Relativity are below any possible desirable sensibility of present experiments, we still believe that it remains interesting to study the possible phenomenological effects of quadratic gravity as a way of imagining test of falsifiability of General Relativity, and maybe also some test of other modified theory of gravity with different origins.

This small section is divided in two parts:

- in the first subsection we present the shadows of astrophysical compact objects, that is, the topological surface over which lie all the innermost stable orbits of photons, for solutions of Einstein-Weyl gravity and Starobinski's model. We will see that not all the solutions will have a shadow, but it will be the case for all the solutions with a large mass; moreover, as we are accustomed by now, we see that an attractive contribution of the tensor mode or a repulsive contribution of the scalar mode lead to an increase in the shadow with respect to General Relativity, while an attractive contribution of the tensor mode or an attractive contribution of the scalar mode leads to a decrease in the shadow;
- in the second subsection we introduce a plethora of quasi-local mass definitions, that is, definitions of the amount of mass inside a sphere of given radius  $r$ ; these definitions will all be coincident in the case of General Relativity but will be different in quadratic gravity. It will be possible then to imagine experiments that, measuring only the gravitational mass of an object with different methods, are able to characterize the potential of the solutions and have an insight into the short-scale nature of the solution. In particular we will show that, as a matter of principle, it is possible to determine the equation of scale of a compact star only with mass measurements.

The results of the first subsection have not been published but are inspired by the ones in [102]; the results of the second subsection instead have been published separately in

[41, 52, 51], and in particular the discussion on the different mass definition is taken by [41].

## 8.1 Shadow of isolated objects

Close to a compact object, the gravitational force can be so strong that any free-falling particle cannot move away from the object. When the gravitational interaction is strong enough to force also free-falling light rays to converge into the object, it is possible to define the so-called photon sphere as the surface defined by the lightlike circular orbits. This is conceptually very different from an event horizon, as an object or a light ray can escape from the gravitational well by using some energy. Nonetheless, this surface will still absorb most of the light, and the object will project a shadow on the light emitted behind with a radius related to the one of this photon sphere. Picturing the shadow is then one of the most detailed and short-scaled measurements of compact objects' geometrical structure. Moreover, in the last years, it has been proven that such measurements are indeed possible [103, 104]. It is then one of the first astrophysical properties to be investigated while looking at modifications of General Relativity at short scales. First, to define the photon ring, let us consider the radial geodesic equation

$$\begin{aligned} \frac{d^2r}{d\tau^2} + \Gamma^r_{\mu\nu} \frac{dx^\mu}{d\tau} \frac{dx^\nu}{d\tau} = \\ = \frac{d^2r}{d\tau^2} + f(r) \left( \frac{1}{2} h'(r) \left( \frac{dt}{d\tau} \right)^2 - \frac{f'(r)}{2f(r)^2} \left( \frac{dr}{d\tau} \right)^2 - r \left( \frac{d\theta}{d\tau} \right)^2 - r \sin^2(\theta) \left( \frac{d\phi}{d\tau} \right)^2 \right) = 0; \end{aligned} \quad (8.1)$$

where  $\tau$  is either the proper time or an affine parameter, if we now specify to circular orbits setting  $\frac{d^2r}{d\tau^2} = \frac{dr}{d\tau} = 0$ , and we fix  $\theta = \pi/2$  without loss of generality, (8.1) becomes

$$\frac{1}{2} h'(r) \left( \frac{dt}{d\tau} \right)^2 - r \left( \frac{d\phi}{d\tau} \right)^2 = 0. \quad (8.2)$$

It is possible to find a similar relation from the line element (2.15) as

$$\epsilon = -h(r) \left( \frac{dt}{d\tau} \right)^2 + r^2 \left( \frac{d\phi}{d\tau} \right)^2, \quad (8.3)$$

where  $\epsilon = -1$  for timelike geodesics and  $\epsilon = 0$  for null geodesics. Given that the photon sphere is defined by circular null orbits, we can set  $\epsilon = 0$  and, putting together (8.2) and (8.3), we find

$$rh'(r) - 2h(r) = 0, \quad (8.4)$$

and the photon ring is defined by the largest root of (8.4). To define the shadow radius, we have to correct the photon ring radius  $r_{pr}$  by a redshift factor and, finally, we have

$$r_{sh} = \frac{r_{pr}}{\sqrt{h(r_{pr})}}, \quad \text{s.t.} \quad rh'(r) - 2h(r) \Big|_{r=r_{pr}} = 0. \quad (8.5)$$

In the case of General Relativity, the photon ring radius and the shadow radius are trivially found as  $r_{pr} = 3M$  and  $r_{sh} = 3\sqrt{3}M$ . At last, we present in Figure 58 the relative difference between the shadow of the object and the one predicted by General Relativity

$$\delta = \frac{r_{sh} - 3\sqrt{3}M}{3\sqrt{3}M} \quad (8.6)$$

in Einstein-Weyl gravity and Starobinski's model. The areas left in white are the ones populated by solutions which *do not have* any photon ring; there is indeed no guarantee that such property exists for all types of solutions. On the contrary, the region with barred red lines is populated by solutions with a shadow radius more than double the one predicted by General Relativity. This has been done for two reasons: the first one is to picture more clearly the differences between solutions with a negative and positive  $\delta$ , and the second is that these solutions are present only in the case of extremely small masses, which are not particularly interesting in this phenomenological context.

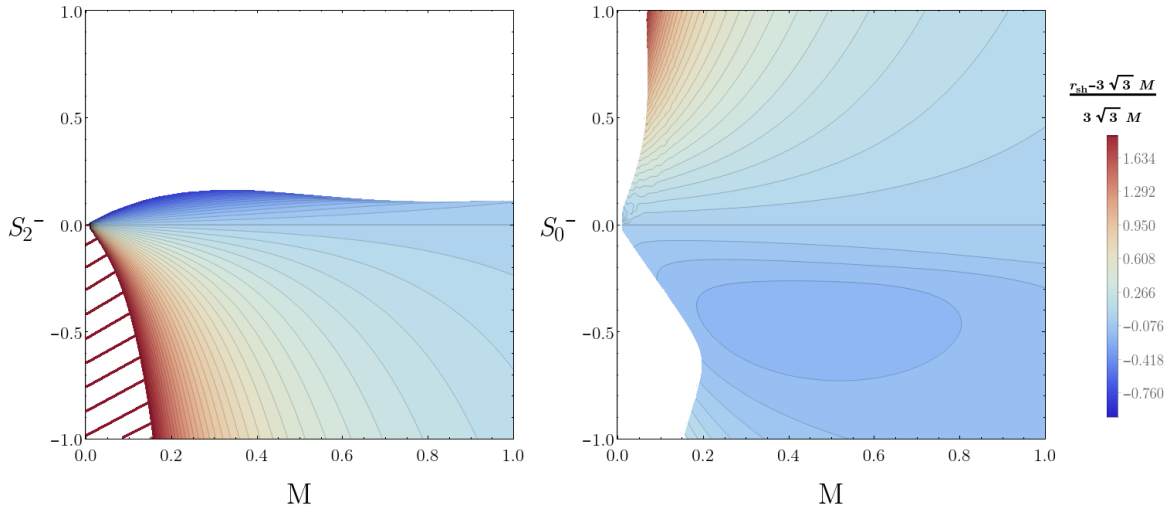


Figure 58: Relative variation between the shadow of the object and the one predicted by General Relativity  $r_{sh} = 3\sqrt{3}M$  in Einstein-Weyl gravity, in the left panel, and in Starobinski's model, in the right panel; the solutions in the white area do not have a shadow, and the ones in the barred red one have a shadow which is more than double the one of General Relativity.

In particular, it seems that all repulsive naked singularities do not have a shadow; however, it is not a surprise considering that they are characterized by a weakening in the gravitational attraction with respect to General Relativity, which actually becomes a gravitational repulsion close to the origin. We also note that an attractive contribution of the tensor Yukawa term leads to an increase in the shadow radius, and a repulsive contribution leads to a decrease, while an attractive contribution of the scalar Yukawa term leads to a decrease in the shadow radius, and a repulsive contribution leads to an increase. As usual, the tensor and scalar terms appear to have opposite effects on the solutions. In particular, this suggests that, in general, wormhole solutions will have a shadow larger

than the one predicted by General Relativity, and attractive naked singularities will have a smaller shadow. Taking into account the results of Subsection 6.2, we then expect as a prediction of quadratic gravity to have shadows that are slightly smaller than the ones predicted by General Relativity. Nonetheless, we also see from Figure 58 that the relative difference becomes less sensitive to the value of the Yukawa charges  $S_0^-$  and  $S_2^-$  as the mass of the solution increases, and then we expect very small variation with respect to the shadow predicted by the Einstein theory.

## 8.2 Mass definitions and mass discrepancies

The definition of energy posed a fundamental problem for General Relativity. Namely, while the energy of the fields populating a spacetime can be described by the stress-energy tensor, there is no concept of gravitational energy density, and the contribution of gravity to the total energy has been open to a large number of interpretations (see for example the discussion in section 11.2 of [105]). While a concept of total energy has been proposed, and it is widely accepted, by Arnowitt, Deser and Misner [44], and other definitions are possible in the case of spacetime with asymptotic timelike Killing vectors [45], the definition of the so-called quasi-local energy, that is the total energy inside a topologically 2-surface, is still a not completely solved puzzle. It is indeed possible to have many quasi-local energy definitions, considering that the requirement of being consistent with the global definitions at large distances is not very stringent. In particular, it is possible to define the quasi-local energy starting from a theoretical point of view [106, 107, 108] or from a phenomenological point of view [109]. In the particular case of quadratic gravity, while the total energy of a static solution is a well-defined concept, and it is proportional to the mass parameter  $M$  of the weak field limit (3.5) and independent from the values of the Yukawa charges  $S_2^-$  and  $S_0^-$ , it is sensible to expect discrepancies in the various possible quasi-local mass definitions. We will start by presenting various quasi-local energy definitions, which we will call quasi-local masses because we are dealing with static spacetimes, and they will always refer to the total energy inside a sphere of radius  $r$ .

**Misner-Sharp mass.** Given a spherically symmetric spacetime with metric

$$ds^2 = g_{ab}dx^a dx^b + r^2 d\Omega^2 \quad (8.7)$$

where  $g_{ab}$  is the induced metric in the effective 1+1 spacetime, the Misner-Sharp mass is defined as

$$r_{,a}r^{,a} = f(r) =: 1 - \frac{2M(x^c)}{r}. \quad (8.8)$$

so that

$$M_{M-S}(r) = \frac{1}{2}r(1 - f(r)) \quad (8.9)$$

in our case. It was originally proposed by Misner and Sharp in the context of spherically symmetric models of gravitational collapse [106] and it was used to represent the energy, or mass, enclosed in a spherical hypersurface at time  $t$ . It is one of the most used definitions in the context of compact stars in quadratic theories of gravity [110, 111, 112, 113, 114].

**Hayward mass.** Hayward [108] proposed a quasi-local mass definition starting from the idea of a 2+2 foliation of the spacetime. He defined a Hamiltonian 2-form, which in the spin-connection formalism can be written as

$$\frac{1}{2\gamma}\mathcal{H} = -dA \left( \mathcal{R} + \theta\tilde{\theta} - \frac{1}{2}\sigma_{ab}\sigma^{ab} - 2\omega_a\omega^a \right), \quad (8.10)$$

where  $dA$  is the 2-form associated with the area of a two-dimensional surface  $\partial\Sigma$ . The quasi-local energy is defined as the integral of this density over  $\partial\Sigma$  as

$$E = -2\gamma \int_{\partial\Sigma} dA \left( \mathcal{R} + \theta\tilde{\theta} - \frac{1}{2}\sigma_{ab}\sigma^{ab} - 2\omega_a\omega^a \right), \quad (8.11)$$

which, however, with our ansatz for the metric, reduces to the Misner-Sharp definition (8.9). This definition also has a theoretical motivation, and there is a solid reason why it has been widely used in extensions of General Relativity.

**Hawking mass.** With a similar idea as the one of Hayward, Hawking proposed a quasi-local mass definition starting from a 2+2 foliation of the spacetime [115]. However, its proposal is inspired by the Gibbons-Hawking-York boundary term and is based on the difference between the extrinsic curvature of a two-dimensional surface embedded in the spacetime and the same surface embedded in a background one. It takes the form

$$E = -2\gamma \int_{\partial\Sigma} dA N ({}^2K - {}^2K_0), \quad (8.12)$$

where  ${}^2K$  is the extrinsic curvature of the two-dimensional surface embedded in the spacetime,  ${}^2K_0$  is the extrinsic curvature of the surface embedded in the background and  $N$  is a lapse function taking into account time translations. When applied to our ansatz for the metric, and considering Minkowski as background, the Hawking mass definition becomes

$$M_{Haw}(r) = \frac{1}{2}r(1 - \sqrt{h(r)f(r)}). \quad (8.13)$$

Nonetheless, we found no previous analysis of solutions in quadratic theories of gravity which used such a definition, and we did not investigate its behavior in detail.

**Komar quasi-local mass.** At last, we present another theoretical mass definition that we believe is of great interest even if, to the best of our knowledge, it has not been considered in any study of solutions of quadratic gravity. In a static spacetime it is indeed always possible to define the mass in a natural way as the conserved quantity associated with the timelike Killing vector

$$M = -4\gamma \int_{\partial\Sigma} dA n_\mu \frac{\kappa^\nu \nabla_\nu \kappa^\mu}{\sqrt{-\kappa_\rho \kappa^\rho}}, \quad (8.14)$$

where  $\kappa^\mu$  is the timelike Killing vector,  $\partial\Sigma$  is a two dimensional surface and  $n^\mu$  is the unit normal to such surface [105]. In General Relativity it can be proved that, in the vacuum, the integral in (8.14) is independent of the choice of  $\partial\Sigma$ , and the definition is well cast; at the same time, in quadratic gravity, this is possible only in the asymptotically infinite region, where it becomes the Komar mass definition (3.8). We can however exploit the definition in (8.14) and consider it as the energy inside the surface  $\partial\Sigma$ ; as usual with our ansatz and units it becomes

$$M_{Kom}(r) = \frac{1}{2} r^2 \sqrt{\frac{f(r)}{h(r)}} h'(r). \quad (8.15)$$

**TOV mass.** In General Relativity, the total mass inside a spherical distribution of matter is most of the time obtained from the  $tt$ -component of the field equations that, with the Misner-Sharp mass definition and our conventions, reads

$$M'(r) = \frac{1}{4\gamma} r^2 \rho(r), \quad (8.16)$$

and which implies

$$M(r) = \int_0^r ds 4\pi s^2 \rho(s). \quad (8.17)$$

The integration extends to the surface  $r = R_*$  defined by  $\rho(R_*) = 0$  in the Tolman-Oppenheimer-Volkoff equations (TOV) for the relativistic stellar structure [116, 117], and reaches the limit value

$$M_{TOV} = \int_0^{R_*} ds 4\pi s^2 \rho(s). \quad (8.18)$$

As it is well known,  $M_{TOV}$  does not coincides with the proper mass inside the star, but fully describes the observational properties of a compact object (neutron star) in General Relativity. This definition is strongly dependent on the equation of motion of General Relativity; however, being sensible in the weak field regime (3.3), it has also been used in quadratic theories of gravity [118, 119].

**Particle potential mass.** To define the mass of a star in terms of observational properties, Resco et al. proposed a definition based on the effective potential of a massive particle [109]. With our ansatz the particle equation of motion reads

$$\frac{1}{2}m\dot{r}^2 + \frac{m f(r)L^2}{2r^2} + \frac{m}{2}(h(r) - 1)\frac{f(r)}{h(r)} = \frac{f(r)}{h(r)}(E - m). \quad (8.19)$$

Comparing the third term on the left hand side of (8.19) with the Newtonian (or General Relativistic) potential energy  $-\frac{mM}{r}$  we can define the mass as

$$M_{Pot}(r) = \frac{1}{2}r(1 - h(r))\frac{f(r)}{h(r)}. \quad (8.20)$$

**Newtonian limit mass.** In the usual non-relativistic limit of General Relativity the gravitational potential is expressed as

$$\phi(r) = \frac{1}{2}(h(r) - 1); \quad (8.21)$$

equating (8.21) to the Newtonian potential  $\phi(r) = -\frac{M}{r}$  we can define the Newtonian limit mass as

$$M_{New}(r) = \frac{1}{2}r(1 - h(r)). \quad (8.22)$$

The motivation behind this definition is conceptually very similar to the one of Resco et al. (8.20), and it could be derived from the particle equation of motion (8.19) imposing that the energy on the right-hand side is independent of the radial coordinate. This definition, however, is particularly useful, being dependent only from the time component of the metric and then associated with the redshift of a photon emitted at radius  $r$  and measured at infinity

$$z(r) = \frac{1 - \sqrt{h(r)}}{\sqrt{h(r)}}, \quad (8.23)$$

and therefore it has already been used in modified theories of gravity [68].

**Kepler's law mass.** Another measurable mass definition is the one that can be inferred from the orbital period using Kepler's Third Law. Assuming that in some limit the Newtonian regime is recovered, one can define the Keplerian mass from a measure of orbital period  $T$

$$\frac{r^3}{T^2} = \frac{M}{4\pi^2}. \quad (8.24)$$

The radial geodesic equation, in the case of a circular orbit on the equatorial plane, can be written as

$$\frac{1}{2}h'(r)\dot{t}^2 - r\dot{\phi}^2 = 0 \quad \Rightarrow \quad \left(\frac{d\phi}{dt}\right)^2 = \frac{1}{2}\frac{h'(r)}{r}, \quad (8.25)$$

and combined with (8.24) give rise to the definition

$$M_{Kep}(r) = \frac{1}{2}r^2h'(r). \quad (8.26)$$

In Figure 59 we collected these mass definitions for all the different types of vacuum solutions in Einstein-Weyl gravity. While there are some important differences between one definition and the other, some general properties can be inferred from these behaviors.

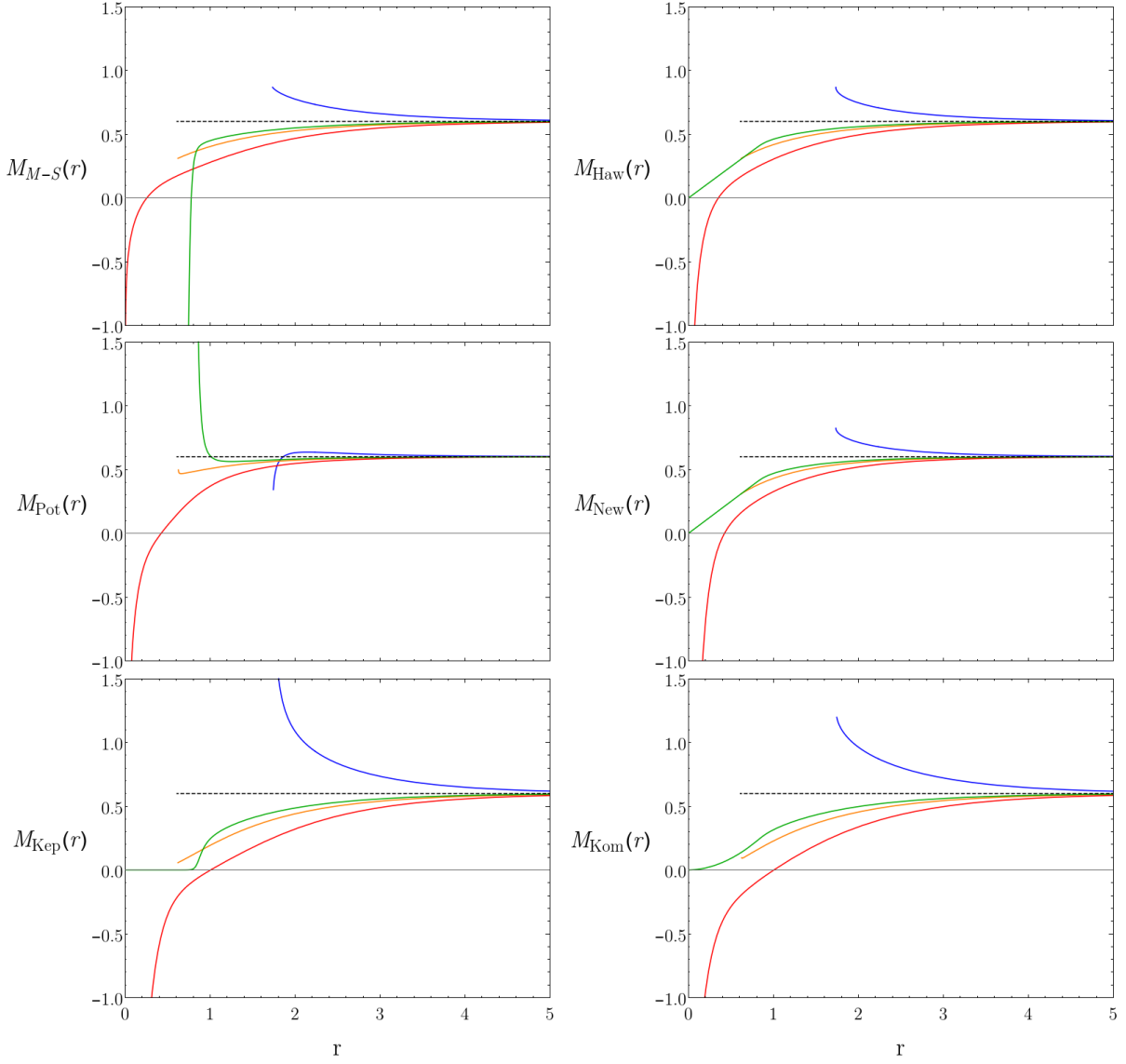


Figure 59: Quasi-local mass definitions for different solutions: in dashed black there is the Schwarzschild metric outside the horizon, in orange there is a non-Schwarzschild black hole outside the horizon, in blue there is a wormhole outside the throat, in green there is an attractive naked singularity and in red a repulsive naked singularity.

All the definitions agree that repulsive naked singularities have a large and negative mass in the origin. On the contrary, with the exception of the Misner-Sharp and the Resco et al. definitions, all the others agree that attractive naked singularities have a vanishing

mass in the origin. The Resco et al. definition is also the only definition for which it can be stated that wormholes have a mass that increases as we get closer to the origin, while all the other solutions have a mass that decreases. Nonetheless, this property is present at large distances for all the definitions considered, and it is the most important from a phenomenological point of view. To focus more on the astrophysical sense of these definitions, we show in Figure 60 the mass-radius relations for the mass definitions considered, evaluated at different distances from the star surface  $d = r - R_*$ ; we note that we did not consider the Hawking definition (8.13), while we considered the TOV one (8.18). Each definition has its specific mass-radius relation and its specific dependence from the distance  $d$ , although it is a general feature that they coincide with the asymptotic limit after a few solar Schwarzschild radii from the surface, except the TOV mass that is identically identified by its value at the star surface.

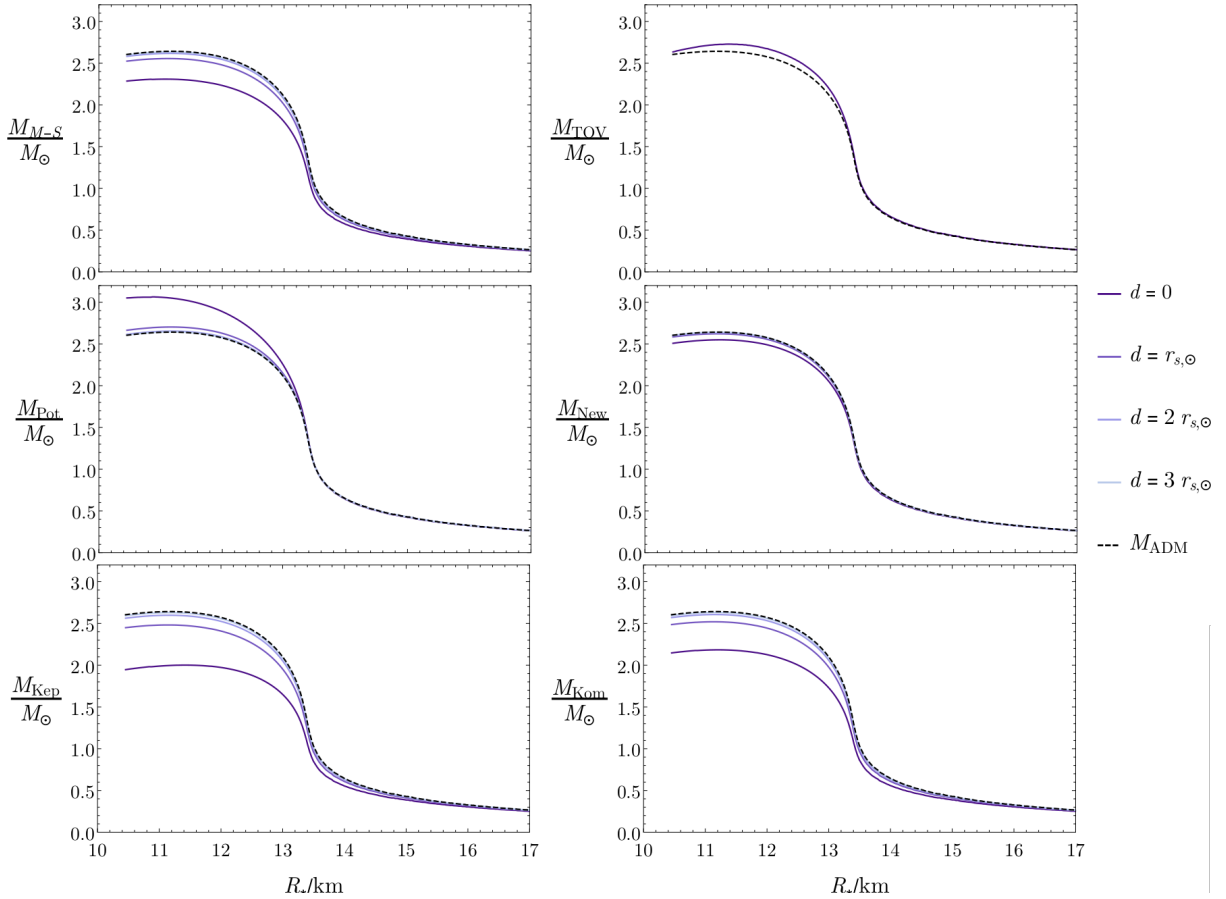


Figure 60: Mass-radius relations for different mass definitions, evaluated at different distances from the star surface.

The large variety in the possible behaviors, and in particular with the mass-radius relations of the same class of solutions, leaves us with two possible approaches to the interpretation of mass in quadratic gravity:

- the only meaningful definition of mass is the asymptotic one  $M$ , and in order to

completely define the gravitational field we have to measure the tensor and scalar charges  $S_2^-$  and  $S_0^-$ ;

- each mass definition describes a particular physical property of the star, and any star analysis has to consider carefully which aspect is under investigation.

While both approaches in the specific case of quadratic gravity seem to be simply different ways of formulating the same problem, we believe that the second approach is more powerful, as it is less dependent on the underlying theory of gravity. In particular, we can reverse our point of view and state that *the presence of discrepancies between different mass definitions can be taken as a strong indication of departure from General Relativity*. Indeed, any metric different from the Schwarzschild one will have a discrepancy between at least two mass definitions, and then this approach leads to an interesting falsifiability mechanism of General Relativity.

Still, we would like to show how these mass discrepancies can be used as a gravitational measure of the microscopical nature of the solutions. As a toy-model example, we can imagine measuring the mass of an object with the redshift of a photon emitted at a radius  $\bar{r}$  by some gas using

$$M_{New}(\bar{r}) = \frac{1}{2}\bar{r}(1 - h(\bar{r})) = \frac{1}{2}\bar{r}\left(1 - \frac{1}{(1 + z(\bar{r}))^2}\right), \quad (8.27)$$

where  $z$  is the redshift, or by the transit of a satellite, assuming that in some limit we can use Kepler's third law, using

$$M_{Kep}(\bar{r}) = \frac{1}{2}\bar{r}^2 h'(\bar{r}) = \left(\frac{2\pi}{T}\right)^2 \bar{r}^3, \quad (8.28)$$

where  $T$  is the orbital period. Both measurements will coincide with the ADM mass parameter  $M$  at infinity but will have discrepancies when evaluated at finite radii. In Figure 61 we show how these mass definitions differ from the asymptotic value if measured at a radius  $\bar{r} = 3M$ , which is the radius of the photon sphere for a Schwarzschild black hole, in the case of Einstein-Weyl gravity; we have removed the area of the phase diagram populated by no-sy wormholes with throat radius greater than  $3M$  which, however, is not relevant in the large mass limit.

As could be expected, the discrepancy increases for small masses but is still present at any scale. In particular, in the limit in which the spacetime at  $\bar{r}$  is already in the linearized regime, the differences become

$$\begin{aligned} M - M_{New}(\bar{r}) &= S_2^- e^{-m_2 \bar{r}} + \frac{1}{2} S_0^- e^{-m_0 \bar{r}}, \\ M - M_{Kep}(\bar{r}) &= S_2^- e^{-m_2 \bar{r}} (1 + m_2 \bar{r}) + \frac{1}{2} S_0^- e^{-m_0 \bar{r}} (1 + m_0 \bar{r}). \end{aligned} \quad (8.29)$$

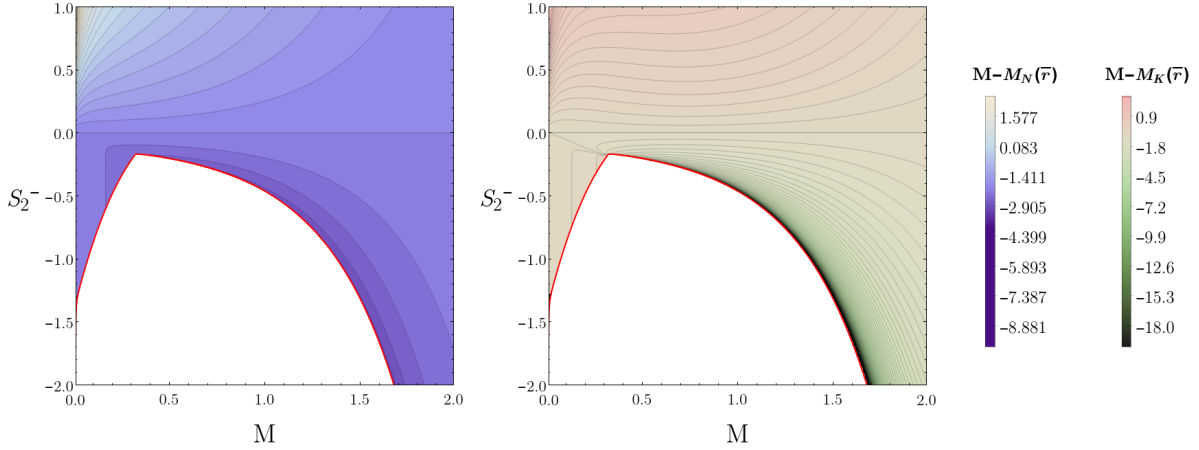


Figure 61: Differences in observable masses measured at infinity and at  $\bar{r} = 3M$ ; in the left panel the mass  $M_N$  is measured by the redshift of a photon, while in the right panel the mass  $M_K$  is measured using Kepler's third law. The white region is removed, being populated by wormholes with throat radius  $r_T > 3M$ .

While both measurements will be exponentially suppressed, is still noticeable the linear dependence from the Yukawa charges  $S_2^-$  and  $S_0^-$ . Thanks to the phase diagram pictured in Figure 10 we can conclude that, as a rule of thumb, repulsive naked singularities will always have a smaller mass when measured closer to the origin, attractive naked singularities will always have a larger mass, and wormholes can have both behaviors; in particular, in the case of Einstein-Weyl gravity it will always be larger, and in Starobinski's model it will always be smaller.

This toy model becomes even more interesting if we consider the case of a neutron star with an orbiting plane. We can indeed consider one mass measurement from the redshift emitted at the star surface

$$M_{New}(R_*) = \frac{1}{2}R_* \left( 1 - \frac{1}{(1 + z(R_*))^2} \right), \quad (8.30)$$

and the mass measured from the transit of the planet, which is considered to be at a distance  $d$  from the star's surface, as

$$M_{Kep}(d) = \left( \frac{2\pi}{T} \right)^2 (R_* + d)^3. \quad (8.31)$$

We believe that this case is more interesting because even if the planet is distant enough from the neutron star to have a Keplerian mass indistinguishable from the ADM one  $M$ , the mass measured by the redshift *will still be different*. In particular, we show in Figure 62 the difference between the two measurements for the case of six different stars with asymptotic masses between  $[0.5 - 2.642] M_\odot$ .

Finally, we conclude with the most interesting aspect of these different mass measurements. If we consider stars with the same asymptotic mass  $M$  but different equations

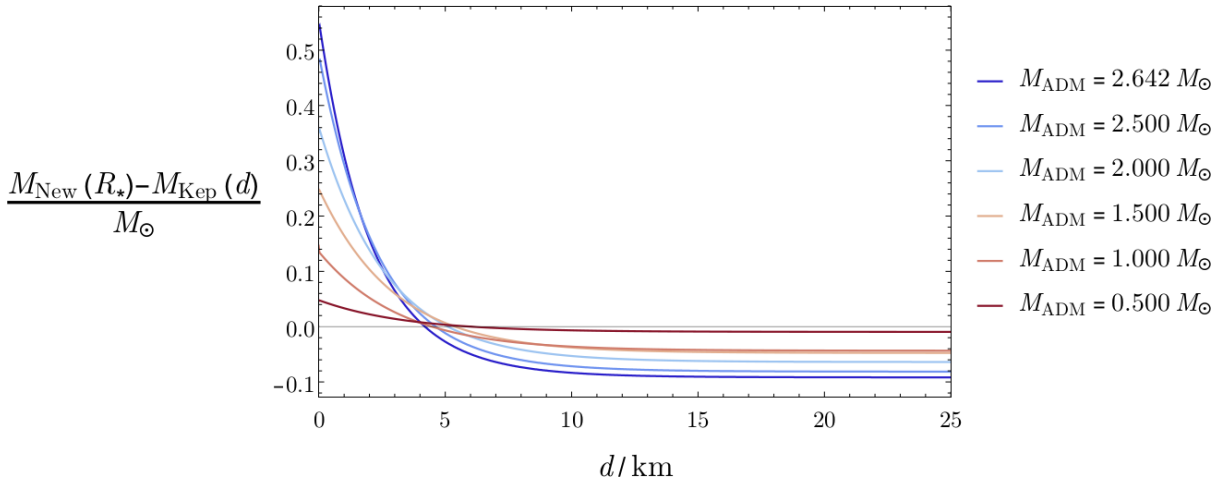


Figure 62: Differences between masses measured with surface redshift or planetary transit, in function of the distance from the star surface, for stars with asymptotic masses in the range  $[0.5 - 2.642] M_{\odot}$ .

of state, we know from the results in Subsection 4.3 that they will have different values of the Yukawa charges. This means that they will also have different quasi-local mass definitions, and then, in principle, *it is possible to study the microscopical nature of the fluid from purely gravitational measurements*. In particular, we show in Figure 63 the difference between the two mass definitions for stars of one solar mass but with different equations of state.

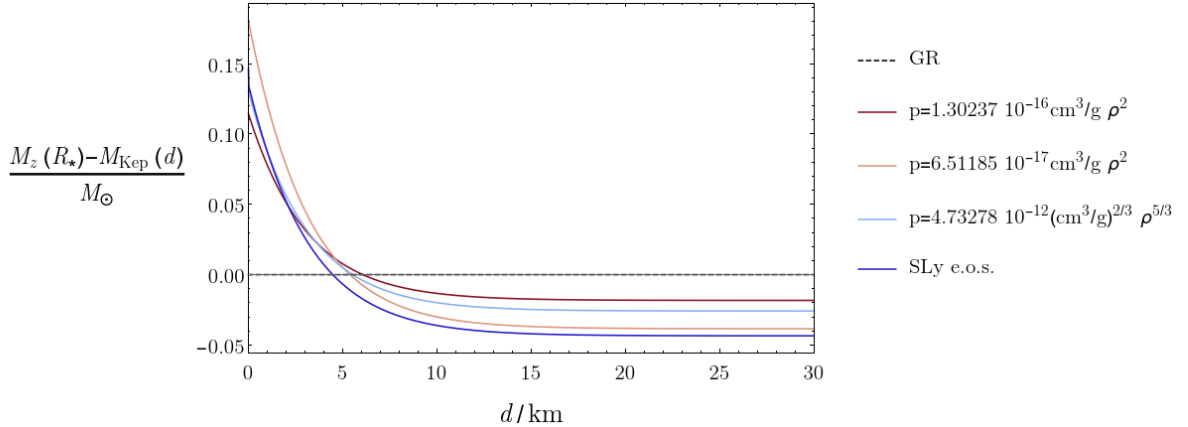


Figure 63: Differences between masses measured with surface redshift or planetary transit, in function of the distance from the star surface, for stars with different equations of state and asymptotic mass  $M = M_{\odot}$ .

Albeit the large range of possibilities for the masses  $m_2$  and  $m_0$  might render a prediction on the equations of state effectively useless, and the natural values of the masses at the order of the Planck mass might render the effective phenomenological prediction many orders of magnitude under the precision of current experiments, the idea of being able to infer the microscopical nature of a compact star exclusively from different measures on its gravitational mass is very intriguing. As a final remark, we would like to stress

one more time that, while using these mass discrepancies as a test of a specific theory of gravity is a utopistic goal, it is still relevant as a falsifiability test of General Relativity.

## Conclusions

In this thesis we analyzed the most simple isolated objects, namely static and spherically symmetric, in the context of very natural extensions of General Relativity at high energies, that is, quadratic theories of gravity. The main goal was to understand the possible contributions to the physical content of our universe of terms quadratic in the curvature tensors in the gravitational action, terms that appear following different approaches to quantum gravity. While a lot of work can still be done in this analysis, we believe that some physical consequences are manifest already in this simplified setting. In Section 2 we presented the two theories under analysis: in the first one, which we called quadratic gravity, General Relativity is corrected by the addition of all possible quadratic combinations of curvature tensors that can be collected in a Ricci scalar squared term and a Weyl tensor squared term; in the second one, which we called scale-invariant gravity, quadratic gravity is modified by the substitution of the only mass-scale present in the theory, that is the Planck mass scale, with a dynamical scalar field. In both cases, we also considered some simplified “sectors” in which some terms are suppressed. In these final remarks, we will separate the discussion on the two theories to focus on the most relevant and physically interesting aspects.

In quadratic gravity, we studied all possible behaviors of static, spherically symmetric and asymptotically flat spacetimes. In order to do that, we had to consider various analytical approximations and integrate numerically between the different approximated solutions with the procedures described in Section 3. In particular, we specify that the asymptotic gravitational potential at large distances is characterized by the total mass  $M$  and the charges  $S_2^-$  and  $S_0^-$  of two contributions with a Yukawa-like form associated with a tensor and scalar mode, respectively. In Section 4 we studied the relation between the relative values of these three parameters and the behavior of the metric at short scales, in Section 5 we presented the main geometric properties of the different families of solutions found, in Section 6 we studied their stability and, finally, in Section 7 we studied the black hole evaporation process and in Section 8 some possible phenomenological properties. We now briefly summarize the results for the different types of solutions of quadratic gravity.

**Black holes.** Together with the Schwarzschild metric, a family of non-Schwarzschild black holes also exists. Thanks to a theorem we presented in Subsection 2.1, they are present in a simplified setting, called Einstein-Weyl gravity, in which also the Weyl tensor squared term is present and then  $S_0^- = 0$ . In contrast with the case of General Relativity, for this type of black hole, as the radius of the event horizon decreases, their total mass and entropy increase while their temperature decreases. In particular, for non-Schwarzschild

black holes with a horizon radius smaller than a specific value, namely  $r_H = 0.876$  in numerical units, the Yukawa term in the asymptotic gravitational potential will have a repulsive contribution, and as the horizon radius gets to zero, the mass and entropy reach a finite value, while the temperature vanishes. For black holes with a horizon radius larger than that specific value, on the contrary, as the horizon radius increases, both the mass and entropy become large and negative, and the temperature increases indefinitely. Both the negative mass and negative entropy are a signal of the presence at the classical level of the ghost instabilities present in the quantized version of quadratic gravity. The analysis of dynamical perturbations confirmed a recent statement for which both Schwarzschild and non-Schwarzschild black holes are unstable under the specific radius  $r_H = 0.876$ . If we assume that an evaporating black hole will always remain in a stable phase, stability, together with the peculiar Thermodynamics of non-Schwarzschild black holes, implies that at the present time there should be extremely repulsive isolated objects; not being the case, we conclude by stating that either quadratic gravity is a flawed theory of gravity, black holes are not physical solutions of quadratic gravity, or that the final stages of black hole evaporation have to be in a dynamically unstable phase. As to Schwarzschild black holes, being present in a zero-measure region of the phase diagram, they do not appear to be the generic vacuum solution of quadratic gravity.

**Repulsive naked singularities.** Solutions characterized in general by either a negative mass or a positive value of the tensor charge  $S_2^-$ , which is characterized by the repulsive contribution of a tensor mode, are naked singularities with a repulsive gravitational interaction close to the origin. This type of singularity cannot be reached by a massive particle, and provides an extreme blueshift to particles emitted close to it. They will then be completely different from black holes, as they will not have a shadow, they cannot be reached, and an orbiting gas will emit photons with extremely high frequencies. Their behavior under dynamical perturbations appears to be stable only in the case of large masses and small values of Yukawa charges. Moreover, if an experiment measures the object's mass as perceived by an observer close to it, it will always detect a smaller value than the one measured at large distances. Due to their “emitting” nature, they do not seem plausible candidates to substitute black holes as solutions describing compact objects.

**Attractive naked singularities.** Solutions characterized by a positive mass and an attractive contribution of the scalar mode, and then a negative value of  $S_0^-$ , are naked singularities with an attractive gravitational interaction close to the origin. These solutions are a peculiarity of quadratic gravity and find no similar counterparts in General

Relativity. A free-falling object will always reach the singularity and, as it gets closer, it will experience extreme tidal forces in the radial direction. Contrary to what happens for repulsive naked singularities, photons that move away from the singularity experience an extreme redshift and will reach spatial infinity with very low frequencies. They have a shadow, which, however, is always slightly smaller than the one of a Schwarzschild black hole with the same mass. Thanks to their attractive nature, they seem to be stable under linear perturbations, most likely as the perturbations reach the singularity and they cannot escape from it. Generically speaking, an experiment that measures the object's mass as perceived by an observer close to it will always detect a larger value than the one measured at large distances. They do not appear to have particularly unphysical properties, and they could be good candidates to be generic solutions representing compact objects.

**Non-symmetric wormholes.** Solutions with a positive mass and competing contributions of the two Yukawa terms, that is, one is attractive and the other is repulsive, will generally be wormhole solutions. In quadratic gravity, wormholes are solutions that connect an asymptotically flat spacetime with another one that has a singularity at spatial infinity, at a specific radius called throat. The gravitational force will be attractive towards the throat in the asymptotically flat patch and repulsive in the second one. Similarly to what happens for attractive naked singularities, free-falling objects will experience extreme tidal forces close to the singularity, and photons which go towards spatial infinity in the asymptotically flat patch will be very redshifted. In contrast with naked singularities, however, they have a shadow larger than the one of a Schwarzschild black hole with the same mass. The analysis of linear perturbation seems to confirm the behavior typical to many traversable wormhole solutions, that is, they are all unstable. While they share many properties with attractive naked singularities, they do not appear to be generic solutions of quadratic gravity.

**Compact stars.** As global properties, compact stars are not qualitatively different from those present in General Relativity. As for the additional modes of quadratic gravity, non-vacuum solutions are favored by a repulsive contribution of the tensor mode and an attractive contribution of the scalar one; in particular, they have an asymptotic potential which is a transition between the one of attractive and repulsive naked singularities. The main effect of the quadratic terms is a major weakening of the gravitational interaction, with a smaller internal pressure able to sustain much more massive stars. As for vacuum solutions, the Weyl tensor squared term has a much stronger effect than the Ricci scalar squared one. A relevant aspect is that the equation of state has an impact on the value of the Yukawa charges, and then two stars with the same total mass but

composed of two different fluids have a different gravitational potential closer to their surface. In particular, if a star's mass is measured both at large distances and, for example, by the redshift of a photon emitted at the star's surface, the two results will be different and sensitive to the equation of state of the fluid. However, natural values of the free parameters of the theory force the possible phenomenological deviations from General Relativity to be much smaller than the precision of current experiments.

In scale-invariant gravity, we studied analytical solutions of General Relativity whenever they are considered as solutions of this more complex theory. In particular, we considered their stability under linear perturbations and with a semiclassical analysis of the Euclidean action. Scale-invariant gravity is indeed known to have two de Sitter solutions in cosmological settings, of which one has a zero value of the scalar field and is unstable, and one has a non-zero value of the scalar field and is stable. There is also a numerical solution that describes a transition between the two solutions, which can model inflation and reheating with good accuracy. In the static and spherically symmetric setting, there are indeed two Schwarzschild-de Sitter solutions, and our analysis of linear perturbations showed that the one with a zero scalar field is unstable and the one with a non-zero field is stable. The semiclassical analysis instead relies on the idea that, in the semiclassical limit of a path integral formulation of quantum gravity, a solution that is in a relative minimum of the action will tunnel into a solution in a true minimum (or at least in a relative minimum with a smaller action). To evaluate the Euclidean action of Schwarzschild-de Sitter black holes, for which the standard approach cannot be used because they have two horizons, we developed a technique that can be applied to all the theories for which the boundary terms are known. In particular, the Euclidean action will be given precisely by the boundary terms evaluated on the horizons. The semiclassical analysis has shown that the unstable solution has a transition into the stable one, indeed confirming the numerical results of the cosmological setting. Moreover, there is much evidence that the presence of black holes stabilizes the unstable pure de Sitter configuration, and the transition to the stable one is slower.

To conclude, including quadratic terms in the action greatly expands the number of possible vacuum solutions representing isolated objects. All the solutions still present a singularity in the origin, but some have a physical structure for which the singularity is not particularly problematic. Nonetheless, the theory's intrinsic instabilities also impact classical solutions, and most of them are unstable. However, in the case of black holes, dynamical instability is the only way out from the thermodynamical instability which would completely spoil the physical predictions of the theory. Imposing scale symmetry

by substituting the Planck mass scale with a dynamical scalar field seems to constrain such instabilities. While we do not know the impact on exotic geometries, and we know that instabilities are still present, there is much evidence that scale invariance protects unstable solutions from being completely disrupted and leads them through a transition into a stable form. While for actual physical predictions it would be necessary to study rotating solutions (for which we show only some very timid and preliminary steps in Appendix B), we believe that the analysis done in this thesis gives an insight into the possible directions that can be fruitful, and the ones that do not seem to lead to physical situations, in the study of these natural extensions of General Relativity.

# Appendices

## A Tachyonic black holes

Motivated by the results in the asymptotic safety approach to quantum gravity [120, 121] which show that the value of the parameter  $\alpha$  in (2.5) is negative at the fixed point, in [24] we investigated the case of black holes for which  $m_2^2 < 0$ . The massive particle with spin  $S = 2$  is then not only a ghost but also a tachyon and, for this reason, we called the black hole solutions found in this case “tachyonic black holes”. Nonetheless, it seems that the scalar mass remains real and then the theorem 1 can still be applied, and black holes can be considered in the case of Einstein-Weyl gravity. The linear theory can be solved analytically, and the metric takes the form

$$\begin{aligned} h(r) &= 1 - \frac{2M}{r} + 2A_2 \frac{\cos(|m_2|r + \phi_2)}{r}, \\ f(r) &= 1 - \frac{2M}{r} + A_2 \frac{\cos(|m_2|r + \phi_2)}{r} + A_2|m_2| \sin(|m_2|r + \phi_2), \end{aligned} \quad (\text{A.1})$$

where  $|m_2|$  is the modulus of the imaginary mass, and  $\phi_2$  is an additional parameter that has to be included as we cannot remove one free parameter by requiring asymptotic flatness as done in (3.4) to obtain (3.5). In fact imposing asymptotic flatness forces the solution to be the Schwarzschild one, having the last term in the definition of  $f(r)$  not vanishing at large distances. It is indeed necessary to impose  $A_2|m_2| \ll 1$  for the linear solution to be consistent. The shooting method can be used exactly as in the standard case using equations (2.40) with  $m_2^2 = -1$  with boundaries (A.1) and (3.28), and in general will find results as the one shown in Figure 64 as an example.

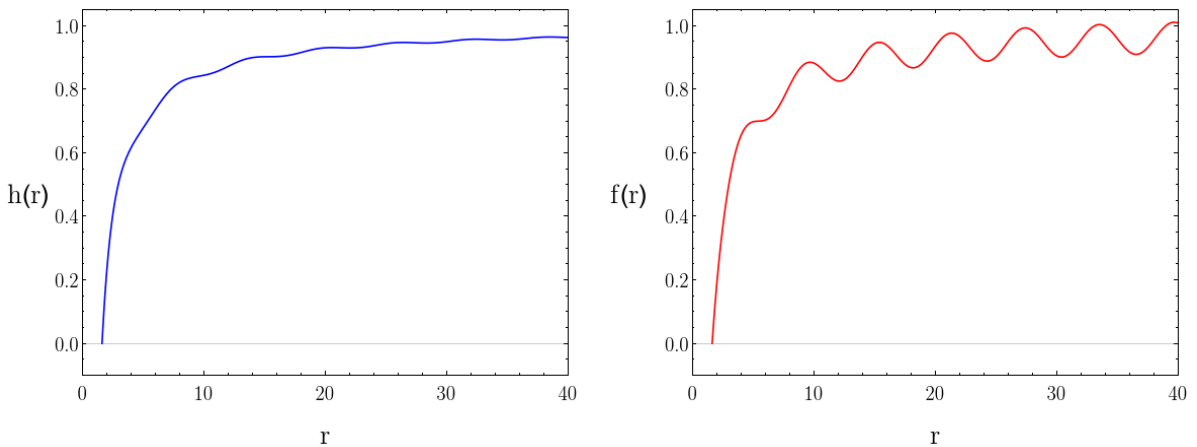


Figure 64: Metric of a tachyonic black hole with mass  $M = 0.746$ , amplitude  $A_2 = -0.170$  and phase  $\phi_2 = \pi/2$ .

From the right plot of the  $f(r)$  metric function the non-asymptotically flat nature of

the solution is manifest, and from the left plot of the  $h(r)$  is manifest that, on the other hand, the Newtonian asymptotic potential  $\phi(r) \sim \frac{1}{2}(h(r) - 1)$  will have suppressed oscillations. An oscillatory solution with similar features was already found in the context of asymptotically safe gravity in [122] by looking at minima of the Euclidean action for a Starobinski model with imaginary mass  $m_0^2 < 0$ , and also appeared in a linearized higher derivative theory in [123], where they were compared to Friedel oscillations in plasma [124]. The concluding remarks of [122] where that an external observer will see an average of the metric over an interval determined by the length scales at which the experiments are being done, more than the metric itself; these remarks can also be applied to our case, and having oscillations with periodicity  $T = 2\pi/|m_2|$ , it is sufficient to do experiments at length scales larger than  $\sim l_2 = 1/m_2$  to not being able to detect deviations from General Relativity. We highlight this property by showing in Figure 65 the metric of the black hole solution of the previous example at large distances, its moving average over intervals of  $\Delta r = 2, 4, 6$ , and the corresponding Schwarzschild metric.

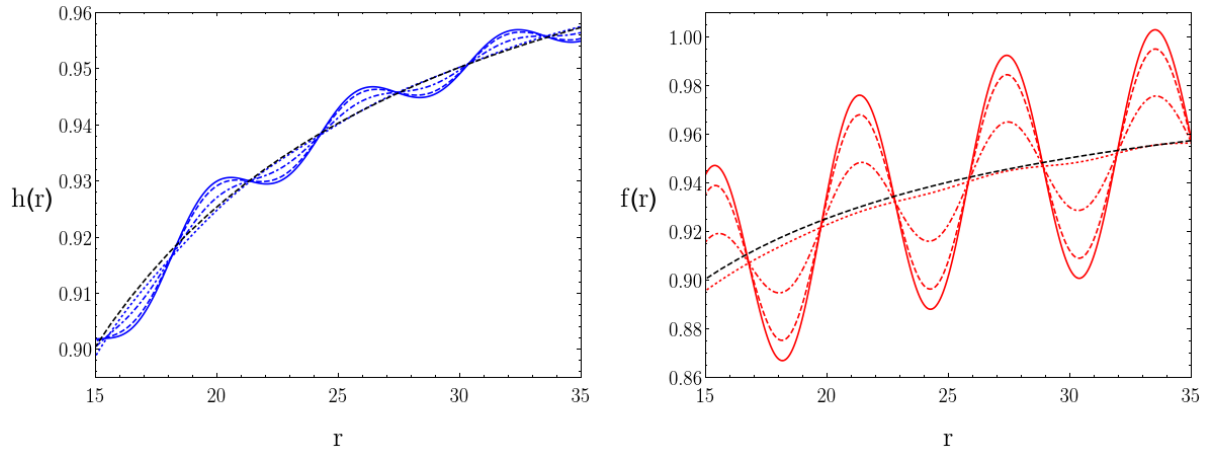


Figure 65: Metric of a tachyonic black hole with mass  $M = 0.746$ , amplitude  $A_2 = -0.170$  and phase  $\phi_2 = \pi/2$  in solid blue and red lines, in dashed blue and red the metric we have shown the moving average over an interval of  $\Delta r = 2$ , in dot-dashed blue and red the metric we have shown the moving average over an interval of  $\Delta r = 4$ , in dotted blue and red the metric we have shown the moving average over an interval of  $\Delta r = 6$  and in dashed black there is the Schwarzschild metric with mass  $M = 0.746$ .

We can perform an analysis similar to the one made in the non-tachyonic case and derive the relations between the different parameters describing the black holes either at spatial infinity or close to the horizon. However, we must note that in this case the parameter  $M$  is not the ADM mass of the solution. Employing (3.6), the total energy results indeed divergent

$$E \sim 2\gamma \lim_{r \rightarrow \infty} 4\pi r^2 \left( \frac{2M}{r^2} - 2A_2 \frac{\cos(|m_2|r + \phi_2)}{r^2} - 2A_2|m_2| \frac{\sin(|m_2|r + \phi_2)}{r} \right) \rightarrow \infty. \quad (\text{A.2})$$

This is actually no surprise, because tachyonic black holes are not asymptotically flat solutions, and the standard definitions of mass cannot be used. A suitable non-Minkowski vacuum solution should be derived, in order to remove its contribution from the energy of black holes and define the total energy of the solutions. We can still call the parameter  $M$  the mass of the solution only if we assume that there is a certain limit in which the metric average is well approximated by a Schwarzschild solution with the same parameter  $M$ . We present in Figure 66 the parameter space both for the asymptotic parameters and the parameters at the horizon. Having an additional parameter  $\phi_2$ , black holes populate an area of the parameter space, of which we presented some one-dimensional sectors of constant phase. We note that changing the phase as  $\phi_2 \rightarrow \phi_2 + \pi$  will not change the parameters at the horizon, while it will change the asymptotic parameters as  $(M, A_2) \rightarrow (M, -A_2)$ . It also seems that black holes densely populate the area of small mass  $M$ , but need larger values of the amplitude  $A_2$  to go to larger mass values, leaving the region around Schwarzschild black holes free.

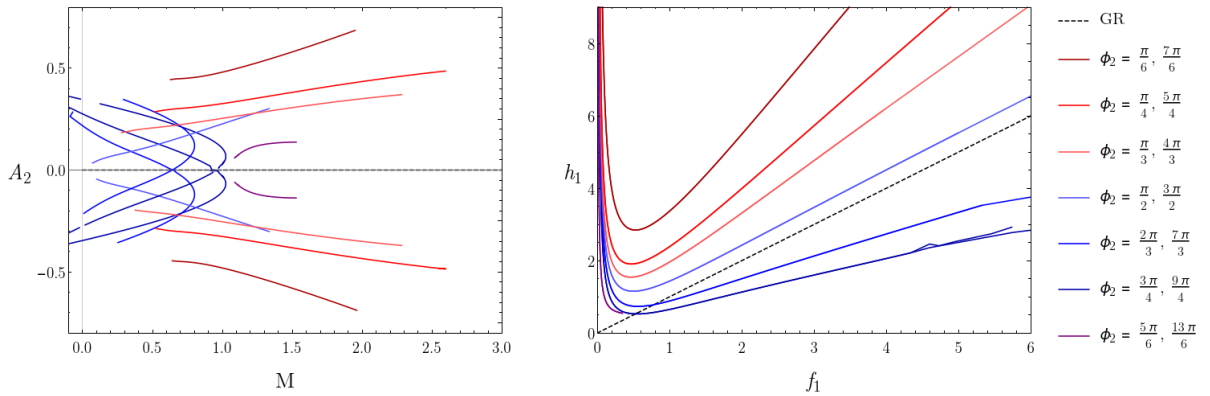


Figure 66: Parameter space for tachyonic black holes, on the left there are the asymptotic ones, that are the “mass” parameter  $M$  and the amplitude  $A_2$ , and on the right there are the ones at the horizon, that are the first derivatives of the metric  $f_1$  and  $h_1$ ; we used the same colors for solutions with a difference of  $\pi$  in their phases  $\phi_2$ , as they have the same parameters at the horizon and the asymptotic parameters can be found one from the other as  $(M, A_2) \rightarrow (M, -A_2)$ .

In Figure 67 we also present the thermodynamical properties of tachyonic black holes, that is, the Hawking temperature and Wald definition of entropy, in terms of the horizon radius. Also in this case there is no proof that these definitions represent actual physical properties, as both definitions rely on the possibility of defining the total energy of the solution. Nonetheless, if we make the strong assumption that it is possible to define a Thermodynamics of these black holes, and that the thermodynamical properties will be defined in the same way as it is done for standard black holes, it is interesting to note that tachyonic black holes have particularly standard temperatures and entropies. While at a quantitative level they differ from the definitions for Schwarzschild black holes, the

temperature is still proportional to a negative power of the horizon radius, that is, it decreases for larger black holes, and the entropy is proportional to a power of the area, with a vanishing entropy for a vanishing black hole.

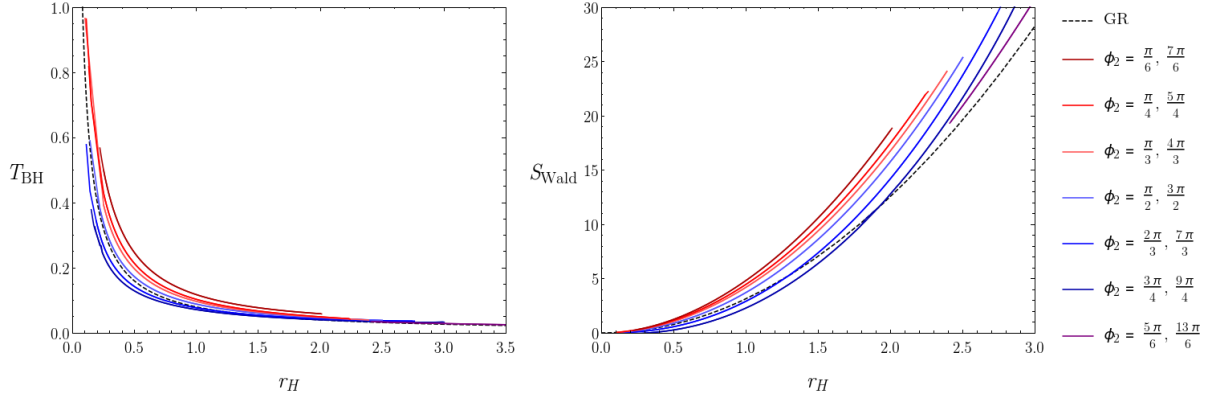


Figure 67: Thermodynamical parameters for tachyonic black holes in terms of the horizon radius; on the left there is the Hawking temperature  $T_{BH}$  and on the right the Wald definition of entropy  $S_{Wald}$ .

While regarding the stability of these solutions, however, due to the negative value of the squared mass  $m_2^2$ , the potential of perturbation (6.21) will go at a negative value at large distances; in units of  $|m_2|$ , the potential will indeed go to  $V(r) \rightarrow -1$  as  $r \rightarrow \infty$ . This property made all the tachyonic black hole solutions considered extremely unstable under linear perturbations, as can be seen by the example shown in Figure 68. From the plot of the potential is manifest both the solution's oscillating nature and the potential's negative limit at large distances. On the contrary, the time evolution of the perturbations at radius  $r_\infty = 50$  does not have oscillations even at very early times, and it seems to diverge as a power law.

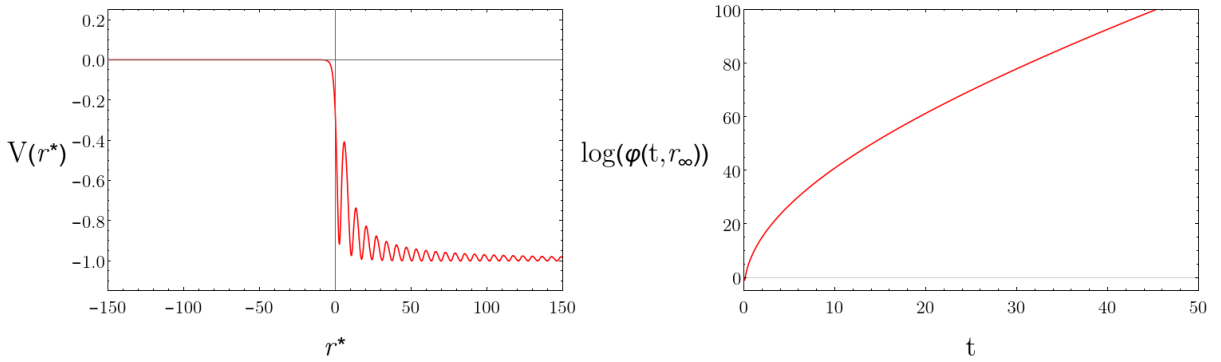


Figure 68: Linear perturbations of a tachyonic black hole with mass  $M = 0.746$ , amplitude  $A_2 = -0.170$  and phase  $\phi_2 = \pi/2$ ; in the left panel there is the potential for perturbations in terms of the tortoise coordinate, while in the right panel there is the time evolution of the perturbation at radius  $r_\infty = 50$ .

More importantly, however, is that the potential has the negative limit  $V(r) \rightarrow -1$  as  $r \rightarrow \infty$  also in the case of Schwarzschild black holes. As shown in Figure 69 the

potential reaches this limit without oscillations, which is sufficient to produce a power law divergence of the perturbations.

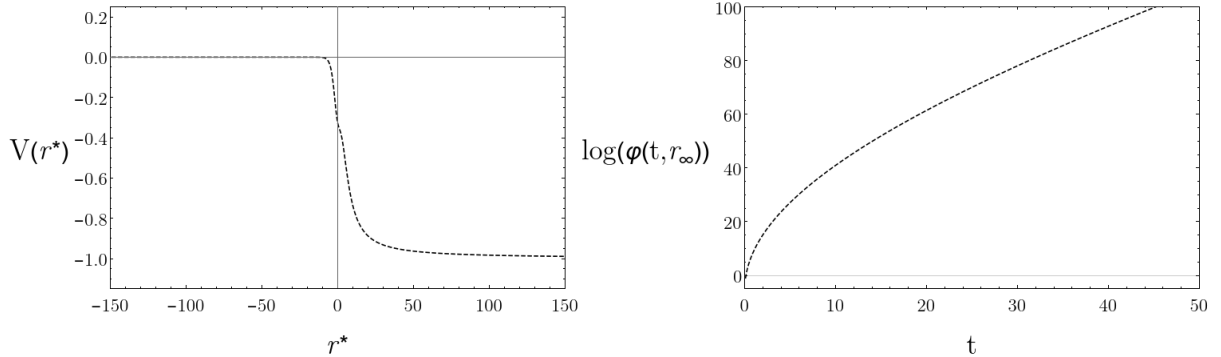


Figure 69: Linear perturbations of a Schwarzschild black hole with mass  $M = 0.75$  in the tachyonic case; in the left panel there is the potential for perturbations in terms of the tortoise coordinate, while in the right panel there is the time evolution of the perturbation at radius  $r_\infty = 50$ .

From our analysis, it seems that all the black hole solutions considered are unstable, regardless of their parameters. The negative limit of the potential will probably lead all the solutions of the theory into an unstable phase, and then we believe that these solutions cannot model astrophysical objects.

## B Rotating solutions and Newman-Janis algorithm

One of the initial goals of this thesis was to derive a rotating counterpart to the spherically symmetric solutions of quadratic gravity, as current observations indicate that the astrophysical black holes of our universe are indeed represented by rotating solutions. We did not manage to produce any sensible result, but we would like to present in this appendix a strong constraint on the possible approaches that we found while working on this problem.

The ansatz for the metric for a stationary axisymmetric solution, that is, a rotating solution, can be written using a Boyer-Lindquist form as

$$ds^2 = -H(r, \theta)dt^2 + J(r, \theta)dtd\phi + \frac{dr^2}{F(r, \theta)} + (r^2 + a \cos^2(\theta))d\theta^2 + G(r, \theta)d\phi^2, \quad (\text{B.1})$$

where we considered the  $g_{\theta\theta}$  component of the metric to be equal to the corresponding flat one in oblate spheroidal coordinates and  $a$  indicates the oblateness, which can also be written as

$$ds^2 = -H(r, \chi)dt^2 + J(r, \chi)dtd\phi + \frac{dr^2}{F(r, \chi)} + \frac{r^2 + a\chi^2}{1 + \chi^2}d\theta^2 + G(r, \chi)d\phi^2, \quad (\text{B.2})$$

where  $\chi = \cos \theta$ , and that will be useful in the following discussion. It is clear that the equations of motion of (B.1) will be much more complicated than the already very complicated ones of the spherically symmetric case (2.20). Unfortunately, also the linearized equations of motion are much more complicated and cannot be solved analytically. The difficulty of finding rotating solutions in modified theories of gravity has then attracted the attention of many physicists to the Newman-Janis algorithm, a procedure (or trick, as it is also called) to derive rotating solutions acting on a seed static and spherically symmetric ansatz (see for example [125]). Following [126] or [127], the procedure works as follows:

- write the static and spherically symmetric metric in advanced null coordinates

$$ds^2 = -h(r)du^2 + \sqrt{\frac{h(r)}{f(r)}}dudr + r^2d\theta^2 + r^2 \sin^2(\theta)d\phi^2; \quad (\text{B.3})$$

- express the inverse metric in terms of a null tetrad

$$g^{\mu\nu} = l^\mu n^\nu + n^\mu l^\nu - m^\mu \bar{m}^\nu - \bar{m}^\mu m^\nu, \quad (\text{B.4})$$

where

$$l^\mu l_\mu = n^\mu n_\mu = m^\mu m_\mu = 0, \quad l^\mu n_\mu = -m^\mu \bar{m}_\mu = 1, \quad l^\mu m_\mu = n^\mu m_\mu = 0, \quad (\text{B.5})$$

that with our ansatz can be written as

$$l^\mu = \delta_r^\mu, \quad n^\mu = \sqrt{\frac{f(r)}{h(r)}} \delta_u^\mu - \frac{1}{2} f(r) \delta_r^\mu, \quad m^\mu = \frac{1}{\sqrt{2} r} \left( \delta_\theta^\mu + \frac{i}{\sin(\theta)} \delta_\phi^\mu \right); \quad (\text{B.6})$$

- extend the coordinates in the complex plane as

$$x^\mu \rightarrow z^\mu = x^\mu + i y^\mu(x), \quad (\text{B.7})$$

where the  $y^\mu(x)$  are functions of the real coordinates  $x^\mu$ , and then extend also the tetrad in the complex plane

$$l^\mu(x) \rightarrow l_{\mathbb{C}}^\mu(z), \quad n^\mu(x) \rightarrow n_{\mathbb{C}}^\mu(z), \quad m^\mu(x) \rightarrow m_{\mathbb{C}}^\mu(z), \quad (\text{B.8})$$

with the requirement that whenever  $z^\mu = \bar{z}^\mu$  the original tetrad is found (N.B. this is the most delicate and controversial point, as there is no mathematical or physical rule for the extension of the tetrad);

- perform the complex coordinate transformation

$$\tilde{z}^\mu = z^\mu + i a \cos(\theta) (\delta_u^\mu - \delta_r^\mu), \quad (\text{B.9})$$

under which the tetrad transforms in the standard way

$$\tilde{l}_{\mathbb{C}}^\mu(\tilde{z}) = \frac{\partial \tilde{z}^\mu}{\partial z^\nu} l_{\mathbb{C}}^\nu(z), \quad \tilde{n}_{\mathbb{C}}^\mu(\tilde{z}) = \frac{\partial \tilde{z}^\mu}{\partial z^\nu} n_{\mathbb{C}}^\nu(z), \quad \tilde{m}_{\mathbb{C}}^\mu(\tilde{z}) = \frac{\partial \tilde{z}^\mu}{\partial z^\nu} m_{\mathbb{C}}^\nu(z), \quad (\text{B.10})$$

and then it will take a form dependent on the complex radius  $r$  and angle  $\theta$  as

$$\begin{aligned} \tilde{l}_{\mathbb{C}}^\mu &= \delta_r^\mu, & \tilde{n}_{\mathbb{C}}^\mu &= \sqrt{\frac{f(r, \theta)}{h(r, \theta)}} \delta_u^\mu - \frac{1}{2} f(r, \theta) \delta_r^\mu, \\ \tilde{m}_{\mathbb{C}}^\mu &= \frac{1}{\sqrt{2} (r - i a \cos(\theta))} \left( i a (\delta_u^\mu - \delta_r^\mu) + \delta_\theta^\mu + \frac{i}{\sin(\theta)} \delta_\phi^\mu \right); \end{aligned} \quad (\text{B.11})$$

- construct a new inverse metric using the new tetrad

$$\tilde{g}^{\mu\nu} = \tilde{l}_{\mathbb{C}}^\mu \tilde{n}_{\mathbb{C}}^\nu + \tilde{n}_{\mathbb{C}}^\mu \tilde{l}_{\mathbb{C}}^\nu - \tilde{m}_{\mathbb{C}}^\mu \tilde{m}_{\mathbb{C}}^\nu - \tilde{m}_{\mathbb{C}}^\mu \tilde{m}_{\mathbb{C}}^\nu; \quad (\text{B.12})$$

- using a suitable coordinate transformation

$$\begin{aligned} u &= t - \int dr \sqrt{\frac{f(r, \theta)}{h(r, \theta)}} (r^2 + a^2 \cos^2(\theta)) + a^2 \sin^2(\theta) \\ \phi &= \phi - \int dr \frac{a}{f(r, \theta) (r^2 + a^2 \cos^2(\theta)) + a^2 \sin^2(\theta)}, \end{aligned} \quad (\text{B.13})$$

together with  $\theta = \arccos(\chi)$  we can rewrite the metric in Boyer-Lindquist coordinates as

$$\begin{aligned} ds^2 = & -h(r, \chi)dt^2 - a(1 - \chi^2) \left( h(r, \chi) - \sqrt{\frac{h(r, \chi)}{f(r, \chi)}} \right) dt d\phi + \\ & + \frac{r^2 + a^2\chi^2}{(r^2 + a^2\chi^2)f(r, \chi) + a^2(1 - \chi^2)} dr^2 + \frac{r^2 + a\chi^2}{1 + \chi^2} d\theta^2 + \\ & + (1 - \chi^2) \left( r^2 + a^2\chi^2 - a^2(1 - \chi^2) \left( h(r, \chi) - 2\sqrt{\frac{h(r, \chi)}{f(r, \chi)}} \right) \right) d\phi^2, \end{aligned} \quad (\text{B.14})$$

which is a particular case of (B.2) in which the functions  $H(r, \chi)$ ,  $F(r, \chi)$ ,  $J(r, \chi)$  and  $G(r, \chi)$  satisfy two algebraic equations.

Using this algorithm, it is possible to derive the Kerr metric starting from the Schwarzschild one, and it was used to derive for the first time the Kerr-Newman metric, which was verified to be a solution of the Maxwell-Einstein equations *a posteriori*, starting from the Reissner-Nordström one. In [127] it was used to derive the rotating counterpart of a solution of  $f(R)$  gravity found exploiting Noether symmetry but, at the same time, it has been proven that the Newman-Janis algorithm in quadratic gravity finds solutions which are not solutions of the equations of motion [128]. In the case of quadratic gravity is indeed possible to prove that this second statement is indeed correct, as the Newman-Janis algorithm can produce only the Kerr-Newman metric. In [126] two theorems are proven, that are:

**Theorem 4.** *The only algebraically special spacetimes generated by the Newman-Janis algorithm are Petrov type D.*

and

**Theorem 5.** *The only Petrov type D spacetime generated by the Newman-Janis algorithm with a vanishing Ricci scalar is the Kerr-Newman spacetime.*

and we refer to the original paper for the relative proofs. The first theorem is somehow intuitive and natural, considering that isolated objects are of Petrov type D. The second theorem, however, imposes a strong constraint on the possible solutions. In particular, we present an additional theorem

**Theorem 6.** *All the stationary, axisymmetric and asymptotically flat black hole solutions of quadratic gravity have  $R = 0$  outside the event horizon.*

which can be proven with the same techniques we used for similar no-hair-like theorems in this thesis.

**Proof.** Let us consider a stationary and axisymmetric metric

$$ds^2 = \gamma_{ab}(y)dx^a dx^b + h_{ij}(y)dy^i dy^j, \quad (\text{B.15})$$

where the indices  $a, b$  run over the directions  $t, \phi$  and the indices  $i, j$  over the directions  $r, \theta$ . The trace of the equations of motion (2.10) can be written as

$$\square R - m_0^2 R = D^i D_i R + \frac{1}{2} \gamma^{ab} \partial^i \gamma_{ab} D_i R - m_0^2 R = D^i D_i R + \frac{1}{\sqrt{-\gamma}} D^i \sqrt{-\gamma} D_i R - m_0^2 R = 0, \quad (\text{B.16})$$

where  $D_i$  is the covariant derivative defined by the  $h_{ij}$  metric and  $\gamma$  is the determinant of  $\gamma_{ab}$ . As usual we multiply by  $\sqrt{-\gamma} R$  and integrate in the submanifold defined by the  $y^i$  vectors

$$\begin{aligned} \int_{\Sigma} dr d\theta \sqrt{h} [\sqrt{-\gamma} R D^i D_i R + R D^i \sqrt{-\gamma} D_i R - \sqrt{-\gamma} m_0^2 R^2] = \\ [\sqrt{-\gamma} R D_i R]_{\partial \Sigma} - \int_{\Sigma} dr d\theta \sqrt{h} \sqrt{-\gamma} [(D^i R) (D_i R) + m_0^2 R^2] = 0, \end{aligned} \quad (\text{B.17})$$

and, if  $h_{ij}$  is positive definite, the vanishing of the boundary term requires  $R = 0$  in all the surface  $\Sigma$ . If we consider the surface to be between spatial infinity and a black hole horizon, we have that  $\sqrt{-\gamma} R D_i R \rightarrow 0$  as  $r \rightarrow \infty$  because the spacetime is asymptotically flat, and that  $\sqrt{-\gamma} R D_i R \rightarrow 0$  as  $r \rightarrow r_H$  because  $\gamma \rightarrow 0$  as  $r \rightarrow r_H$  for the definition of the event horizon. Being the spacetime axisymmetric, the surface  $\Sigma$  is independent of the choice of angle  $\phi$ , and the black hole has zero Ricci scalar outside the horizon.  $\square$

Putting together theorems 4, 5 and 6 we conclude that the Newman-Janis algorithm can be used consistently in quadratic gravity only to produce the Kerr metric from a Schwarzschild seed. A more viable approach to the problem of rotating solutions is probably the slowly rotating approximation, which already showed some interesting results for solutions of quadratic gravity [129].

## References

- [1] S. Weinberg, “Critical Phenomena for Field Theorists,” in *14th International School of Subnuclear Physics: Understanding the Fundamental Constituents of Matter*, 8 1976.
- [2] S. Weinberg, *Ultraviolet divergences in quantum theories of gravitation*, pp. 790–831. Cambridge University Press, 1980.
- [3] R. Percacci, “A Short introduction to asymptotic safety,” in *Time and Matter*, pp. 123–142, 10 2011.
- [4] R. Percacci, *An Introduction to Covariant Quantum Gravity and Asymptotic Safety*, vol. 3 of *100 Years of General Relativity*. World Scientific, 2017.
- [5] G. ’t Hooft and M. J. G. Veltman, “One loop divergencies in the theory of gravitation,” *Ann. Inst. H. Poincare Phys. Theor. A*, vol. 20, pp. 69–94, 1974.
- [6] J. Scherk and J. H. Schwarz, “Dual Models for Nonhadrons,” *Nucl. Phys. B*, vol. 81, pp. 118–144, 1974.
- [7] P. Candelas, G. T. Horowitz, A. Strominger, and E. Witten, “Vacuum configurations for superstrings,” *Nucl. Phys. B*, vol. 258, pp. 46–74, 1985.
- [8] D. J. Gross and E. Witten, “Superstring Modifications of Einstein’s Equations,” *Nucl. Phys. B*, vol. 277, p. 1, 1986.
- [9] B. Zwiebach, “Curvature Squared Terms and String Theories,” *Phys. Lett. B*, vol. 156, pp. 315–317, 1985.
- [10] D. Tong, “String Theory,” 1 2009.
- [11] D. Benedetti, “On the number of relevant operators in asymptotically safe gravity,” *EPL*, vol. 102, no. 2, p. 20007, 2013.
- [12] K. Stelle, “Renormalization of Higher Derivative Quantum Gravity,” *Phys. Rev. D*, vol. 16, pp. 953–969, 1977.
- [13] S. W. Hawking and T. Hertog, “Living with ghosts,” *Phys. Rev. D*, vol. 65, p. 103515, 2002.
- [14] D. Anselmi, “On the quantum field theory of the gravitational interactions,” *Journal of High Energy Physics*, vol. 6, p. 86, June 2017.

- [15] D. Anselmi and M. Piva, “Quantum gravity, fakeons and microcausality,” *Journal of High Energy Physics*, vol. 11, p. 21, Nov. 2018.
- [16] J. F. Donoghue and G. Menezes, “Unitarity, stability, and loops of unstable ghosts,” *Phys. Rev. D*, vol. 100, p. 105006, Nov. 2019.
- [17] A. Platania and C. Wetterich, “Non-perturbative unitarity and fictitious ghosts in quantum gravity,” *Phys. Lett. B*, vol. 811, p. 135911, 2020.
- [18] A. Salvio and A. Strumia, “Quantum mechanics of 4-derivative theories,” *Eur. Phys. J. C*, vol. 76, no. 4, p. 227, 2016.
- [19] A. A. Starobinsky, “A New Type of Isotropic Cosmological Models Without Singularity,” *Phys. Lett. B*, vol. 91, pp. 99–102, 1980.
- [20] H. Lü, A. Perkins, C. Pope, and K. Stelle, “Spherically Symmetric Solutions in Higher-Derivative Gravity,” *Phys. Rev. D*, vol. 92, no. 12, p. 124019, 2015.
- [21] J. Podolsky, R. Svarc, V. Pravda, and A. Pravdova, “Explicit black hole solutions in higher-derivative gravity,” *Phys. Rev. D*, vol. 98, no. 2, p. 021502, 2018.
- [22] J. Podolsky, R. Svarc, V. Pravda, and A. Pravdova, “Black holes and other exact spherical solutions in Quadratic Gravity,” *Phys. Rev. D*, vol. 101, no. 2, p. 024027, 2020.
- [23] H. Lü, A. Perkins, C. Pope, and K. Stelle, “Black Holes in Higher-Derivative Gravity,” *Phys. Rev. Lett.*, vol. 114, no. 17, p. 171601, 2015.
- [24] A. Bonanno and S. Silveravalle, “Characterizing black hole metrics in quadratic gravity,” *Phys. Rev. D*, vol. 99, no. 10, p. 101501, 2019.
- [25] K. Goldstein and J. J. Mashiyane, “Ineffective Higher Derivative Black Hole Hair,” *Phys. Rev. D*, vol. 97, no. 2, p. 024015, 2018.
- [26] B. Holdom and J. Ren, “Not quite a black hole,” *Phys. Rev. D*, vol. 95, no. 8, p. 084034, 2017.
- [27] M. Rinaldi and L. Vanzo, “Inflation and reheating in theories with spontaneous scale invariance symmetry breaking,” *Phys. Rev. D*, vol. 94, no. 2, p. 024009, 2016.
- [28] A. Ghoshal, D. Mukherjee, and M. Rinaldi, “Inflation and primordial gravitational waves in scale-invariant quadratic gravity with Higgs,” *JHEP*, vol. 05, p. 023, 2023.

[29] C. Cecchini and M. Rinaldi, “Inflationary helical magnetic fields with a sawtooth coupling,” *Phys. Dark Univ.*, vol. 40, p. 101212, 2023.

[30] S. Vicentini, L. Vanzo, and M. Rinaldi, “Scale-invariant inflation with one-loop quantum corrections,” *Phys. Rev. D*, vol. 99, no. 10, p. 103516, 2019.

[31] B. L. Giacchini, “Experimental limits on the free parameters of higher-derivative gravity,” in *14th Marcel Grossmann Meeting on Recent Developments in Theoretical and Experimental General Relativity, Astrophysics, and Relativistic Field Theories*, vol. 2, pp. 1340–1345, 2017.

[32] K. S. Stelle, “Classical Gravity with Higher Derivatives,” *Gen. Rel. Grav.*, vol. 9, pp. 353–371, 1978.

[33] A. Perkins, *Static spherically symmetric solutions in higher derivatives gravity*. PhD thesis, Imperial College, 2016.

[34] M. Rinaldi, L. Vanzo, S. Zerbini, and G. Venturi, “Inflationary quasiscale-invariant attractors,” *Phys. Rev. D*, vol. 93, p. 024040, 2016.

[35] S. Boudet, F. Bombacigno, G. Olmo, and P. Porfírio, “Quasinormal modes of schwarzschild black holes in projective invariant chern-simons modified gravity,” *Journal of Cosmology and Astroparticle Physics*, vol. 2022, p. 032, may 2022.

[36] W. Nelson, “Static Solutions for 4th order gravity,” *Phys. Rev. D*, vol. 82, p. 104026, 2010.

[37] N. Aghanim *et al.*, “Planck 2018 results. VI. Cosmological parameters,” *Astron. Astrophys.*, vol. 641, p. A6, 2020. [Erratum: *Astron. Astrophys.* 652, C4 (2021)].

[38] Y. Akrami *et al.*, “Planck 2018 results. X. Constraints on inflation,” *Astron. Astrophys.*, vol. 641, p. A10, 2020.

[39] D. Anselmi, E. Bianchi, and M. Piva, “Predictions of quantum gravity in inflationary cosmology: effects of the Weyl-squared term,” *JHEP*, vol. 07, p. 211, 2020.

[40] A. Hindawi, B. A. Ovrut, and D. Waldram, “Consistent spin two coupling and quadratic gravitation,” *Phys. Rev. D*, vol. 53, pp. 5583–5596, 1996.

[41] A. Bonanno and S. Silveravalle, “The gravitational field of a star in quadratic gravity,” *J. Cosmol. Astropart. Phys.*, vol. 08, p. 050, 2021.

[42] R. Svarc, J. Podolsky, V. Pravda, and A. Pravdova, “Exact black holes in quadratic gravity with any cosmological constant,” *Phys. Rev. Lett.*, vol. 121, no. 23, p. 231104, 2018.

[43] A. Bonanno, S. Silveravalle, and A. Zuccotti, “Nonsymmetric wormholes and localized big rip singularities in Einstein-Weyl gravity,” *Phys. Rev. D*, vol. 105, no. 12, p. 124059, 2022.

[44] R. L. Arnowitt, S. Deser, and C. W. Misner, “The Dynamics of general relativity,” *Gen. Rel. Grav.*, vol. 40, pp. 1997–2027, 2008.

[45] A. Komar, “Covariant conservation laws in general relativity,” *Phys. Rev.*, vol. 113, pp. 934–936, 1959.

[46] J. D. Barrow and F. J. Tipler, “Action principles in nature,” *Nature*, vol. 331, pp. 31–34, Jan. 1988.

[47] J.-L. Lehners and K. S. Stelle, “A Safe Beginning for the Universe?,” *Phys. Rev. D*, vol. 100, no. 8, p. 083540, 2019.

[48] J. N. Borissova and A. Eichhorn, “Towards black-hole singularity-resolution in the Lorentzian gravitational path integral,” *Universe*, vol. 7, no. 3, p. 48, 2021.

[49] J. Chojnacki and J. Kwapisz, “Finite action principle and Hořava-Lifshitz gravity: Early universe, black holes, and wormholes,” *Phys. Rev. D*, vol. 104, no. 10, p. 103504, 2021.

[50] W. H. Press, S. A. Teukolsky, W. T. Vetterling, and B. P. Flannery, *Numerical Recipes in FORTRAN: The Art of Scientific Computing*. Cambridge University Press, 1992.

[51] S. Silveravalle and A. Zuccotti, “The phase diagram of Einstein-Weyl gravity,” *Phys. Rev. D*, vol. 107, no. 6, p. 064029, 2023.

[52] S. Silveravalle, “The gravitational field of isolated objects in quadratic gravity,” *Nuovo Cimento Soc. Ital. Fis. C (to be published)*, 2 2022.

[53] M. Calzà, M. Rinaldi, and L. Sebastiani, “A special class of solutions in  $F(R)$ -gravity,” *Eur. Phys. J. C*, vol. 78, no. 3, p. 178, 2018.

[54] G. Cognola, M. Rinaldi, and L. Vanzo, “Scale-invariant rotating black holes in quadratic gravity,” *Entropy*, vol. 17, pp. 5145–5156, 2015.

[55] G. Cognola, M. Rinaldi, L. Vanzo, and S. Zerbini, “Thermodynamics of topological black holes in  $R^2$  gravity,” *Phys. Rev. D*, vol. 91, p. 104004, 2015.

[56] S. W. Hawking and G. F. R. Ellis, *The Large Scale Structure of Space-Time*. Cambridge Monographs on Mathematical Physics, Cambridge University Press, 2 2011.

[57] M. S. Morris and K. S. Thorne, “Wormholes in space-time and their use for interstellar travel: A tool for teaching general relativity,” *Am. J. Phys.*, vol. 56, pp. 395–412, 1988.

[58] M. S. Morris, K. S. Thorne, and U. Yurtsever, “Wormholes, Time Machines, and the Weak Energy Condition,” *Phys. Rev. Lett.*, vol. 61, pp. 1446–1449, 1988.

[59] M. Visser, “Traversable wormholes: Some simple examples,” *Phys. Rev. D*, vol. 39, pp. 3182–3184, 1989.

[60] D. Hochberg and M. Visser, “Geometric structure of the generic static traversable wormhole throat,” *Phys. Rev. D*, vol. 56, pp. 4745–4755, 1997.

[61] C.-M. Claudel, K. S. Virbhadra, and G. F. R. Ellis, “The Geometry of photon surfaces,” *J. Math. Phys.*, vol. 42, pp. 818–838, 2001.

[62] R. R. Silbar and S. Reddy, “Neutron stars for undergraduates,” *Am. J. Phys.*, vol. 72, pp. 892–905, 2004. [Erratum: Am.J.Phys. 73, 286 (2005)].

[63] E. Chabanat, P. Bonche, P. Haensel, J. Meyer, and R. Schaeffer, “A Skyrme parametrization from subnuclear to neutron star densities. 2. Nuclei far from stabilities,” *Nucl. Phys. A*, vol. 635, pp. 231–256, 1998. [Erratum: Nucl.Phys.A 643, 441–441 (1998)].

[64] F. Douchin and P. Haensel, “A unified equation of state of dense matter and neutron star structure,” *Astron. Astrophys.*, vol. 380, p. 151, 2001.

[65] P. Haensel and A. Y. Potekhin, “Analytical representations of unified equations of state of neutron-star matter,” *Astron. Astrophys.*, vol. 428, pp. 191–197, 2004.

[66] F. Sbisà, P. O. Baqui, T. Miranda, S. E. Jorás, and O. F. Piattella, “Neutron star masses in  $R^2$ -gravity,” *Phys. Dark Univ.*, vol. 27, p. 100411, 2020.

[67] D. J. Kapner, T. S. Cook, E. G. Adelberger, J. H. Gundlach, B. R. Heckel, C. D. Hoyle, and H. E. Swanson, “Tests of the gravitational inverse-square law below the dark-energy length scale,” *Phys. Rev. Lett.*, vol. 98, p. 021101, 2007.

[68] A. V. Astashenok, S. D. Odintsov, and A. de la Cruz-Dombriz, “The realistic models of relativistic stars in  $f(R) = R + \alpha R^2$  gravity,” *Class. Quant. Grav.*, vol. 34, no. 20, p. 205008, 2017.

[69] A. Held and J. Zhang, “Instability of spherically symmetric black holes in quadratic gravity,” *Phys. Rev. D*, vol. 107, no. 6, p. 064060, 2023.

[70] T. Regge and J. A. Wheeler, “Stability of a Schwarzschild singularity,” *Phys. Rev.*, vol. 108, pp. 1063–1069, 1957.

[71] F. J. Zerilli, “Effective potential for even-parity regge-wheeler gravitational perturbation equations,” *Phys. Rev. Lett.*, vol. 24, pp. 737–738, Mar 1970.

[72] R. A. Konoplya and A. Zhidenko, “Quasinormal modes of black holes: From astrophysics to string theory,” *Rev. Mod. Phys.*, vol. 83, pp. 793–836, 2011.

[73] C. Gundlach, R. H. Price, and J. Pullin, “Late-time behavior of stellar collapse and explosions. i. linearized perturbations,” *Phys. Rev. D*, vol. 49, pp. 883–889, Jan 1994.

[74] B. Wang, C. Molina, and E. Abdalla, “Evolution of a massless scalar field in reissner-nordström anti-de sitter spacetimes,” *Phys. Rev. D*, vol. 63, p. 084001, Feb 2001.

[75] B. Wang, C.-Y. Lin, and C. Molina, “Quasinormal behavior of massless scalar field perturbation in reissner-nordström anti-de sitter spacetimes,” *Phys. Rev. D*, vol. 70, p. 064025, Sep 2004.

[76] C. Molina, P. Pani, V. Cardoso, and L. Gualtieri, “Gravitational signature of schwarzschild black holes in dynamical chern-simons gravity,” *Phys. Rev. D*, vol. 81, p. 124021, Jun 2010.

[77] A. Chowdhury and N. Banerjee, “Echoes from a singularity,” *Phys. Rev. D*, vol. 102, no. 12, p. 124051, 2020.

[78] H. Lü, A. Perkins, C. N. Pope, and K. S. Stelle, “Lichnerowicz Modes and Black Hole Families in Ricci Quadratic Gravity,” *Phys. Rev. D*, vol. 96, no. 4, p. 046006, 2017.

[79] G. W. Gibbons, S. A. Hartnoll, and A. Ishibashi, “On the stability of naked singularities,” *Prog. Theor. Phys.*, vol. 113, pp. 963–978, 2005.

[80] P. R. Brady, C. M. Chambers, W. G. Laarakkers, and E. Poisson, “Radiative falloff in schwarzschild–de sitter spacetime,” *Phys. Rev. D*, vol. 60, p. 064003, Aug 1999.

- [81] S. W. Hawking, “Particle Creation by Black Holes,” *Commun. Math. Phys.*, vol. 43, pp. 199–220, 1975. [Erratum: Commun.Math.Phys. 46, 206 (1976)].
- [82] S. W. Hawking, “Black Holes and Thermodynamics,” *Phys. Rev. D*, vol. 13, pp. 191–197, 1976.
- [83] G. W. Gibbons and S. W. Hawking, “Action Integrals and Partition Functions in Quantum Gravity,” *Phys. Rev. D*, vol. 15, pp. 2752–2756, 1977.
- [84] N. N. Bogolyubov, V. V. Tolmachev, and D. V. Shirkov, “A New method in the theory of superconductivity,” *Fortsch. Phys.*, vol. 6, pp. 605–682, 1958.
- [85] R. Gregory, I. G. Moss, N. Oshita, and S. Patrick, “Black hole evaporation in de Sitter space,” *Class. Quant. Grav.*, vol. 38, no. 18, p. 185005, 2021.
- [86] P. Candelas, “Vacuum Polarization in Schwarzschild Space-Time,” *Phys. Rev. D*, vol. 21, pp. 2185–2202, 1980.
- [87] D. N. Page, “Particle Emission Rates from a Black Hole: Massless Particles from an Uncharged, Nonrotating Hole,” *Phys. Rev. D*, vol. 13, pp. 198–206, 1976.
- [88] S. W. Hawking, “Quantum Gravity and Path Integrals,” *Phys. Rev. D*, vol. 18, pp. 1747–1753, 1978.
- [89] J. D. Bekenstein, “Black holes and the second law,” *Lett. Nuovo Cim.*, vol. 4, pp. 737–740, 1972.
- [90] J. D. Bekenstein, “Generalized second law of thermodynamics in black hole physics,” *Phys. Rev. D*, vol. 9, pp. 3292–3300, 1974.
- [91] R. M. Wald, “Black hole entropy is the Noether charge,” *Phys. Rev. D*, vol. 48, no. 8, pp. 3427–3431, 1993.
- [92] V. Iyer and R. M. Wald, “Some properties of Noether charge and a proposal for dynamical black hole entropy,” *Phys. Rev. D*, vol. 50, pp. 846–864, 1994.
- [93] Z.-Y. Fan and H. Lu, “Thermodynamical First Laws of Black Holes in Quadratically-Extended Gravities,” *Phys. Rev. D*, vol. 91, no. 6, p. 064009, 2015.
- [94] B. J. Carr and S. W. Hawking, “Black holes in the early Universe,” *Mon. Not. Roy. Astron. Soc.*, vol. 168, pp. 399–415, 1974.
- [95] S. Shankaranarayanan, “Temperature and entropy of Schwarzschild-de Sitter space-time,” *Phys. Rev. D*, vol. 67, p. 084026, 2003.

[96] C. W. Robson, L. D. M. Villari, and F. Biancalana, “Global Hawking Temperature of Schwarzschild-de Sitter Spacetime: a Topological Approach,” 2 2019.

[97] S. W. Hawking and D. N. Page, “Thermodynamics of Black Holes in anti-De Sitter Space,” *Commun. Math. Phys.*, vol. 87, p. 577, 1983.

[98] S. N. Solodukhin, “Boundary terms of conformal anomaly,” *Phys. Lett. B*, vol. 752, pp. 131–134, 2016.

[99] E. K. Morvan, J. P. van der Schaar, and M. R. Visser, “On the Euclidean Action of de Sitter Black Holes and Constrained Instantons,” *SciPost Phys.*, vol. 14, p. 022, 2023.

[100] D. V. Fursaev and S. N. Solodukhin, “On the description of the Riemannian geometry in the presence of conical defects,” *Phys. Rev. D*, vol. 52, pp. 2133–2143, 1995.

[101] R. Sini and V. C. Kuriakose, “Absorption cross-section of a Schwarzschild-de Sitter black hole,” *Int. J. Mod. Phys. D*, vol. 16, pp. 105–116, 2007.

[102] J. Daas, K. Kuijpers, F. Saueressig, M. F. Wondrak, and H. Falcke, “Probing Quadratic Gravity with the Event Horizon Telescope,” 4 2022.

[103] K. Akiyama *et al.*, “First M87 Event Horizon Telescope Results. I. The Shadow of the Supermassive Black Hole,” *Astrophys. J. Lett.*, vol. 875, p. L1, 2019.

[104] K. Akiyama *et al.*, “First Sagittarius A\* Event Horizon Telescope Results. I. The Shadow of the Supermassive Black Hole in the Center of the Milky Way,” *Astrophys. J. Lett.*, vol. 930, no. 2, p. L12, 2022.

[105] R. M. Wald, *General Relativity*. Chicago, USA: Chicago Univ. Pr., 1984.

[106] C. W. Misner and D. H. Sharp, “Relativistic Equations for Adiabatic, Spherically Symmetric Gravitational Collapse,” *Physical Review*, vol. 136, pp. 571–576, Oct. 1964.

[107] S. W. Hawking, “Gravitational Radiation in an Expanding Universe,” *Journal of Mathematical Physics*, vol. 9, pp. 598–604, Apr. 1968.

[108] S. A. Hayward, “Quasilocal gravitational energy,” *Phys. Rev. D*, vol. 49, pp. 831–839, 1994.

[109] M. Aparicio Resco, A. de la Cruz-Dombriz, F. J. Llanes Estrada, and V. Zapatero Castrillo, “On neutron stars in  $f(R)$  theories: Small radii, large masses and large energy emitted in a merger,” *Phys. Dark Univ.*, vol. 13, pp. 147–161, 2016.

[110] A. S. Arapoglu, C. Deliduman, and K. Y. Eksi, “Constraints on Perturbative f(R) Gravity via Neutron Stars,” *J. Cosmol. Astropart. Phys.*, vol. 07, p. 020, 2011.

[111] M. Orellana, F. Garcia, F. A. Teppa Pannia, and G. E. Romero, “Structure of neutron stars in  $R$ -squared gravity,” *Gen. Rel. Grav.*, vol. 45, pp. 771–783, 2013.

[112] A. V. Astashenok, S. Capozziello, and S. D. Odintsov, “Further stable neutron star models from  $f(R)$  gravity,” *J. Cosmol. Astropart. Phys.*, vol. 12, p. 040, 2013.

[113] S. S. Yazadjiev, D. D. Doneva, K. D. Kokkotas, and K. V. Staykov, “Non-perturbative and self-consistent models of neutron stars in  $R$ -squared gravity,” *J. Cosmol. Astropart. Phys.*, vol. 06, p. 003, 2014.

[114] C. Deliduman, K. Y. Eksi, and V. Keles, “Neutron star solutions in perturbative quadratic gravity,” *J. Cosmol. Astropart. Phys.*, vol. 05, p. 036, 2012.

[115] S. Hawking and G. T. Horowitz, “The Gravitational Hamiltonian, action, entropy and surface terms,” *Class. Quant. Grav.*, vol. 13, pp. 1487–1498, 1996.

[116] R. C. Tolman, “Static solutions of Einstein’s field equations for spheres of fluid,” *Phys. Rev.*, vol. 55, pp. 364–373, 1939.

[117] J. R. Oppenheimer and G. M. Volkoff, “On Massive neutron cores,” *Phys. Rev.*, vol. 55, pp. 374–381, 1939.

[118] E. Santos, “Neutron stars in generalized  $f(R)$  gravity,” *Astrophys. Space Sci.*, vol. 341, pp. 411–416, 2012.

[119] S. Capozziello, M. De Laurentis, R. Farinelli, and S. D. Odintsov, “Mass-radius relation for neutron stars in  $f(R)$  gravity,” *Phys. Rev. D*, vol. 93, no. 2, p. 023501, 2016.

[120] D. Benedetti, P. F. Machado, and F. Saueressig, “Asymptotic safety in higher-derivative gravity,” *Mod. Phys. Lett. A*, vol. 24, pp. 2233–2241, 2009.

[121] Y. Hamada and M. Yamada, “Asymptotic safety of higher derivative quantum gravity non-minimally coupled with a matter system,” *Journal of High Energy Physics*, vol. 8, p. 70, Aug. 2017.

- [122] A. Bonanno and M. Reuter, “Modulated Ground State of Gravity Theories with Stabilized Conformal Factor,” *Phys. Rev. D*, vol. 87, no. 8, p. 084019, 2013.
- [123] J. Boos, “Gravitational Friedel oscillations in higher-derivative and infinite-derivative gravity?,” *Int. J. Mod. Phys. D*, vol. 27, no. 14, p. 1847022, 2018.
- [124] J. Friedel, “Electronic structure of primary solid solutions in metals,” *Advances in Physics*, vol. 3, no. 12, pp. 446–507, 1954.
- [125] T. Adamo and E. T. Newman, “The Kerr-Newman metric: A Review,” *Scholarpedia*, vol. 9, p. 31791, 2014.
- [126] S. P. Drake and P. Szekeres, “Uniqueness of the Newman-Janis algorithm in generating the Kerr-Newman metric,” *Gen. Rel. Grav.*, vol. 32, pp. 445–458, 2000.
- [127] S. Capozziello, M. De Laurentis, and A. Stabile, “Axially symmetric solutions in  $f(R)$ -gravity,” *Class. Quant. Grav.*, vol. 27, p. 165008, 2010.
- [128] D. Hansen and N. Yunes, “Applicability of the Newman-Janis Algorithm to Black Hole Solutions of Modified Gravity Theories,” *Phys. Rev. D*, vol. 88, no. 10, p. 104020, 2013.
- [129] S. N. Sajadi and S. H. Hendi, “Slowly rotating solution of quadratic gravity: An analytical approximation method,” *Nucl. Phys. B*, vol. 987, p. 116070, 2023.